

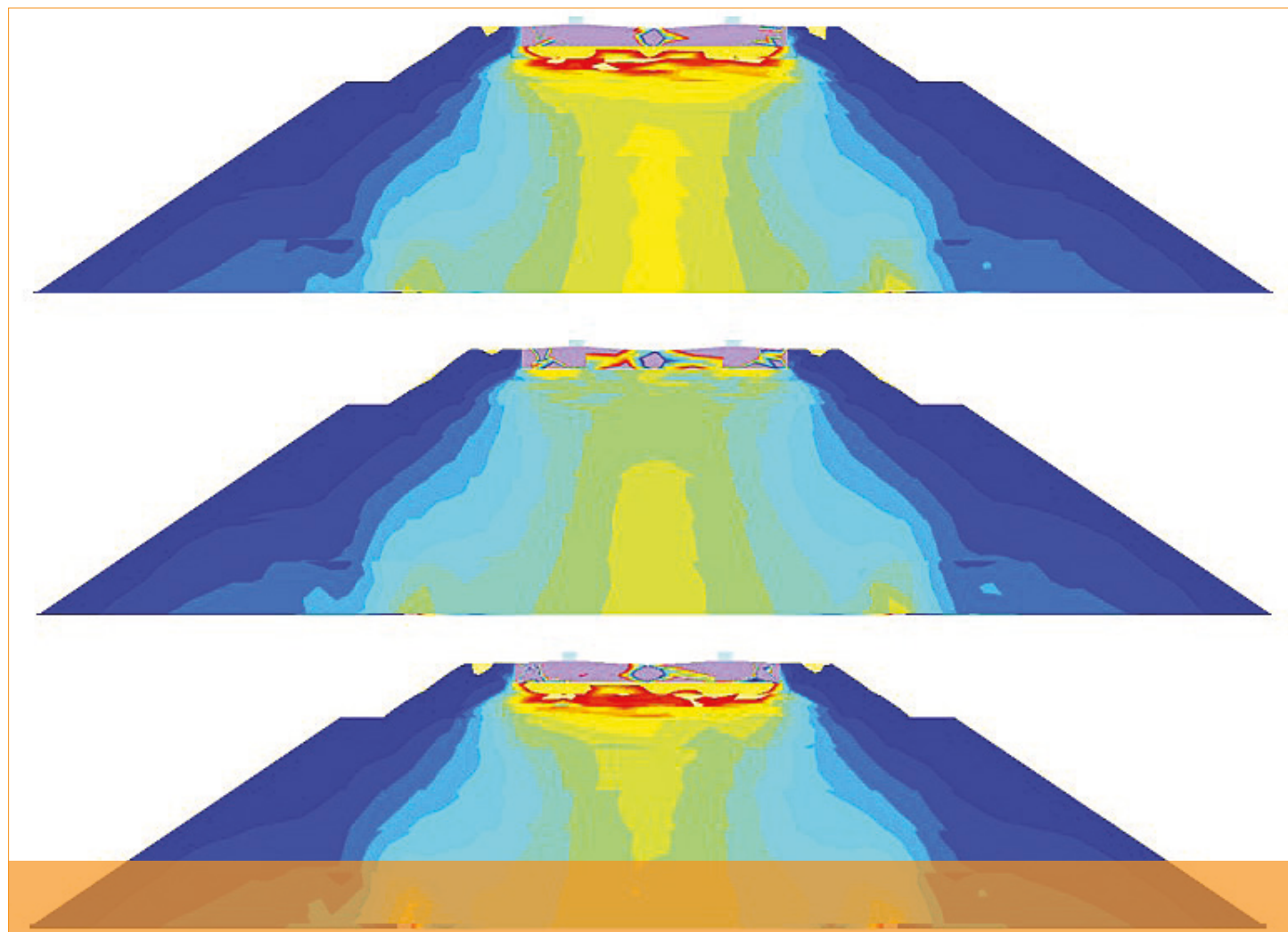


Research reports of the Finnish Transport Agency
28/2017

Antti Kallainen
Pauli Kolisoja

Pile supported embankment slabs under railway track line

**3D FEM simulations on the effect of load models on the
vertical stress levels exposed to slab structures**



Antti Kallialainen, Pauli Kolisoja

Pile supported embankment slabs under railway track line

3D FEM simulations on the effect of load models on the
vertical stress levels exposed to slab structures

Research reports of the Finnish Transport Agency
28/2017

Finnish Transport Agency
Helsinki 2017

Verkkojulkaisu pdf (www.liikennevirasto.fi)

ISSN-L 1798-6656

ISSN 1798-6664

ISBN 978-952-317-416-0

Finnish Transport Agency

P.O.Box 33

FI-00521 HELSINKI

Tel. +358(0)295 34 3000

Antti Kallainen and Pauli Kolisoja: Pile supported embankment slabs under railway track line. Finnish Transport Agency, Engineering and Environment Department. Helsinki 2017. Research reports of the Finnish Transport Agency 28/2017. 43 pages and 4 appendices. ISSN-L 1798-6656, ISSN 1798-6664, ISBN 978-952-317-416-0.

Keywords: Pile supported embankment slab, Finite element method, Railway track structure, Modeling

Summary

The design of railway structures is based on European standards. The specified traffic loads used in dimensioning are presented in EN 1991-2 “Actions on structures Part 2: Traffic loads on bridges” and EN 15528 “Railway applications. Line categories for managing the interface between load limits of vehicles and infrastructure”. The EU Commission regulation No 1299/2014 rules that structures, earthworks and earth pressure effects should be designed according to EN 1991-2 when the structure is new or replaced and according to EN 15528 if the structure if an existing structure is renewed or upgraded. With these regulations, the technical specifications of interoperability (TSI) for loads on railway structures are guaranteed. However, the standard EN 1991-2 is prepared to be applied on bridges and at some cases has been evaluated inappropriate for buried structures.

The aim of the study was to observe the effects of different load models on the vertical stress levels of pile supported embankment slabs under railway structures. The study was conducted with PLAXIS 3D software. Simulations included seven different load models and three different embankment thicknesses, or slab installation depths.

The used calculation model has been verified with actual field data. The field data used for verification is taken from a project where a railway embankment located on soft soil area was heavily instrumented and loaded with a special loading car having an axle load of 25 tonnes. The comparison of stress-strain relationship has been conducted only at top parts of the railway structure since the field data represents embankment on soft soil area and the models in this study have a stiff base. The measured and modeled results had good correlation and it is safe to assume the model used in this study provides credible results. Three main load models were studied more thoroughly. Load model A (LM71), which TSI determines to be applied on slab structures, though it is intended for bridges; load model F (LM-GEO), which is conceptual load model providing an alternative solution to load model A (LM71) (standard EN 1991-2) having line load groups to simulate the actual train load instead of point load group in load model A (LM71); and load model G (E4) (standard EN 15528) which is used for existing infrastructure for 25 ton axle load.

Based on the obtained results load models A (LM71) and F (LM-GEO) are very close to each other in load intensity, or maximum stress increase due train load whereas load model G (E4) provides a smaller load intensity. This is mainly due to distances between load groups. Load model G has always two point loads representing one bogey of a wagon and the distances between bogies are more realistic compared to the actual vehicles. Load model A also has a point load group representing two consecutive bogies but the distance between point loads is fixed. Load model F (LM-GEO), on the other hand, has a replication of the point load group of load model A (LM71) depicted as a line load.

Load model A (LM71) also seems to produce the highest stresses in the most intensively loaded areas. The effect is observable when the installation depth of a pile supported embankment slab is less than 5 meters but seems to vanish as the installation depth increases.

The differences between load models seem to contract as the examined section is getting longer. The total traffic loads at the observed maximum section were close to each other. On the other hand, load model A (LM71) results as the highest local load effects due to combination of point loads and line loads and their sequence. Though the total load throughout the slab structure is similar to other load models, the maximum traffic load is roughly half of the live load other load model produce to a single pile.

The obtained results indicate that the load model has a significant effect on the load effects. A load model intended for bridge design is also ruled to be applied on earthworks, which obviously leads to uneconomical structures and increasing constructions costs.

Antti Kalliainen ja Pauli Kolisoja: Ratarakenteessa oleviin paalulaattoihin kohdistuvat pystyjännitykset. Liikennevirasto, teknikka ja ympäristö -osasto. Helsinki 2017. Liikenneviraston tutkimuksia ja selvityksiä 28/2017. 43 sivua ja 4 liitettä. ISSN-L 1798-6656, ISSN 1798-6664, ISBN 978-952-317-416-0.

Avainsanat: Paalut, laatat, elementtimenetelmä, radat, rakenteet, mallinnus

Tiivistelmä

Rautatierakenteiden suunnittelu perustuu eurooppalaisiin standardeihin. Määritellyt liikennekuormat, joita käytetään mitoituksessa, esitetään suunnittelustandardissa EN 1991-2 "RAKENTEIDEN KUORMAT Osa 2: Siltojen liikennekuormat" ja EN 15528 "Kiskoliikenne. Ratalinjojen luokitus. Rautatievaunujen kuormitusrajat ja infrastruktuuri". EU:n komission asetus N:o 1299/2014 määrää, että rakenteet, maanrakennustyöt ja maanpaineen vaikutukset tulee suunnitella EN 1991-2 mukaisilla kuormilla, jos kyseessä on uusi tai korvattava rakenne. EN 15528 mukaisia mitoituskuormia voidaan käyttää, jos olemassa oleva rakennetta uudistetaan tai parannetaan. Näiden säännösten avulla varmistetaan, että ratarakenteet on suunniteltu yhteentoimivuuden teknisten eritelmien (YTE) mukaisesti. Suunnittelunormi EN 1991-2 on kuitenkin nimensä mukaisesti tarkoitettu ensisijaisesti siltarakenteiden suunnittelua varten ja jossain tapauksissa on todettu, ettei se sellaisenaan soveltu hyvin maan sisällä olevien rakenteiden mitoittamiseen.

Tämän tutkimuksen tavoitteena oli tarkastella erilaisten kuormakaavioiden aiheuttamia pystyjännitystasoja ratarakenteeseen asennettujen paalulaattojen pinnalla. Tutkimuksessa käytetty malli on tehty kolmiulotteisella, elementtimenetelmään perustuvalla PLAXIS 3D-ohjelmistolla. Tutkimuksessa tarkasteltiin seitsemää erilaista kuormakaaviota ja kolmea paalulaatan päällä olevaa pengerpaksuutta.

Tutkimuksessa käytetty laskentamalli on verifioitu mittausdatan avulla. Mittausdatat on poimittu Korialla vuonna 1999 tehdyistä instrumentointikohteesta. Kohteessa mitattiin ratarakenteeseen mobilisoituvia siirtymä- ja jännitystasoja, kun rakennetta kuormitettiin liikkuvalla kalustolla, jonka akselipaino oli 25 tonnia. Mallista on poimittu jännitysmuodonmuutostilaa kuvaavia suureita ja verrattu niitä mitattuihin vastaaviin arvoihin. Verratut suureet vastasivat toisiaan hyvin ja tulosten perusteella voidaan olettaa, että tutkimuksessa käytettävä malli kuvaaa kuormitetun ratarakenteen jännitysmuodon muutostilaa realistikesti.

Laskentatulosten perusteella tutkimuksessa käytettyjen kuormakaavioiden paalulaatan pinnalle aiheuttama jännityslisäys ratarakenteen keskilinjalla on jotakuinkin saman suuruinen lukuun ottamatta kuormakaaviota G (E4), jonka projisoima kuormitusintensiteetti on muiden kuormakaavioiden maksimiavroja pienempi. Kuormakaaviot A (LM71) ja F (LM-GEO) ovat luonnollisista syistä hyvin lähellä toisiaan, sillä kuormakaavio F (LM-GEO) on viivakuomaprosjektilo kuormakaavion A (LM71) neljän pistekuorman ryhmästä. Kuormakaavion A neljän pistekuorman ryhmässä vaunun telejä simuloivat kuormat ovat kuitenkin kiinteällä etäisyydellä toisistaan, kun taas kuormakaaviossa G (E4) kahden peräkkäisen telin välinen etäisyys on suurempi ja vastaa paremmin todellista raiteilla liikkuvaa kalustoa.

Kuormakaavio A (LM71) tuottaa suurimman kuormitusintensiteetin lisäksi suurimman kokonaiskuorman lisäksen suurimman kuormituksen (pistekuormaryhmän) alueella. Ero muihin kuormakaavioihin on havaittava, kun paalulaatan päällä olevan penkereen paksuus on alle 5 metriä. Pengerpaksuuden kasvaessa eri kuormakaavioiden välistet erot kuitenkin näyttävät tasoittuvan. Vastaavasti tapahtuu myös radan pituussunnassa. Jos tarkastellaan eniten kuormitettua aluetta, kuormakaavio A (LM71) tuottaa suurimman lisäkuorman. Kun

kuormakaaviolla F (LM-GEO) ja G (E4) lisätään viiva- ja pistekuormaryhmien lukumäärää, laatalle aiheutuva kokonaiskuorma on likimäärin yhtä suuri kaikilla kuormakaavio-tyypeillä.

Toisaalta, jos tarkastellaan yhdelle paalulle kohdistuvaa kokonaiskuormaa, havaitaan, että kuormakaavio G (E4) tuottaa yhden paalun rasitukseksi vain noin puolet muihin kuormakaavioihin verrattuna, vaikka koko laatan alueella kokonaiskuorma on likipitän saman suuruinen.

Tulokset osoittavat, että kuormituskaavioilla on huomattava vaikutus kuormituksen vaikuttuihin ratarakenteessa. Säännöksistä johtuen silloille kehitettyä kuormituskaaviota joudutaan soveltamaan myös maarakenteissa, mikä johtaa selvästi epätaloudellisiin rakenteisiin.

Antti Kalliainen och Pauli Kolisoja: Vertikalspänningar som riktas mot pålplattor i spårkonstruktionen. Trafikverket, teknik och miljö avdelningen. Helsingfors 2017. Trafikverkets undersökningar och utredningar 28/2017. 43 sidor och 4 bilagor. ISSN-L 1798-6656, ISSN 1798-6664, ISBN 978-952-317-416-0.

Sammanfattning

Projekteringen av järnvägskonstruktioner baseras på europeiska standarder. De fastställda trafiklaster som används vid dimensionering presenteras i konstruktionsstandarden EN 1991-2 "LASTER PÅ BÄRVERK Del 2: "Trafiklast på broar" och EN 15528 "Rälstrafik. Järnvägar. Linjekategorier för hantering av samverkan mellan lastgränser för fordon och infrastruktur". Europeiska kommissionens förordning nr 1299/2014 föreskriver att konstruktioner, jordbyggnadsarbeten och jordtryckseffekter ska projekteras med laster enligt EN 1991-2, när det handlar om en ny konstruktion eller en konstruktion som ska ersättas. Dimensioneringslaster enligt EN 15528 kan användas när en befintlig konstruktion förnyas eller förbättras. Genom dessa bestämmelser säkerställs att bankonstruktioner blir projekterade enligt de tekniska specifikationerna för driftskompatibilitet (TSD). I enlighet med sitt namn är dock konstruktionsnormen EN 1991-2 i första hand avsedd för projektering av brokonstruktioner och i vissa fall har man konstaterat att normen som sådan inte lämpar sig väl för dimensionering av konstruktioner i jord.

Målet med denna undersökning var att granska de vertikallastnivåer som olika lastmodeller orsakar på ytan av pålplattor som är monterade i spårkonstruktionen. Modellen som användes i undersökningen är gjord med den tredimensionella programvaran PLAXIS 3D, som baseras på finita elementmetoden. I undersökningen studerade man sju olika lastmodeller och tre banvallstjocklekar ovanpå pålplattan.

Den beräkningsmodell som användes i undersökningen har verifierats med hjälp av mätdata. Mätdata plockades ur ett instrumenteringsobjekt som genomfördes i Koria år 1999. I objektet mätte man förflyttnings- och spänningsnivåer som mobiliseras mot spårkonstruktionen, när konstruktionen belastades med en rörlig utrustning vars axelvikt var 25 ton. Ur modellen har man plockat storheter som beskriver spänning-formförändrings-tillståndet och jämfört dem med motsvarande uppmätta värden. De jämförda värdena motsvarade varandra väl och baserat på resultaten kan man anta att den vid undersökningen använda modellen beskriver spårkonstruktionens spänning-formförändrings-tillstånd på ett realistiskt sätt.

Baserat på beräkningsresultaten är spänningssökningen vid spårkonstruktionens centrumlinje som de i undersökningen använda lastmodellerna orsakar på ytan av pålplattan ungefär lika stor, utom för lastmodell G (E4) vars projicerade belastningsintensitet är mindre än de övriga lastmodellernas maximivärden. Lastmodellerna A (LM71) och F (LM-GEO) ligger av naturliga orsaker mycket nära varandra, eftersom lastmodell F (LM-GEO) är en linjelastprojektion av en grupp av fyra punktlaster i lastmodell A (LM71). De laster som simulerar vagnboggarna i gruppen av fyra punktlaster i lastmodell A ligger dock på fasta avstånd från varandra, medan i lastmodell G (E4) avståndet mellan två efter varandra följande boggier är större och bättre motsvarar den utrustning som rör sig på rälsen.

Förutom den största belastningsintensiteten producerar lastmodell A (LM71) också den största totallastökningen inom området för den största belastningen (punktlastgruppen). Skillnaden mot de övriga lastmodellerna är märkbar när banvallens tjocklek ovanför pålplattan är mindre än 5 meter. Skillnaderna mellan de olika lastmodellerna verkar dock utjämns när banvallens tjocklek ökar. Motsvarande händer också i spårets längdriktning.

Om man granskar det mest belastade området producerar lastmodell A (LM71) den största tilläggslasten. När antalet linje- och punktlastgrupper ökas i lastmodellerna F (LM-GEO) och G (E4), blir den på plattan orsakade totallasten i det närmaste lika stor med alla lastmodelltyper.

Om man å andra sidan granskar den totallast som riktas mot en påle, upptäcker man att lastmodell G (E4) som enpålsbelastning endast producerar cirka hälften jämfört med de övriga lastmodellerna, trots att totallasten är i det närmaste lika stor över hela plattans område.

Resultaten visar att lastmodellen har en betydande inverkan på lastens effekter i spar konstruktionen. På grund av bestämmelserna tvingas man tillämpa en för broar utvecklas lastmodell även i jordkonstruktioner, vilket leder till klart oekonomiska konstruktioner.

Foreword

The aim of this research report is to study the effects of different load models on the vertical stress levels of pile supported embankment slabs under railway structures with help of three-dimensional Finite Element Model.

This study has been accomplished in Unit of Earth and Foundation Structures at Tampere University of Technology. M.Sc. Antti Kallainen has been responsible of the modeling work and writing this research report. Professor Pauli Kolisoja has supervised the study at Tampere university of Technology.

This study is produced for purposes of Finnish Transport Agency. Geotechnical Advisor Panu Tolla (FTA) and Head of bridge engineering department Sami Noponen (Sweco Finland) have instructed and supervised this study.

Helsinki, June 2017

Finnish Transport Agency
Engineering and Environment

Table of contents

1	INTRODUCTION	11
2	3D FEM MODEL.....	13
2.1	Material models.....	14
2.2	Track components and calculation parameters.....	14
2.2.1	Rail	14
2.2.2	Rail pads.....	15
2.2.3	Sleepers.....	15
2.2.4	Ballast	15
2.2.5	Substructure layers	16
2.2.6	Pile supported embankment slab	16
2.3	Load models.....	17
3	MODEL VERIFICATION	18
3.1	Vertical stresses.....	18
3.2	Strain levels	19
4	RESULTS	22
4.1	The load intensity on top of the pile supported embankment slab	22
4.2	Vertical stress distributions at cross-sections.....	24
4.3	Vertical effective stress distributions on top of the pile supported embankment slab	26
4.4	Total traffic load on the slab.....	35
5	CONCLUSIONS.....	42
	REFERENCES.....	43
	APPENDICES	
	Appendix A	Load intensities on top of the pile supported embankment slab
	Appendix B	Vertical stress distributions at cross-sections
	Appendix C	Vertical stress planes on top of the slab structure
	Appendix D	Longitudinal stress planes on top of the slab structure

1 Introduction

The design of railway structures is based on European standards. The specified traffic loads used in dimensioning are presented in EN 1991-2 “Actions on structures Part 2: Traffic loads on bridges” and EN 15528 “Railway applications. Line categories for managing the interface between load limits of vehicles and infrastructure”. The EU Commission regulation No 1299/2014 rules that structures, earthworks and earth pressure effects should be designed according to EN 1991-2 when the structure is new or replaced and according to EN 15528 if the structure is an existing structure is renewed or upgraded. With these regulations, the technical specifications of interoperability (TSI) for loads on railway structures are guaranteed.

However, the EN 1991-2 is mainly intended for bridge structures and some problems have been identified when applying these loads on geotechnical structures. The EN 1991-2 does not specifically consider geotechnical or buried structures but refers them as earthworks and earth pressure effects. This leads to somewhat irrelevant load factor α since the factor should be used for both bridges and buried structures (e.g. pile supported embankment slabs). In addition, the required load model LM71 for traffic loads differs from both actual train loads and load models presented in EN 15528. Applying LM71 on buried structures usually leads to more complicated structural design, especially in case of pile supported embankment slabs in soft soil areas.

The aim of the study was to observe the effects of different load models on the vertical stress levels of pile supported embankment slabs under railway structures. An earlier study (Nemlander 2015) suggested that for 25 (metric) ton axle loads, the load models presented in EN 15528 produce a significantly lower stress level on top of buried slab structure compared to load model LM71 presented in EN 1991-2.

The study was conducted with PLAXIS 3D software (version 2013.01). Simulations included seven different load models and three different embankment thicknesses, or slab installation depths. The model used in this project is based on an earlier research (Kallialainen et. al. 2014) in which the railway track components were studied in bearing capacity perspective.

The used simulation model and load models are presented in chapter 2. The aggregate components of the track, especially, have model parameters deviating from traditional geotechnical parameters. For example, the stiffness parameters of ballast layers have been derived from triaxial test data (Nurmikolu & Kolisoja 2010). The strength parameters of ballast material have been derived from several sources (e.g. Skoglund 2002, Indraratna et. al. 2011). All the parameters for soil layers presented in chapter 2 also represent cyclic state. This is the main reason both stiffness and strength values of these parameters might appear high but are mandatory when simulating cyclic state with quasi-static calculation procedure.

The used calculation model has been verified with actual field data. The verification is presented in chapter 3. The field data used for verification is taken from a project (Kolisoja et. al. 2000), where a railway embankment located on soft soil area was heavily instrumented and loaded with a special loading car having an axle load of 25 tonnes. The comparison of stress-strain relationship has been conducted only at top

parts of the railway structure since the field data represents embankment on soft soil area and the models in this study have a stiff base.

A summary of calculation results is presented in chapter 4 and the main observations are gathered in conclusions (chapter 5).

2 3D FEM Model

The model developed for the purposes of this study was created with PLAXIS 3D which is a finite element software that has been developed especially for the analysis of deformation and stability in geotechnical engineering projects. (Kallialainen et. al 2016)

PLAXIS uses 10-node tetrahedral elements for soil layers and 6-node plate elements. Plate elements are based on Mindlin's plate theory (Bathe 1982). User can define the desirable refinement for elements and the program calculates the target element size based on the outer model geometry dimensions. In addition, user can affect the meshing procedure by defining the relative element size factor, polyline angle tolerance and surface angle tolerance. (Brinkreve et. al. 2012) In this project, the finest mesh at automatic meshing procedure was used, i.e. target element size was 0.5, polyline tolerance angle was 30° and surface angle tolerance 15° respectively. (Kallialainen et. al 2016)

The model created for this study is illustrated in figure 1 and consists of a straight and flat railway section. The length of modeled track is 36.86 meters which is equal to 61 sleepers with 0.61 m spacing. The loads are produced with point loads representing wheel loads of a 25 ton axle and with line loads presented in figure 2. Simulations were calculated with pure static 25 ton axle load (characteristic load), with respective line loads and with dynamic load factor 1.25. The dynamic load factor was chosen instead of factor α presented in EN 1991-2 since the α factor used for bridge structures has been evaluated high when applied to buried structures. The value 1.25 is a commonly used value for dynamic impact on railway structures in Finland.

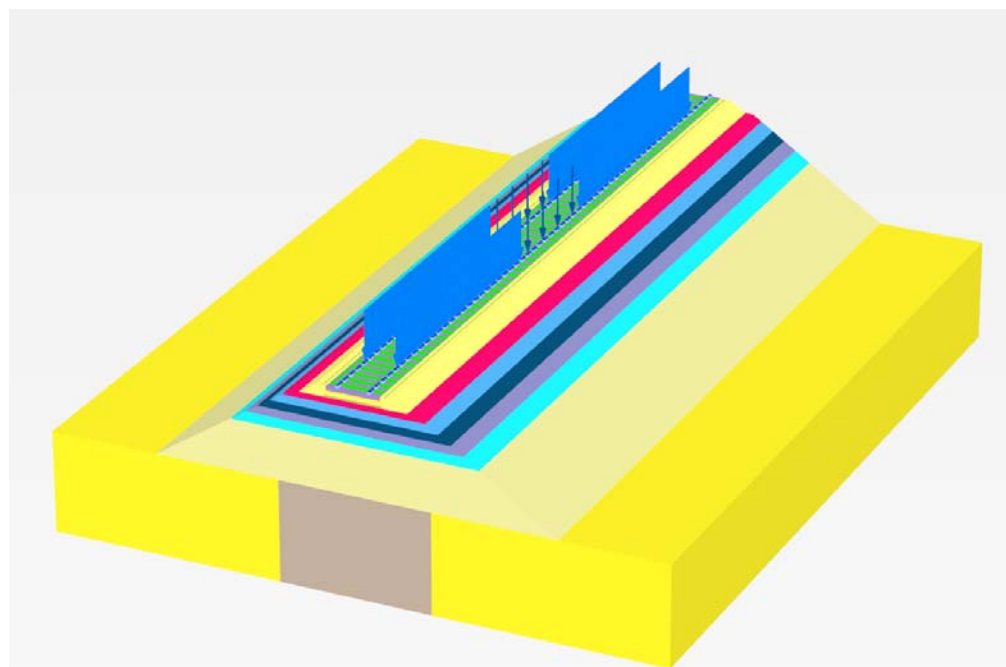


Figure 1. Schematic picture of the FE-model, embankment thickness is 5 meters, load model A (LM71-25).

2.1 Material models

PLAXIS contains several different material models within the software. The material models used in this track model are shortly described. The Hardening-Soil Model (HS) is an advanced model for the simulation of soil behavior. Limiting states of stresses are described by means of the friction angle, φ , the cohesion, c , and the dilatancy angle, ψ . Soil stiffness is described by using three different input stiffnesses: the triaxial loading stiffness, E_{50} , the triaxial unloading stiffness, E_{ur} , and the oedometer loading stiffness, E_{oed} . All these stiffnesses relate to a reference stress, 100 kPa in this study. The HS model was chosen for aggregate materials (ballast, subballast and frost protection layers) since the yield surface is not fixed but can expand due to plastic straining. The hardening rules can be divided into two main types of hardening, namely shear and compression hardening. Shear hardening is used to model plastic strains due to primary deviatoric loading. Compression hardening is used to model irreversible strains in oedometric and isotropic loading. Therefore, the stiffnesses of aggregate layers are more appropriate on both sides of the yield surface i.e. when subjected to deviatoric loading, the soil stiffness decreases simultaneously with the development of irreversible strains. The Linear Elastic Model (LE) was chosen for other components of this track model. (Kalliainen et. al 2016)

2.2 Track components and calculation parameters

In the FE-model the railway track superstructure consist of rails, rail pads, sleepers and ballast. Rails are modeled as plate elements. Base plates and sleepers are modelled using linear elastic soil elements. Material model for ballast is Hardening Soil. Railway substructure layers are modeled using HS-model.

2.2.1 Rail

Rail profile simulated is 60 E1. The necessary parameters and measures are presented in table 1.

Table 1. Rail properties.

Rail type	Cross-section area A	Moment of inertia I	EA	EI
Unit	m^2	m^4	N/m	Nm^2/m
60 E1	$7.67 * 10^{-3}$	$3.038 * 10^{-5}$	$1.61 * 10^9$	$6.380 * 10^6$
Rail type	Rail foot width	Artificial height of Plate element	E_{12}	G_{12} when $v=0$
Unit	m	m	GPa	GPa
60 E1	0.150	0.135	<u>22.68</u>	<u>11.34</u>

2.2.2 Rail pads

Rail pads were modeled as linear elastic block elements. The stiffness of a standard pad was determined similar to the commonly used rubber pad type (Vossloh Zw 900 NT) in Finland. The moduli value of a standard pad in this model is based on static compression tests. Taking the prestress due to the fastening systems into account, the stiffness of the pad was determined between 30 and 70 kN load to provide pad stiffness to match the track conditions. The stiffness of a standard pad in this model was approximately 80 MN/mm. The actual thickness of modeled pad was 8 mm. In the first simulations the pads were modeled as 10 mm thick, 140 mm x 180 mm elements having a moduli value of 100 MPa. Due to some difficulties at the meshing procedure of software, the thickness of the pad was decoupled to avoid meshing failure. Therefore, also the moduli values of simulated pad stiffnesses were decoupled. The moduli value used in simulations was 1,000 MPa. Since the modeled pad material was rubber, a realistic Poisson's Ratio is close to 0.5. A maximum value available in used software, 0.495 was chosen.

2.2.3 Sleepers

The sleeper type modeled was pre-stressed concrete monoblock B97. A single sleeper could be modeled accurately but the tilted surfaces at sleeper and ballast interfaces caused failure in meshing procedure of the actual model. Therefore the actual sleeper used in the model was somewhat simplified as illustrated in table 2. The moment of inertia of the sleeper was matched with the actual sleeper at sleeper end, in the middle of the sleeper and at rail seat section. Moduli value used for concrete sleeper was 40 GPa ($v = 0$).

Table 2. *Sleeper dimensions.*

Sleeper material	Length of sleeper	Width of sleeper	Height of sleeper
Unit	m	m	m
Concrete	2.600	0.260	1)
Height of B97 monoblock sleeper		Moment of inertia at calculated cross-section	Modeled height of the sleeper
Unit	m	m^4	m
At sleeper end	0.198	$1.508 * 10^{-4}$	1) 0.185
At rail seat section	0.2325	$2.274 * 10^{-4}$	1) 0.210
In the middle of sleeper	0.185	$9.992 * 10^{-5}$	1) 0.165

2.2.4 Ballast

Ballast was modeled in three separate layers under the sleeper area. Thickness of upper layer was 120 mm and thicknesses of middle and lower layers were 110 mm, respectively. The HS-model parameters are shown in table 3.

Table 3. HS-model parameters for ballast layers.

Parameter	c'	ϕ'	ψ	E_{50}^{ref}	E_{oed}^{ref}	E_{ur}^{ref}	ν_{ur}	m	p^{ref}	K_0^{nc}	f
Unit	kPa	°	°	MPa	MPa	MPa	-	-	kPa	-	-
Upper ballast layer	20	45	10	275	230	550	0.2	0.5	100	0.300	0.9
Middle ballast layer	20	45	10	250	210	500	0.2	0.5	100	0.300	0.9
Lower ballast layer	20	45	10	225	190	450	0.2	0.5	100	0.300	0.9

2.2.5 Substructure layers

Railway substructure consisted of subballast layer (thickness 300 mm) and frost protection layers. Each frost protection layer was 400 mm thick. The simulations represented a new railway structure. The current practice is to use crushed rock aggregates in construction of railway track substructures. In addition, when the embankment thickness was 5 meters, a 2.5 meters thick rockfill layer was modeled below the frost insulation layers. The HS-model parameters used in simulations are presented in table 4.

Table 4. HS-model parameters for substructure layers.

Parameter	c'	ϕ'	ψ	E_{50}^{ref}	E_{oed}^{ref}	E_{ur}^{ref}	ν_{ur}	m	p^{ref}	K_0^{nc}	f
Unit	kPa	°	°	MPa	MPa	MPa	-	-	kPa	-	-
Subballast											
Crushed rock	10	45	5	250	210	500	0.2	0.5	100	0.300	0.9
Frost protection layers											
Layer 1	10	45	5	180	150	360	0.2	0.5	100	0.300	0.9
Layer 2	10	45	5	170	145	340	0.2	0.5	100	0.300	0.9
Layer 3	10	45	5	160	135	320	0.2	0.5	100	0.300	0.9
Layer 4	10	45	5	150	130	300	0.2	0.5	100	0.300	0.9
Rockfill											
	0.1	40	10	120	120	250	0.2	0.5	100	0.357	0.9

2.2.6 Pile supported embankment slab

The slab was modeled as a massive linear elastic soil element. The width of a slab element was 3.9 meters, when embankment thickness was 1.4 meters, 4.9 meters when embankment thickness was 2.5 meters and 7.4 meters when embankment thickness was 5 meters. The slab block has a moduli value of 20 GPa ($v = 0.1$).

2.3 Load models

Load models used in the simulations are illustrated in figure 2. Load models used in simulations were:

- A: standard LM71 load model (EN 1991-2), which is currently used in dimensioning of slab structures
- B: Point load group of LM71 has been replaced with a line load “LM-GEO”. LM-GEO is a suggested load model to replace the point load group representing two consecutive bogies in load model LM71.
- C: One point load group of LM71
- D: Three consecutive point load groups of LM71
- E: One line load “LM-GEO”
- F: Three consecutive line load groups “LM-GEO”
- G: Load model E4 (EN 15528)

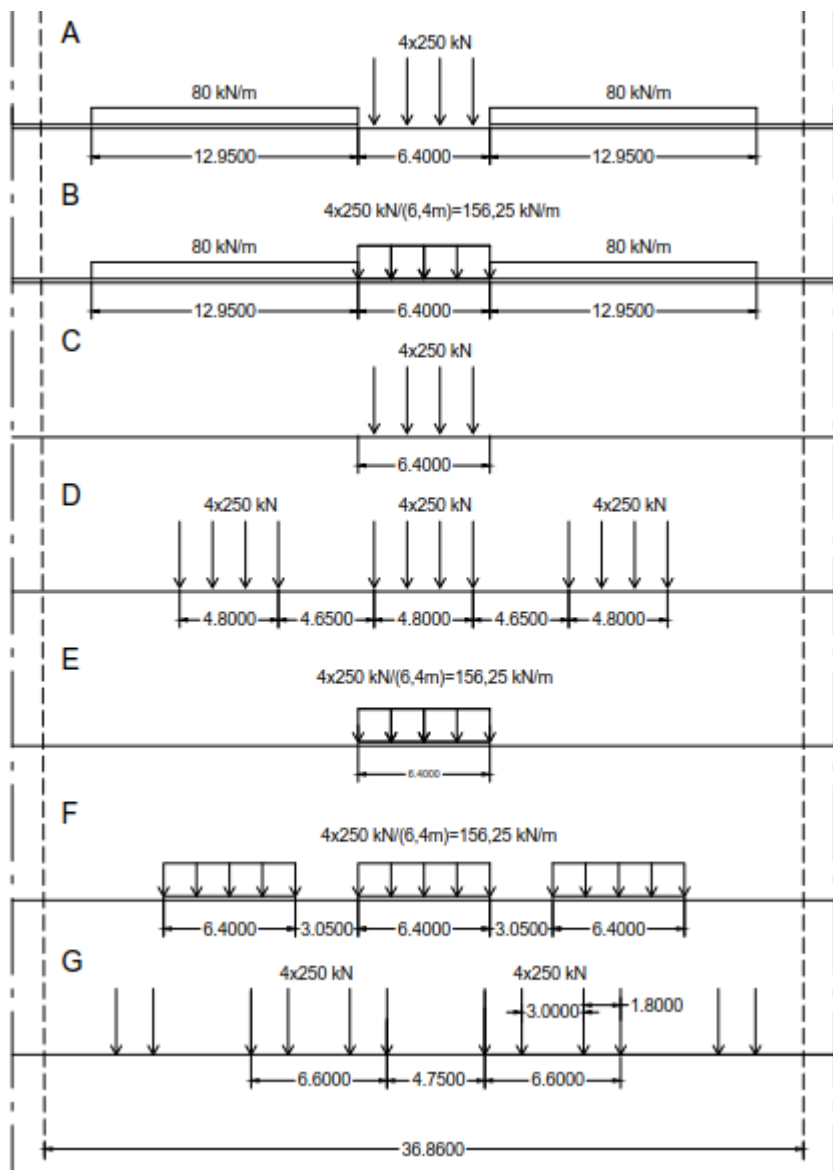


Figure 2. Load model dimensions and simulation model length 36.86 meters.

3 Model verification

The model components have earlier been studied in a simulation series presented in Kallainen et. al. 2014. The study provides one solution to analyze the stress-strain relationships of a railway structure using advanced 3D FEM software. The simulation series also compares the stresses and strains of track components caused by a change of a single track component property at a time. Based on the results of study, the model provides a credible stress-strain relationship with current model specification. Therefore, the basic idea of the model structure is also used in this study. The model has been updated for the specifications of this study.

In the following chapters the stress and strain levels the model produces have been compared to measured data. The measured data is applied from a research "Instrumentation and modelling of track structure, 250 kN and 300 kN axle loads" (Kolisoja et. al. 2000), where a railway track was heavily instrumented and stress-strain relationship was measured using a specific wagon having axle load of 250 kN.

3.1 Vertical stresses

Vertical stresses were measured in Koria 1999 (Kolisoja et. al 2000). The measured values are compared to modeled effective stresses at same depth. The load model in these comparisons is LM71 (type A) which the currently used load model in structural dimensioning. The measured effective vertical stresses (or earth pressures) at level -0.7 meters from the rail seat are illustrated in figure 3. The modeled effective vertical stresses are shown in figure 4, respectively. The modeled values include the weight of the structures, approximately 15 kPa. The model produces approximately 100 kPa peak value, and an area under loaded sleepers, where the effective stress is between 80 and 90 kPa. Based on this information, the stress the load model induces is approximately 65-75 kPa. The measured values transducer P4 provides in figure 3 are at the same levels than modeled values.

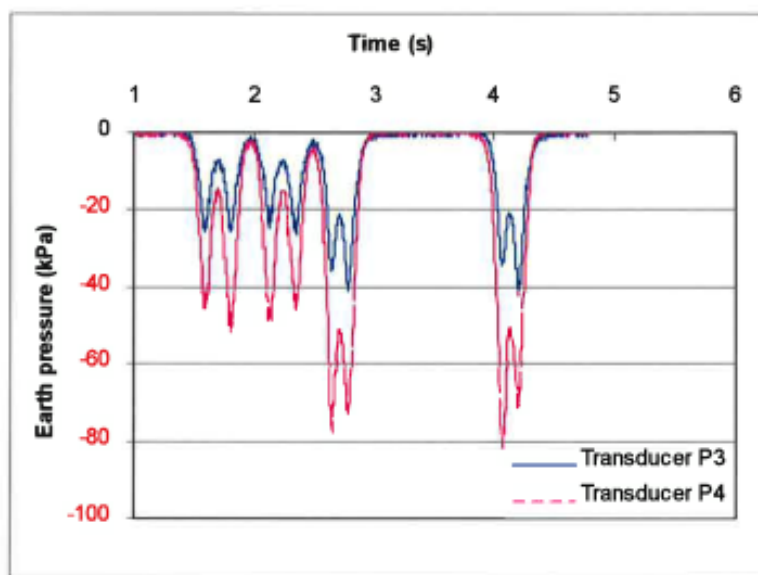


Figure 3. Vertical earth pressures at the level of -0.7 meters. (Kolisoja et. al. 2000)

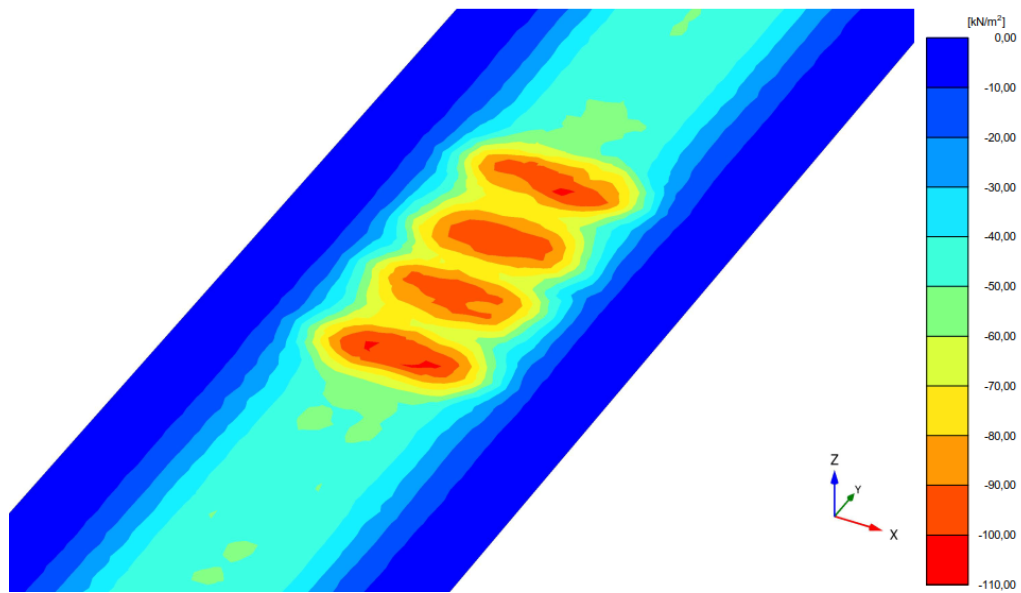


Figure 4. Modeled vertical effective stresses including the dead load (approximately 15 kPa) at the level of -0.7 meters.

3.2 Strain levels

Vertical and lateral strains were also measured at the same depth in Koria. The results of vertical strains are presented in figure 5. The respective modeled strains are presented in figure 6. The measured vertical strains were between 300 and 400 $\mu\text{m}/\text{m}$ whereas the modeled values vary between 280 and 450 $\mu\text{m}/\text{m}$ under the sleeper area.

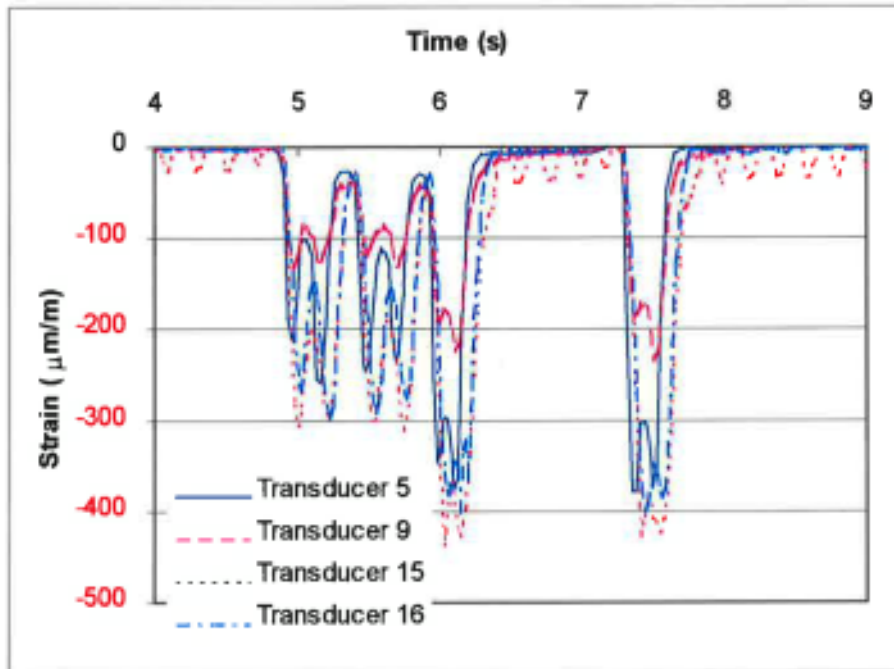


Figure 5. Measured vertical strains at the level of -0.7 meters. (Kolisoja et. al. 2000)

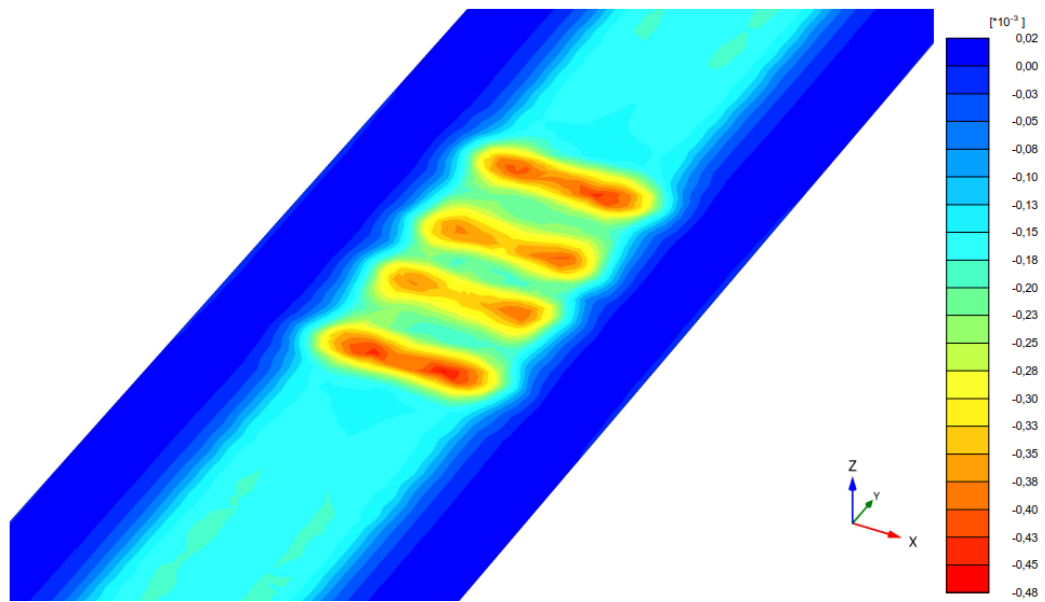


Figure 6. Modeled vertical strains at the level of -0.7 meters.

The measured lateral strains are illustrated in figure 7. Based on the measured data, the lateral strains are between 50 and 100 $\mu\text{m}/\text{m}$. The modeled lateral (or transverse) strains are illustrated in figure 8. The modeled values are in the range of 70-110 $\mu\text{m}/\text{m}$.

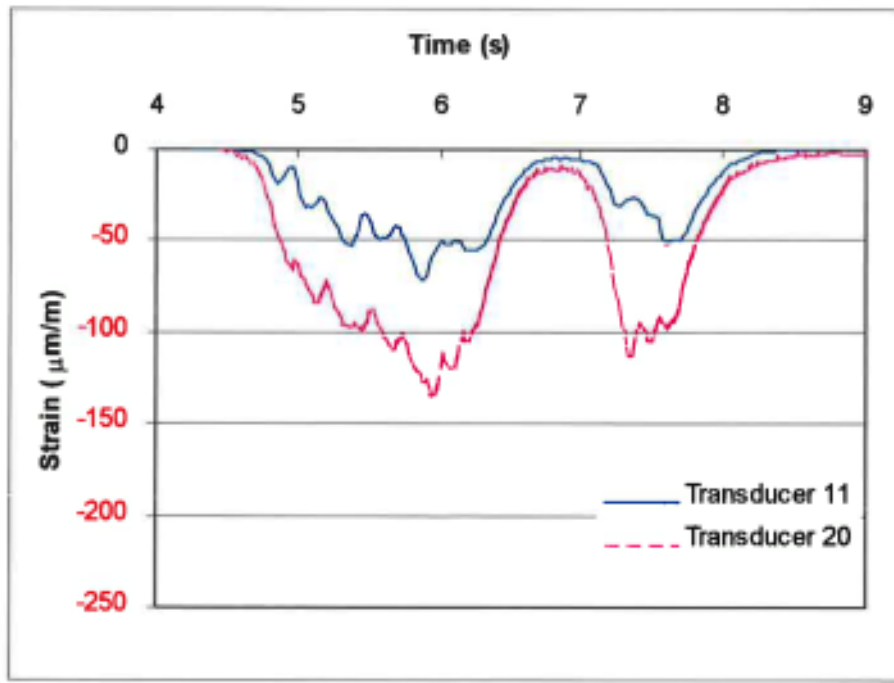


Figure 7. Measured lateral strains at the level of -0.7 meters. (Kolisoja et. al. 2000)

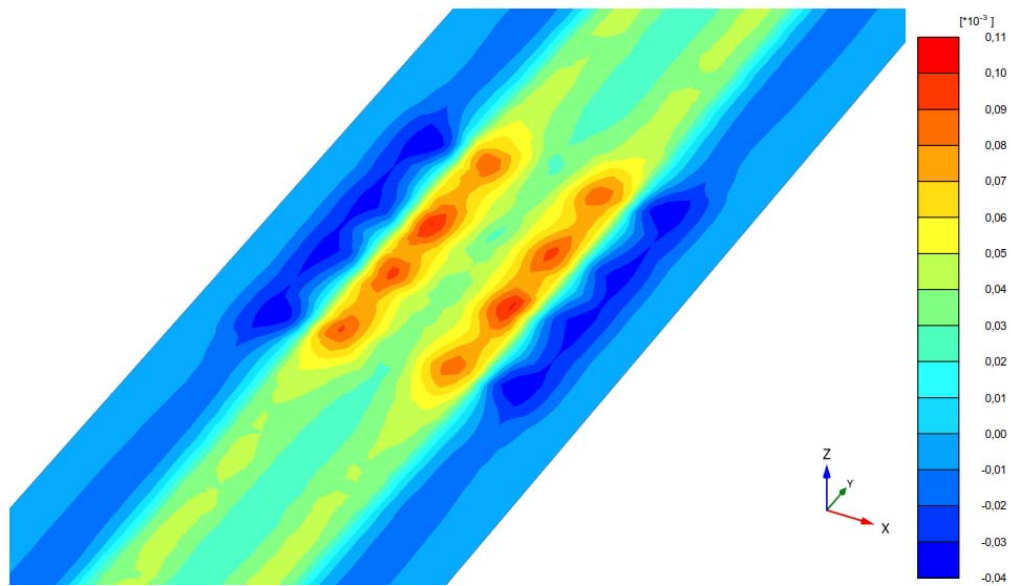


Figure 8. Modeled lateral strains at the level of -0.7 meters.

Based on the comparisons between measured and modeled values it can be concluded that the calculation model used in this project provides a credible stress-strain relationship. The comparison was made only at one and certain level. On the other hand, the earlier versions of the calculation model have been widely analyzed. The simulation series Kalliainen et. al. 2014 reported also includes a wide variety of sensitivity analysis for model components. Therefore, the results the model used in this study provides a realistic stress and strain levels at different track components.

4 Results

4.1 The load intensity on top of the pile supported embankment slab

The load intensities have been presented as a line section along the track centerline on top of the slab structure. The intensity represents the total maximum load the load model projects to the slab. Weight of the structures (dead load) is subtracted from the shown results.

All results are presented in appendix A. Figures 9-11 illustrate an example of the results. Figures 9-11 show that load models A and F are very close to each other in local load intensity (maximum stress increase due train load) whereas load model G provides a smaller load intensity. This is mainly due to distances between load groups. Load model G has always two point loads representing one bogey of a wagon and the distances between bogies are more realistic compared to the actual vehicles. Load model A also has a point load group representing two consecutive bogies but the distance between point loads is fixed. Load model F, on the other hand, has a replication of the point load group of load model A depicted as a line load.

Due to unlimited line load sections on both sides point load group in load model A, the total load effect is more widely spread (lateral coordinates 13.00...23.87) compared to the load model F (Figure 9). Similar effects can also be observed in figures 10 and 11. Based on the obtained results the load intensities do not solely define the principles of the dimensioning.

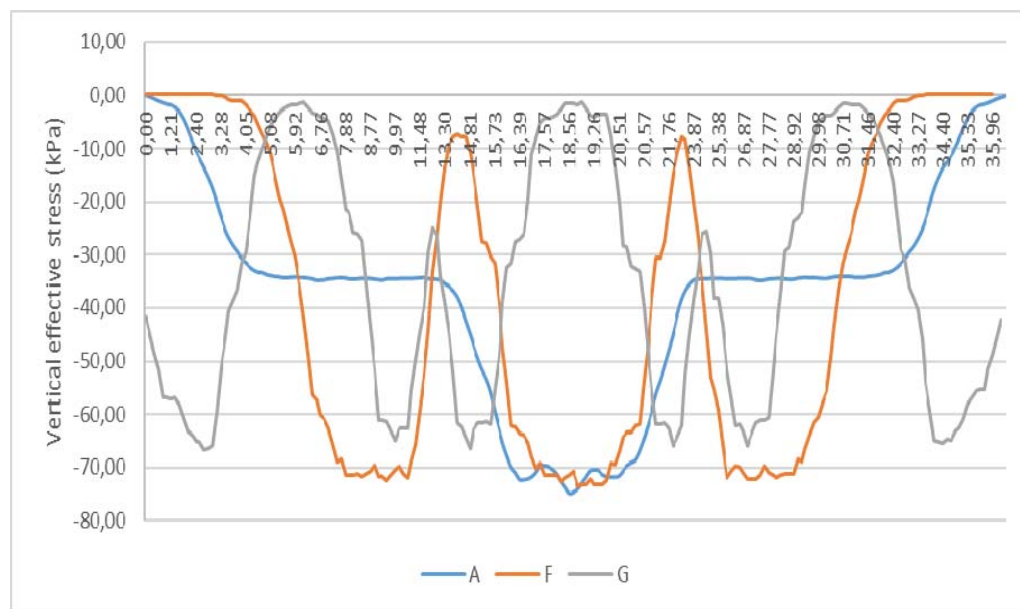


Figure 9. The load intensity on top of the slab structure along the track centerline, slab installation depth 1.4 meters, load models A (LM71), F (LM-GEO) and G (E4) including dynamic load factor 1.25.

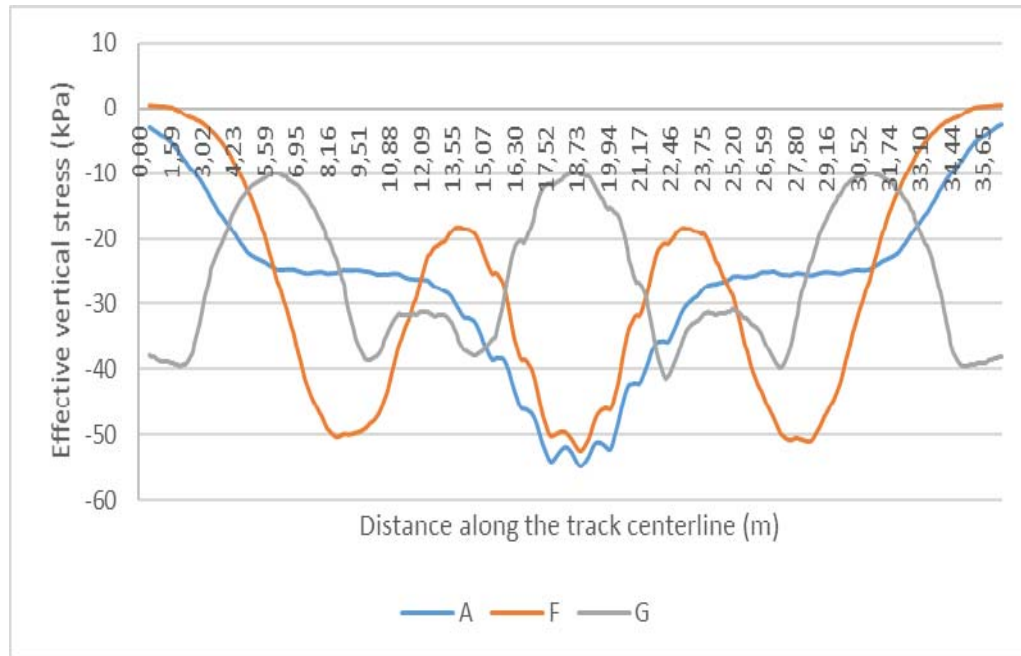


Figure 10. The load intensity on top of the slab structure along the track centerline, slab installation depth 2.5 meters, load models A (LM71), F (LM-GEO) and G (E4) including dynamic load factor 1.25.

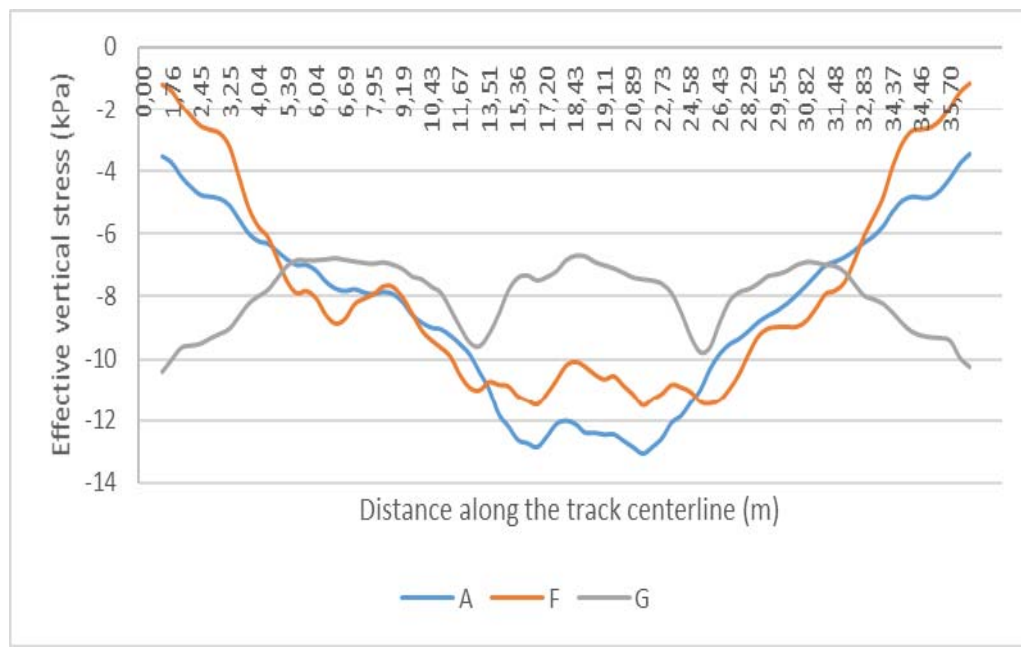


Figure 11. The load intensity on top of the slab structure along the track centerline, slab installation depth 5 meters, load models A (LM71), F (LM-GEO) and G (E4) including dynamic load factor 1.25.

4.2 Vertical stress distributions at cross-sections

To gain a better comprehension on how the load distributes in a railway track structure the cross-sections of the most intensively loaded areas were defined. All the vertical stress distributions are presented in Appendix B. Calculation results for load models A, F and G at different slab installation depths are presented in figures 12-14. These stress distributions include the dead load of the railway structure.

The difference of line load and point load can be observed on the top parts of the railway structure. When the cross section is defined at the point load spot, the load intensity is higher especially at the ballast layer. The vertical stress level is in these cases higher at the center area of the embankment structure. However, the most unexpected result at the cross sections is the magnitude of vertical stress inside the embankment structure. Based on the obtained results the vertical stress level does not systematically decrease as a function of depth. Actually, the stiff slab under the embankment supports the structure and as a result the stresses inside the embankment distribute less than the dead load of the structure increases.

On the other hand, the differences in load distribution the different load models produce appear to diminish as the embankment height grows.

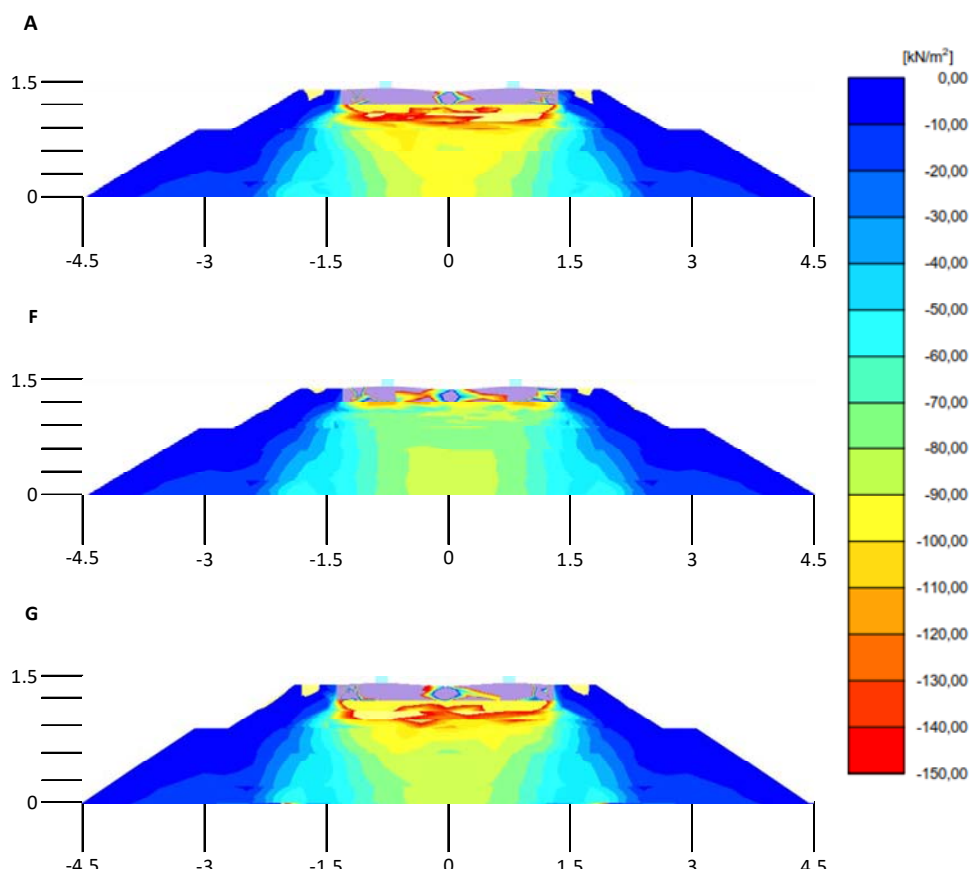


Figure 12. Total vertical stress distributions at the most intensively loaded cross sections of a modeled track, slab installation depth 1.4 meters, load models A (LM71), F (LM-GEO) and G (E4) including dynamic load factor 1.25.

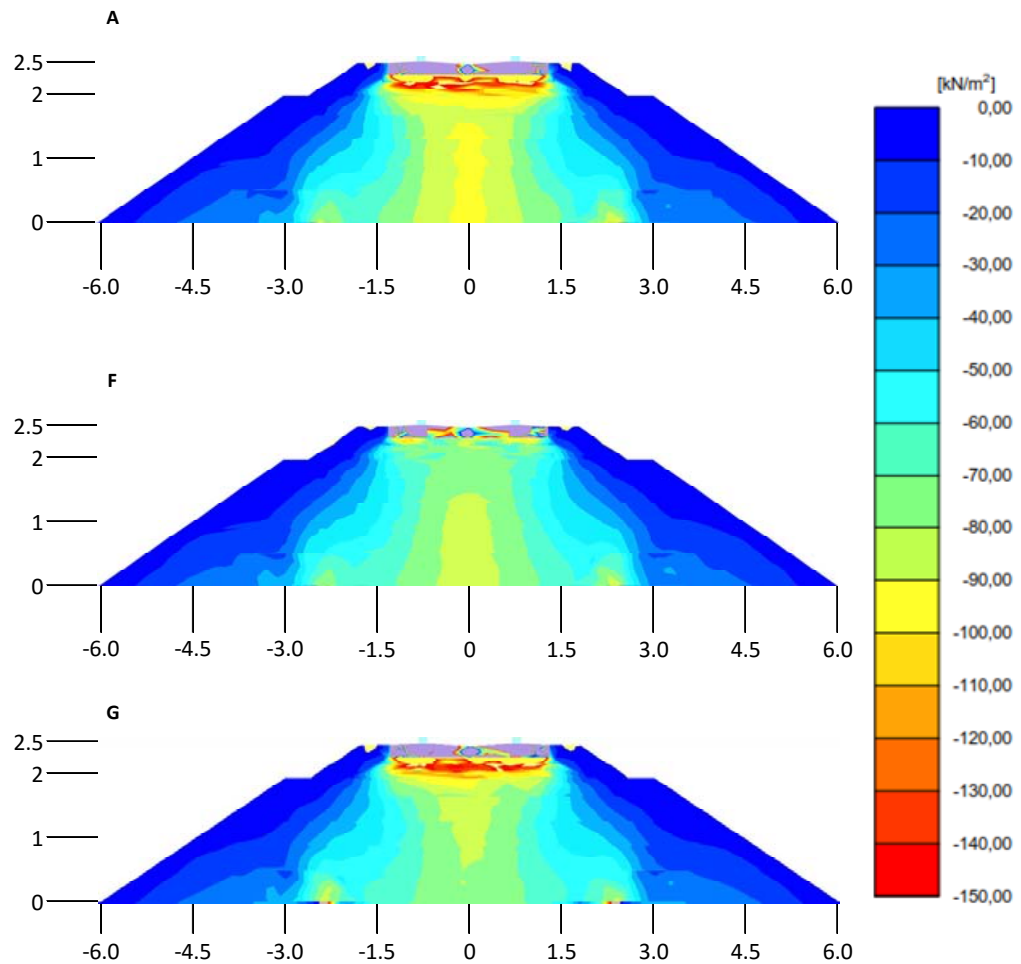


Figure 13. Total vertical stress distributions at the most intensively loaded cross sections of a modeled track, slab installation depth 2.5 meters, load models A (LM71), F (LM-GEO) and G (E4) including dynamic load factor 1.25.

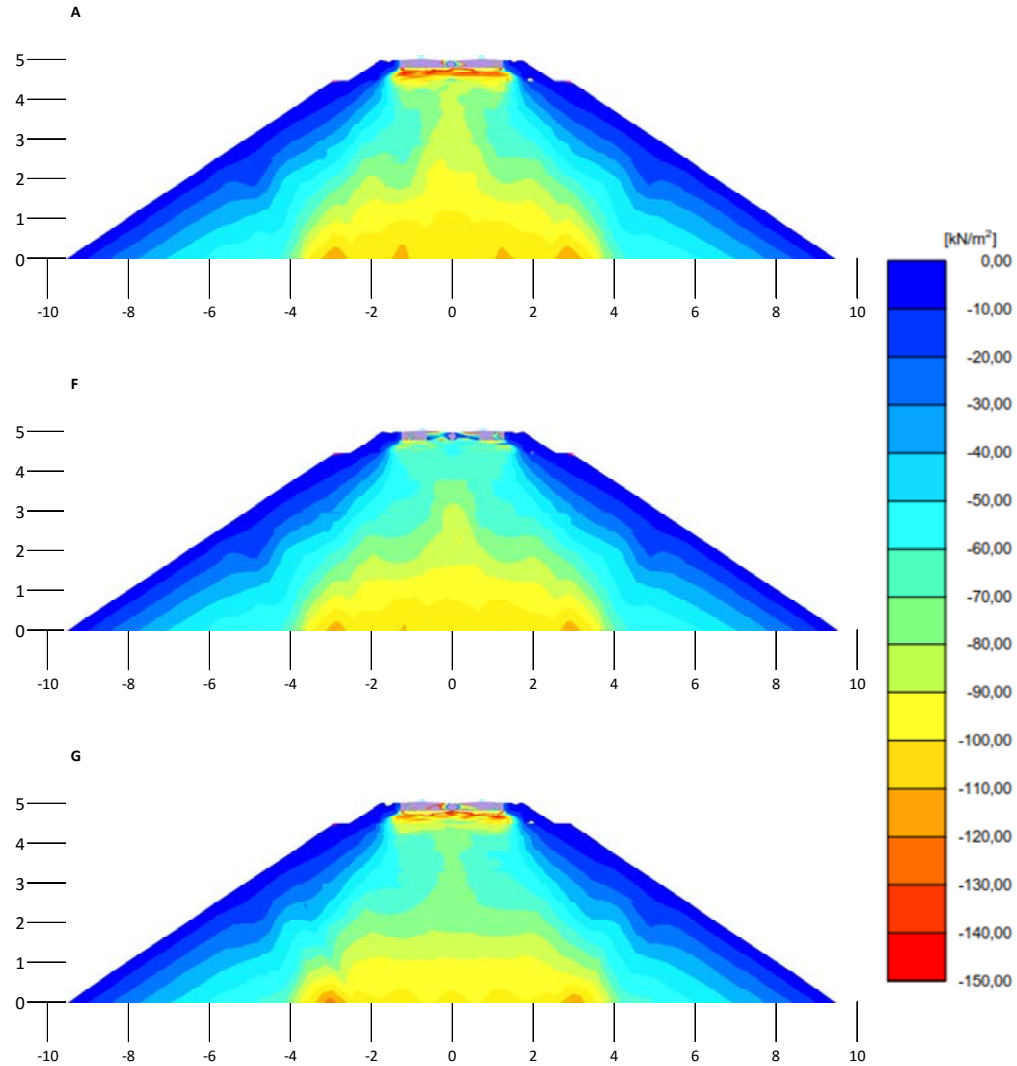


Figure 14. Total vertical stress distributions at the most intensively loaded cross sections of a modeled track, slab installation depth 5 meters, load models A (LM71), F (LM-GEO) and G (E4) including dynamic load factor 1.25

4.3 Vertical effective stress distributions on top of the pile supported embankment slab

The stress distribution planes on top of the embankments structure provide the best available tool to analyze the differences of the load models. All the vertical stress distributions on top of the slab are presented in Appendix C.

For a better understanding of the stress distribution on top of the slab, the longitudinal stress planes were also observed. The longitudinal stress planes are presented in Appendix D.

The stress distribution planes of load models A, F and G (slab installed at the depth of 1.4 meters) are presented in figures 15-17. The corresponding stress planes of installation depth 2.5 meters are presented in figures 18-20 and planes having the installation depth of 5 meters are shown in figures 21-23. These distribution planes include the dead load of the railway structure. In addition, these curves were plotted with unfiltered data and all the stresses are defined from embankment structure (soil stresses) to avoid analyzing the stresses of the concrete structure. For this reason, some calculatory stress peaks occur in figures 15-23 at the boundary areas of the slab structure.

It is obvious that the stress levels vary in these plane views but as the embankment height increases, the stress distributions become more equalized as the effects of actual point or line loads spread in the track structure.

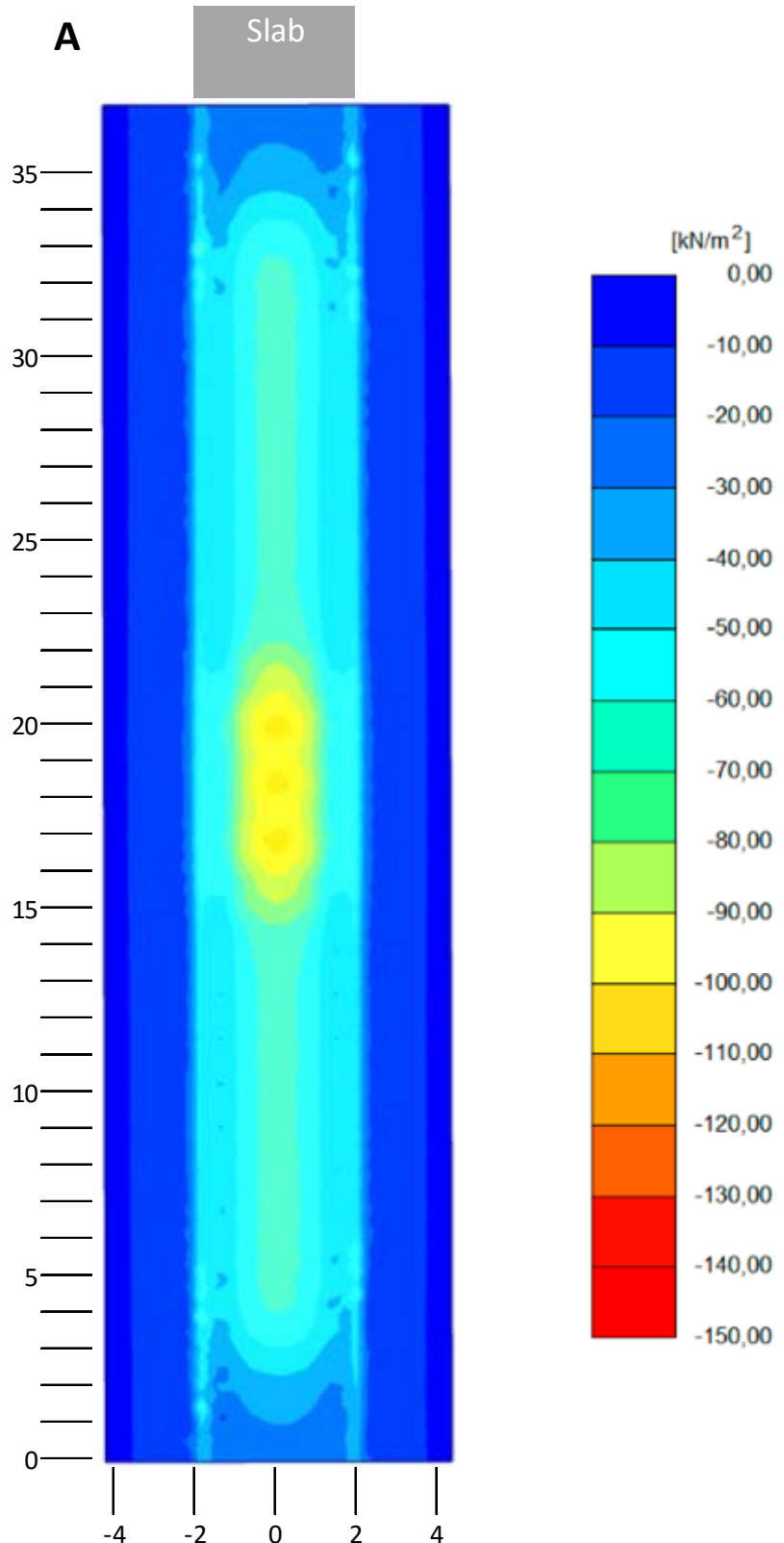


Figure 15. Total vertical stress distributions on a plane on top of the slab structure, slab installation depth 1.4 meters, load model A (LM71) including dynamic load factor 1.25.

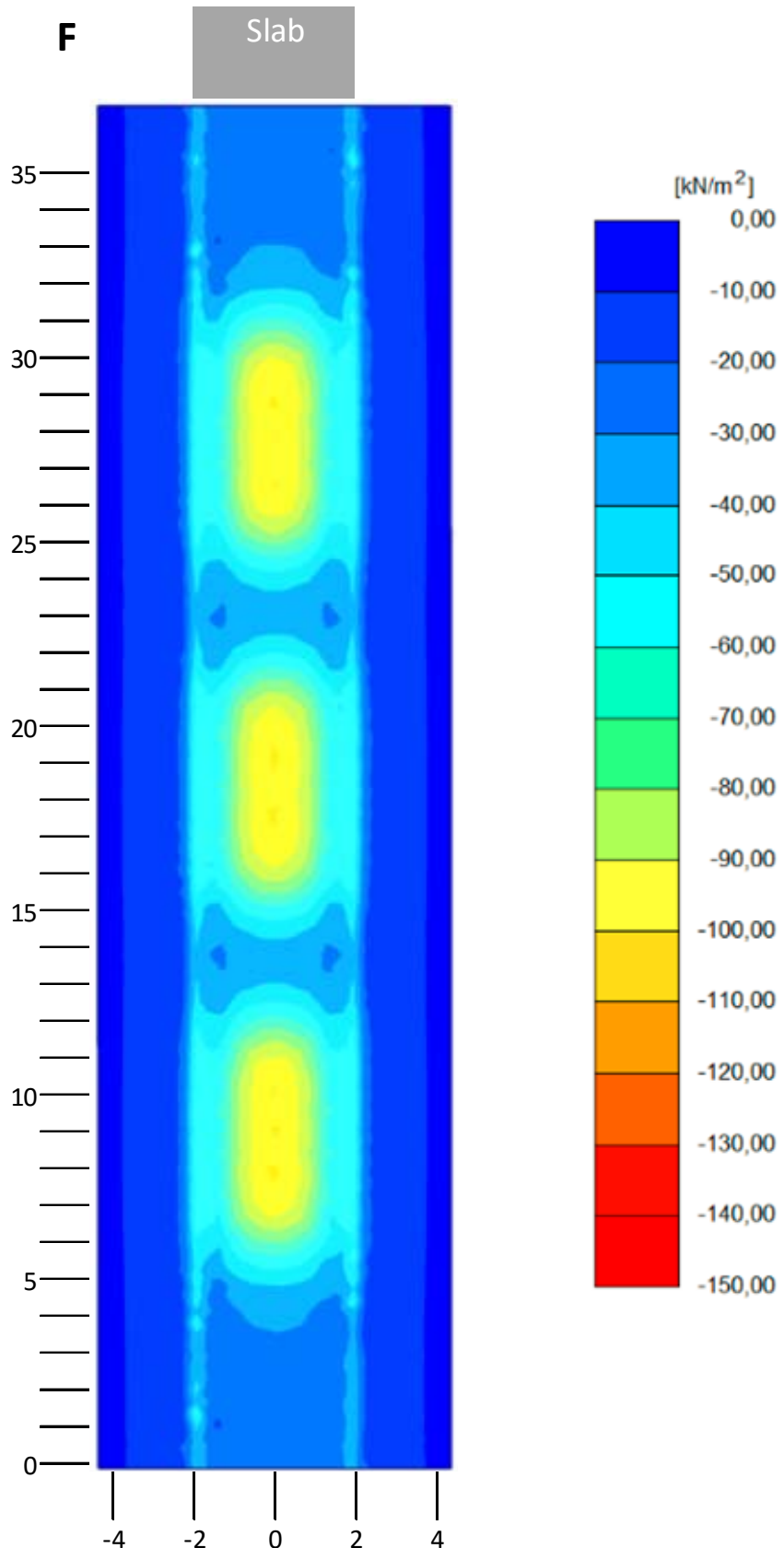


Figure 16. Total vertical stress distributions on a plane on top of the slab structure, slab installation depth 1.4 meters, load model F (LM-GEO) including dynamic load factor 1.25.

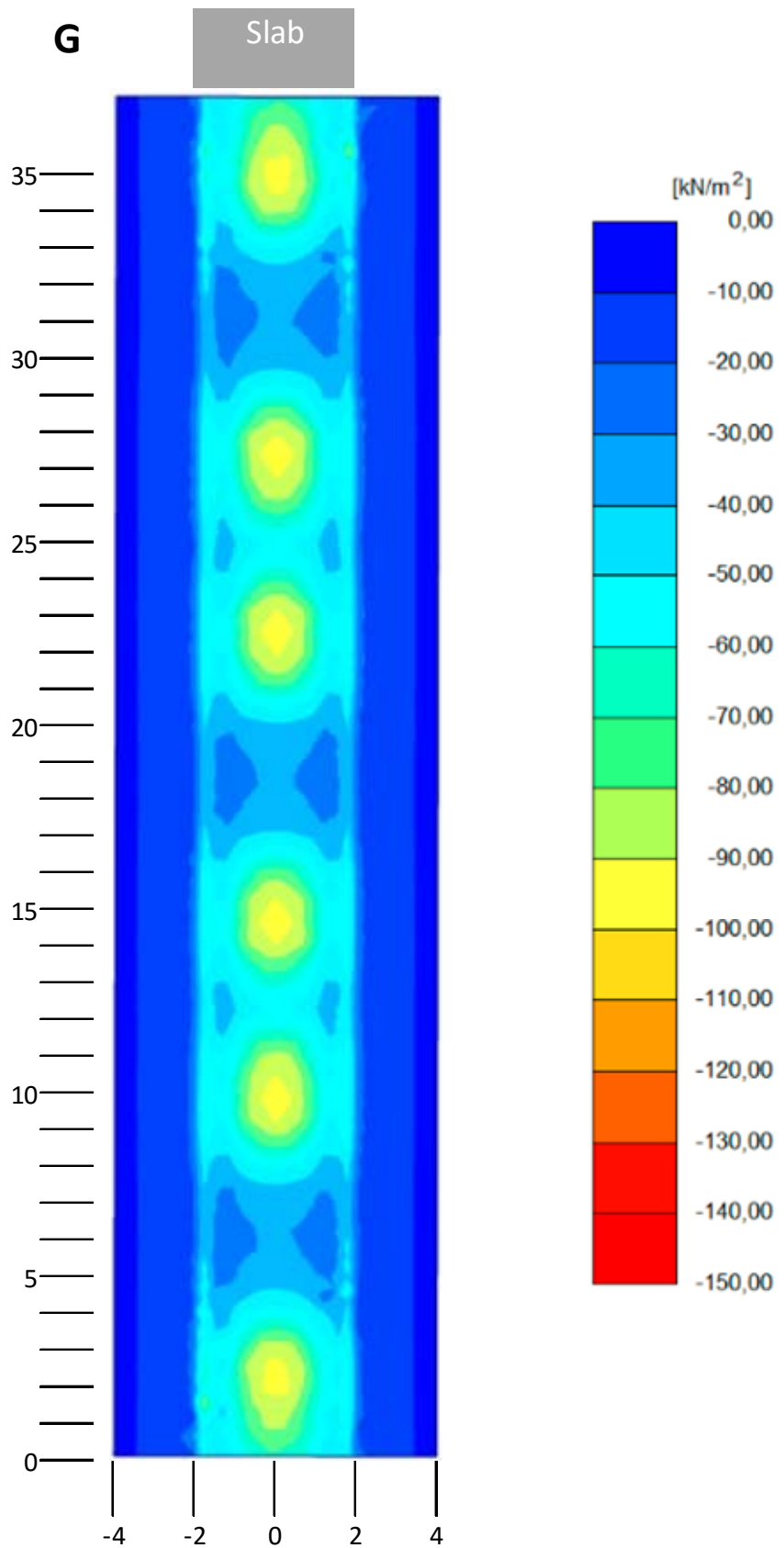


Figure 17. Total vertical stress distributions on a plane on top of the slab structure, slab installation depth 1.4 meters, load model G (E4) including dynamic load factor 1.25.

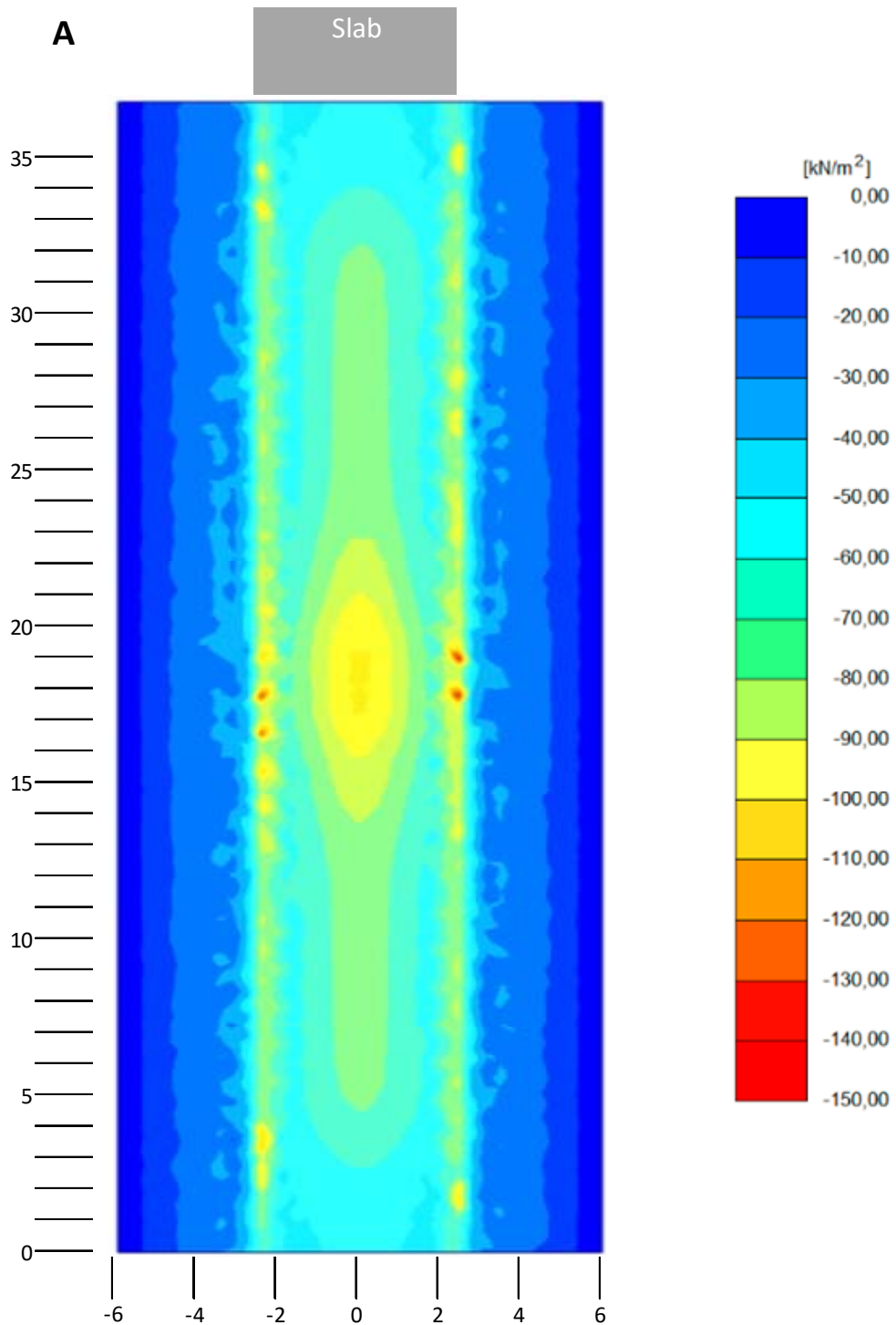


Figure 18. Total vertical stress distributions on a plane on top of the slab structure, slab installation depth 2.5 meters, load model A (LM71) including dynamic load factor 1.25.

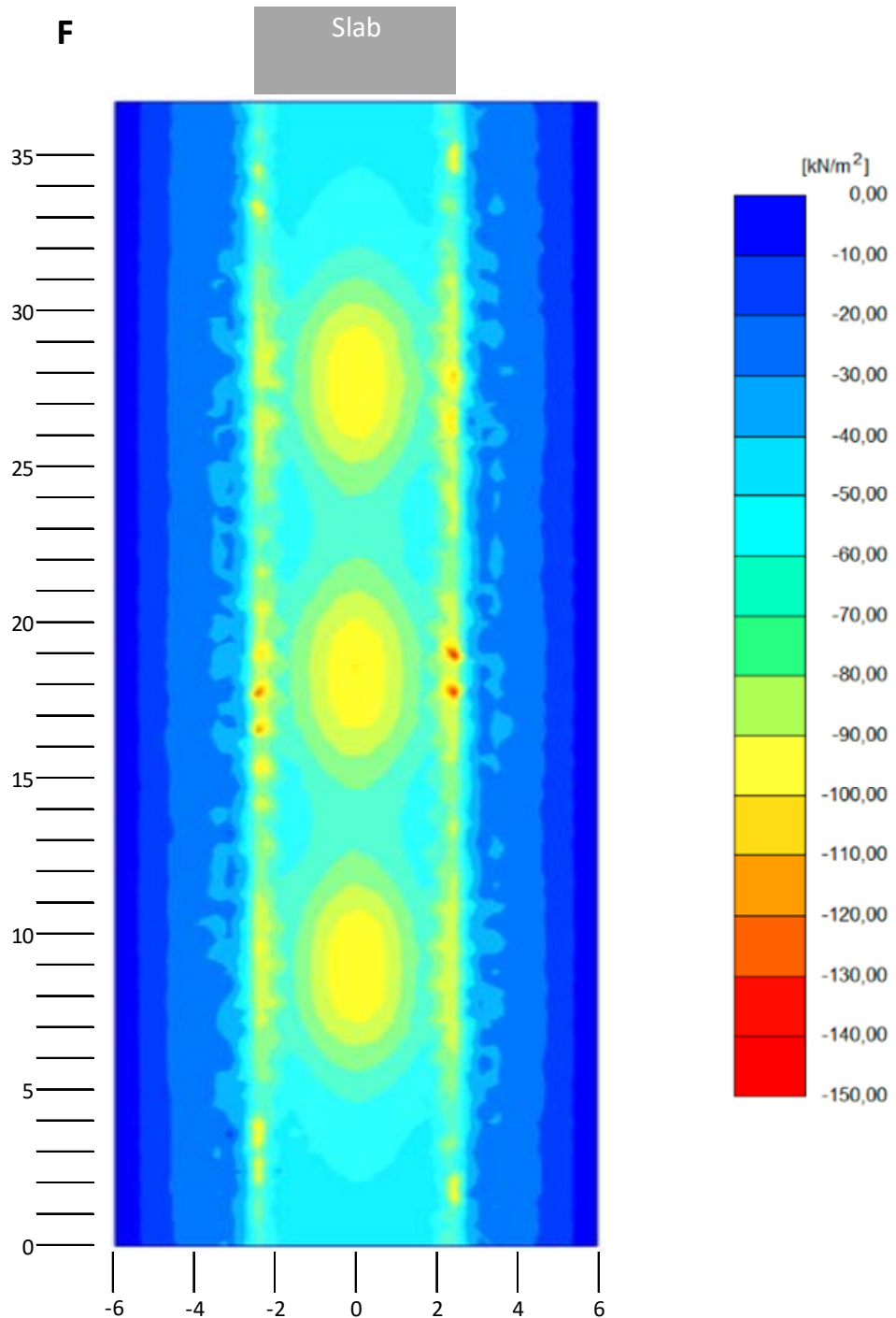


Figure 19. Total vertical stress distributions on a plane on top of the slab structure, slab installation depth 2.5 meters, load model F (LM-GEO) including dynamic load factor 1.25.

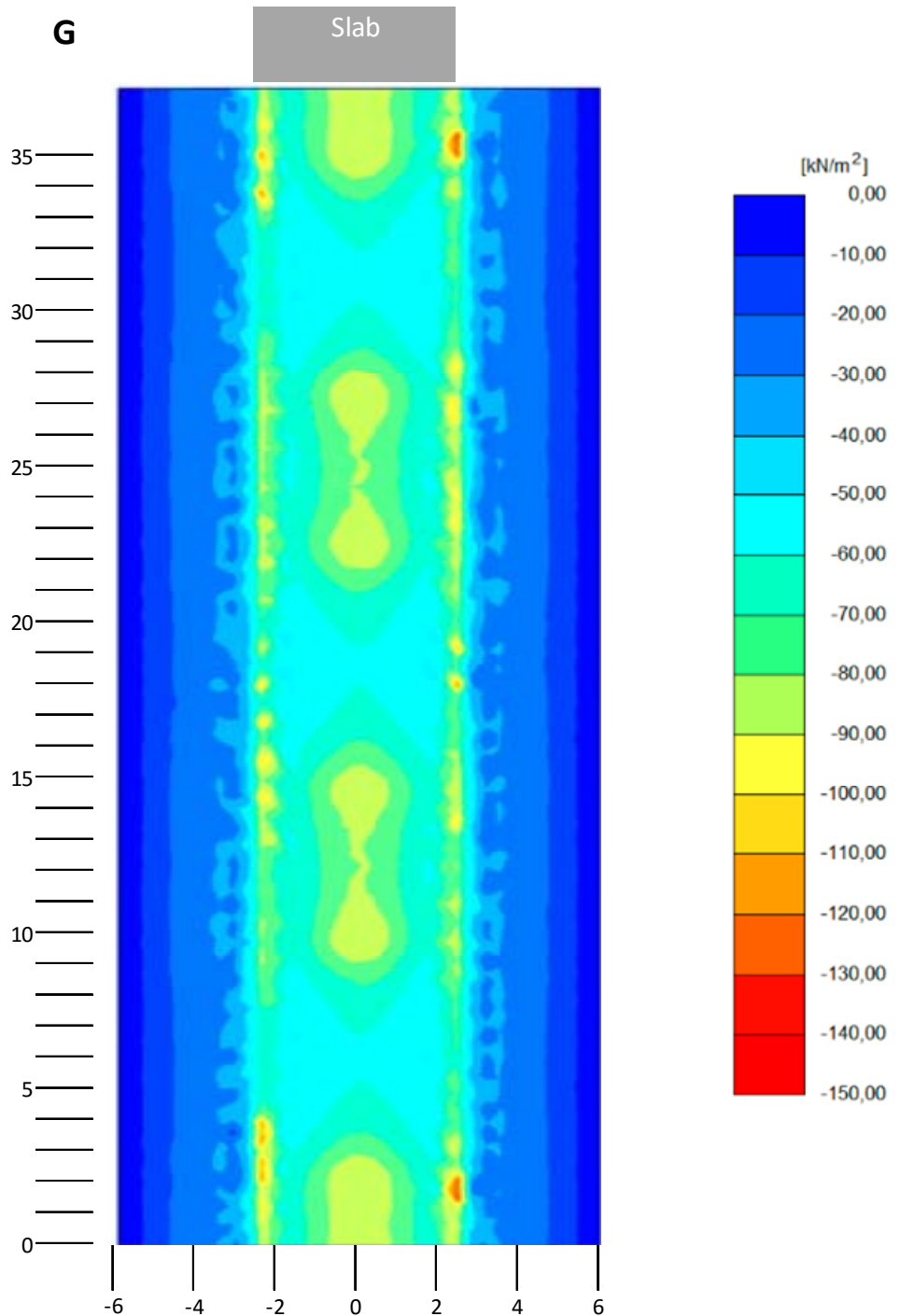


Figure 20. Total vertical stress distributions on a plane on top of the slab structure, slab installation depth 2.5 meters, load model G (E4) including dynamic load factor 1.25.

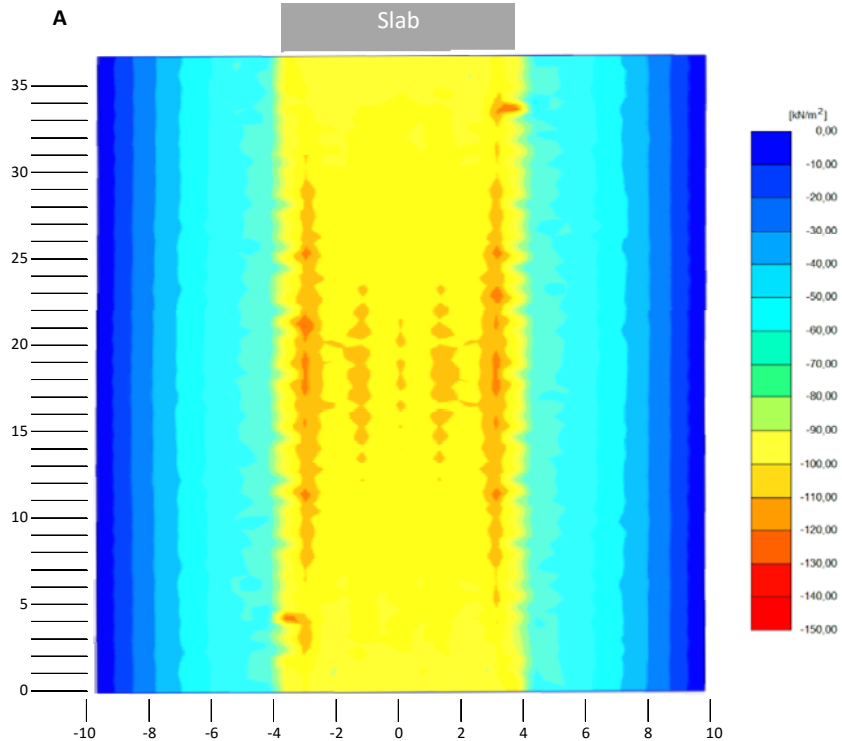


Figure 21. Total vertical stress distributions on a plane on top of the slab structure, slab installation depth 5 meters, load model A (LM71) including dynamic load factor 1.25.

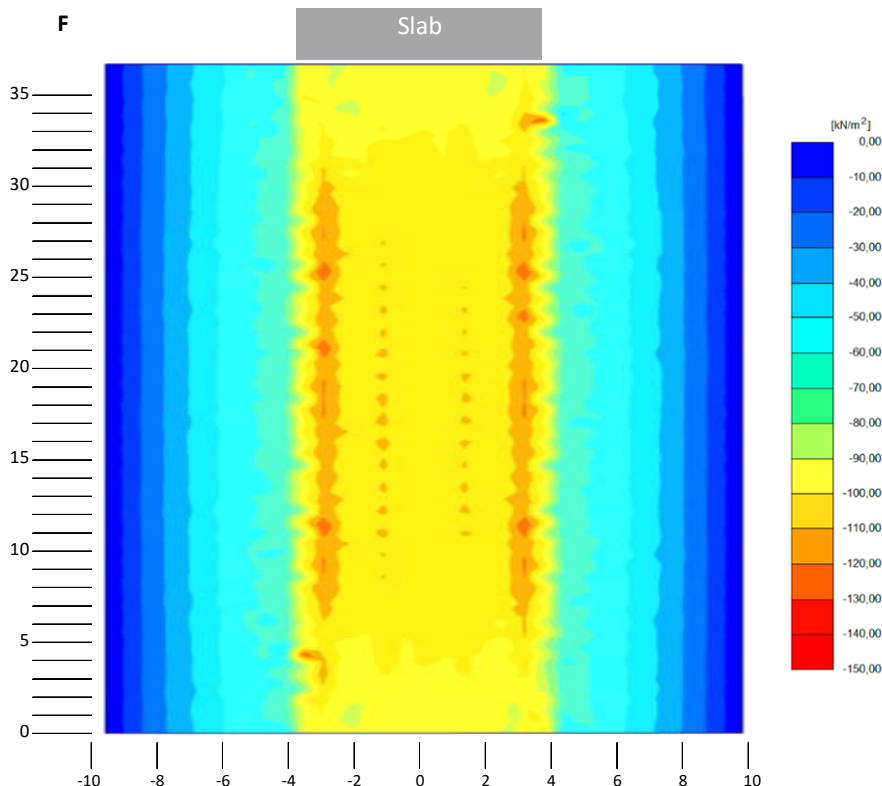


Figure 22. Total vertical stress distributions on a plane on top of the slab structure, slab installation depth 5 meters, load model F (LM-GEO) including dynamic load factor 1.25.

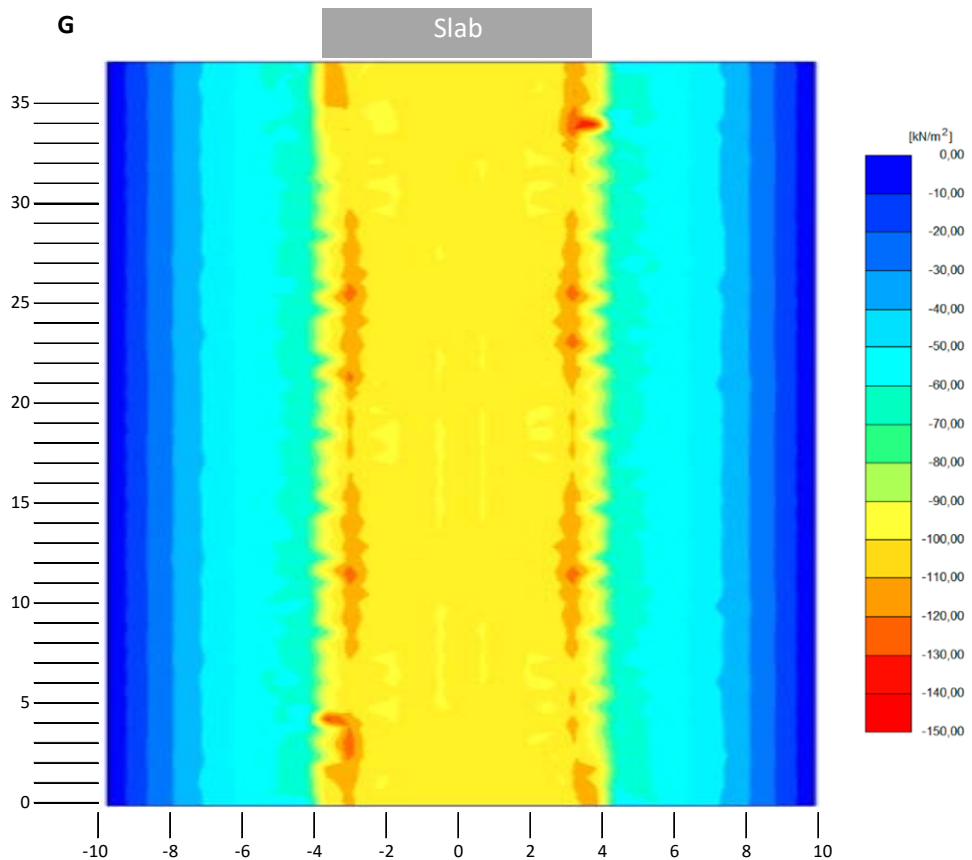


Figure 23. Total vertical stress distributions on a plane on top of the slab structure, slab installation depth 5 meters, load model G (E4) including dynamic load factor 1.25.

4.4 Total traffic load on the slab

The most significant consideration of dimensioning of a pile supported embankment slab is the total load accumulating to the slab structure. The total load of the slab structures were defined with help of the stress distribution planes. First, all the stress points of the model that were geometrically in the slab area were defined. Then the effective vertical stresses were aggregated at both the loaded and unloaded stage. Finally, the total load of the slab structured was calculated with help of slab area and number of stress points over that area. The total vertical loads are shown in tables 5 and 6. The corresponding total longitudinal loads are presented in tables 7 and 8. Although the horizontal load effects due to traction or breaking of the train have a significant effect on the railway structure, the analysis of these forces have not been included in this study.

Table 5. Total vertical loads on the slab structure, characteristic load.

Slab installation depth 1.4 meters				Characteristic load	
Load model	Number of stress points	Area of the slab (m ²)	Stress points/slab m ²	Sum of effective stresses at stress points	Total load (kN)
A (LM71)	12972	143,754	90,237	254632,9	2822
F (LM-GEO)	12972	143,754	90,237	256891,5	2847
G (E4)	12972	143,754	90,237	249661,4	2767
Slab installation depth 2.5 meters				Characteristic load	
Load model	Number of stress points	Area of the slab (m ²)	Stress points/slab m ²	Sum of effective stresses at stress points	Total load (kN)
A (LM71)	16218	180,614	89,794	223550,9	2490
F (LM-GEO)	16218	180,614	89,794	222035,9	2473
G (E4)	16218	180,614	89,794	225670,8	2513
Slab installation depth 5 meters				Characteristic load	
Load model	Number of stress points	Area of the slab (m ²)	Stress points/slab m ²	Sum of effective stresses at stress points	Total load (kN)
A (LM71)	6584	272,764	24,13808	51852,8	2148
F (LM-GEO)	6584	272,764	24,13808	50286,2	2083
G (E4)	6584	272,764	24,13808	51930,3	2151

Table 6. Total vertical loads on the slab structure, including dynamic load factor 1.25.

Slab installation depth 1.4 meters				Dynamic load factor	
Load model	Number of stress points	Area of the slab (m ²)	Stress points/slab m ²	Sum of effective stresses at stress points	Total load (kN)
A (LM71)	12972	143,754	90,237	318154,7	3526
F (LM-GEO)	12972	143,754	90,237	321420,4	3562
G (E4)	12972	143,754	90,237	311991,1	3457
Slab installation depth 2.5 meters				Dynamic load factor	
Load model	Number of stress points	Area of the slab (m ²)	Stress points/slab m ²	Sum of effective stresses at stress points	Total load (kN)
A (LM71)	16218	180,614	89,794	281188,5	3131
F (LM-GEO)	16218	180,614	89,794	282421,9	3145
G (E4)	16218	180,614	89,794	282702,6	3148

Slab installation depth 5 meters				Dynamic load factor	
Load model	Number of stress points	Area of the slab (m ²)	Stress points/slab m ²	Sum of effective stresses at stress points	Total load (kN)
A (LM71)	6584	272,764	24,138083	64477,9	2671
F (LM-GEO)	6584	272,764	24,138083	62439,1	2587
G (E4)	6584	272,764	24,138083	64517,5	2673

Table 7. Total longitudinal loads on the slab structure, characteristic load.

Slab installation depth 1.4 meters				Characteristic load	
Load model	Number of stress points	Area of the slab (m ²)	Stress points/slab m ²	Sum of effective stresses at stress points	Total load (kN)
A (LM71)	12972	143,754	90,237	-5023,9	-56
F (LM-GEO)	12972	143,754	90,237	-6381,7	-71
G (E4)	12972	143,754	90,237	-3957,4	-44
Slab installation depth 2.5 meters				Characteristic load	
Load model	Number of stress points	Area of the slab (m ²)	Stress points/slab m ²	Sum of effective stresses at stress points	Total load (kN)
A (LM71)	16218	180,614	89,794	20311,1	226
F (LM-GEO)	16218	180,614	89,794	20071,9	224
G (E4)	16218	180,614	89,794	20207,9	225
Slab installation depth 5 meters				Characteristic load	
Load model	Number of stress points	Area of the slab (m ²)	Stress points/slab m ²	Sum of effective stresses at stress points	Total load (kN)
A (LM71)	6584	272,764	24,138	10198,6	423
F (LM-GEO)	6584	272,764	24,138	10696,3	443
G (E4)	6584	272,764	24,138	10985,4	455

Table 8. Total longitudinal loads on the slab structure, including dynamic load factor 1.25.

Slab installation depth 1.4 meters				Dynamic load factor	
Load model	Number of stress points	Area of the slab (m ²)	Stress points/slab m ²	Sum of effective stresses at stress points	Total load (kN)
A (LM71)	12972	143,754	90,237	-6841,5	-76
F (LM-GEO)	12972	143,754	90,237	-9719,5	-108
G (E4)	12972	143,754	90,237	-6020,1	-67

Slab installation depth 2.5 meters				Dynamic load factor	
Load model	Number of stress points	Area of the slab (m ²)	Stress points/slab m ²	Sum of effective stresses at stress points	Total load (kN)
A (LM71)	16218	180,614	89,794	22560,2	251
F (LM-GEO)	16218	180,614	89,794	22670,8	252
G (E4)	16218	180,614	89,794	24396,5	272
Slab installation depth 5 meters				Dynamic load factor	
Load model	Number of stress points	Area of the slab (m ²)	Stress points/slab m ²	Sum of effective stresses at stress points	Total load (kN)
A (LM71)	6584	272,764	24,138	12965,2	537
F (LM-GEO)	6584	272,764	24,138	13555,8	562
G (E4)	6584	272,764	24,138	13931,8	577

The obtained results in tables 5 and 6 indicate that there is no significant differences between the studied load models. In practice, when the observed or dimensioned area is long enough, the total load does not vary despite the load model. If the effects of different load models are examined at shorter sections, different load models produce different results. A slab wide, 9.45 meters long sections of the slab was also studied. The results are presented in tables 9 and 10. The section of 9.45 meters was chosen since it is the distance of two consecutive bogies in load model G (E4). Based on the results obtained, the load model A (LM71) gives the most intensive total load on the slab structure when the observed section is shorter whereas the load model G (E4) produces the lowest values.

Table 9. Total vertical loads on the slab structure at most intensively loaded 9.45 meters section, characteristic load

Slab installation depth 1.4 meters				Characteristic load	
Load model	Number of stress points	Area of the slab (m ²)	Stress points/slab m ²	Sum of effective stresses at stress points	Total load (kN)
A (LM71)	3444	36,855	93,447	107562,5	1151
F (LM-GEO)	3444	36,855	93,447	86277,1	923
G (E4)	3367	36,855	91,358	81867,9	896
Slab installation depth 2.5 meters				Characteristic load	
Load model	Number of stress points	Area of the slab (m ²)	Stress points/slab m ²	Sum of effective stresses at stress points	Total load (kN)
A (LM71)	4162	46,305	89,882	89468,4	995
F (LM-GEO)	4162	46,305	89,882	72880,9	811
G (E4)	4112	46,305	88,803	64675,8	728

Slab installation depth 5 meters				Characteristic load	
Load model	Number of stress points	Area of the slab (m ²)	Stress points/slab m ²	Sum of effective stresses at stress points	Total load (kN)
A (LM71)	1699	69,93	24,295724	18921,7	779
F (LM-GEO)	1699	69,93	24,295724	16403,7	675
G (E4)	1682	69,93	24,052624	12971,2	539

Table 10. Total vertical loads on the slab structure at most intensively loaded 9.45 meters section including dynamic load factor 1.25.

Slab installation depth 1.4 meters				Dynamic load factor	
Load model	Number of stress points	Area of the slab (m ²)	Stress points/slab m ²	Sum of effective stresses at stress points	Total load (kN)
A (LM71)	3444	36,855	93,447	134494,4	1439
F (LM-GEO)	3444	36,855	93,447	107966,6	1155
G (E4)	3367	36,855	91,358	102463,1	1122
Slab installation depth 2.5 meters				Dynamic load factor	
Load model	Number of stress points	Area of the slab (m ²)	Stress points/slab m ²	Sum of effective stresses at stress points	Total load (kN)
A (LM71)	4162	46,305	89,882	112373,8	1250
F (LM-GEO)	4162	46,305	89,882	91657,9	1020
G (E4)	4112	46,305	88,803	81247,9	915
Slab installation depth 5 meters				Dynamic load factor	
Load model	Number of stress points	Area of the slab (m ²)	Stress points/slab m ²	Sum of effective stresses at stress points	Total load (kN)
A (LM71)	1699	69,93	24,295724	23529,9	968
F (LM-GEO)	1699	69,93	24,295724	20466,4	842
G (E4)	1682	69,93	24,052624	16010,6	666

The results observed at a 9.45 meters section clearly indicate that from dimensioning point of view, the desired load model affects to the structural dimensioning. Therefore the most intensively loaded area was yet reduced to an area a single pile supports. A commonly used pile spacing in Finland is 2.5 meters. Technically, one pile supports an area of 6.25 m². It should be noted, that from structural perspective the effects of adjacent piles are to be perceived. In this study the most intensively loaded 6.25 m² was defined and a theoretical maximum traffic load directing to one pile support area was calculated. The results are shown in tables 11 and 12. Based on the obtained results, load model A and F produce quite similar maximum load to one pile. This is comprehensible since regardless the type of loading (point or line load), the

accumulated total load is similar at a 6.4 meters section. Load model G, instead, produces roughly half of the load on a single pile compared to A and F.

Table 11. Total vertical loads on the slab structure at support area of a single pile, characteristic load.

Slab installation depth 1.4 meters				Characteristic load	
Load model	Number of stress points	Area of the slab (m ²)	Stress points/slab m ²	Sum of effective stresses at stress points	Total load (kN)
A (LM71)	180	6,25	28,800	8434,4	293
F (LM-GEO)	180	6,25	28,800	8449,8	293
G (E4)	160	6,25	25,600	5222,9	204
Slab installation depth 2.5 meters				Characteristic load	
Load model	Number of stress points	Area of the slab (m ²)	Stress points/slab m ²	Sum of effective stresses at stress points	Total load (kN)
A (LM71)	172	6,25	27,520	5975,7	217
F (LM-GEO)	172	6,25	27,520	5644,4	205
G (E4)	160	6,25	25,600	3212,1	125
Slab installation depth 5 meters				Characteristic load	
Load model	Number of stress points	Area of the slab (m ²)	Stress points/slab m ²	Sum of effective stresses at stress points	Total load (kN)
A (LM71)	78	6,25	12,48	805,5	65
F (LM-GEO)	78	6,25	12,48	648,7	52
G (E4)	64	6,25	10,24	347,8	34

Table 12. Total vertical loads on the slab structure at support area of a single pile including dynamic load factor 1.25.

Slab installation depth 1.4 meters				Dynamic load factor	
Load model	Number of stress points	Area of the slab (m ²)	Stress points/slab m ²	Sum of effective stresses at stress points	Total load (kN)
A (LM71)	180	6,25	28,800	10661,7	370
F (LM-GEO)	180	6,25	28,800	10712,5	372
G (E4)	160	6,25	25,600	6635,5	259

Slab installation depth 2.5 meters				Dynamic load factor	
Load model	Number of stress points	Area of the slab (m ²)	Stress points/slab m ²	Sum of effective stresses at stress points	Total load (kN)
A (LM71)	172	6,25	27,520	7633,1	277
F (LM-GEO)	172	6,25	27,520	7278,9	264
G (E4)	160	6,25	25,600	4077,2	159
Slab installation depth 5 meters				Dynamic load factor	
Load model	Number of stress points	Area of the slab (m ²)	Stress points/slab m ²	Sum of effective stresses at stress points	Total load (kN)
A (LM71)	78	6,25	12,48	938,1	75
F (LM-GEO)	78	6,25	12,48	761,1	61
G (E4)	64	6,25	10,24	406,4	40

5 Conclusions

The aim of the study was to compare the effects that varying load models produce on the vertical stress levels of a railway structure. The main issue was to study the effects on the induced vertical stress level on top of pile supported embankment slab. Seven different load models and three different slab installation depths were simulated totaling 21 simulations. The load models used in this project were the currently used dimensioning model LM71 (EN 1991-2) and E4 (EN 15528). In addition, altogether five derivatives of load model LM71 were used.

The 3D FEM simulation model used in this project has been developed in previous studies for bearing capacity analysis purposes but was assessed suitable for this study since the main issue to solve was the stress level at the base of a railway embankment. The model results were also evaluated with help of field data. Based on the correlations between modeled and measured results the model provides a credible stress-strain relationship.

Load model LM71 seems to produce the highest stresses in the most intensively loaded areas. The effect is observable when the installation depth of a pile supported embankment slab is less than 5 meters but seems to vanish as the installation depth increases.

The differences between load models seem to contract as the examined section lengthens. The total traffic loads at the observed maximum section were close to each other. On the other hand, load model A (LM71) results as the highest local load effects due to a combination of point loads and line loads and their sequence. Load model F (LM-GEO) seems to produce similar total stress levels than load model A (LM71) but local stresses are smaller due to discontinuous load model. Furthermore, the point load groups of load model A (LM71) could be replaced with line load groups of load model F (LM-GEO) in case of dimensioning of buried structures, especially in cases the depth of buried structure is at least 1.4 meters. Load model G (E4) provides an interesting result. Though the total load throughout the slab structure is similar to other load models, the maximum traffic load is roughly 30...40 percent lower compared to other load models produce to a single pile.

The stress distributions inside the embankment structure were partly surprising. The stiff slab base appears to concentrate the vertical stresses to middle parts of the embankment whereas on more flexible base the stresses distribute at cross sectional direction. Similar results were observed in a project modelling the slab structures under road embankments (Andersson-Berlin 2017).

Though the aim of this study was to evaluate the vertical stress levels exposing to the slab structures, longitudinal stresses were also glimpsed. The results were quite complicated to interpret. The development of longitudinal and cross-sectional stresses need to be further investigated in other studies.

References

- Andersson-Berlin, K. (2017). Tieliikennetrien aiheuttamien jännitysten mallinnus. *In Finnish*. Helsinki 2017. Liikenneviraston tutkimuksia ja selvityksiä 14/2017. 36 p., 6 app.
- Bathe, K.J. (1982). Finite element analysis in engineering analysis. Prentice-Hall, New Jersey.
- Brinkreve, R.B.J., Engin, E & Swolfs, W.M. (2012). PLAXIS 3D 2012. User Manuals. Plaxis bv, The Netherlands.
- EN 1991-2. (2008) Eurocode 1. Actions on structures. Part 2: Traffic loads on bridges.
- EN 15528. (2008). Railway applications – Line categories for managing the interface between load limits of vehicles and infrastructure. 18p., 38 app.
- Indraratna, B., Salim, W. & Rujikiatkamjorn, C. (2011). Advanced Rail Geotechnology – Ballasted Track. CRC Press, The Netherlands. 414 p.
- Kallialainen, A., Kolisoja, P. & Nurmikolu, A. (2014). Radan 3D-rakennemalli ja ratarakenteen kuormituskestävyyys. *In Finnish*. Helsinki 2014. Liikenneviraston tutkimuksia ja selvityksiä 55/2014. 174 p.
- Kallialainen, A., Kolisoja, P. & Nurmikolu, A. (2016) 3D Finite element model as a tool for analyzing the structural behavior of a railway track. Publications of International Conference on Transportation Geotechnics (ICTG 2016). Guimaraes, Portugal 2016; 143:820-7.
- Kolisoja, P., Järvenpää, I. & Mäkelä, E. (2000). Instrumentation and Modelling of Track Structure, 250 kN and 300 kN Axle Loads. Helsinki 2000. Publications of Finnish Rail Administration A10/2000. 99p, 4 app. Available at:
http://www2.liikennevirasto.fi/julkaisut/pdf4/rhk_2000_a10.pdf
- Nemlander, R. (2015). Junan jarrukuorman välittymisen pengeraatalalle. *In Finnish*. Helsinki 2015. Liikenneviraston tutkimuksia ja selvityksiä 35/2015. 133p., 11 app.
- Nurmikolu, A. & Kolisoja, P. (2010). Sepelinpuhdistuksen vaikutukset raidesepelin ominaisuuksiin. *In Finnish*. Helsinki 2010. Liikenneviraston tutkimuksia ja selvityksiä 11/2010. 64 p., 3 app.
- Skoglund, K. A. (2002). A Study of Some Factors in Mechanistic Railway Track Design. Eng.D Thesis. Norwegian University of Science and Technology (NTNU), Faculty of Engineering and Technology. 160 p., 37 app.

Load intensities on top of the pile supported embankment slab

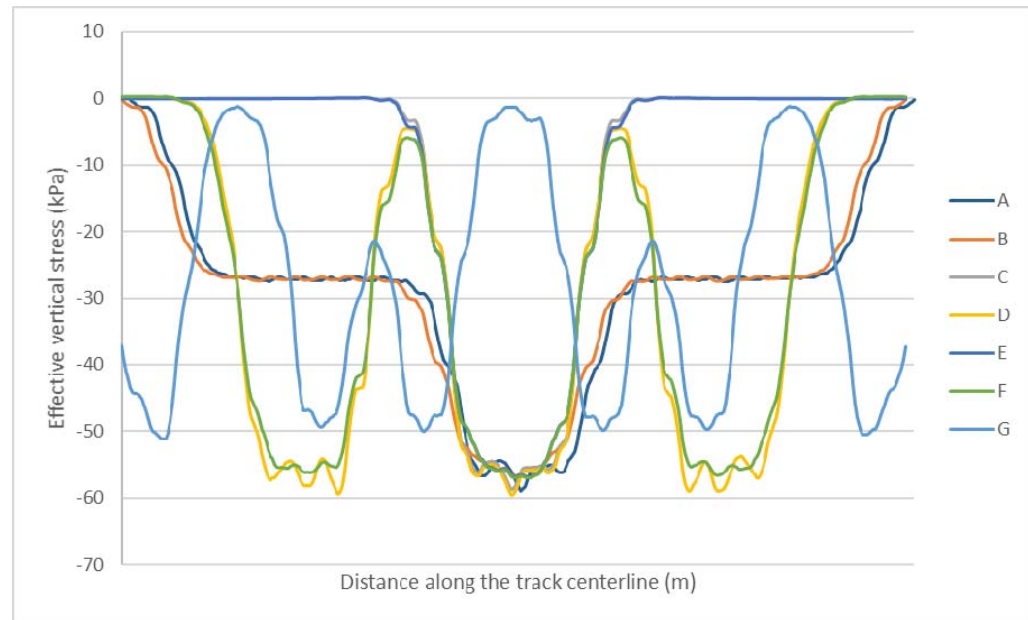


Figure 1. Load intensity, slab installation depth 1.4 meters, characteristic load.

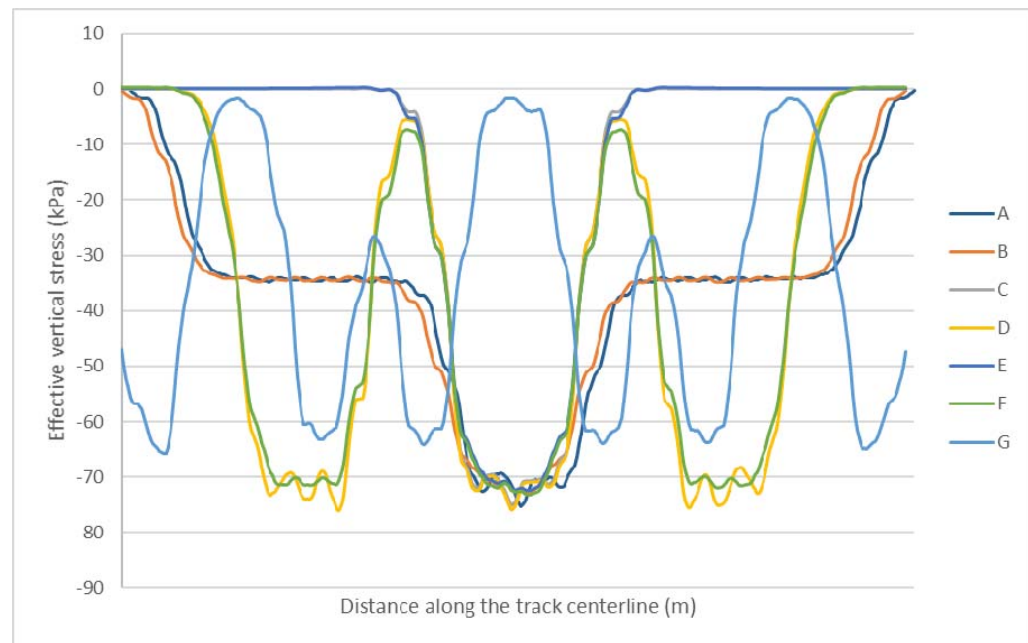


Figure 2. Load intensity, slab installation depth 1.4 meters including dynamic load factor 1.25.

Appendix A / 2 (3)

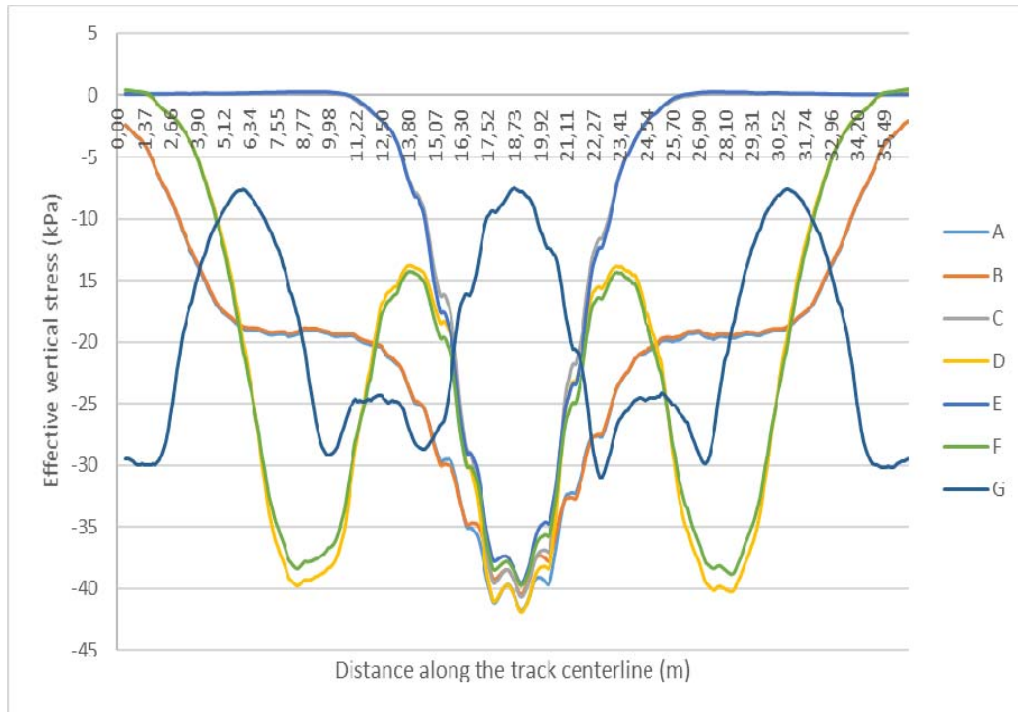


Figure 3. Load intensity, slab installation depth 2.5 meters, characteristic load.

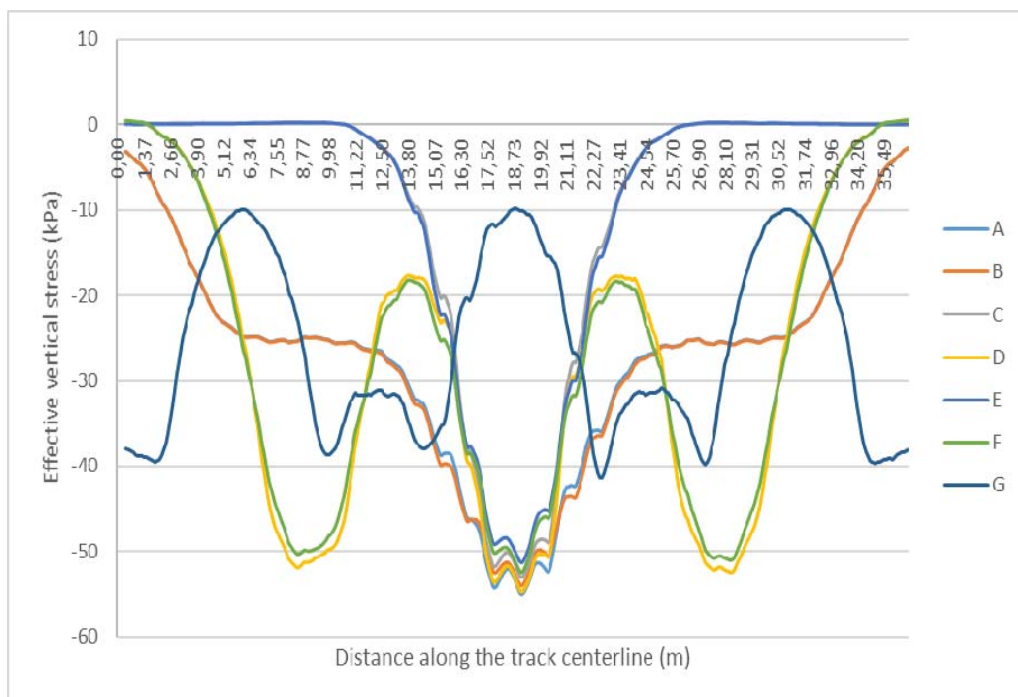


Figure 4. Load intensity, slab installation depth 2.5 meters including dynamic load factor 1.25.

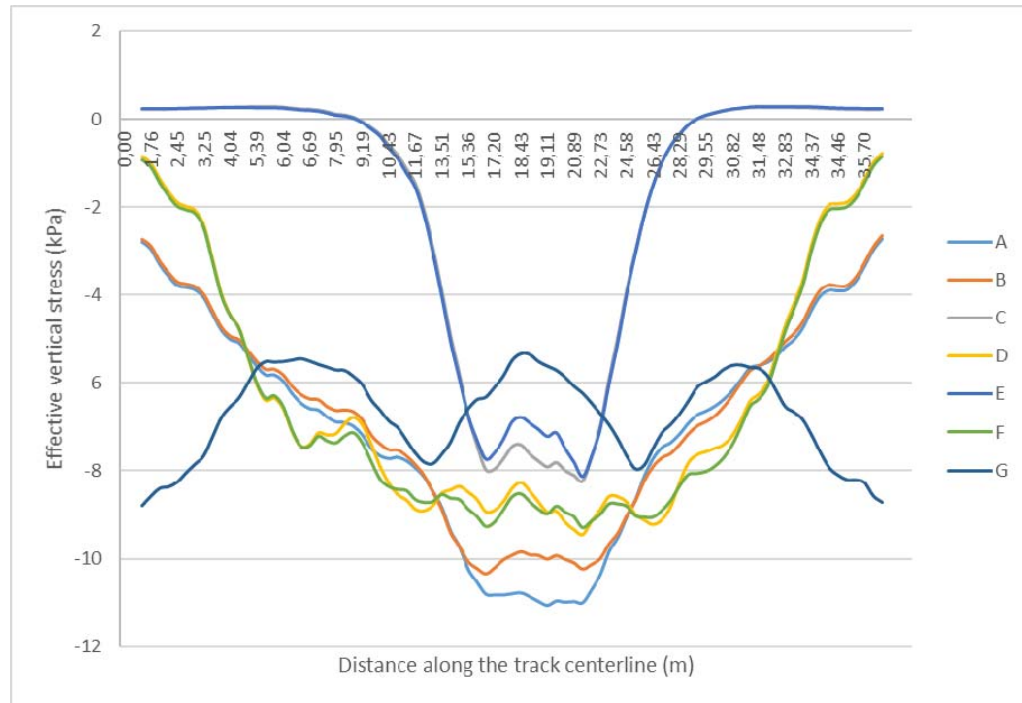


Figure 5. Load intensity, slab installation depth 5 meters, characteristic load.

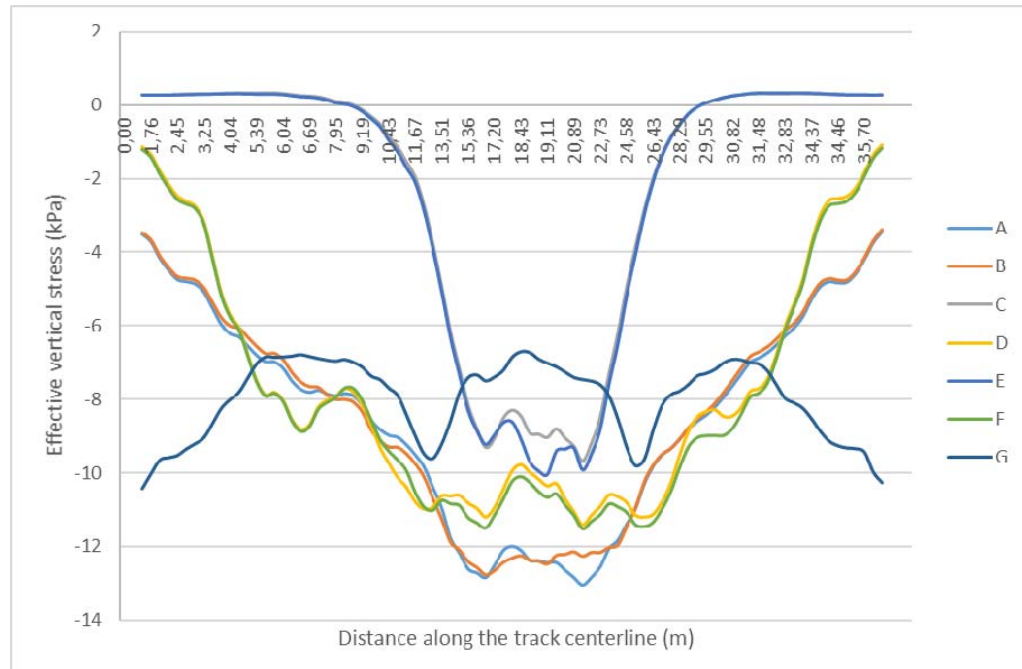


Figure 6. Load intensity, slab installation depth 5 meters including dynamic load factor 1.25.

Vertical stress distributions at cross-sections

Cross-sections at the point load or line load group area.

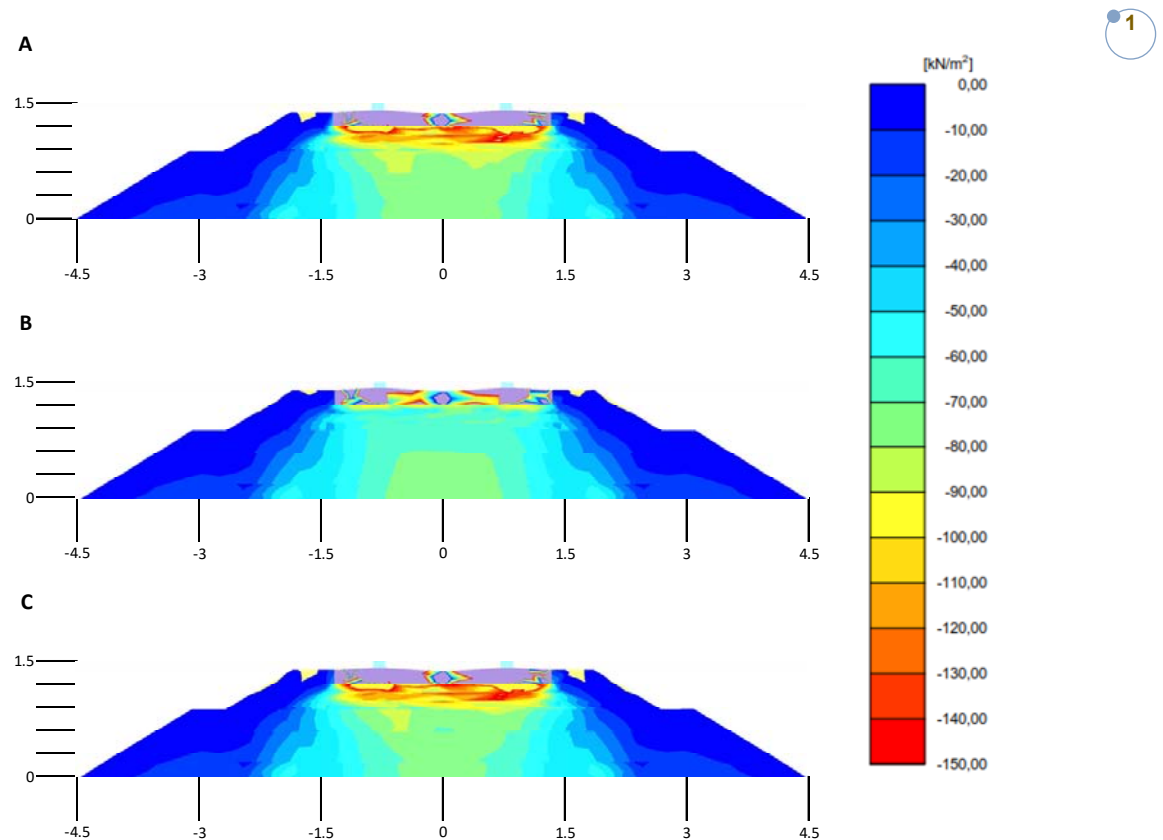


Figure 1. Total vertical stress distributions at cross-sections, load modes A to C, slab installation depth 1.4 meters, characteristic load.

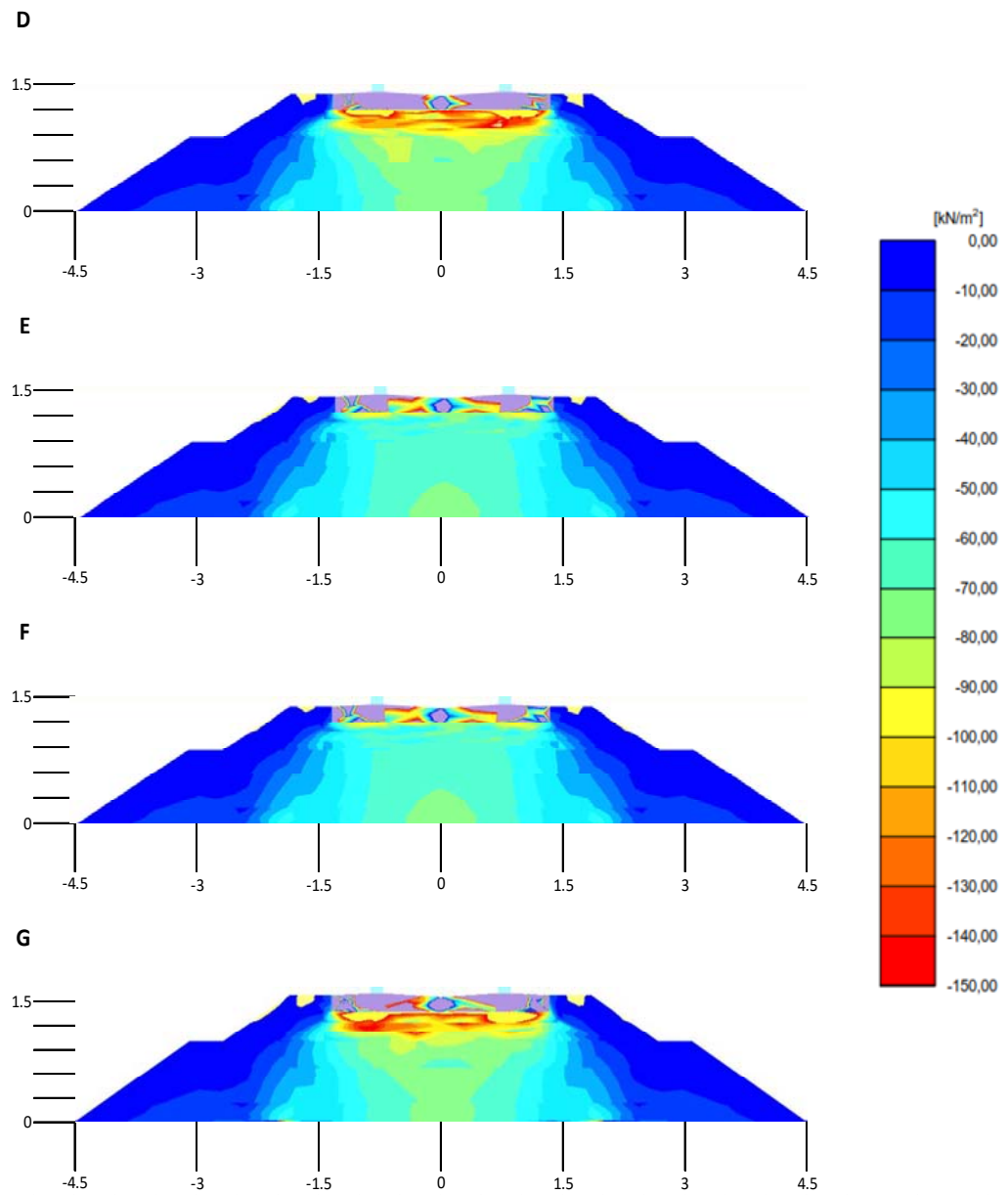


Figure 2. Total vertical stress distributions at cross-sections, load modes D to G, slab installation depth 1.4 meters, characteristic load.

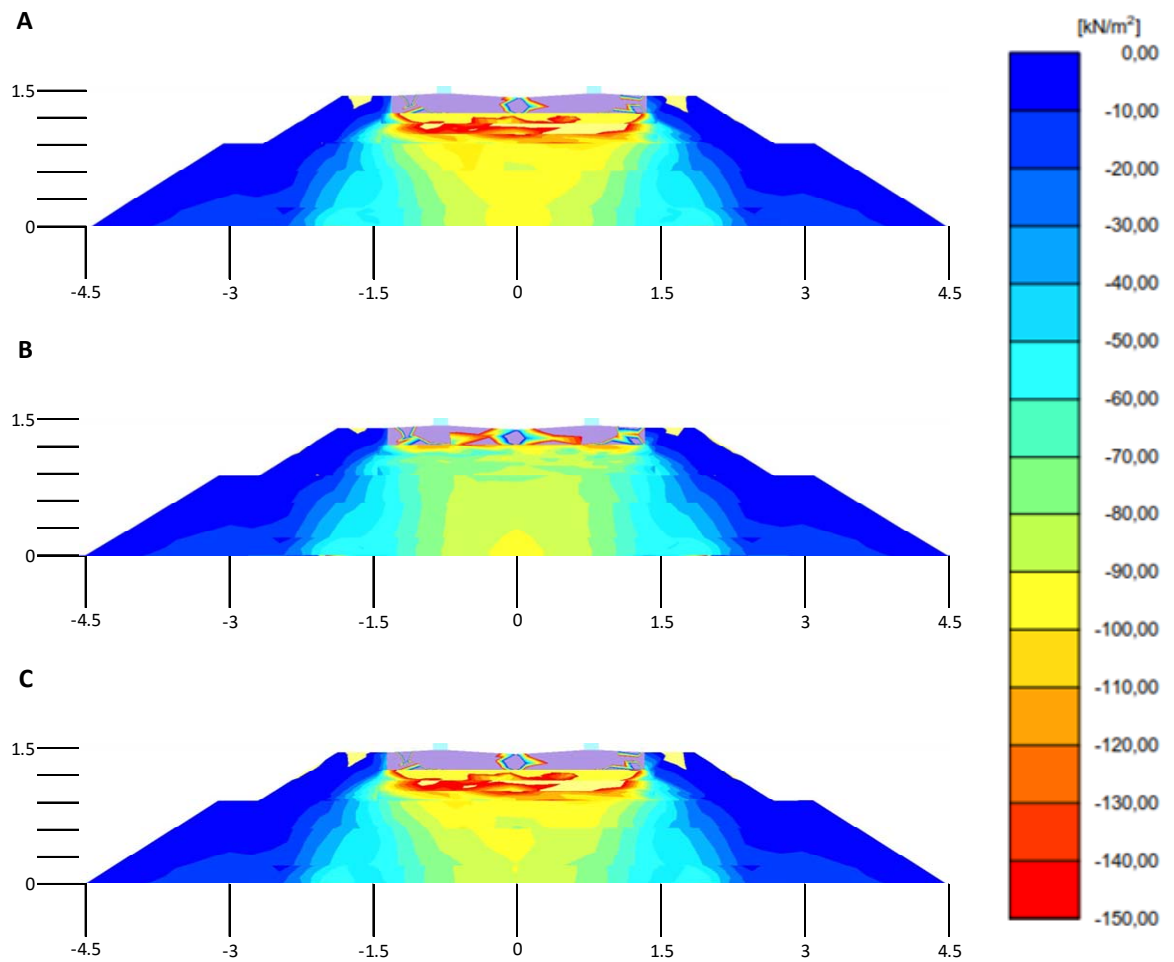


Figure 3. Total vertical stress distributions at cross-sections, load modes A to C, slab installation depth 1.4 meters, including dynamic load factor 1.25.

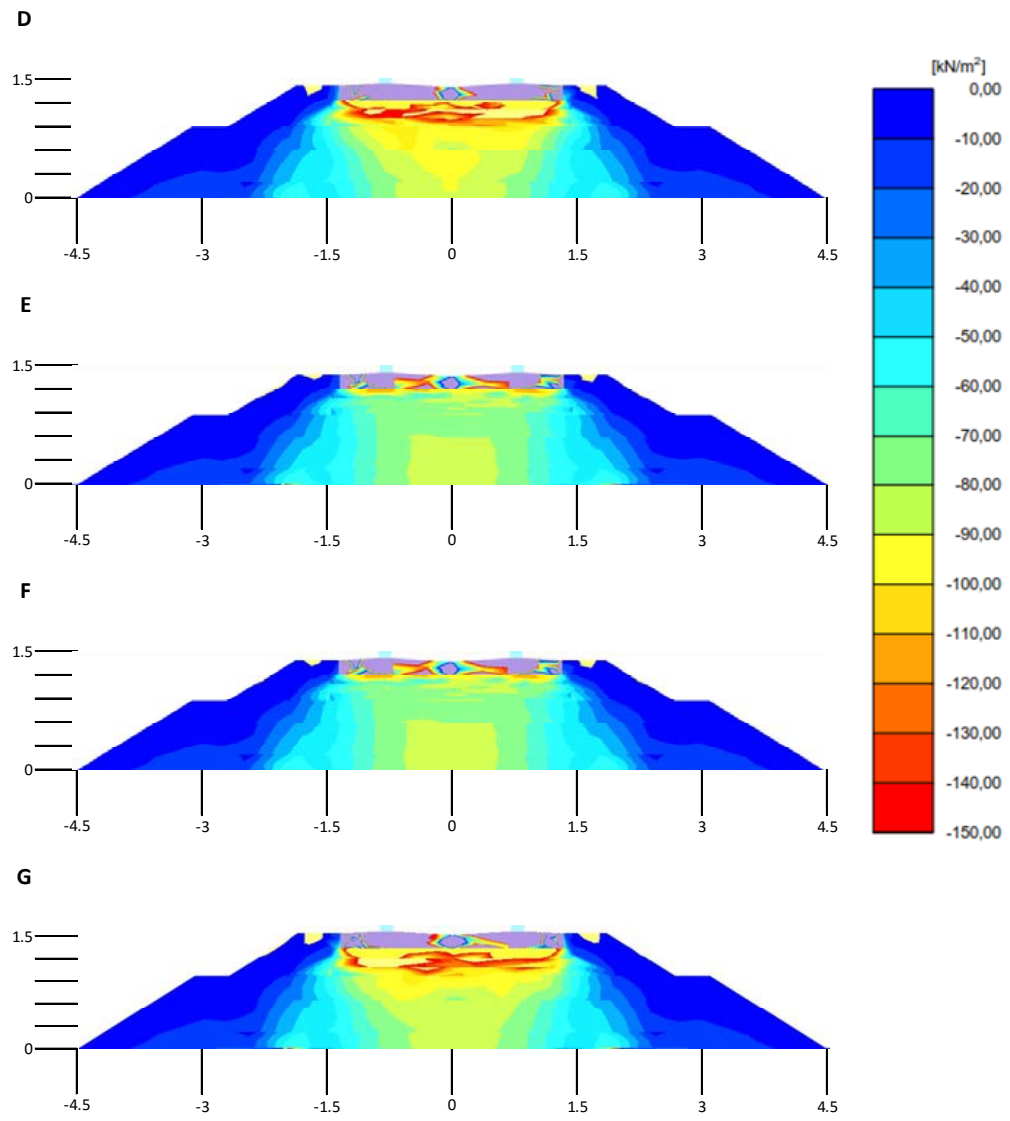


Figure 4. Total vertical stress distributions at cross-sections, load modes D to G, slab installation depth 1.4 meters, including dynamic load factor 1.25..

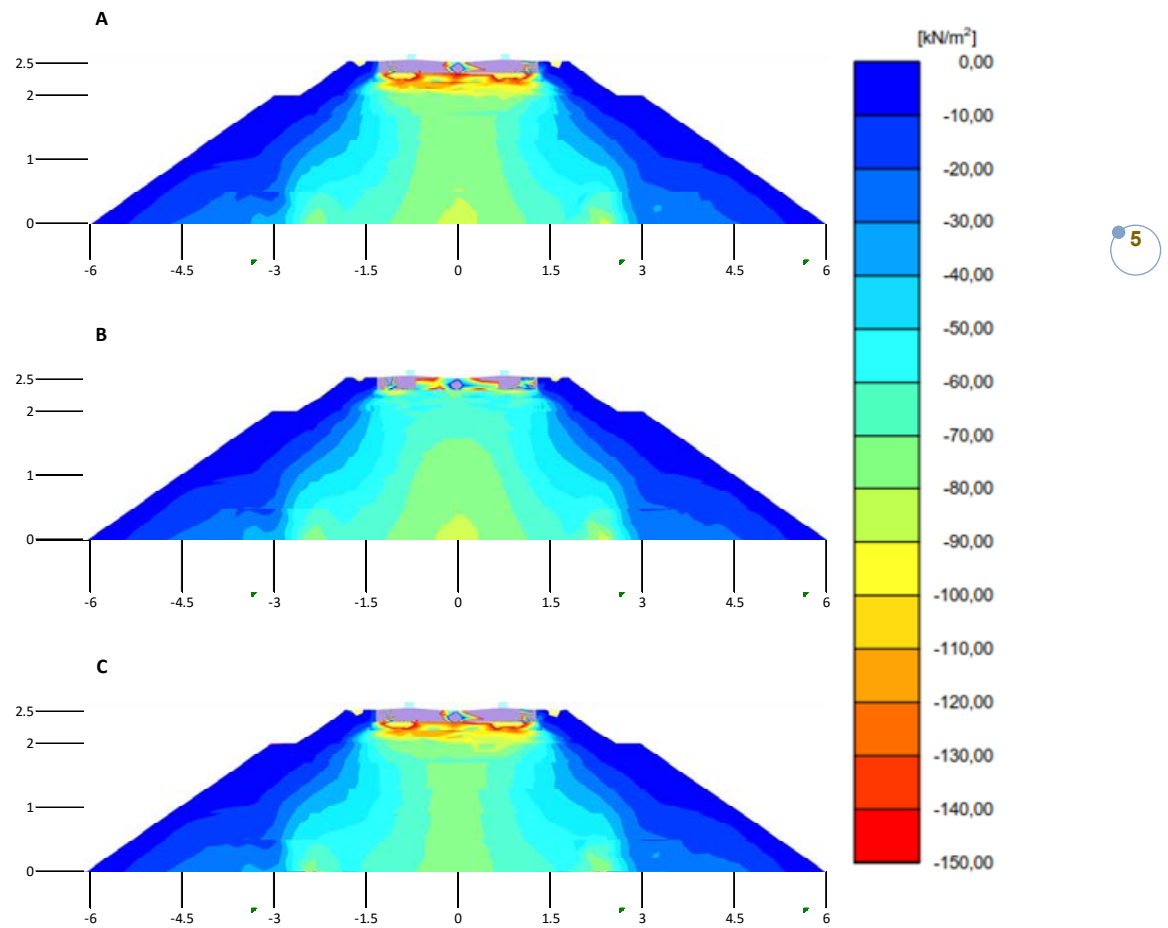


Figure 5. Total vertical stress distributions at cross-sections, load modes A to C, slab installation depth 2.5 meters, characteristic load.

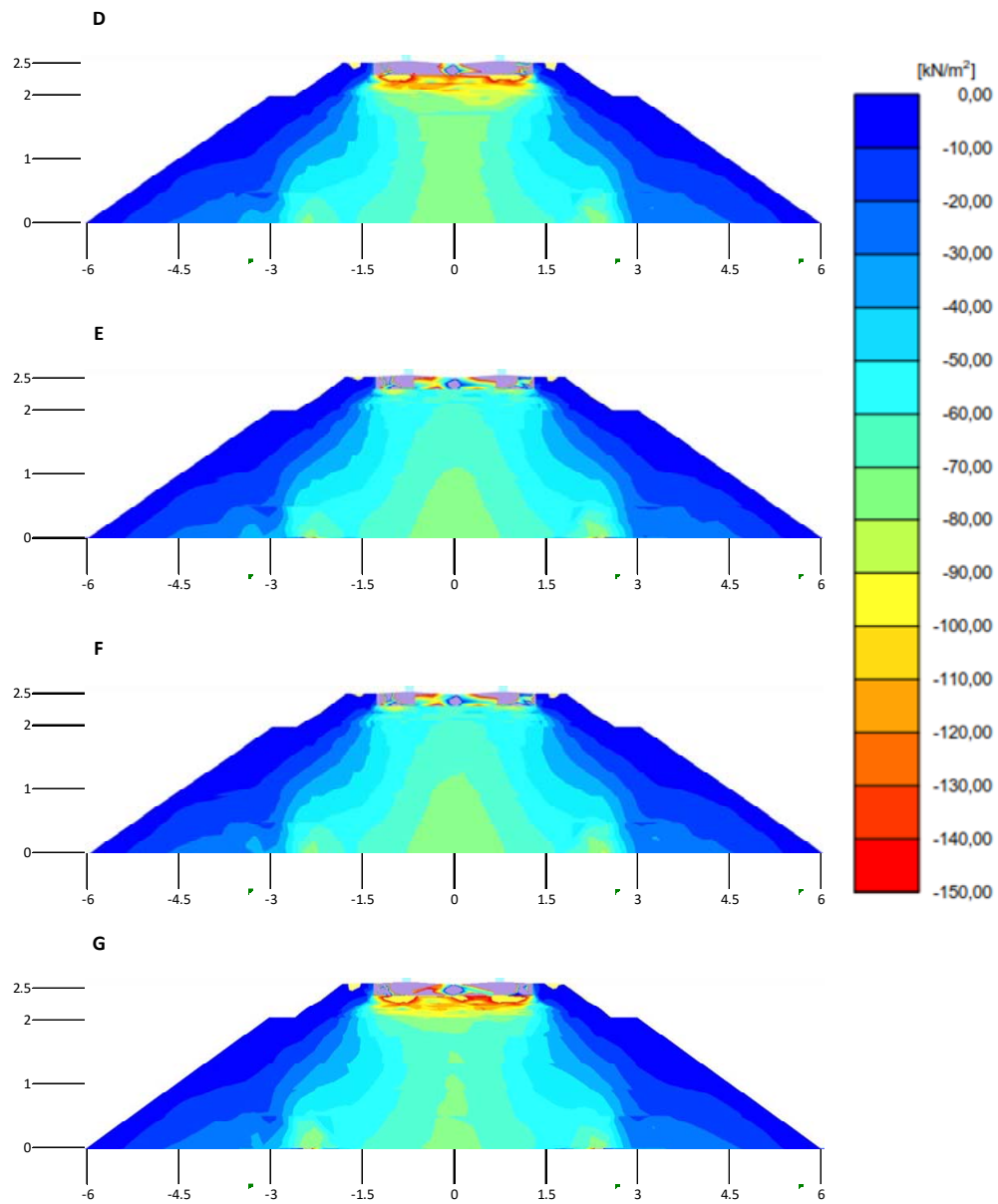


Figure 6. Total vertical stress distributions at cross-sections, load modes D to G, slab installation depth 2.5 meters, characteristic load.

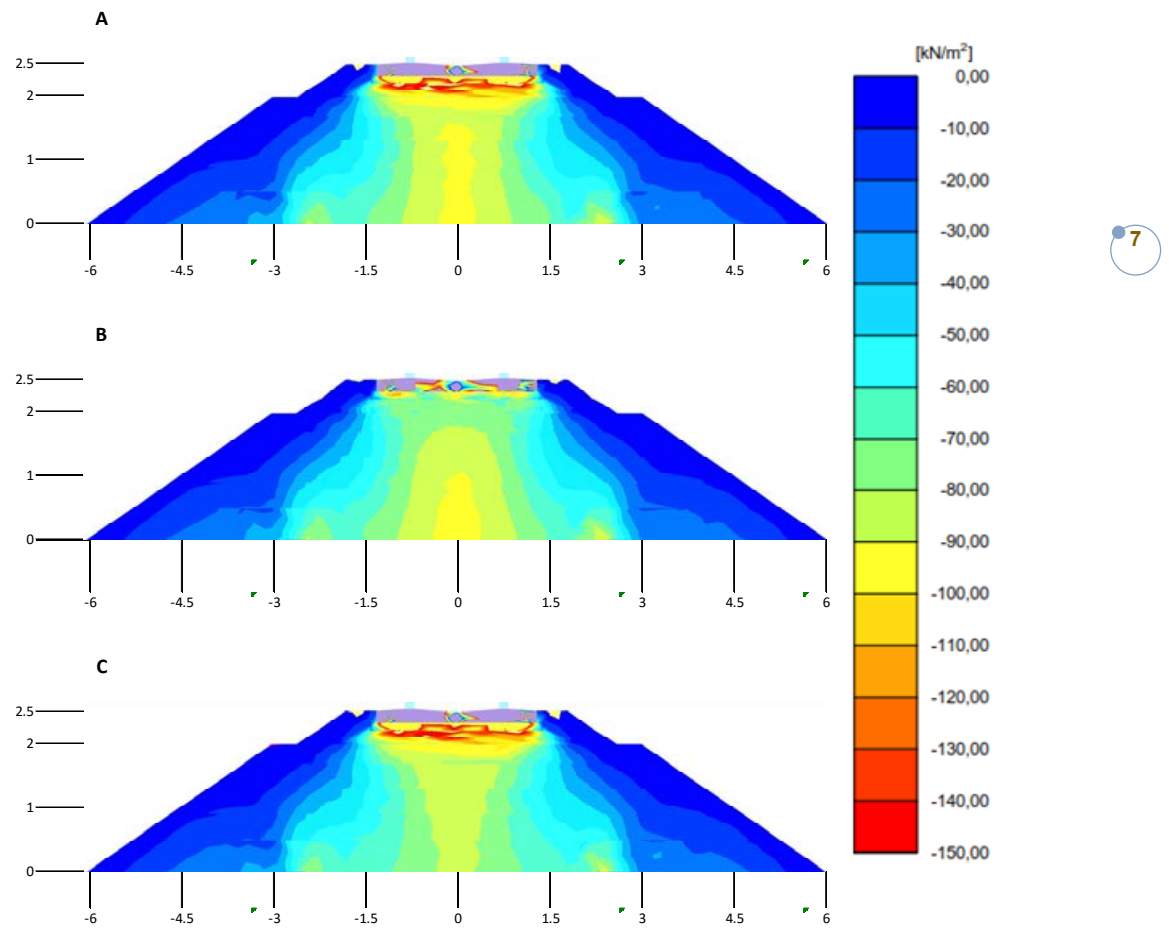


Figure 7. Total vertical stress distributions at cross-sections, load modes A to C, slab installation depth 2.5 meters, including dynamic load factor 1.25.

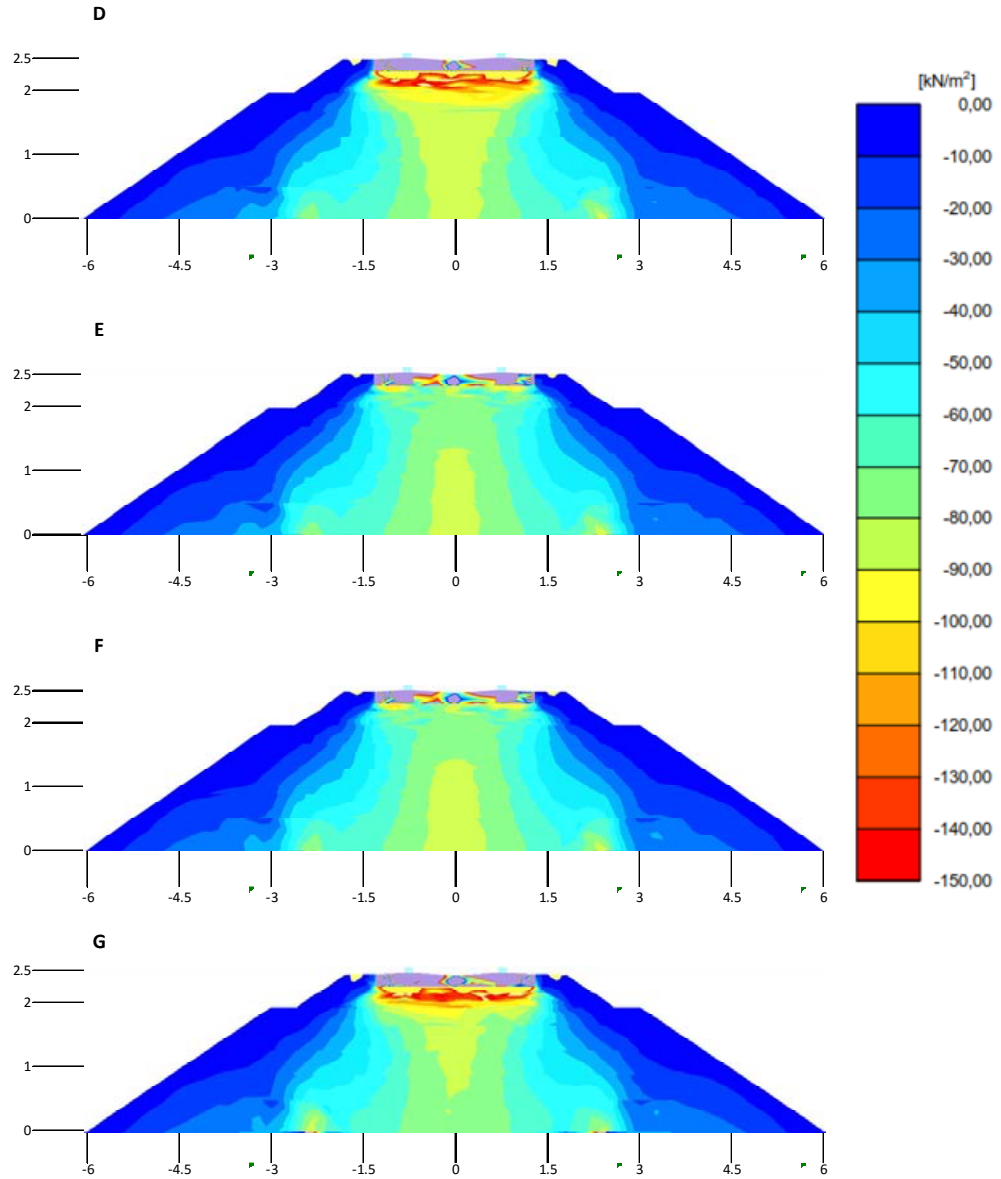


Figure 8. Total vertical stress distributions at cross-sections, load modes D to G, slab installation depth 2.5 meters, including dynamic load factor 1.25.

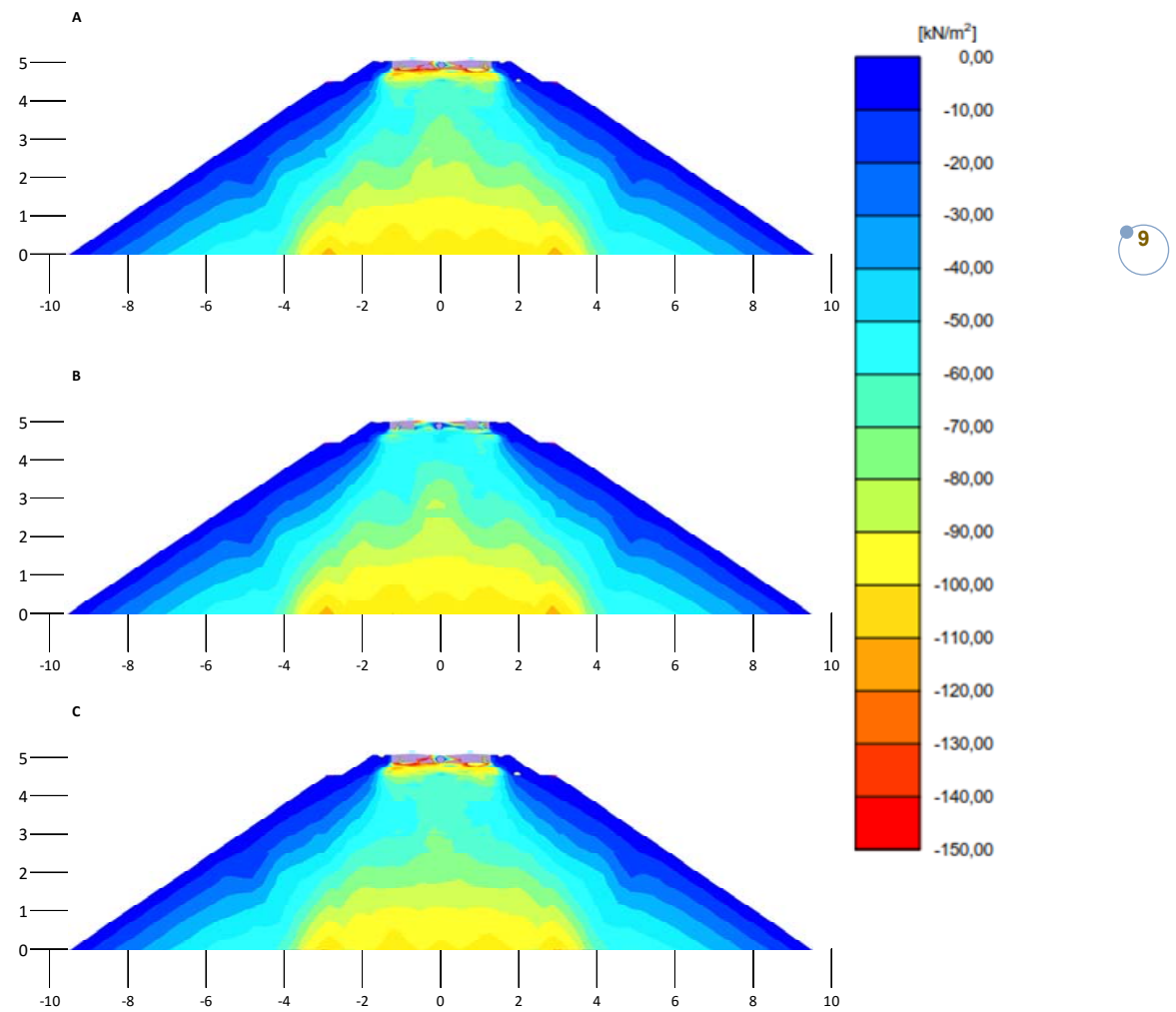


Figure 9. Total vertical stress distributions at cross-sections, load modes A to C, slab installation depth 5 meters, characteristic load.

Appendix B / 10 (12)

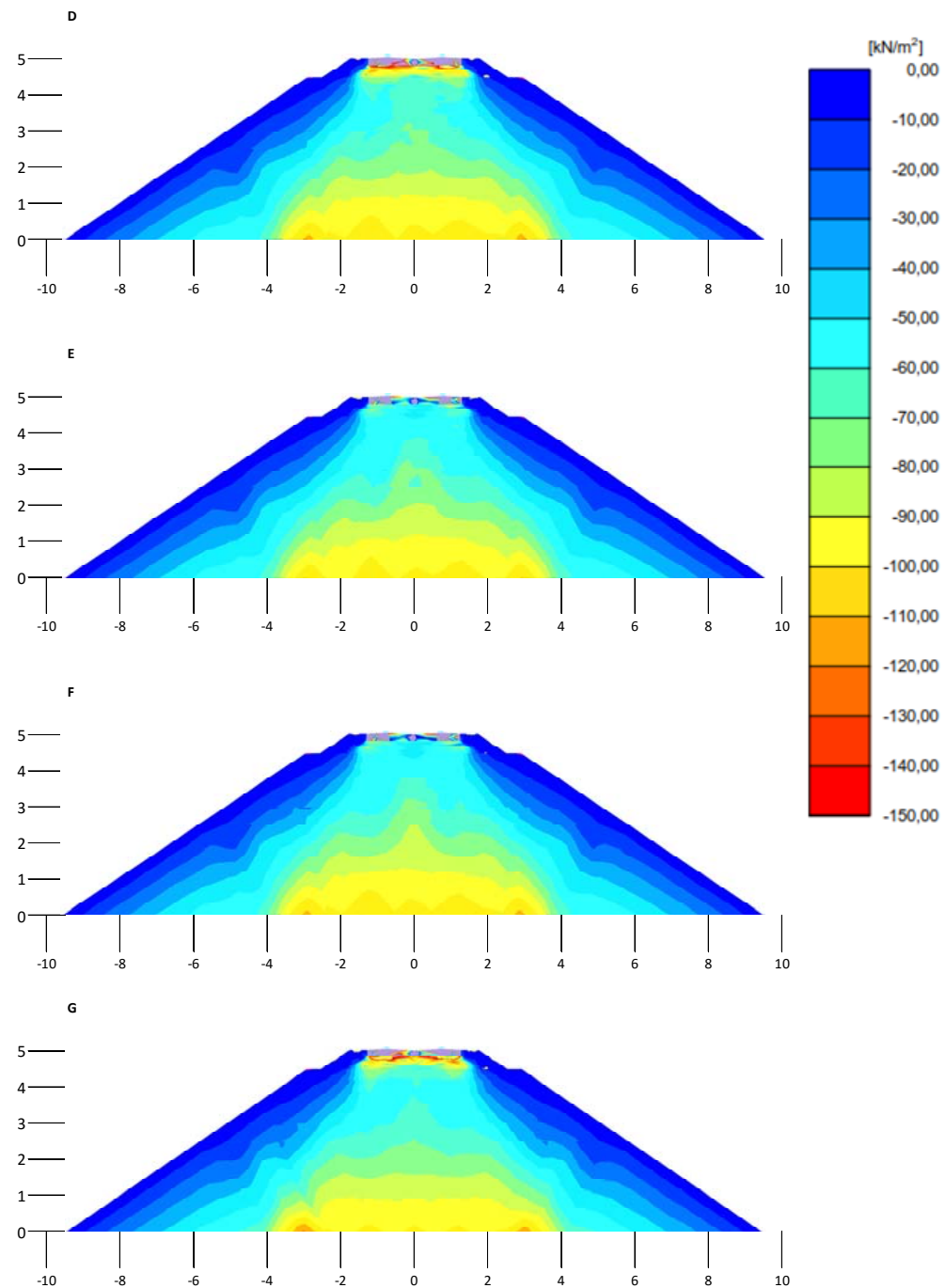


Figure 10. Total vertical stress distributions at cross-sections, load modes D to G, slab installation depth 5 meters, characteristic load.

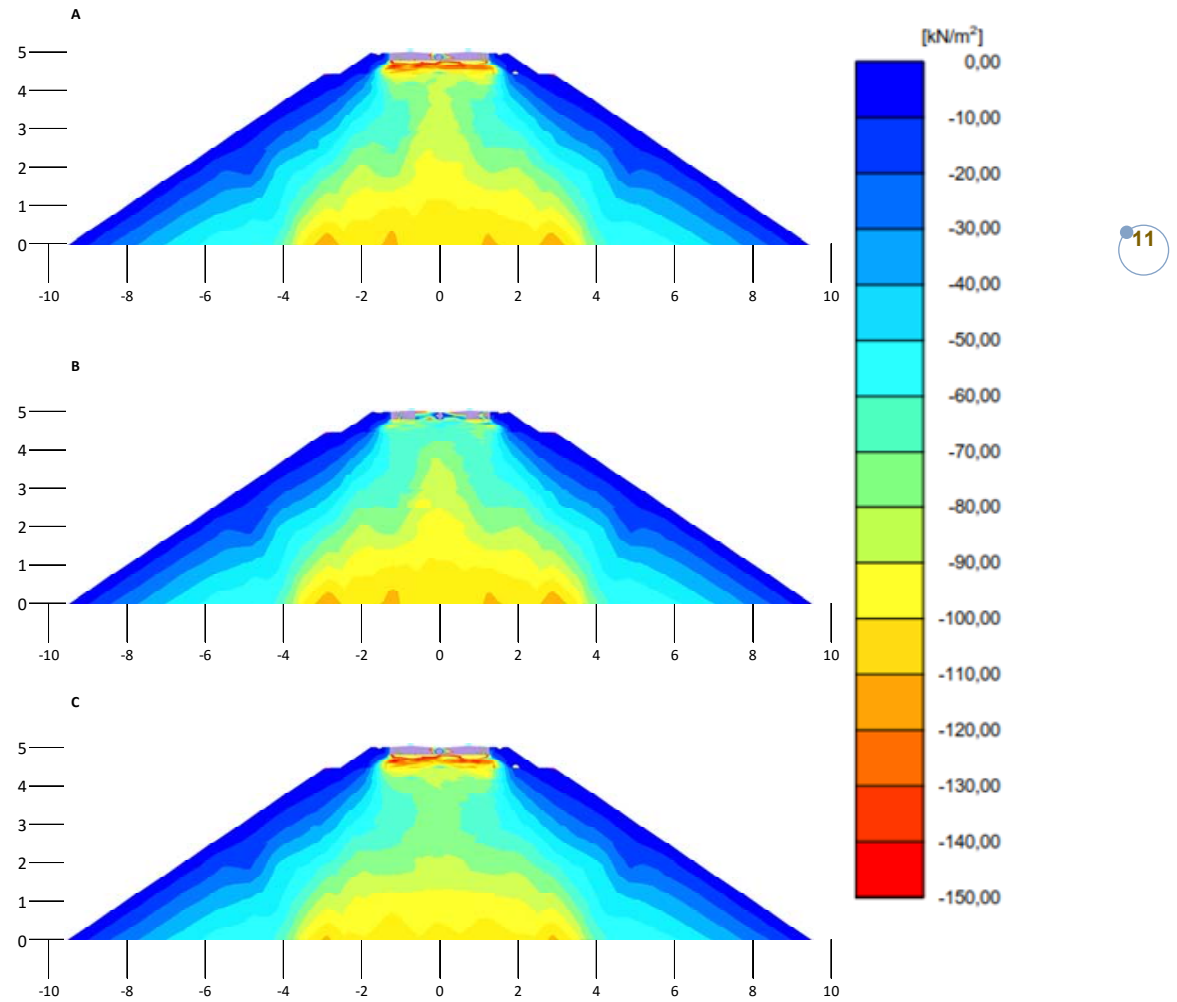


Figure 11. Total vertical stress distributions at cross-sections, load modes A to C, slab installation depth 5 meters, including dynamic load factor 1.25.

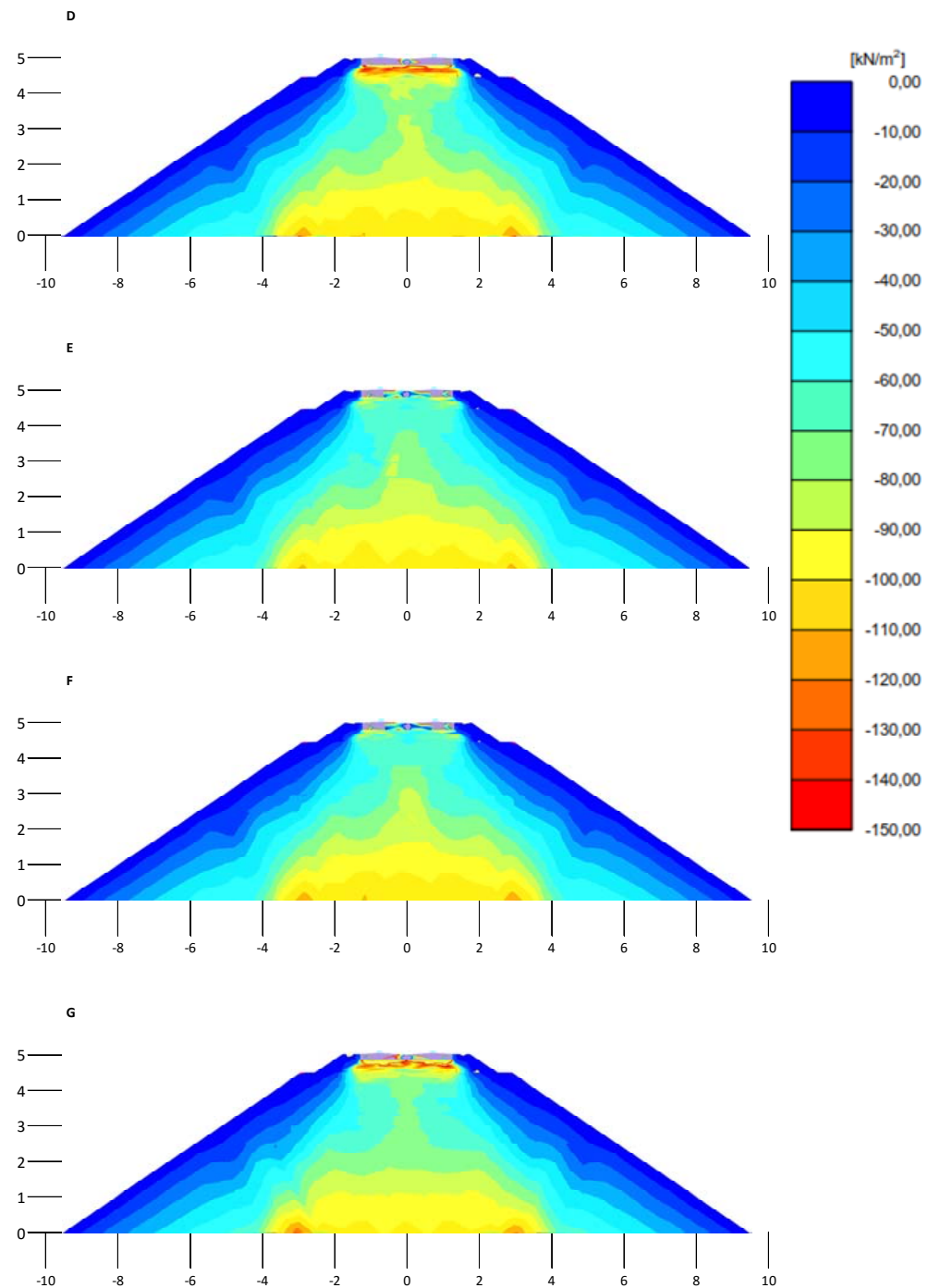


Figure 12. Total vertical stress distributions at cross-sections, load modes D to G, slab installation depth 5 meters, including dynamic load factor 1.25.

Vertical stress planes on top of the slab structure

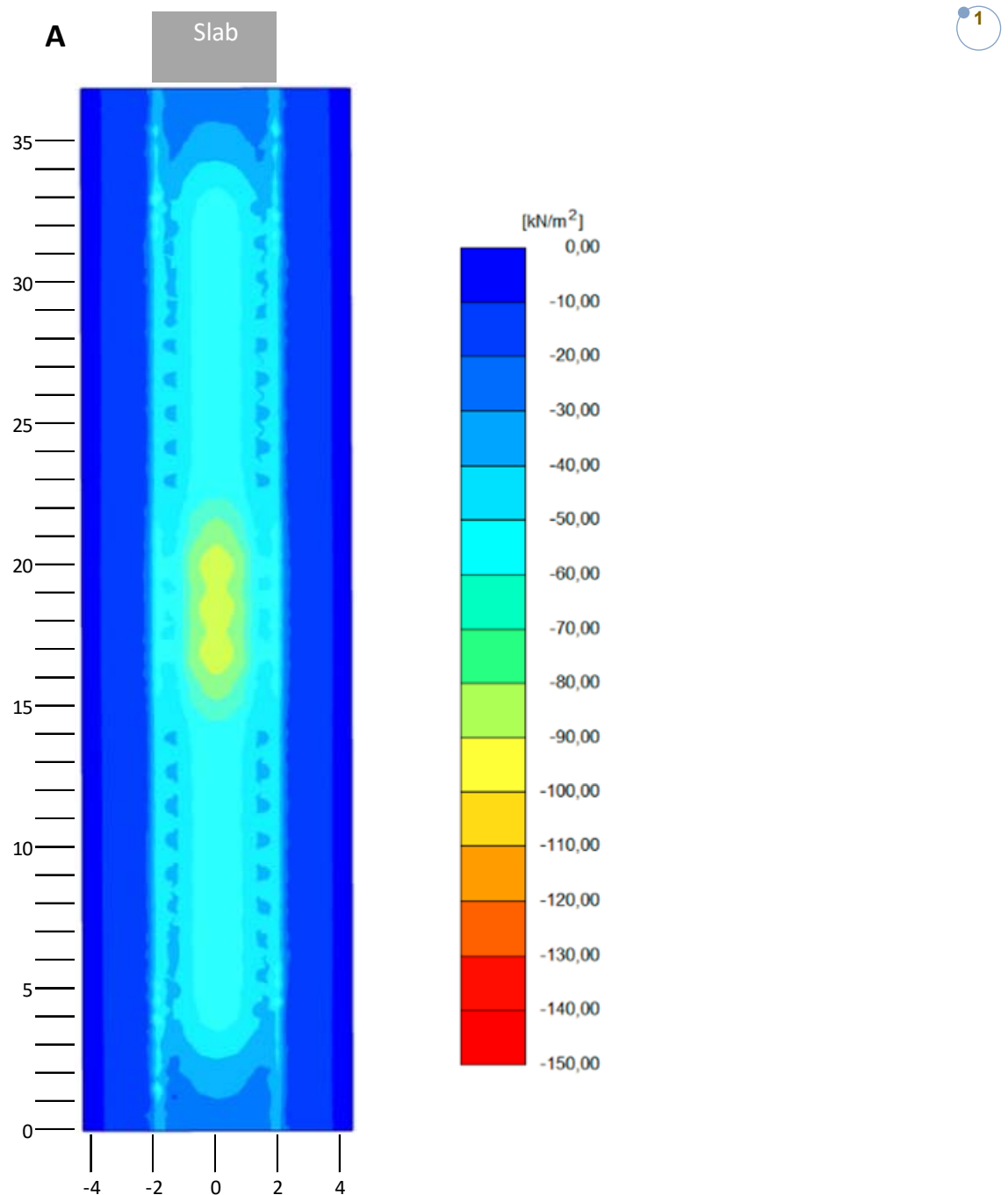


Figure 1. Total vertical stresses, load model A, slab installation depth 1.4 meters, characteristic load.

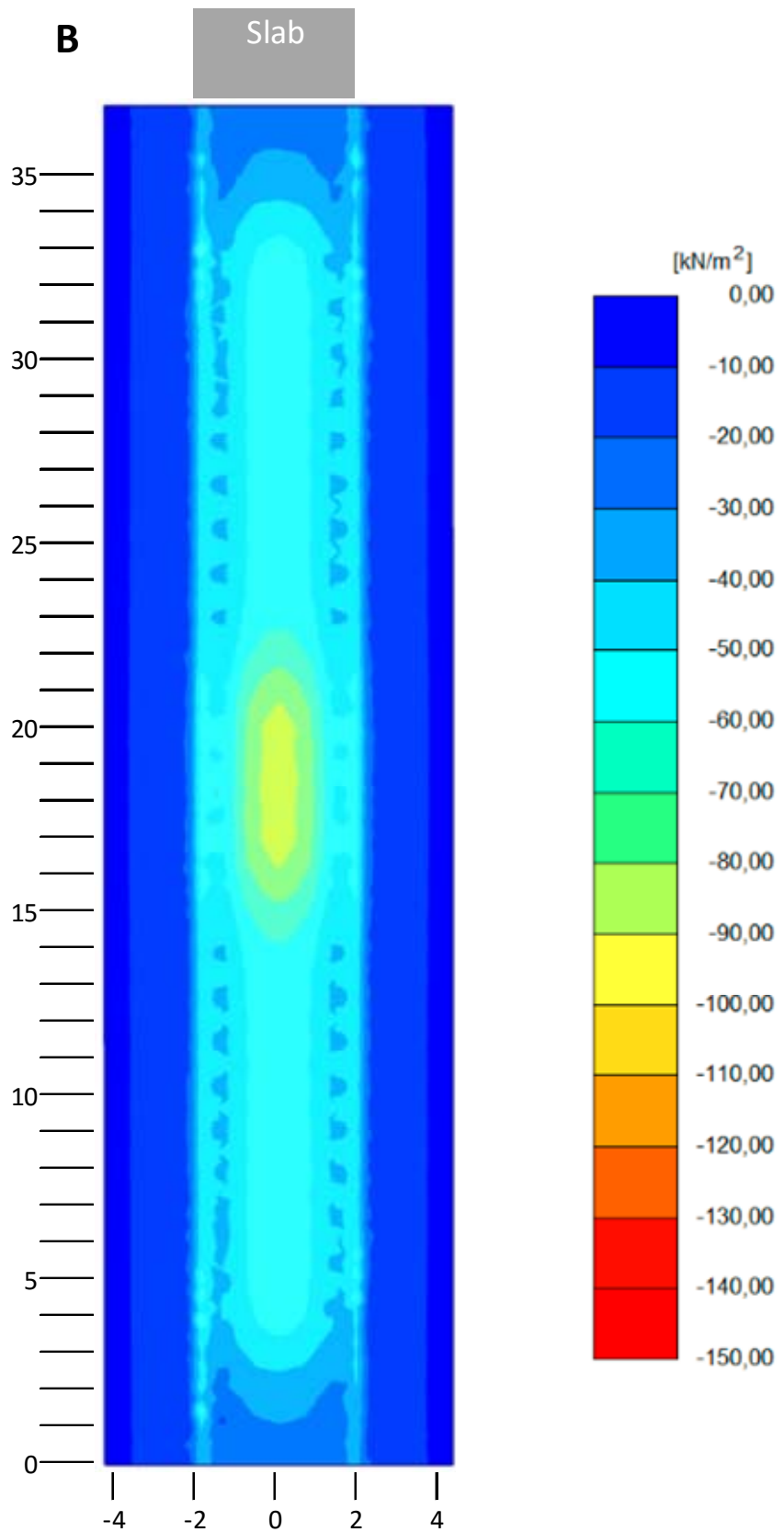


Figure 2. Total vertical stresses, load model B, slab installation depth 1.4 meters, characteristic load.

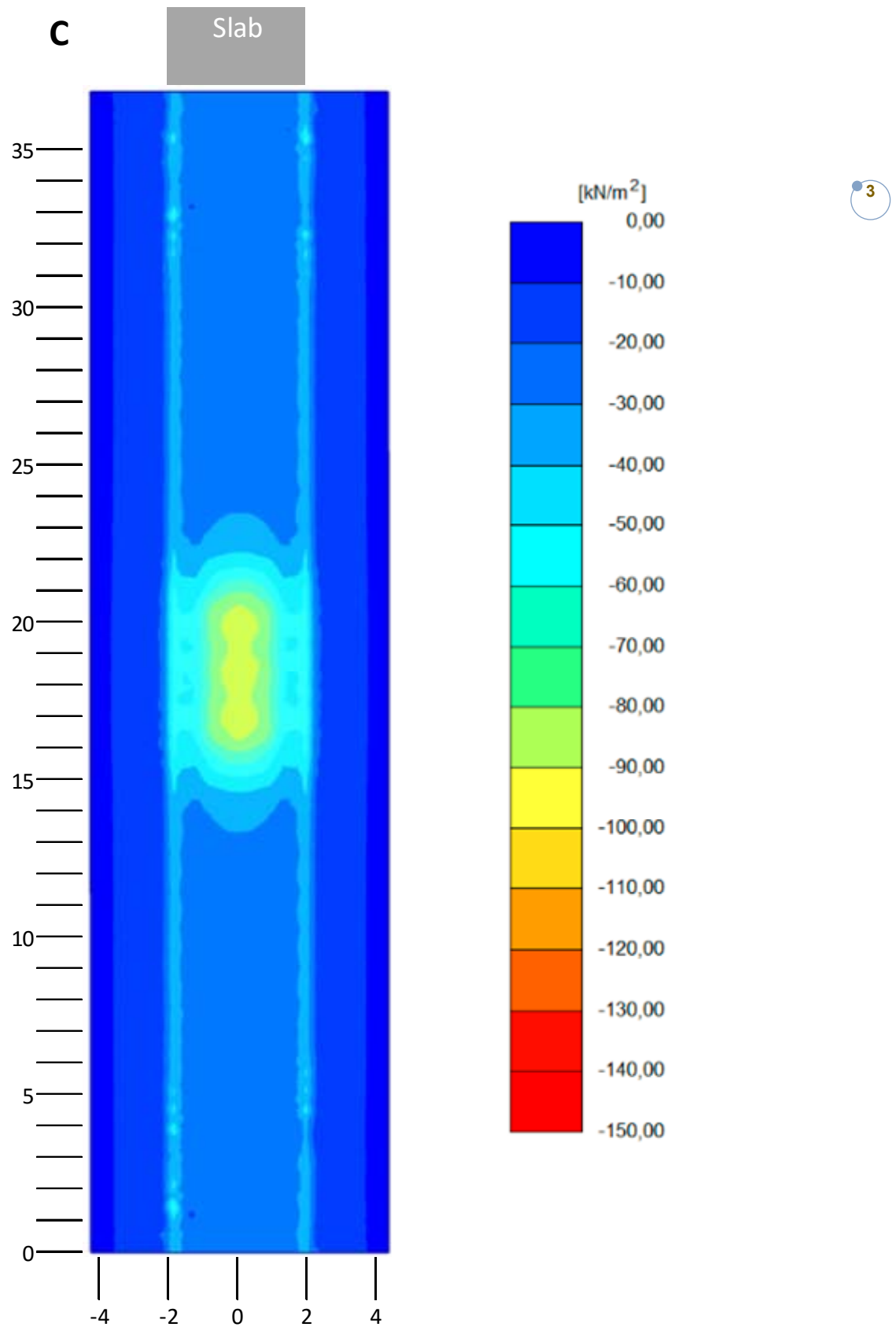


Figure 3. Total vertical stresses, load model C, slab installation depth 1.4 meters, characteristic load.

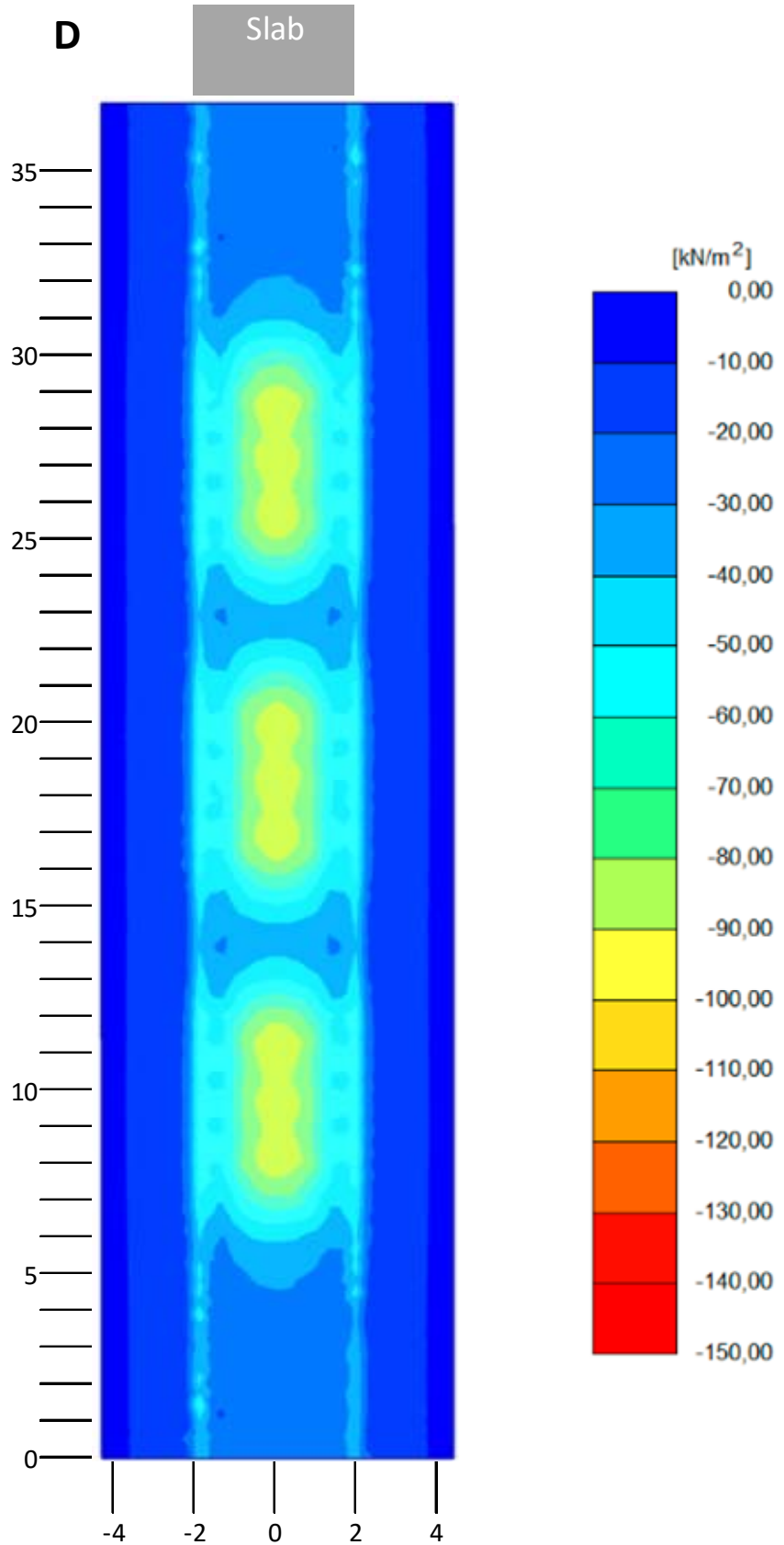


Figure 4. Total vertical stresses, load model D, slab installation depth 1.4 meters, characteristic load.

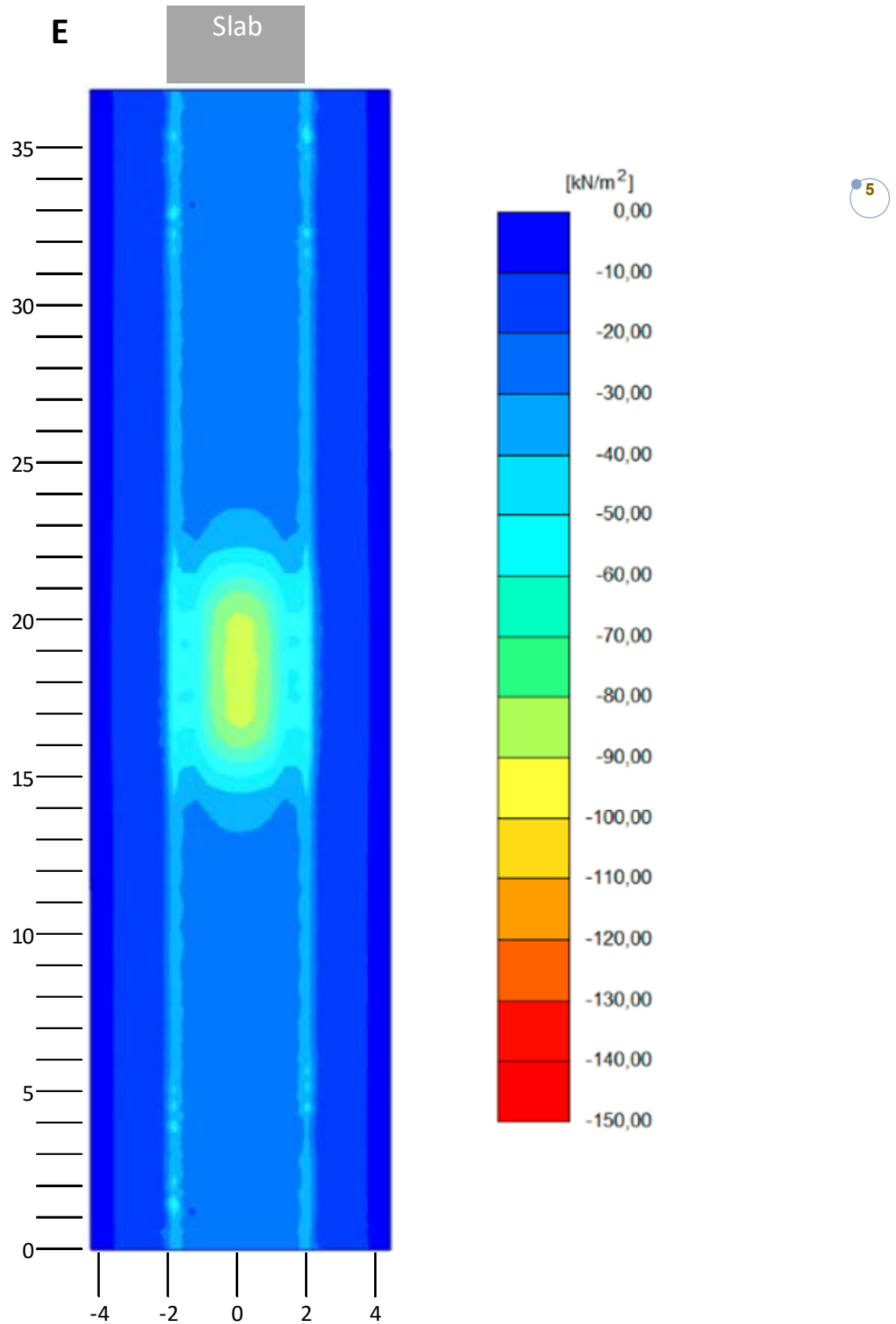


Figure 5. Total vertical stresses, load model E, slab installation depth 1.4 meters, characteristic load.

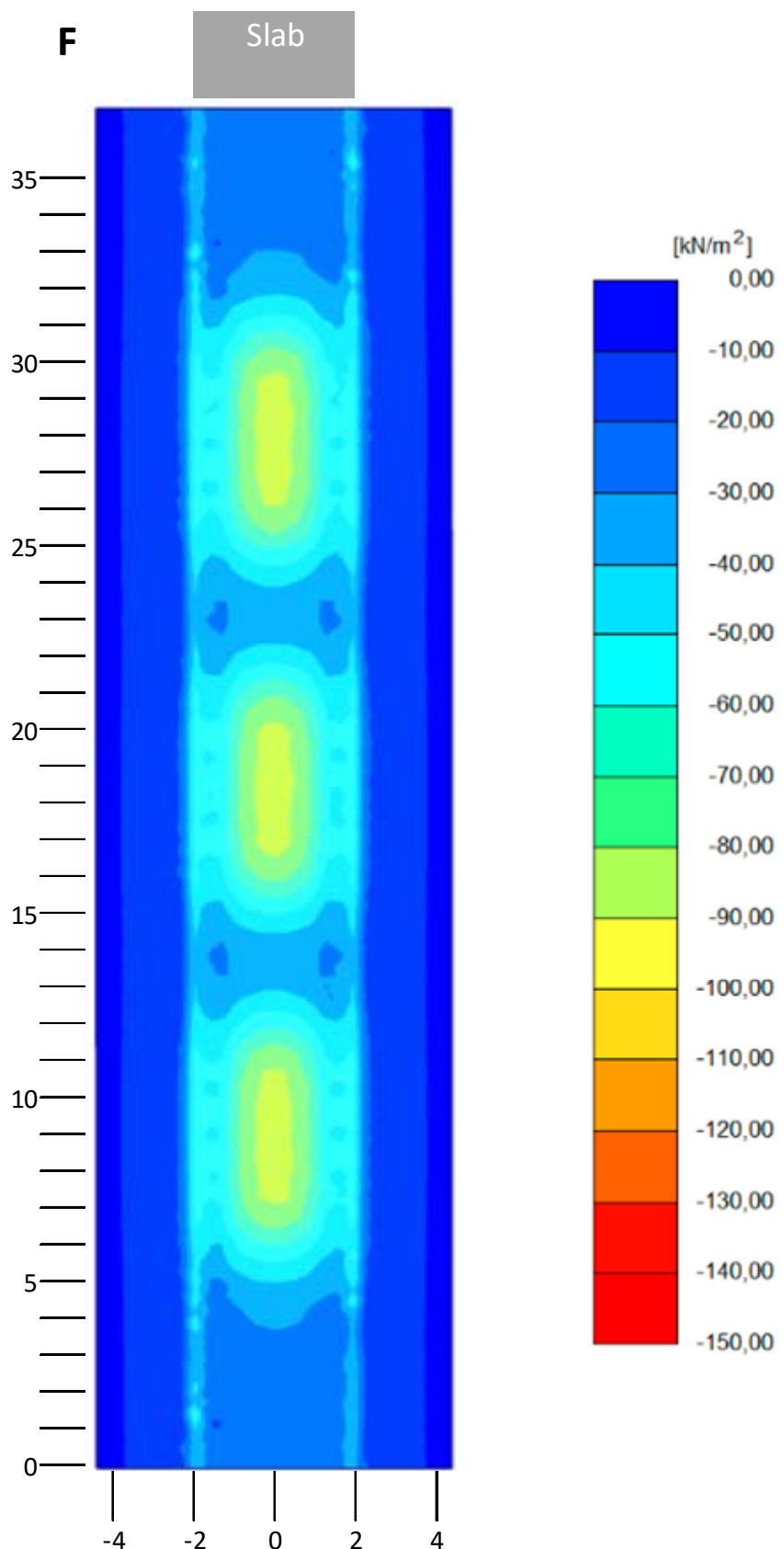


Figure 6. Total vertical stresses, load model F, slab installation depth 1.4 meters, characteristic load.

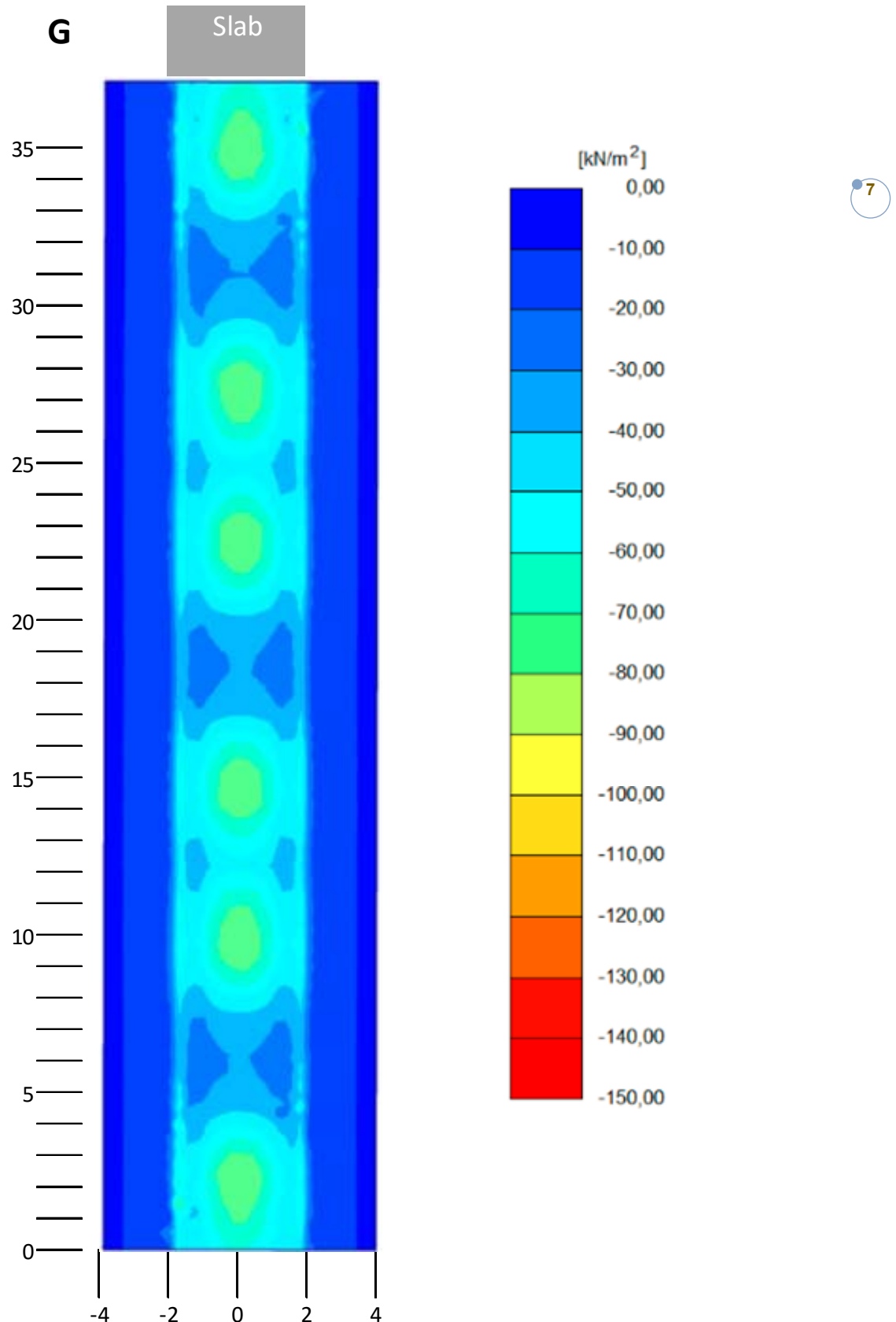


Figure 7. Total vertical stresses, load model G, slab installation depth 1.4 meters, characteristic load.

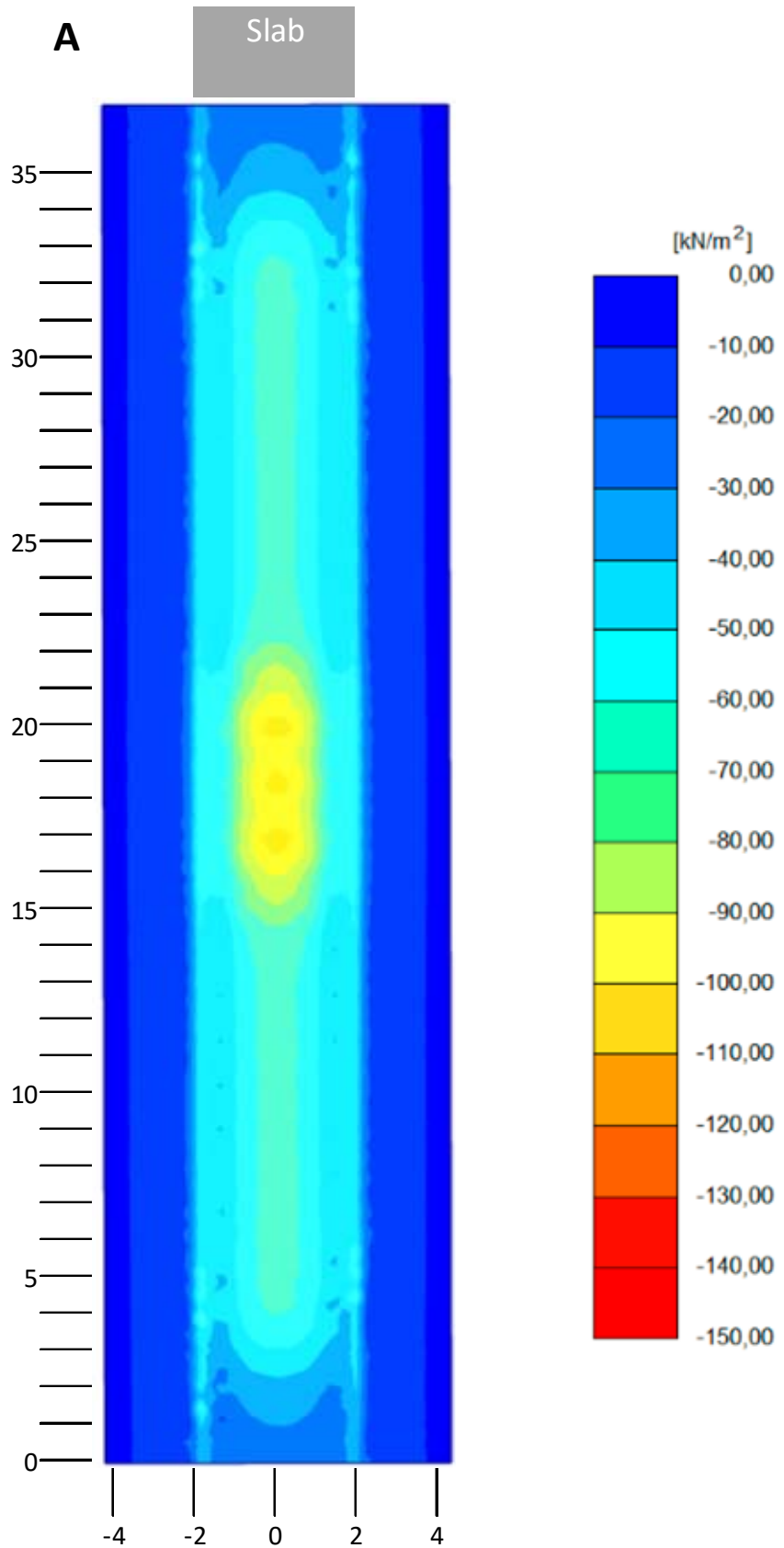


Figure 8. Total vertical stresses, load model A, slab installation depth 1.4 meters, including dynamic load factor 1.25.

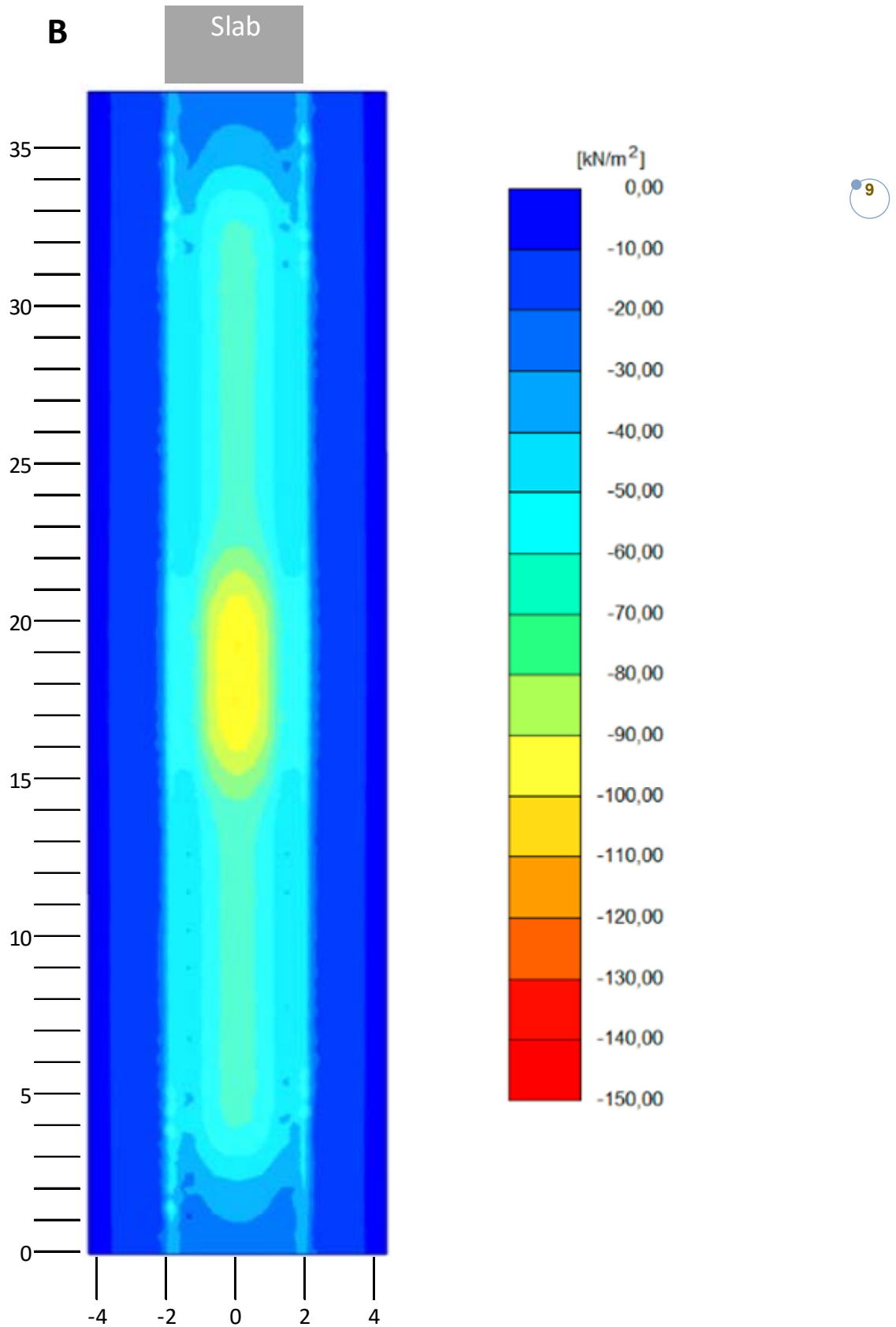


Figure 9. Total vertical stresses, load model B, slab installation depth 1.4 meters, including dynamic load factor 1.25.

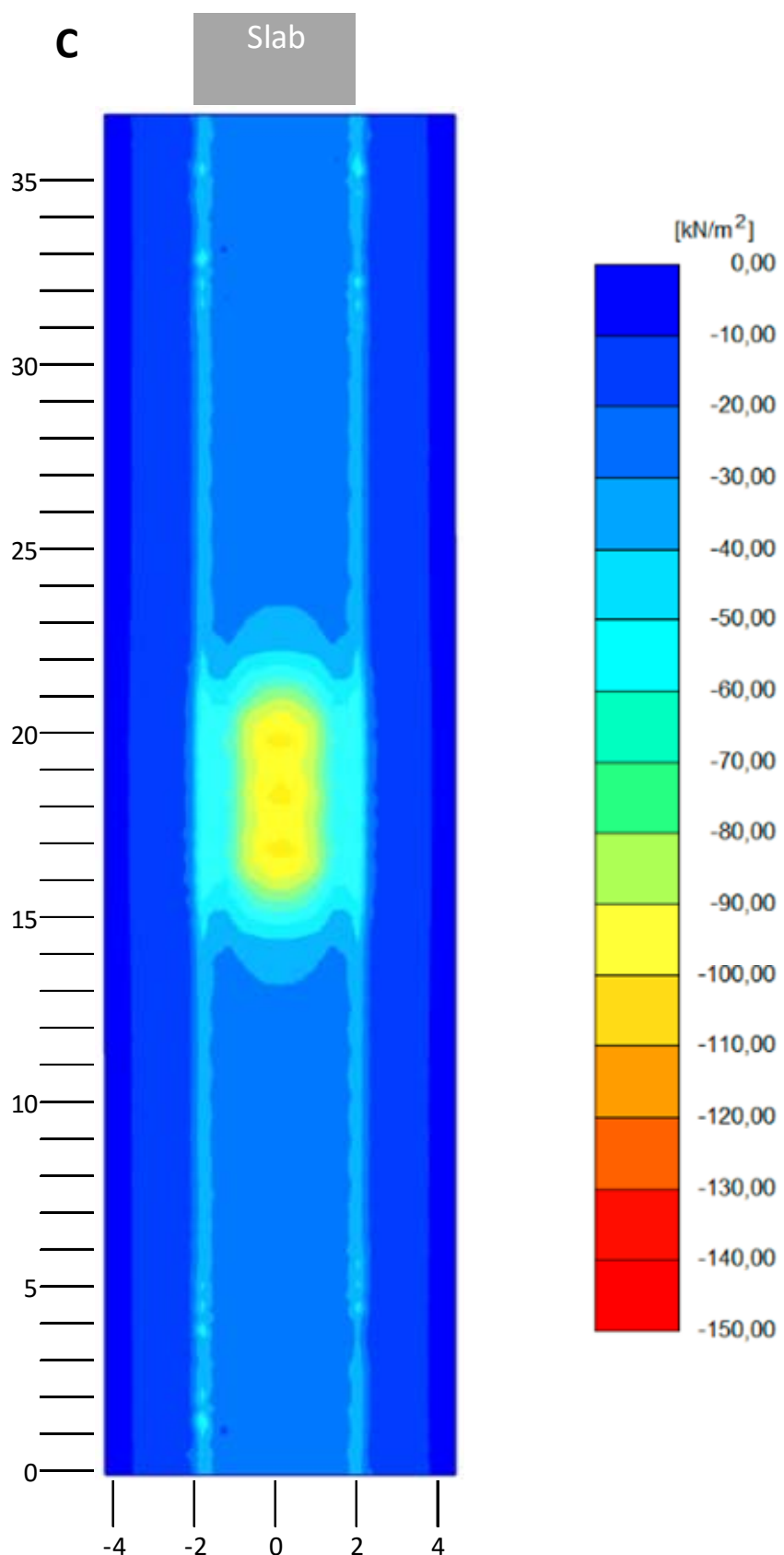


Figure 10. Total vertical stresses, load model C, slab installation depth 1.4 meters, including dynamic load factor 1.25.

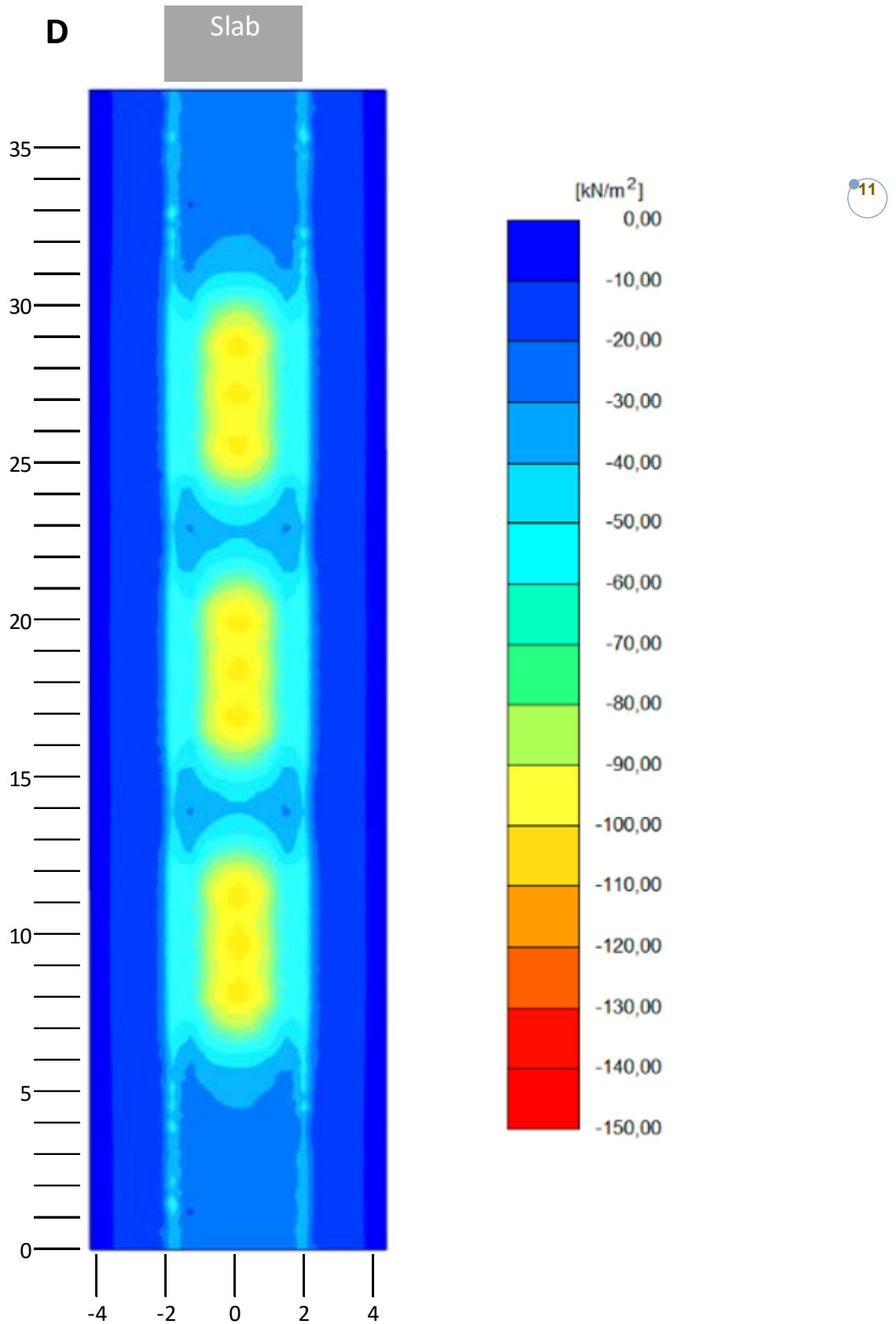


Figure 11. Total vertical stresses, load model D, slab installation depth 1.4 meters, including dynamic load factor 1.25.

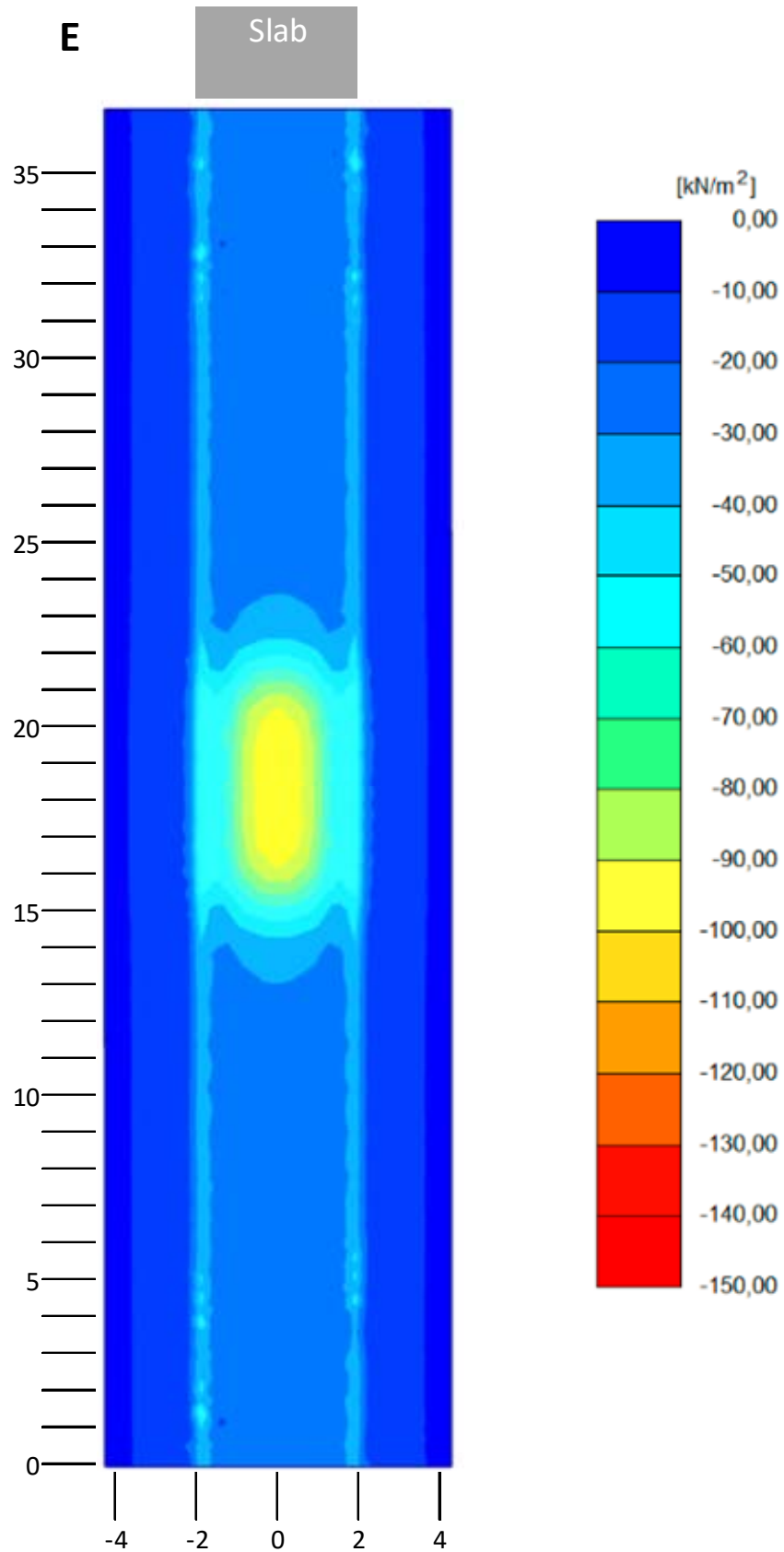


Figure 12. Total vertical stresses, load model E, slab installation depth 1.4 meters, including dynamic load factor 1.25.

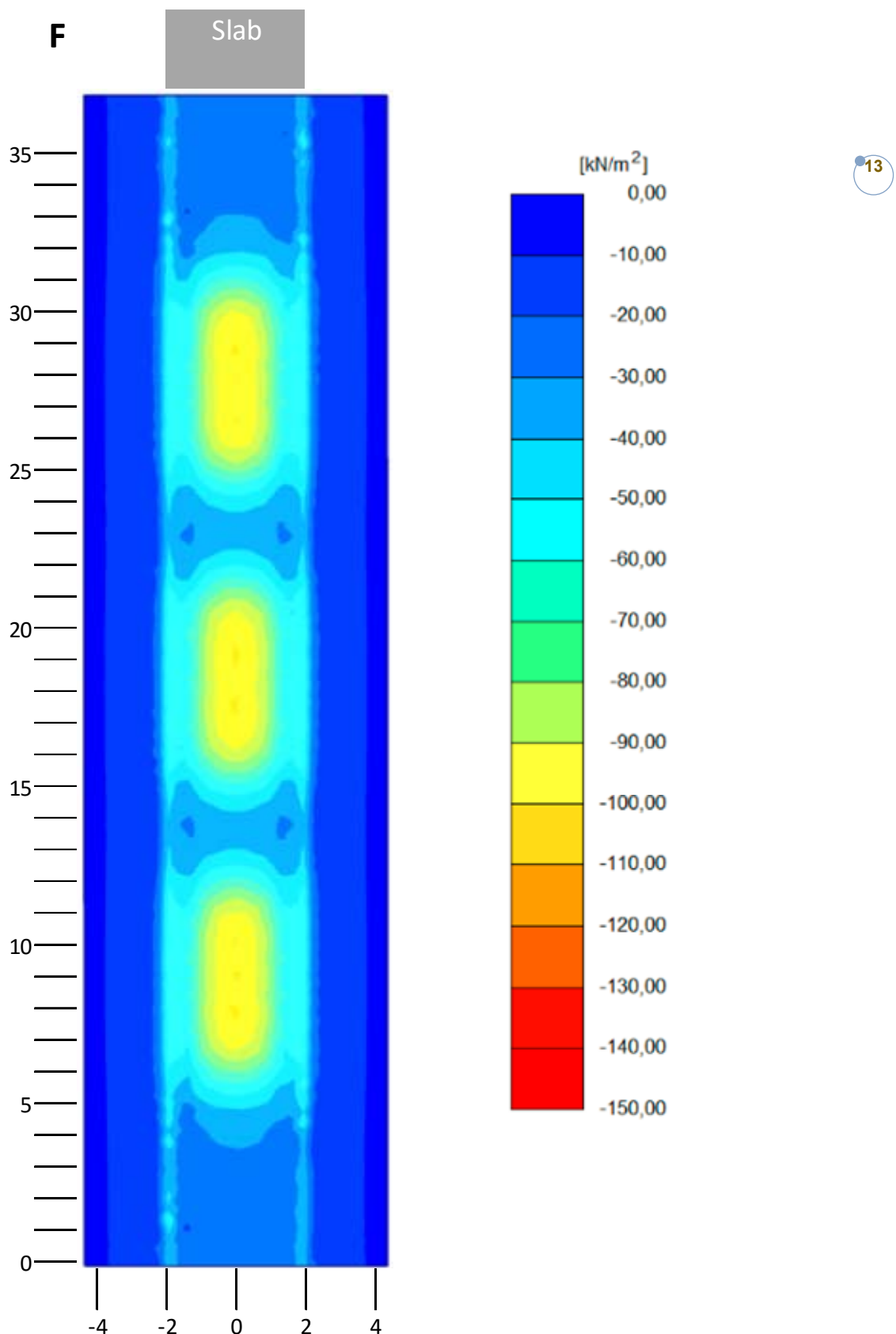


Figure 13. Total vertical stresses, load model F, slab installation depth 1.4 meters, including dynamic load factor 1.25.

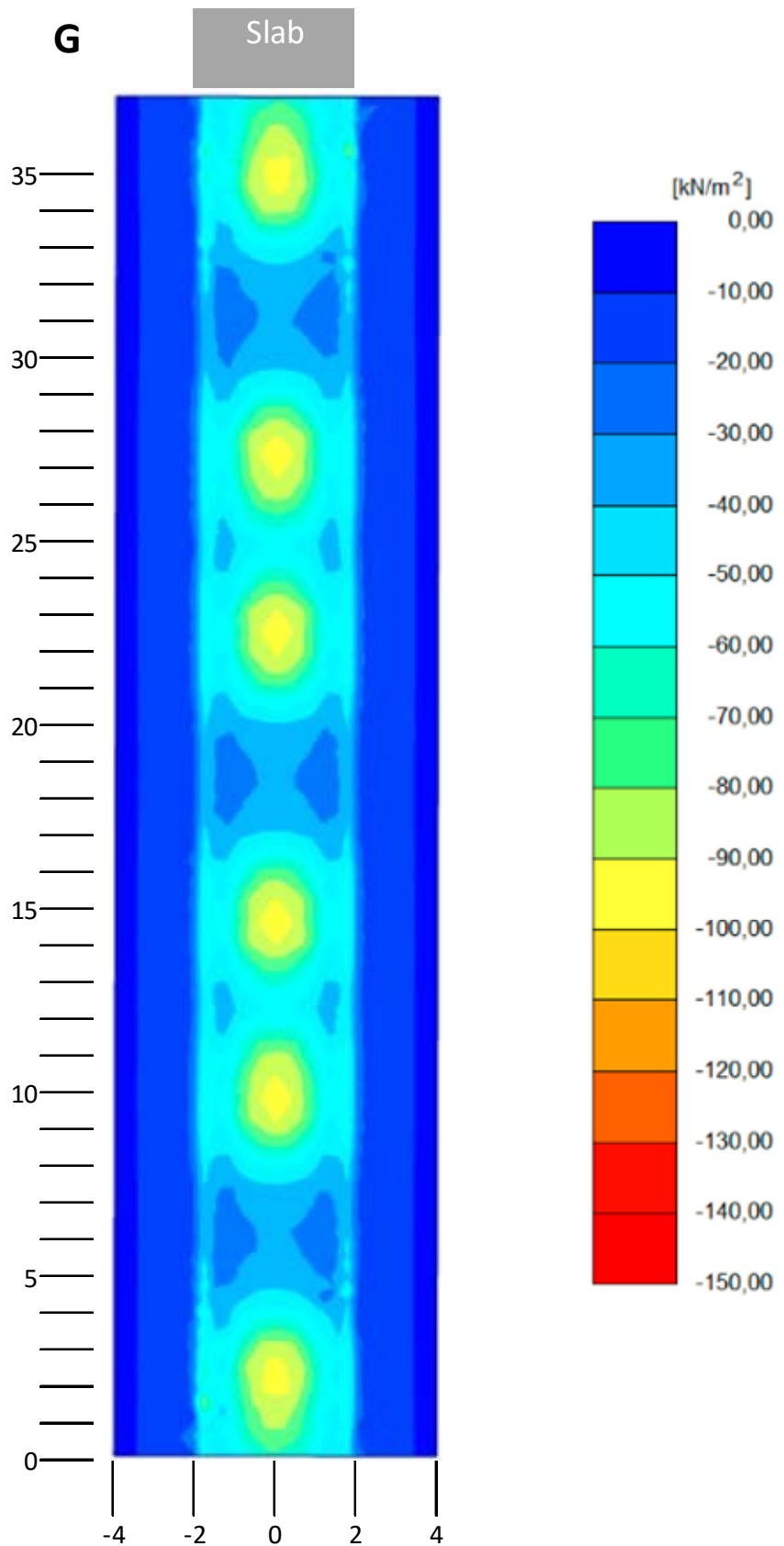


Figure 14. Total vertical stresses, load model G, slab installation depth 1.4 meters, including dynamic load factor 1.25.

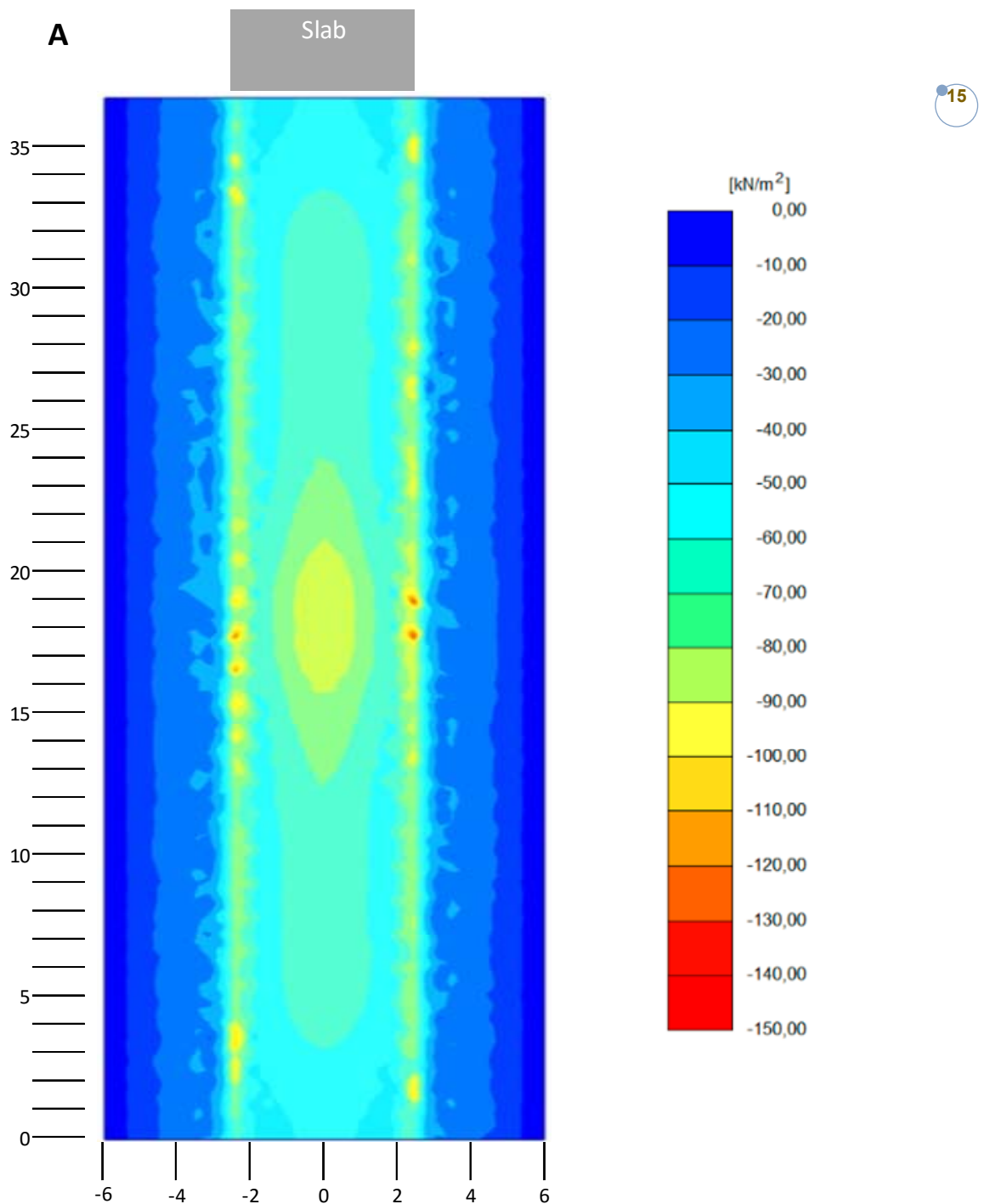


Figure 15. Total vertical stresses, load model A, slab installation depth 2.5 meters, characteristic load.

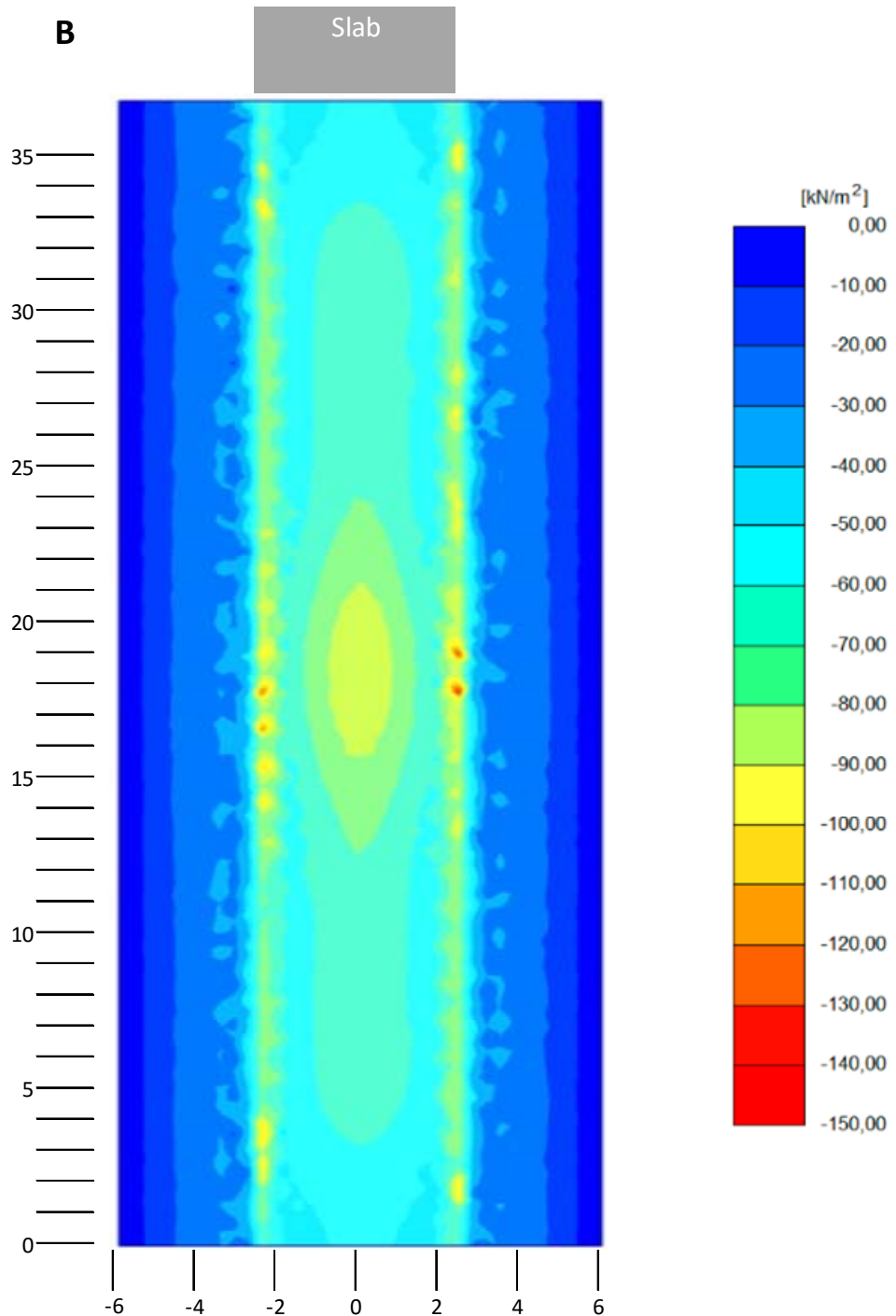


Figure 16. Total vertical stresses, load model B, slab installation depth 2.5 meters, characteristic load.

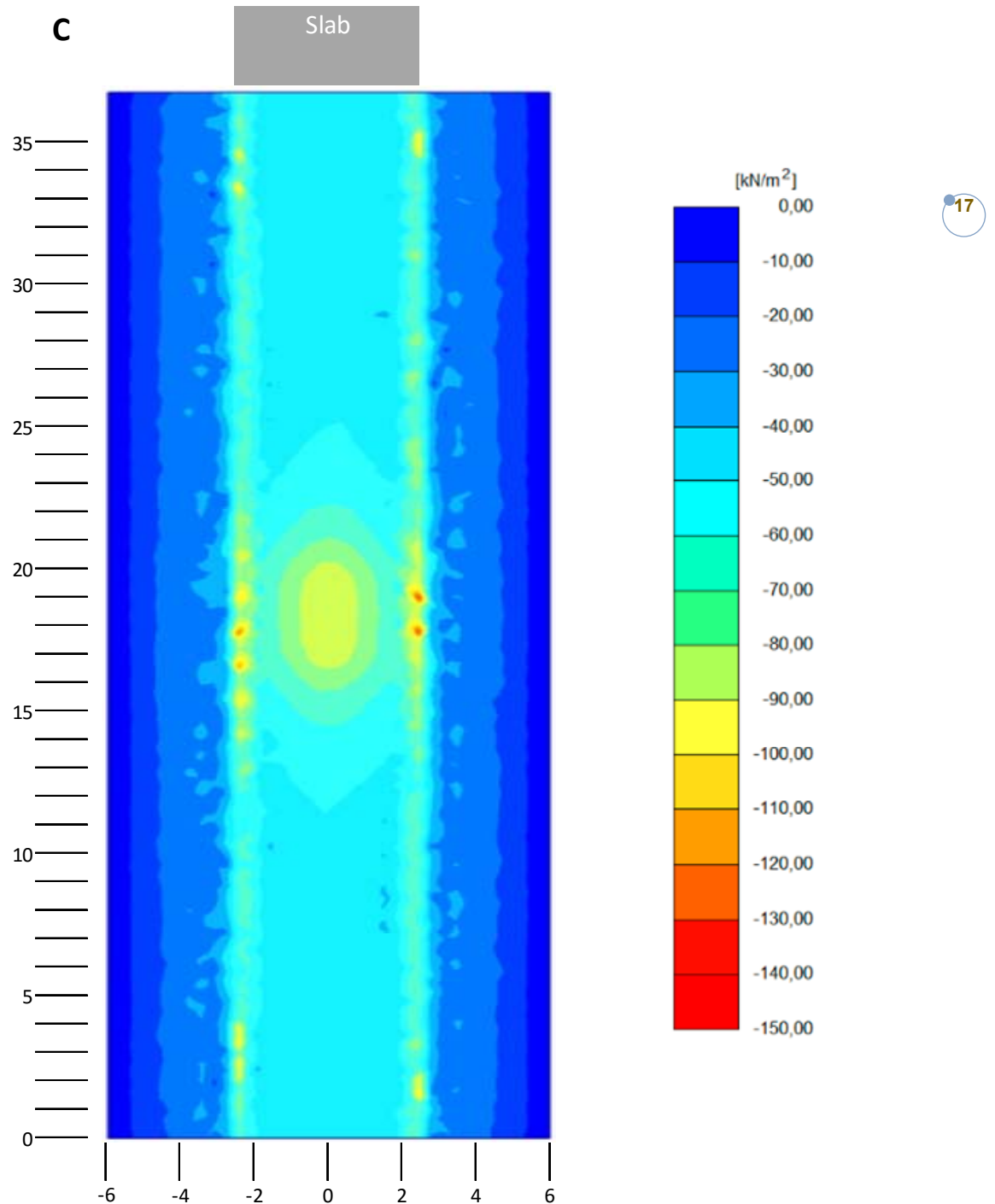


Figure 17. Total vertical stresses, load model C, slab installation depth 2.5 meters, characteristic load.

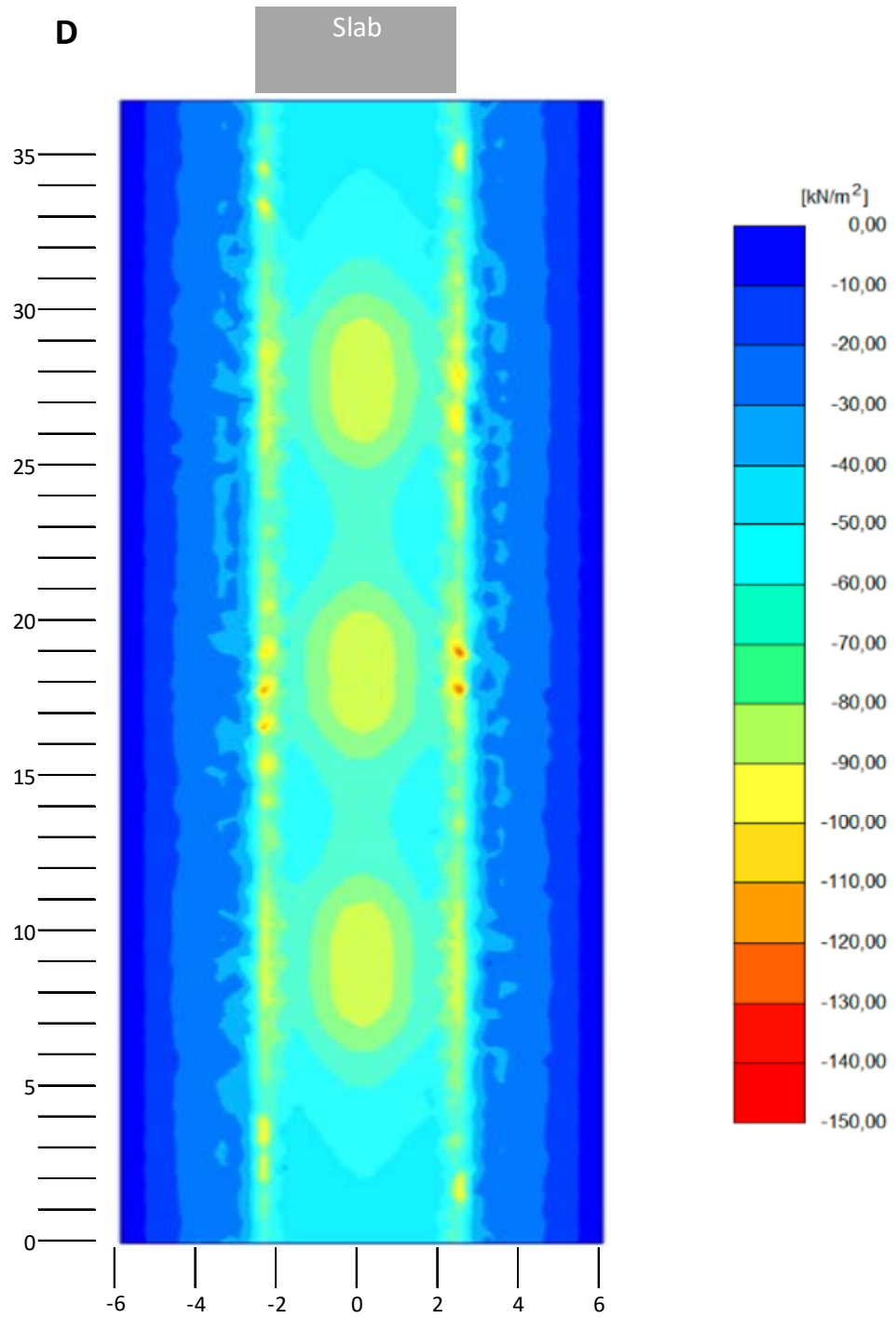


Figure 18. Total vertical stresses, load model D, slab installation depth 2.5 meters, characteristic load.

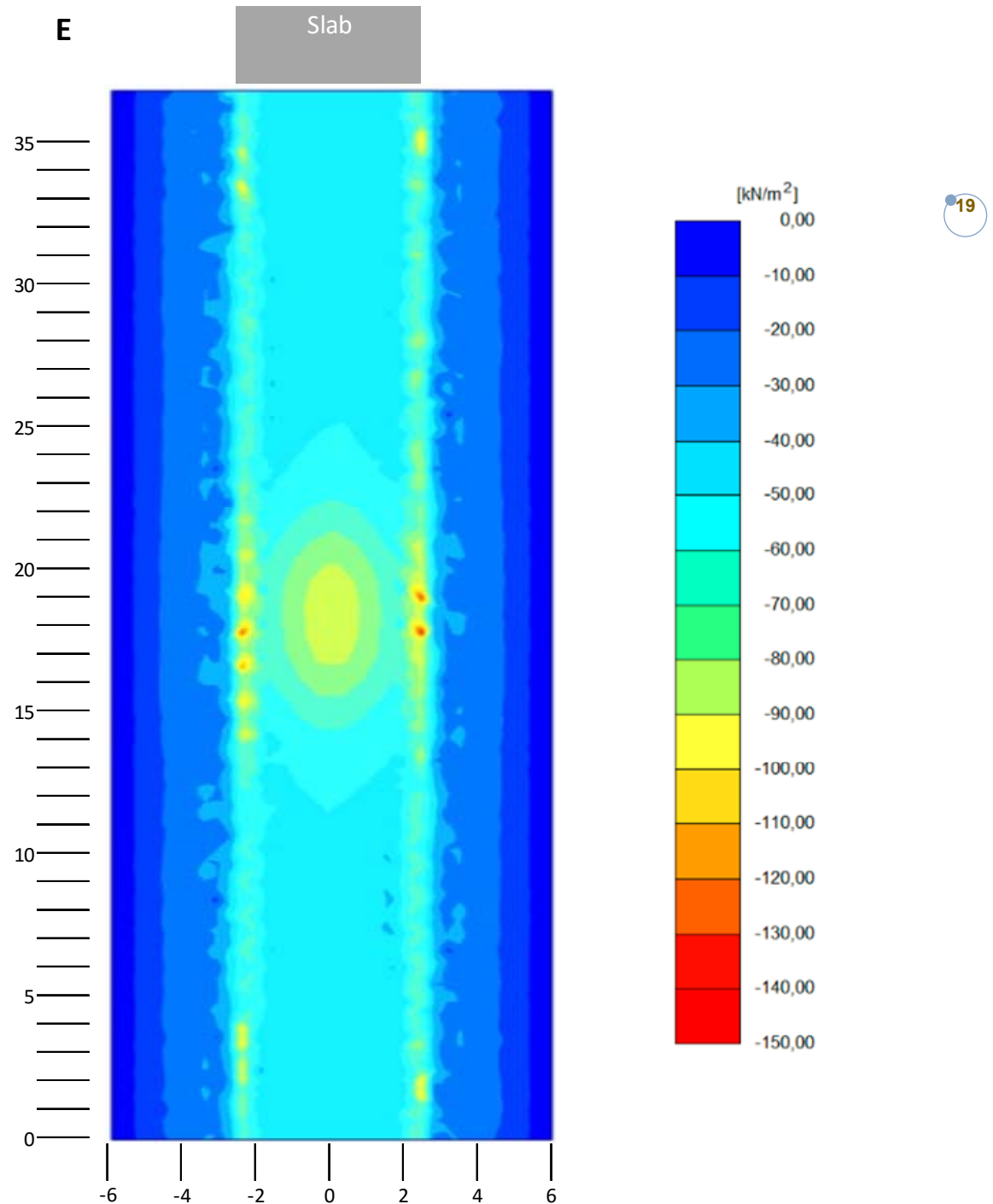


Figure 19. Total vertical stresses, load model E, slab installation depth 2.5 meters, characteristic load.

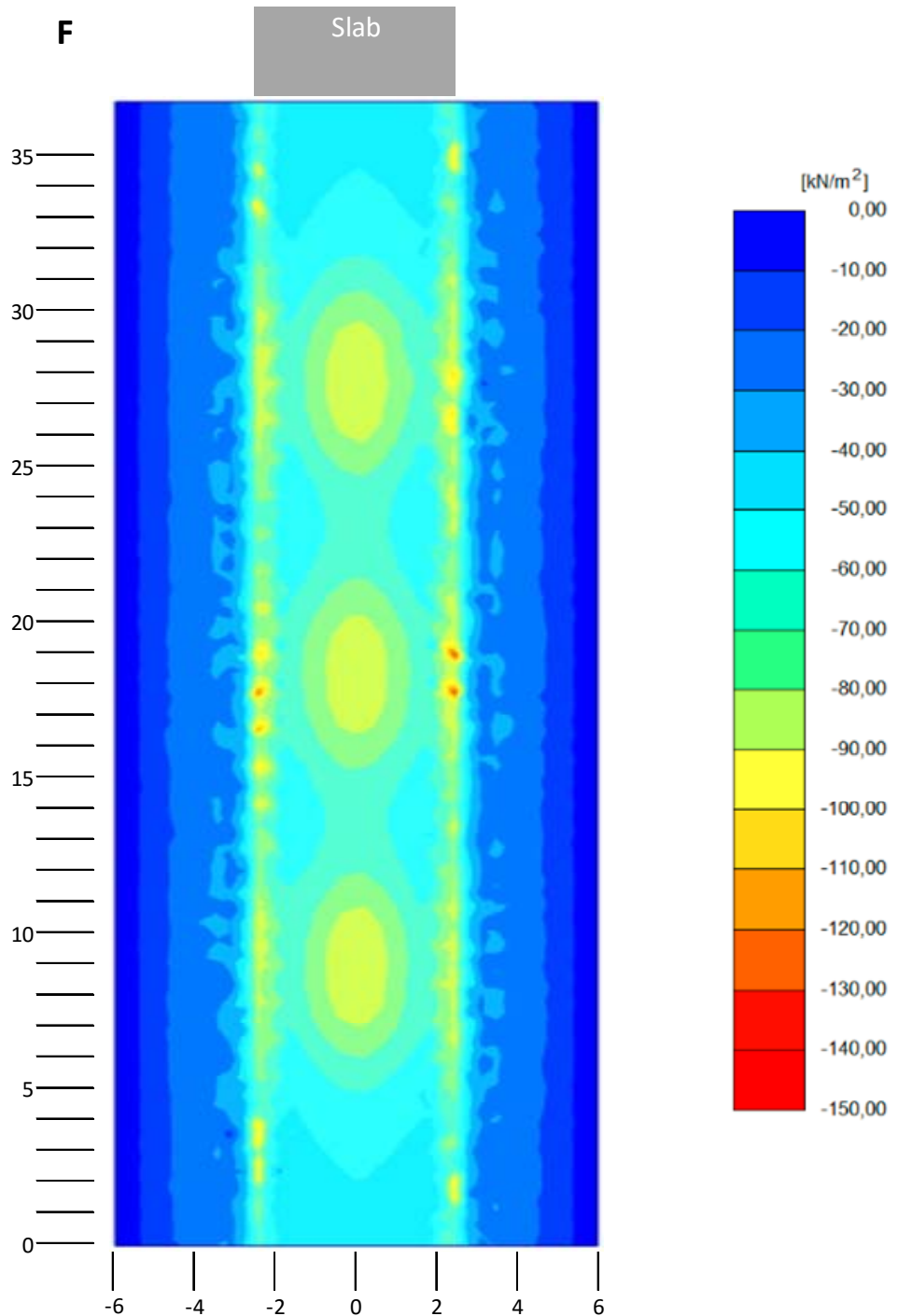


Figure 20. Total vertical stresses, load model F, slab installation depth 2.5 meters, characteristic load.

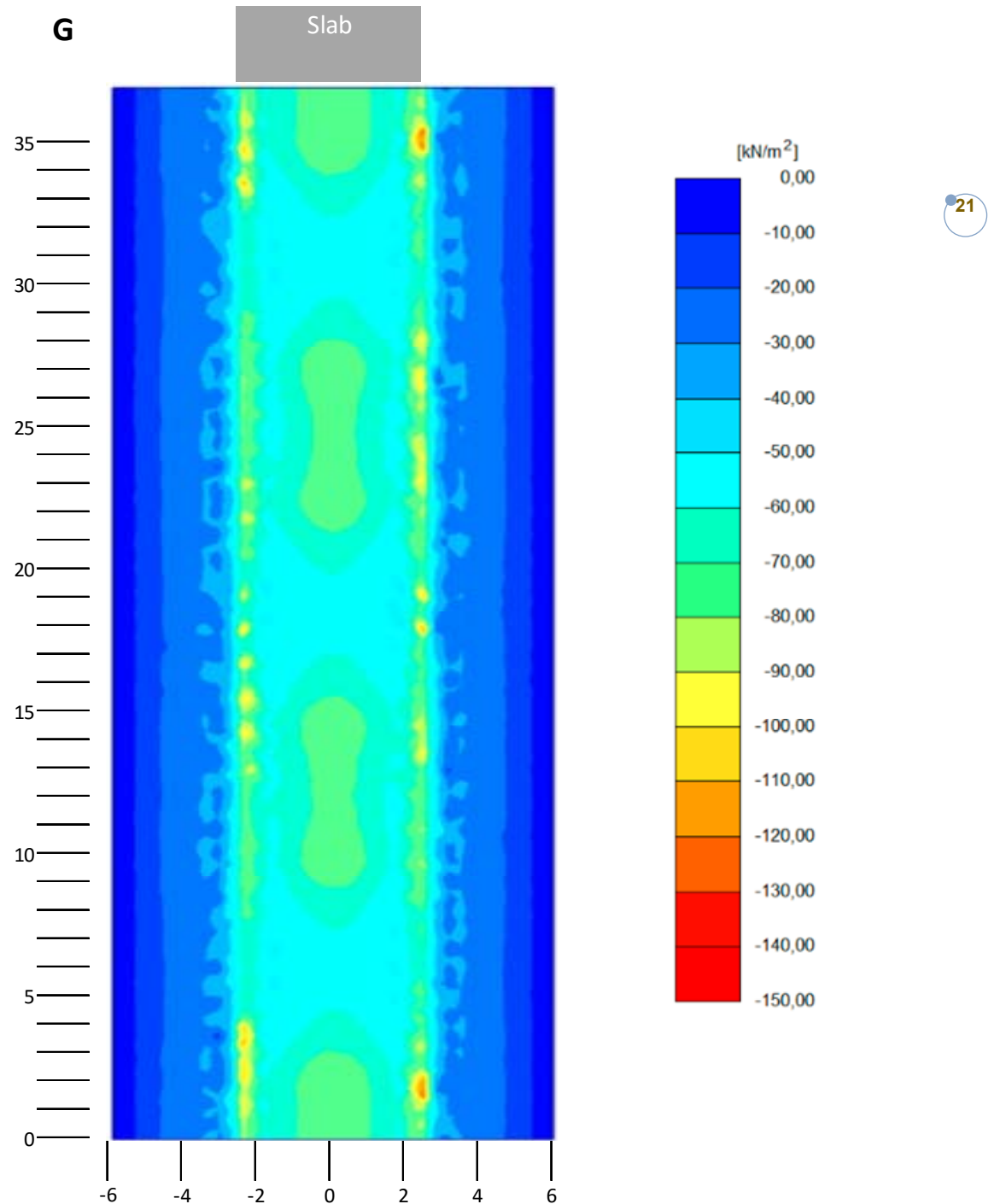


Figure 21. Total vertical stresses, load model G, slab installation depth 2.5 meters, characteristic load.

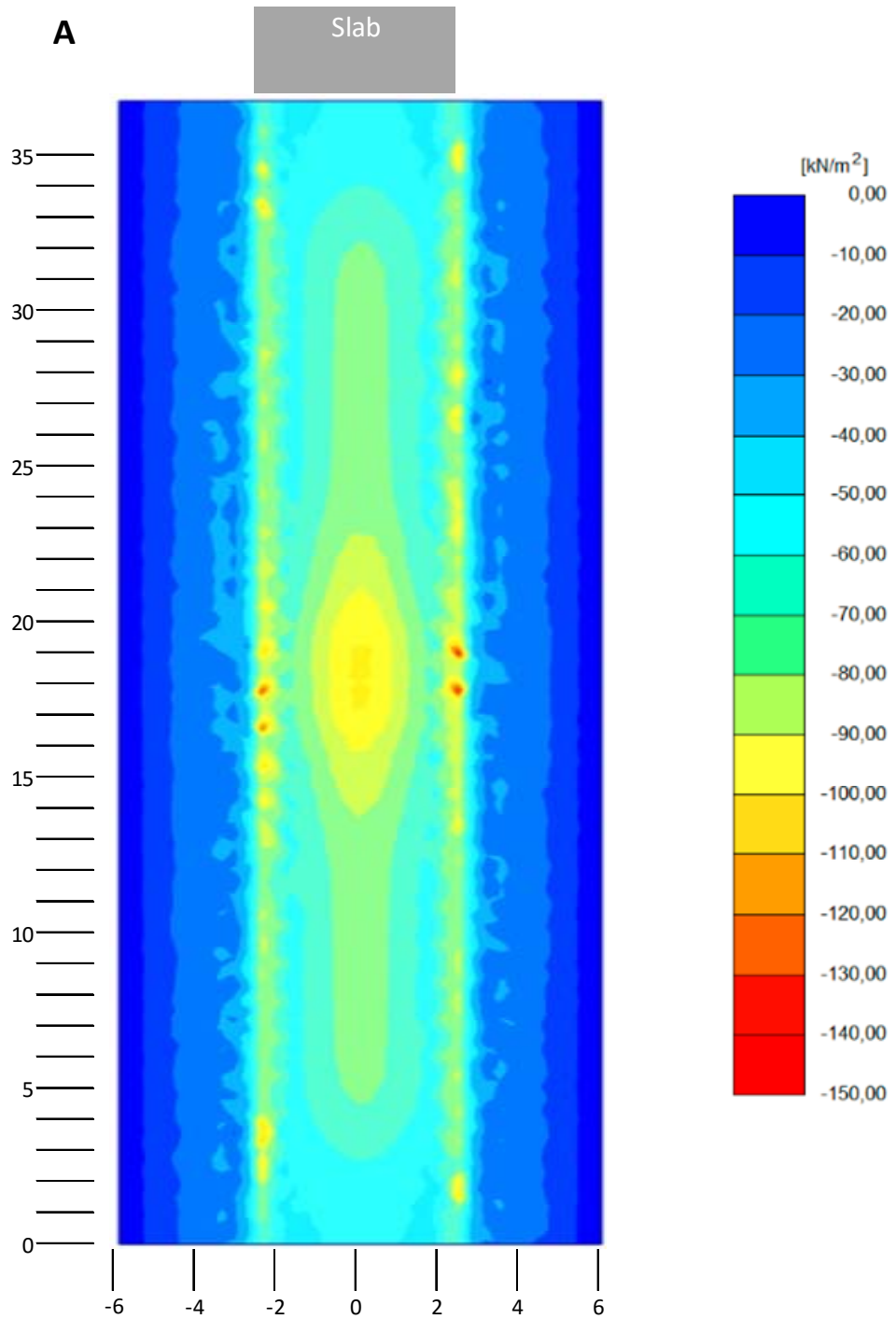


Figure 22. Total vertical stresses, load model A, slab installation depth 2.5 meters, including dynamic load factor 1.25.

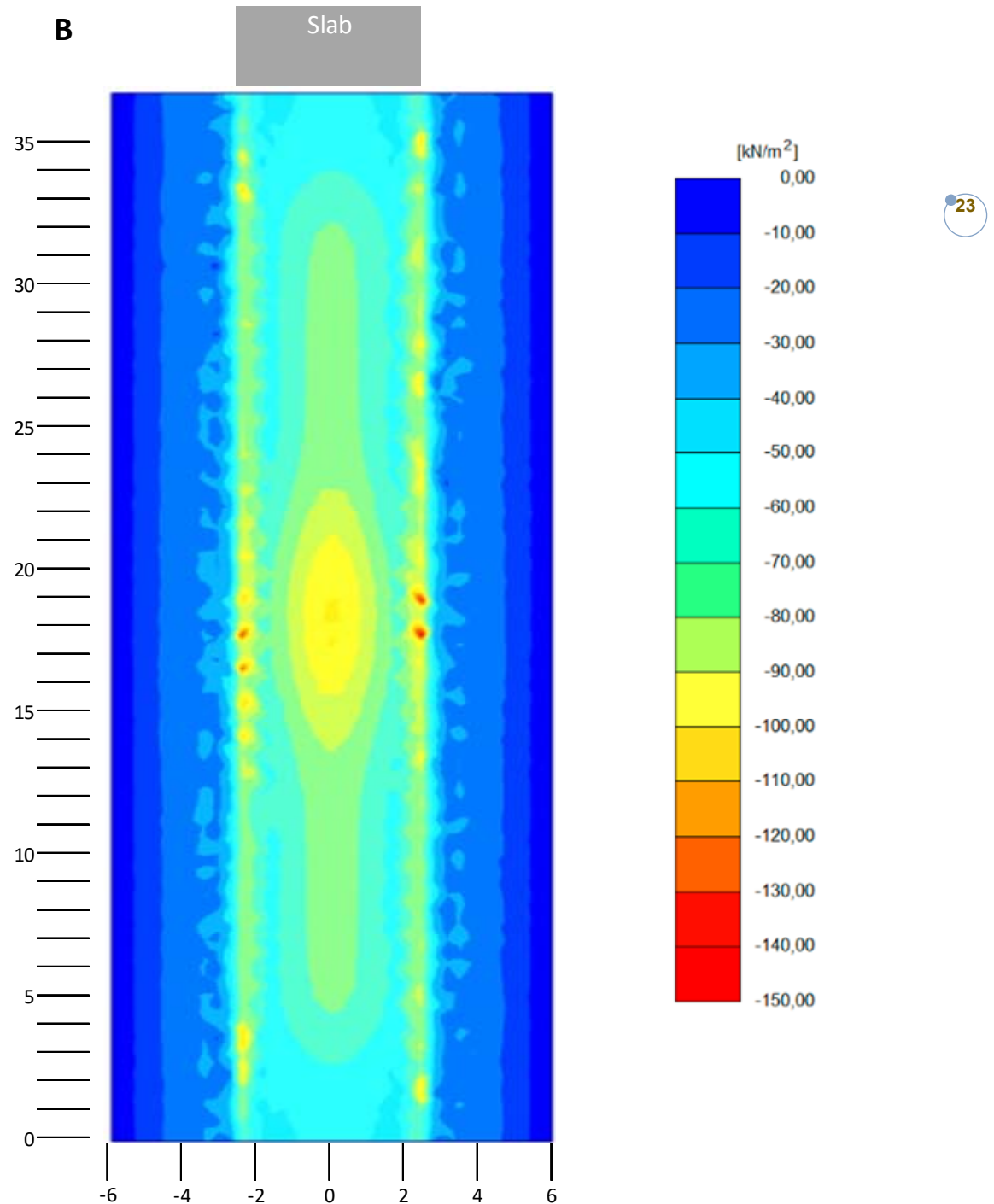


Figure 23. Total vertical stresses, load model B, slab installation depth 2.5 meters, including dynamic load factor 1.25.

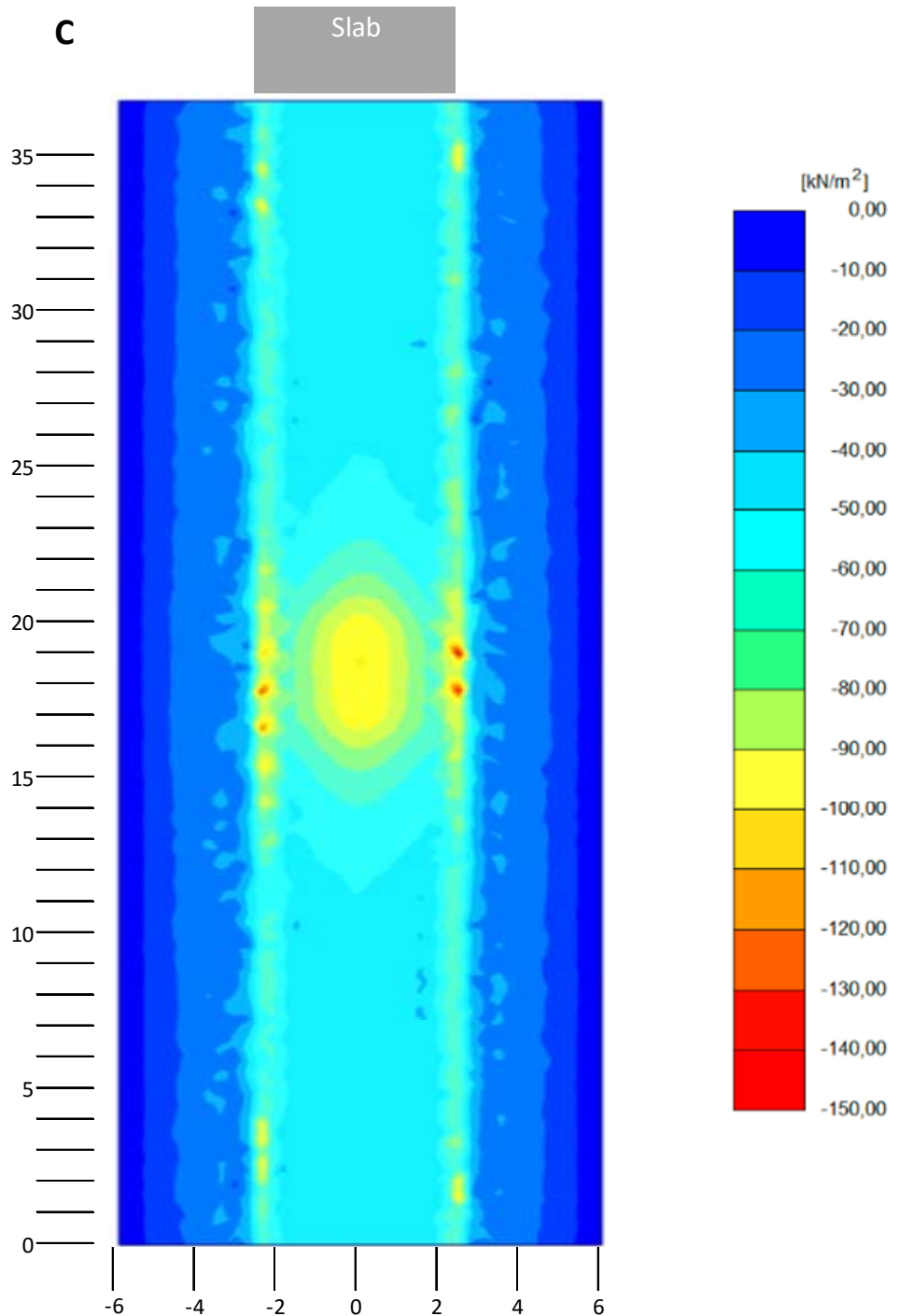


Figure 24. Total vertical stresses, load model C, slab installation depth 2.5 meters, including dynamic load factor 1.25.

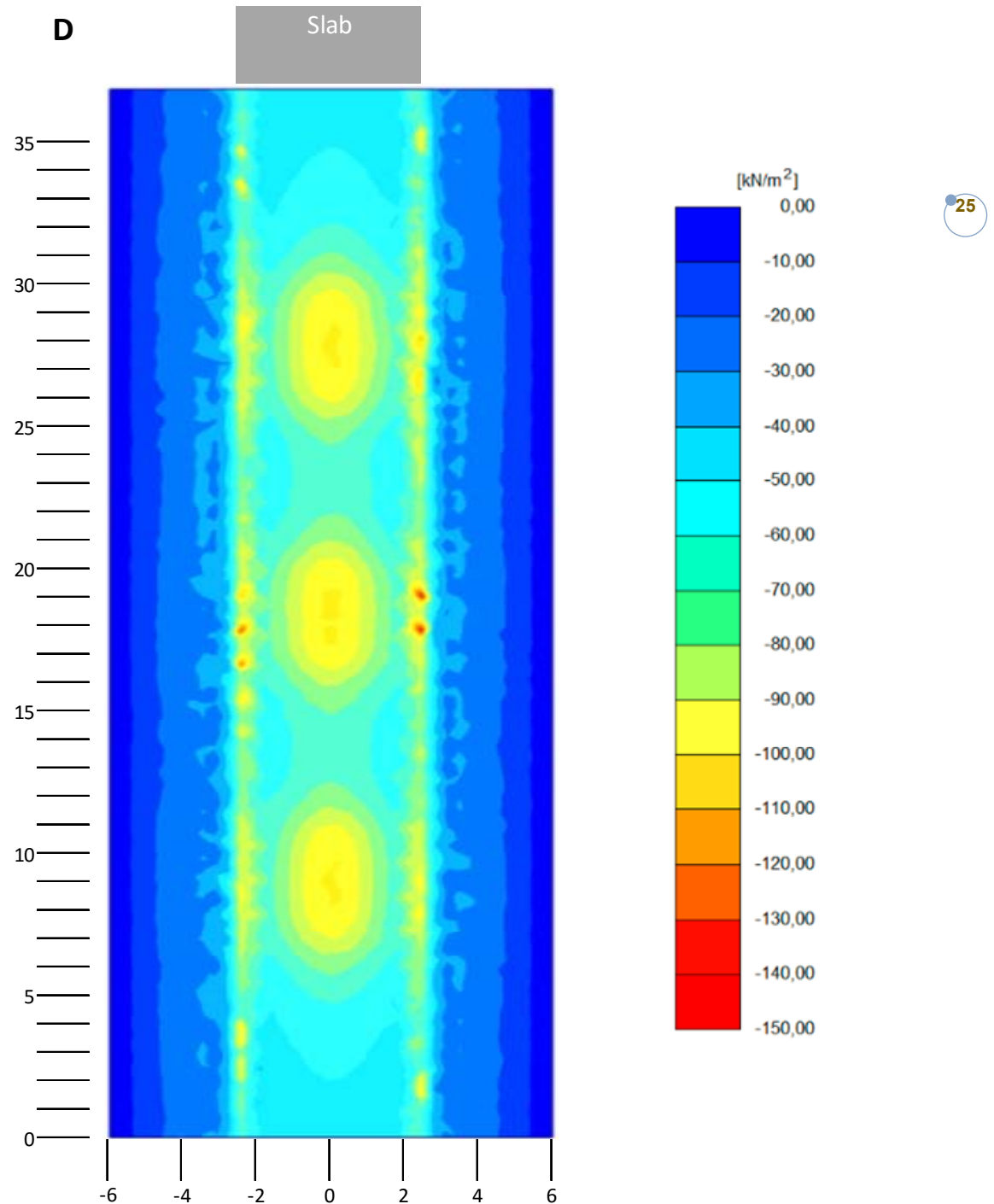


Figure 25. Total vertical stresses, load model D, slab installation depth 2.5 meters, including dynamic load factor 1.25.

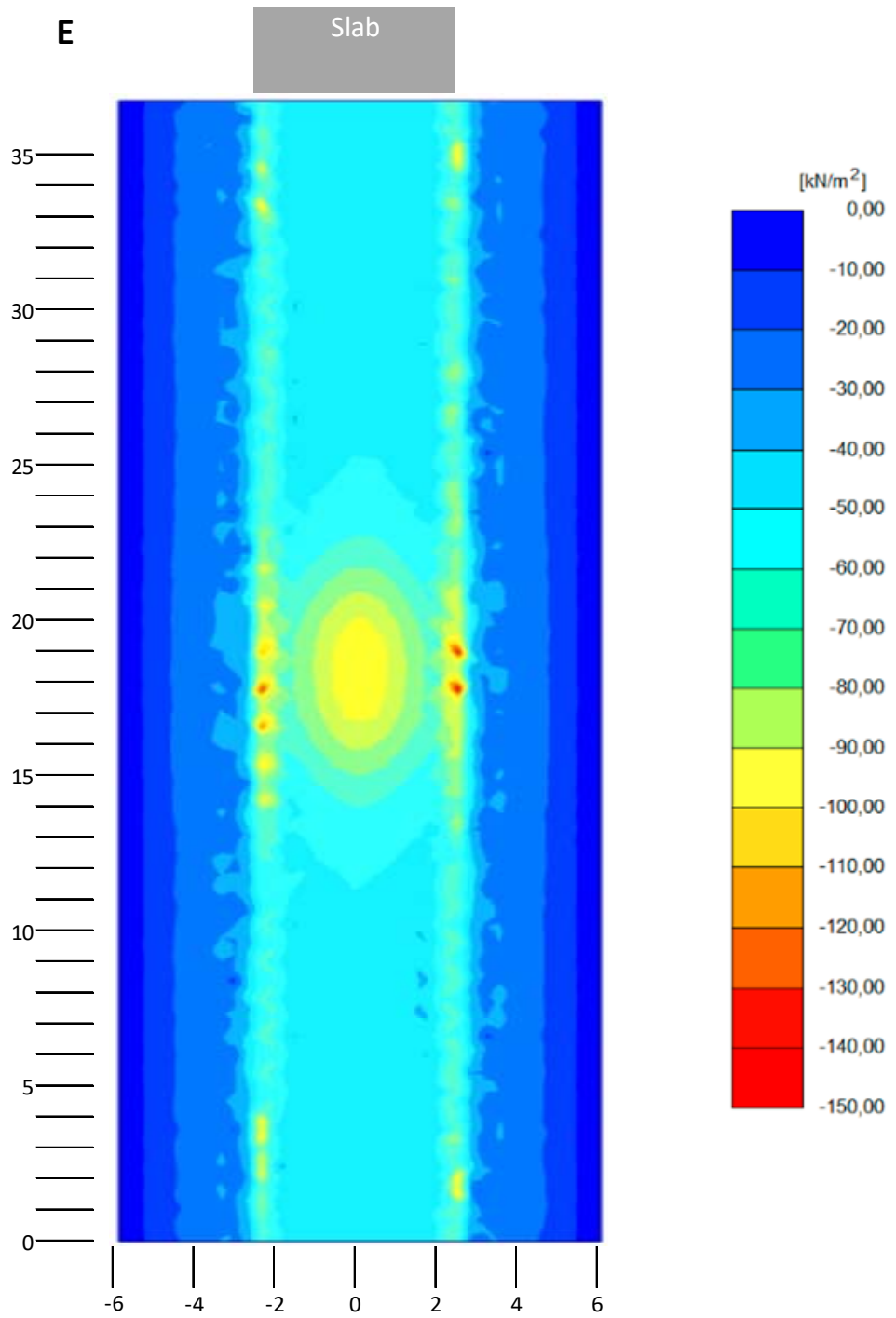


Figure 26. Total vertical stresses, load model E, slab installation depth 2.5 meters, including dynamic load factor 1.25.

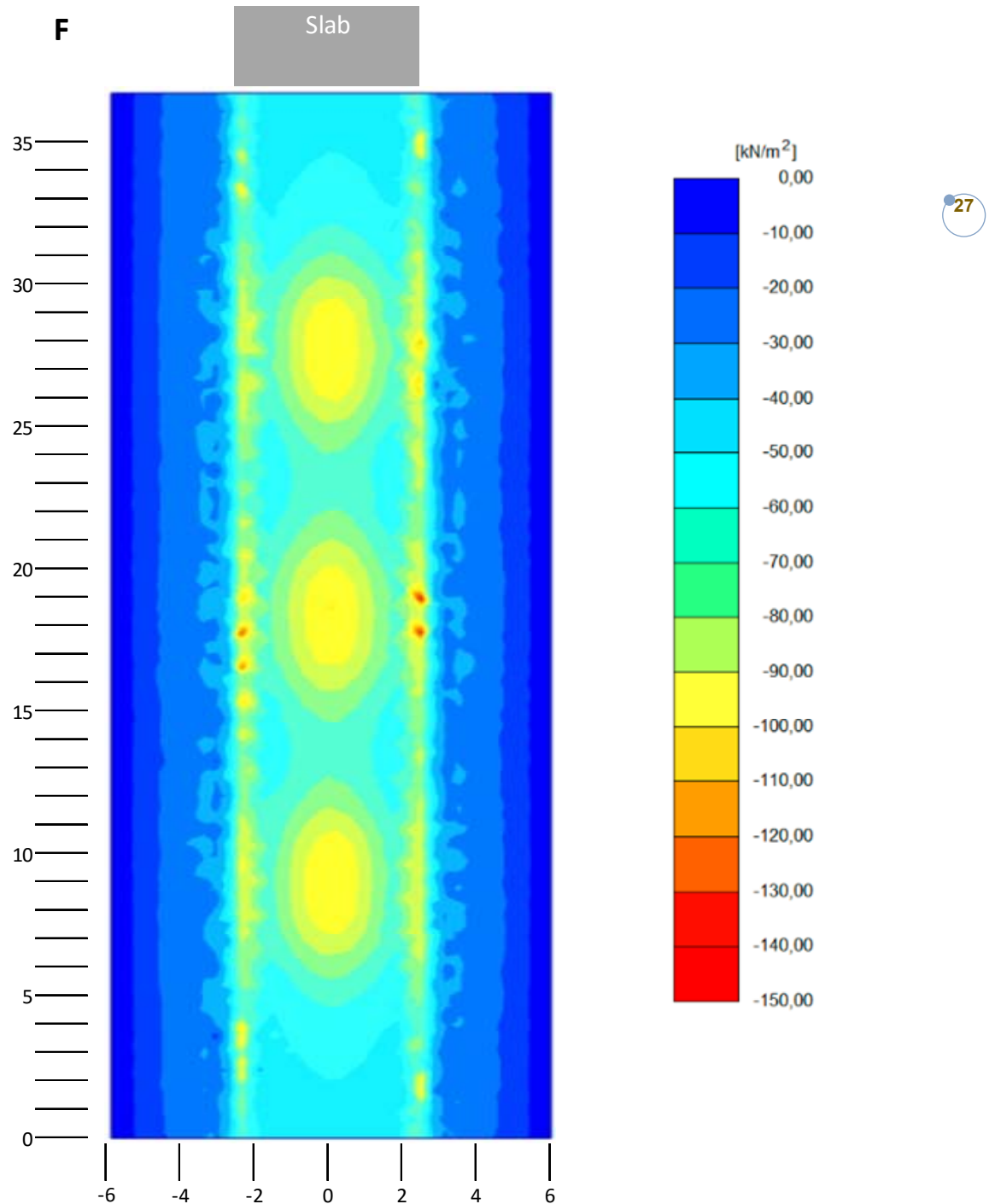


Figure 27. Total vertical stresses, load model F, slab installation depth 2.5 meters, including dynamic load factor 1.25.

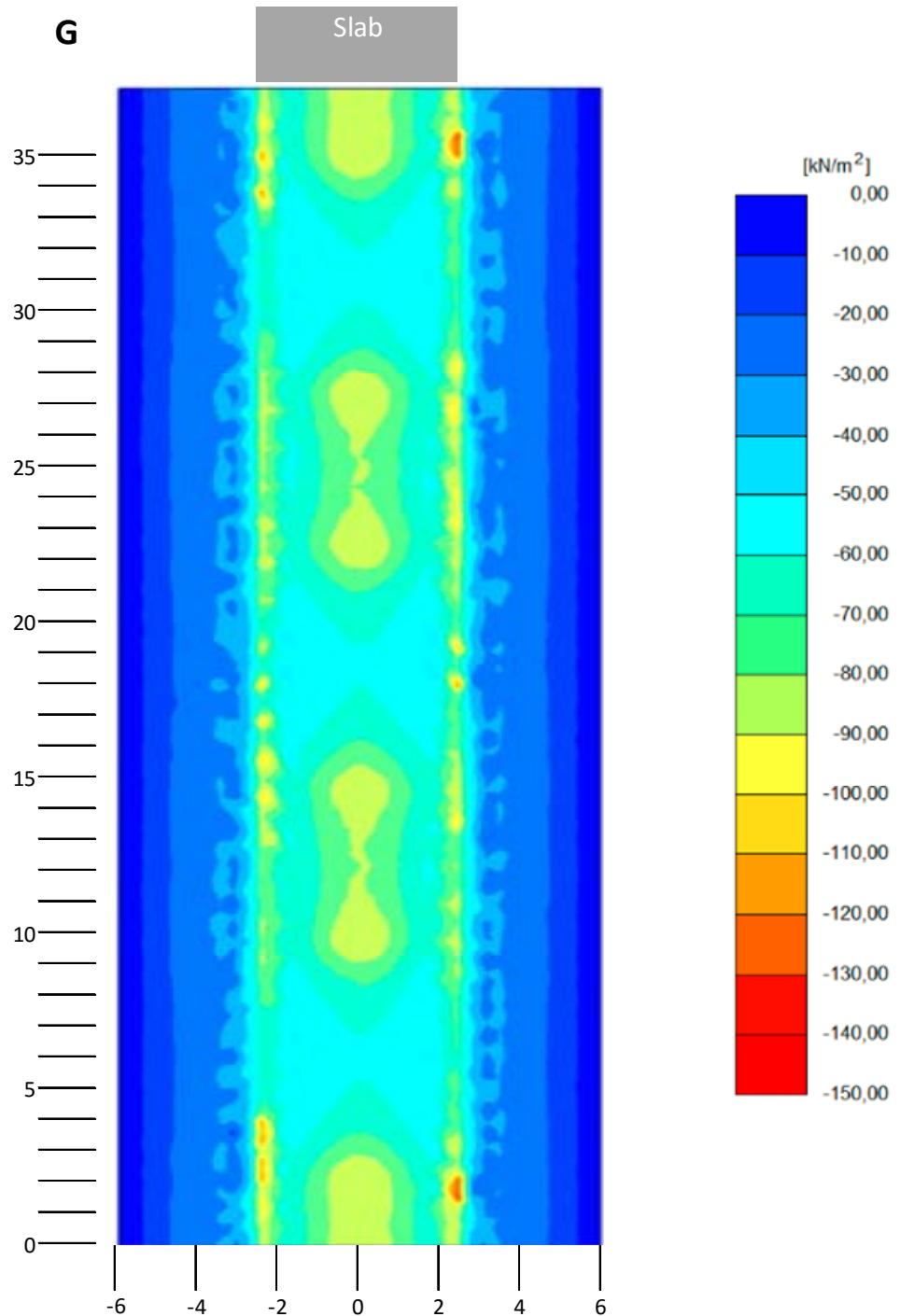


Figure 28. Total vertical stresses, load model G, slab installation depth 2.5 meters, including dynamic load factor 1.25.

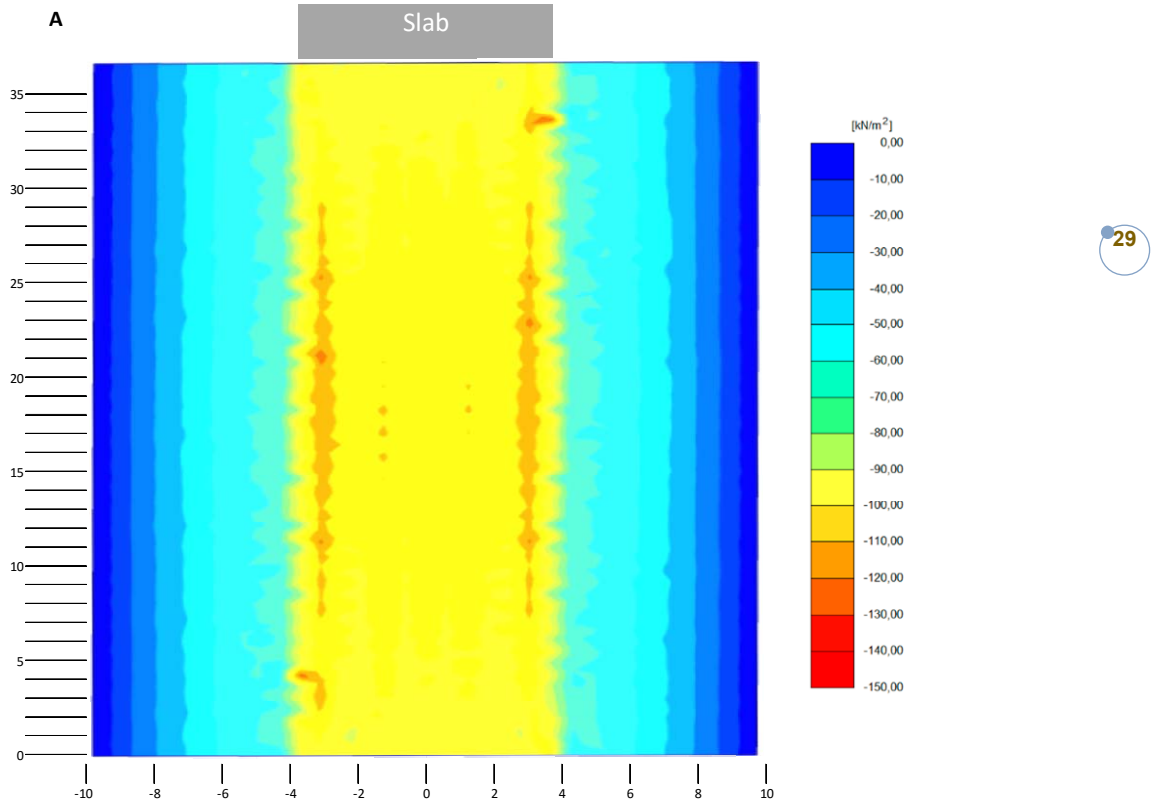


Figure 29. Total vertical stresses, load model A, slab installation depth 5 meters, characteristic load.

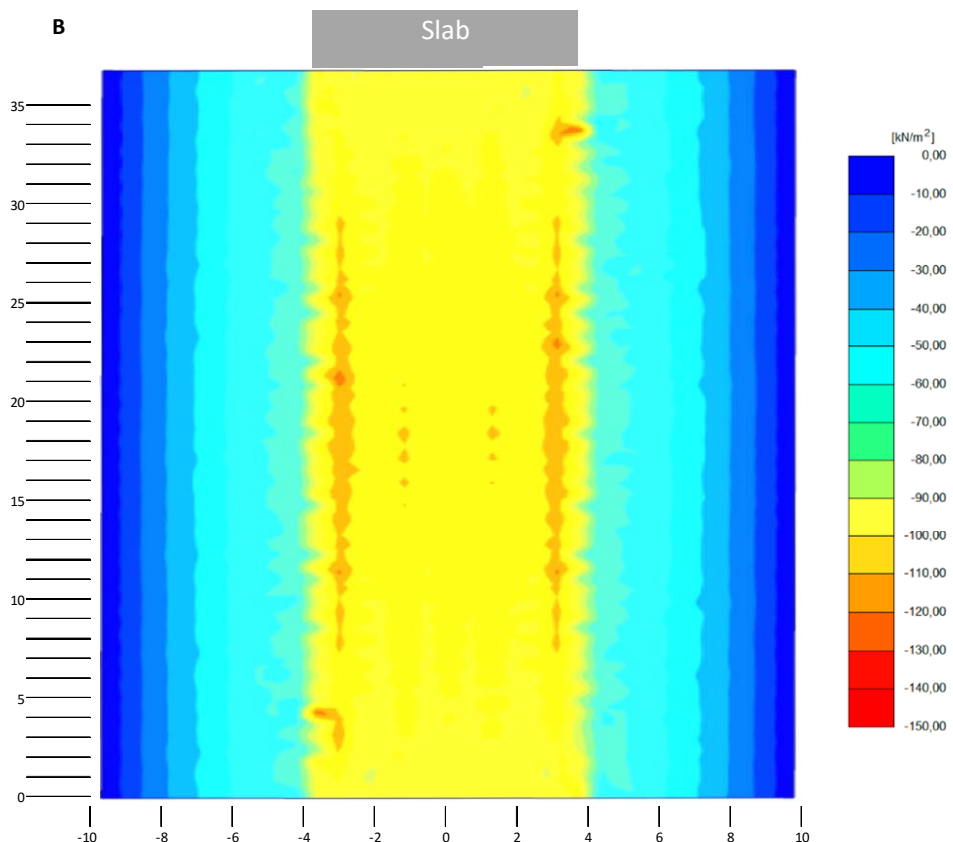


Figure 30. Total vertical stresses, load model B, slab installation depth 5 meters, characteristic load.

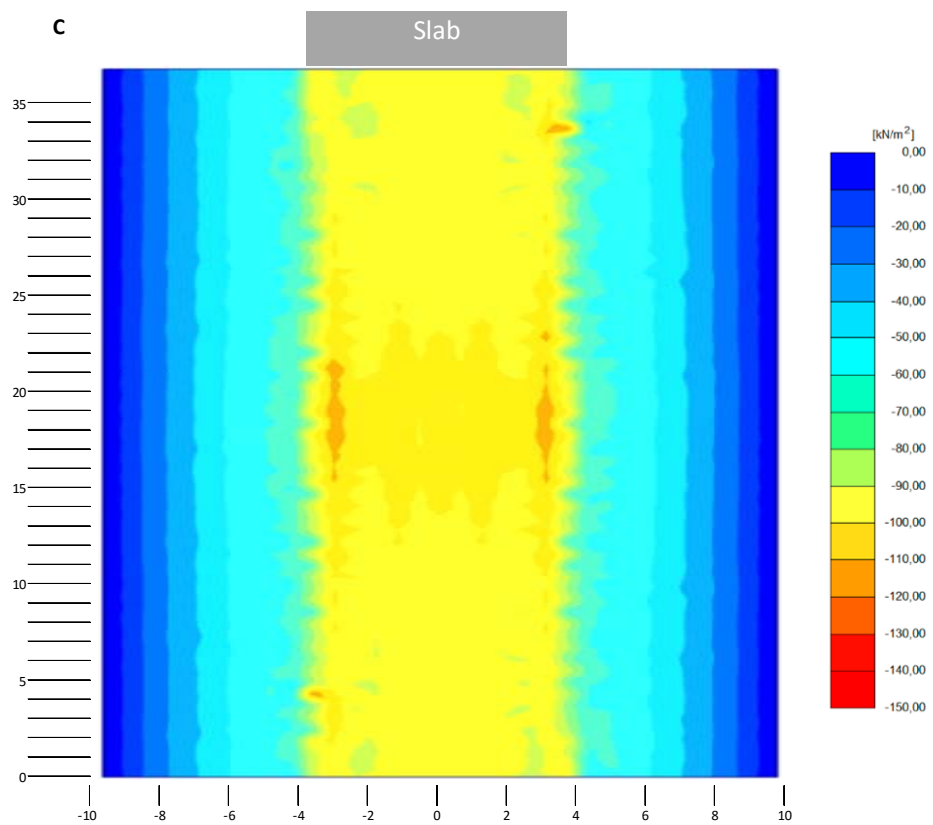


Figure 31. Total vertical stresses, load model C, slab installation depth 5 meters, characteristic load.

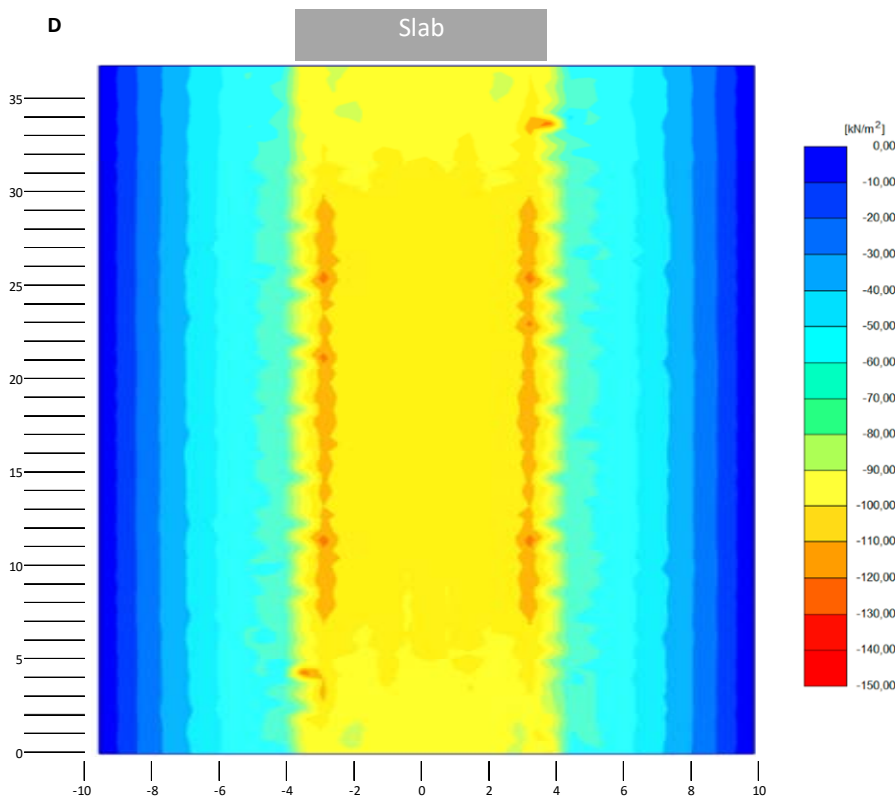


Figure 32. Total vertical stresses, load model D, slab installation depth 5 meters, characteristic load.

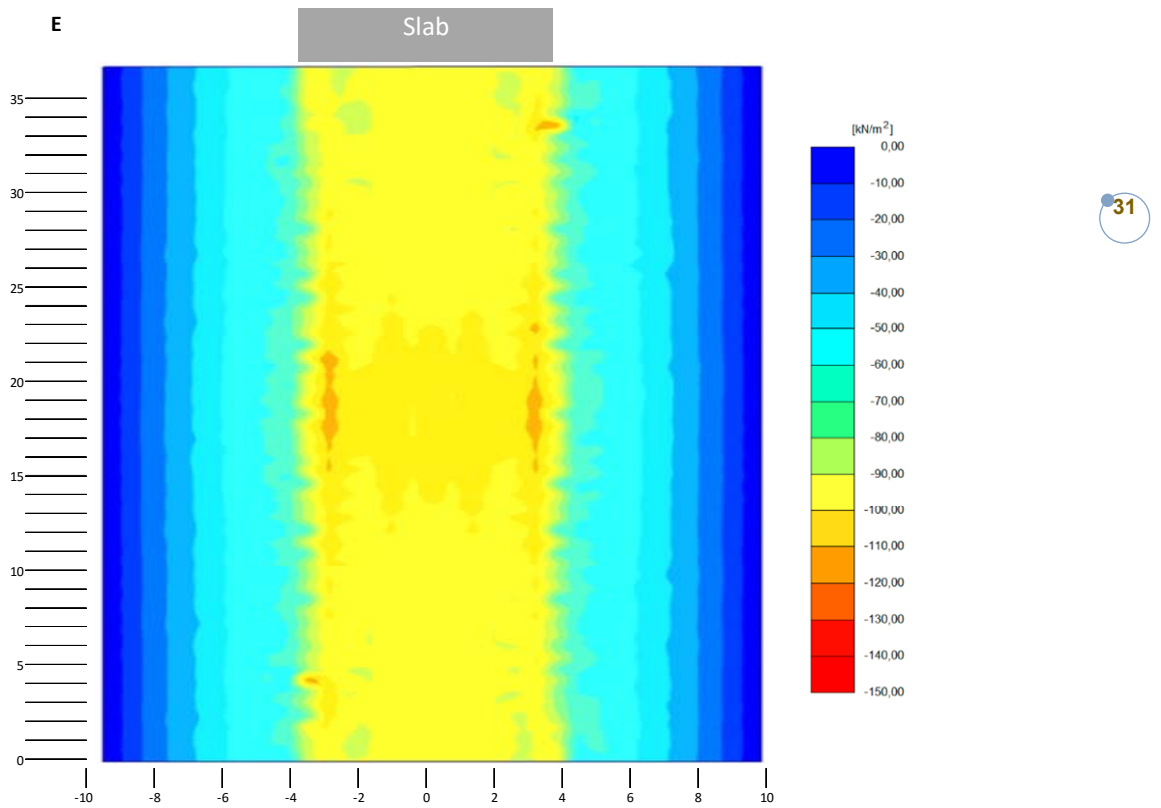


Figure 33. Total vertical stresses, load model E, slab installation depth 5 meters, characteristic load.

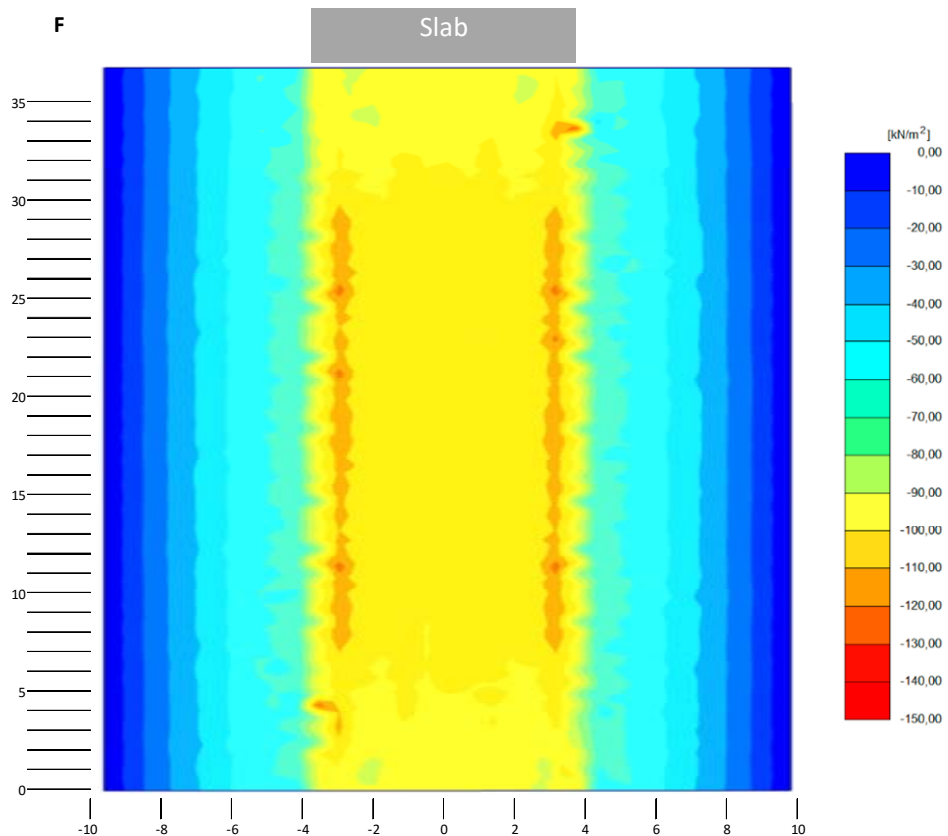


Figure 34. Total vertical stresses, load model F, slab installation depth 5 meters, characteristic load.

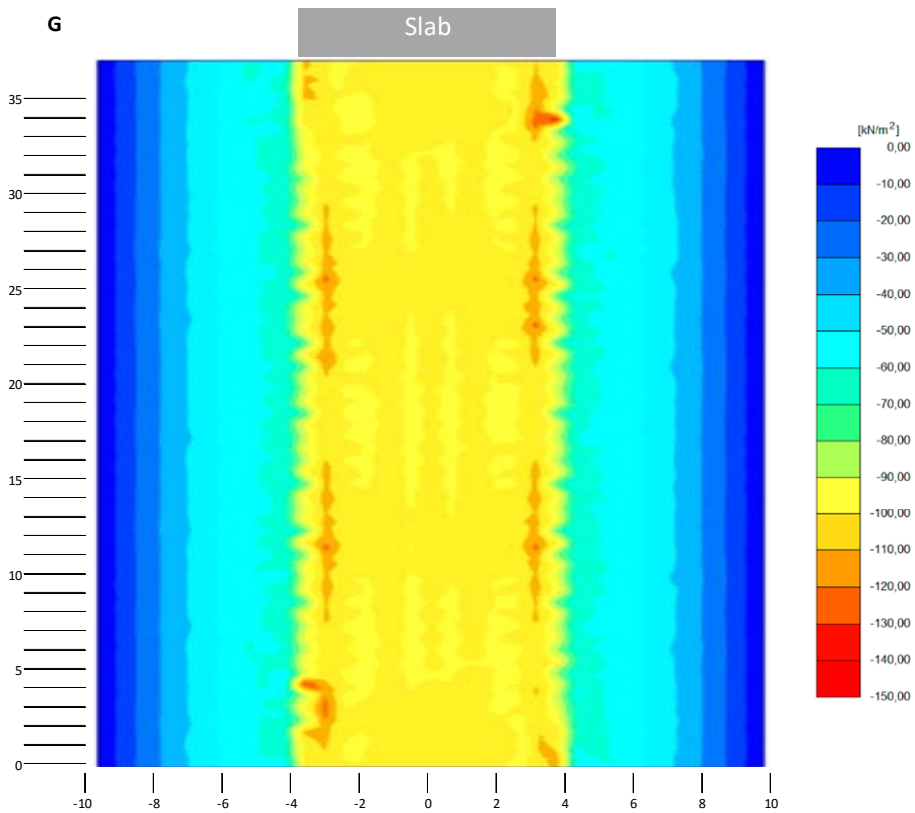


Figure 35. Total vertical stresses, load model G, slab installation depth 5 meters, characteristic load.

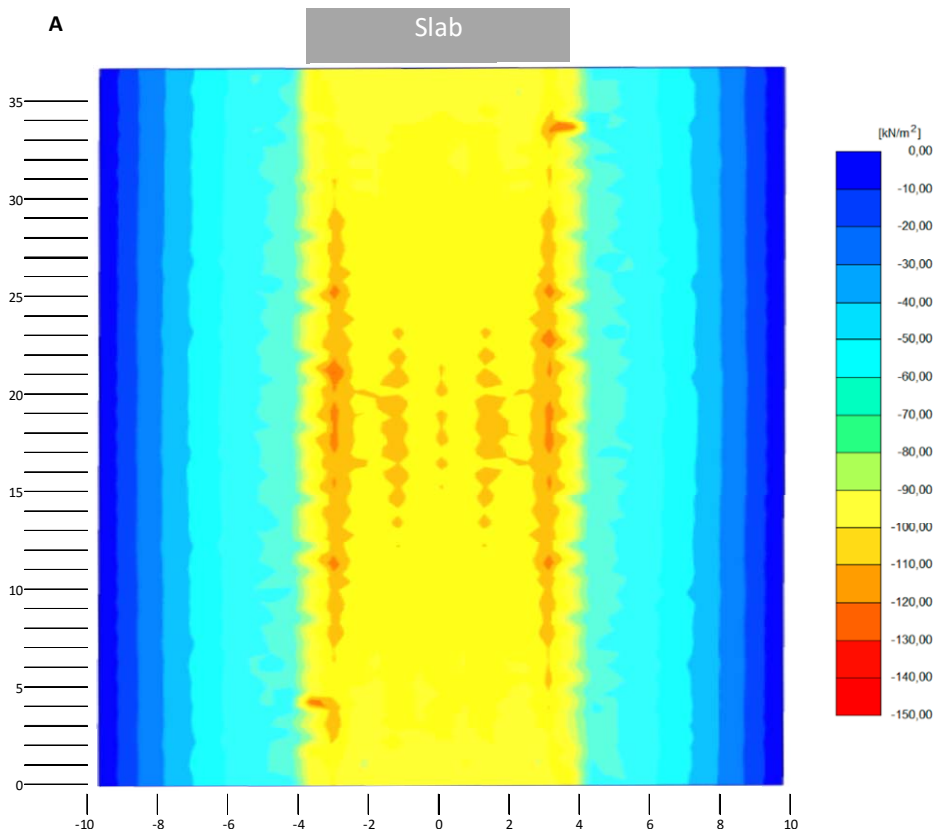


Figure 36. Total vertical stresses, load model A, slab installation depth 5 meters, including dynamic load factor 1.25.

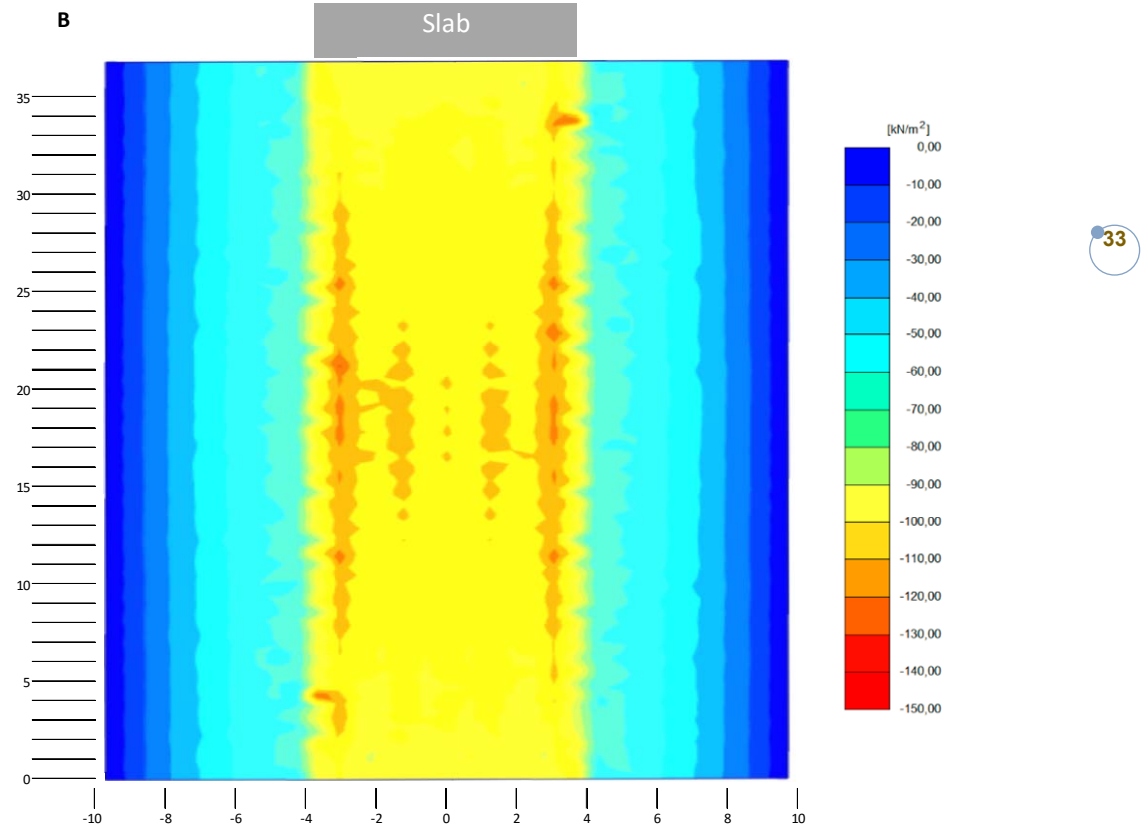


Figure 37. Total vertical stresses, load model B, slab installation depth 5 meters, including dynamic load factor 1.25.

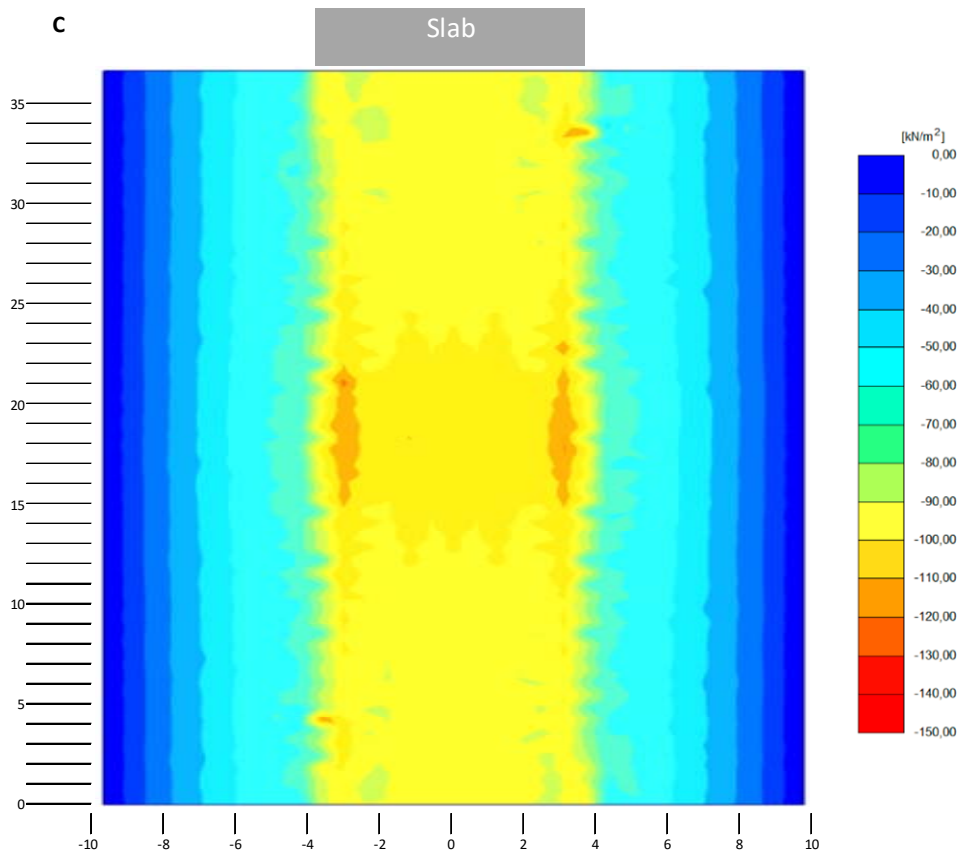


Figure 38. Total vertical stresses, load model C, slab installation depth 5 meters, including dynamic load factor 1.25.

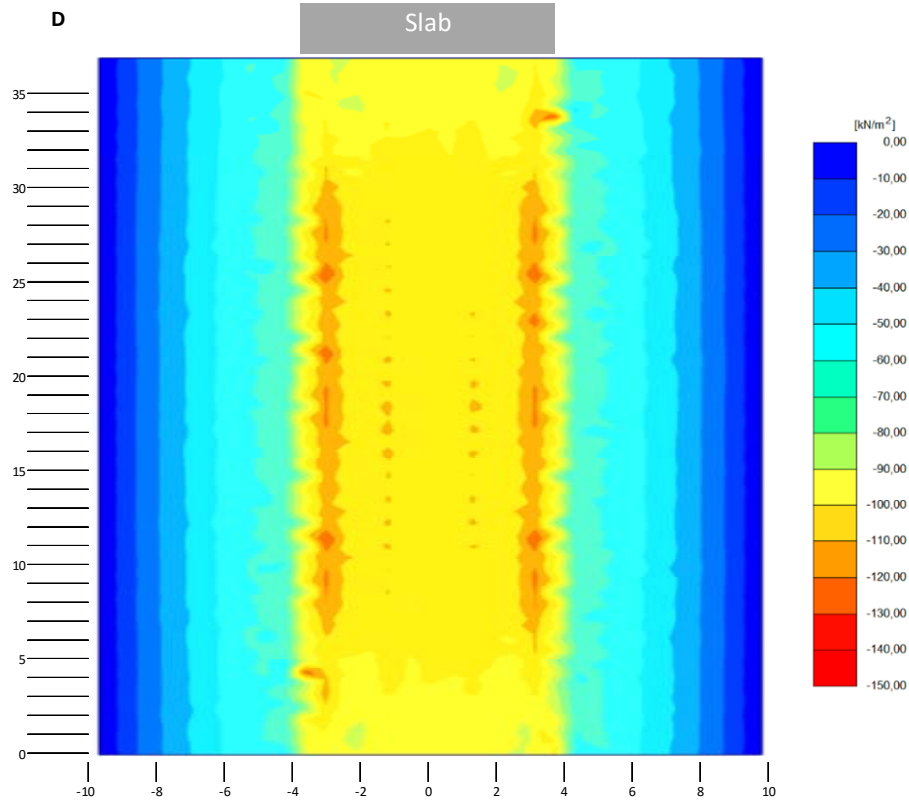


Figure 39. Total vertical stresses, load model D, slab installation depth 5 meters, including dynamic load factor 1.25.

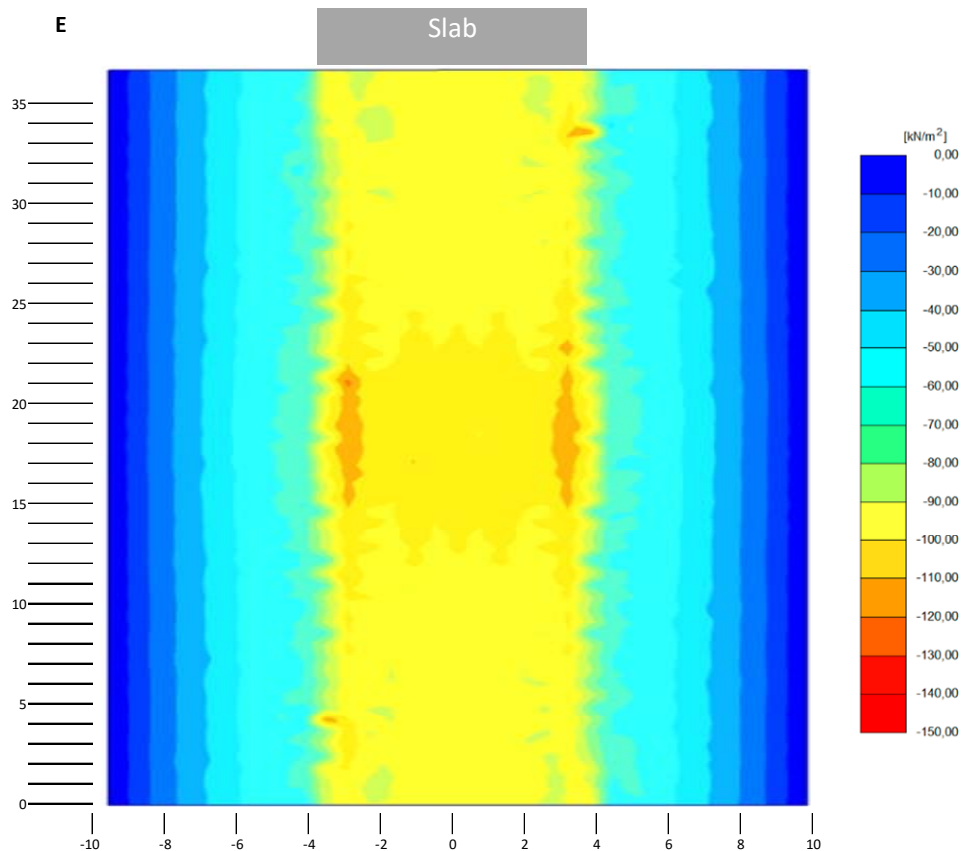


Figure 40. Total vertical stresses, load model E, slab installation depth 5 meters, including dynamic load factor 1.25.

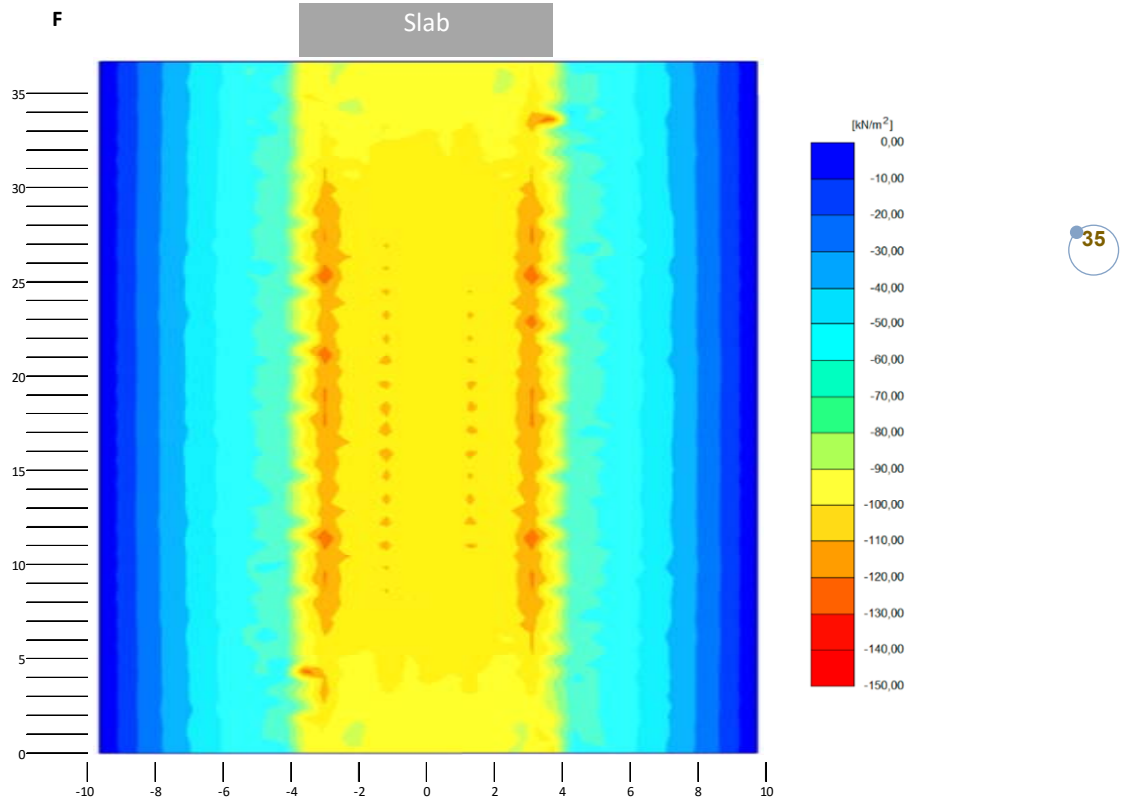


Figure 41. Total vertical stresses, load model F, slab installation depth 5 meters, including dynamic load factor 1.25.

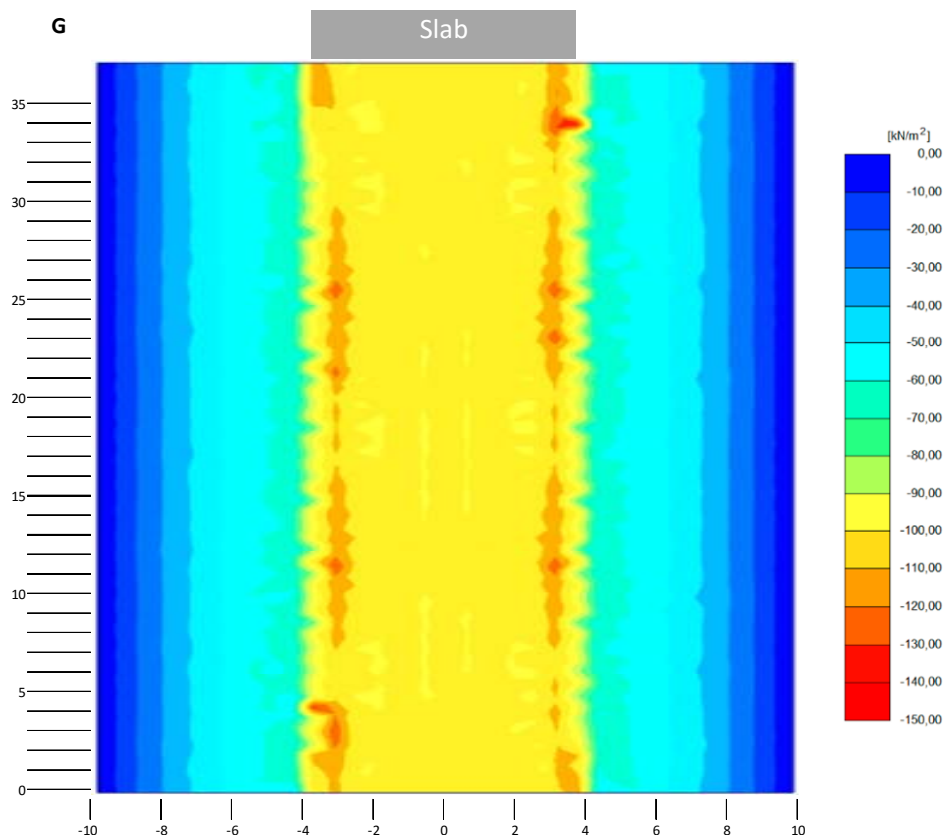


Figure 42. Total vertical stresses, load model F, slab installation depth 5 meters, including dynamic load factor 1.25.

Longitudinal stress planes on top of the slab structure

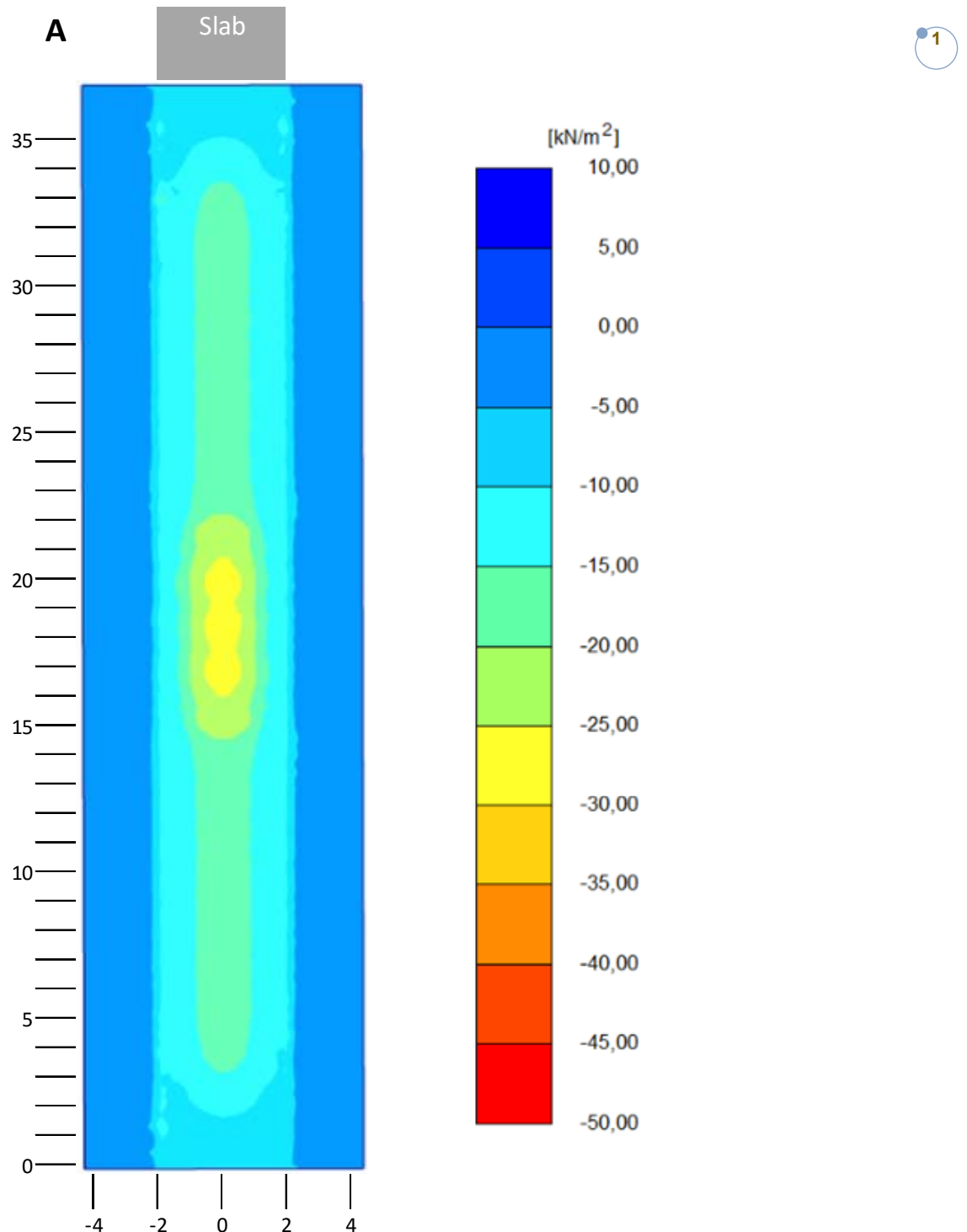


Figure 1. Longitudinal stresses, load model A, slab installation depth 1.4 meters, characteristic load.

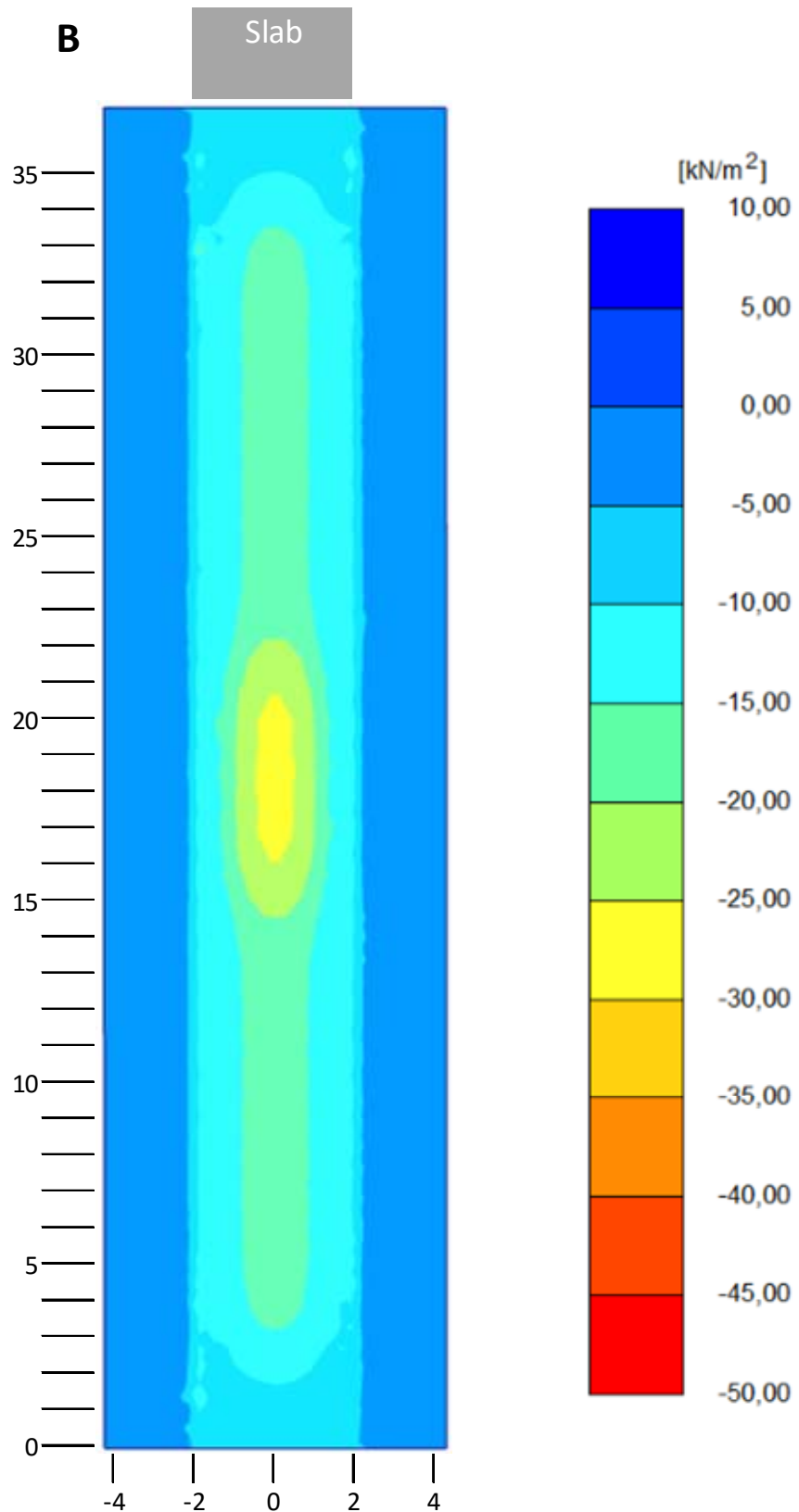


Figure 2. Longitudinal stresses, load model B, slab installation depth 1.4 meters, characteristic load.

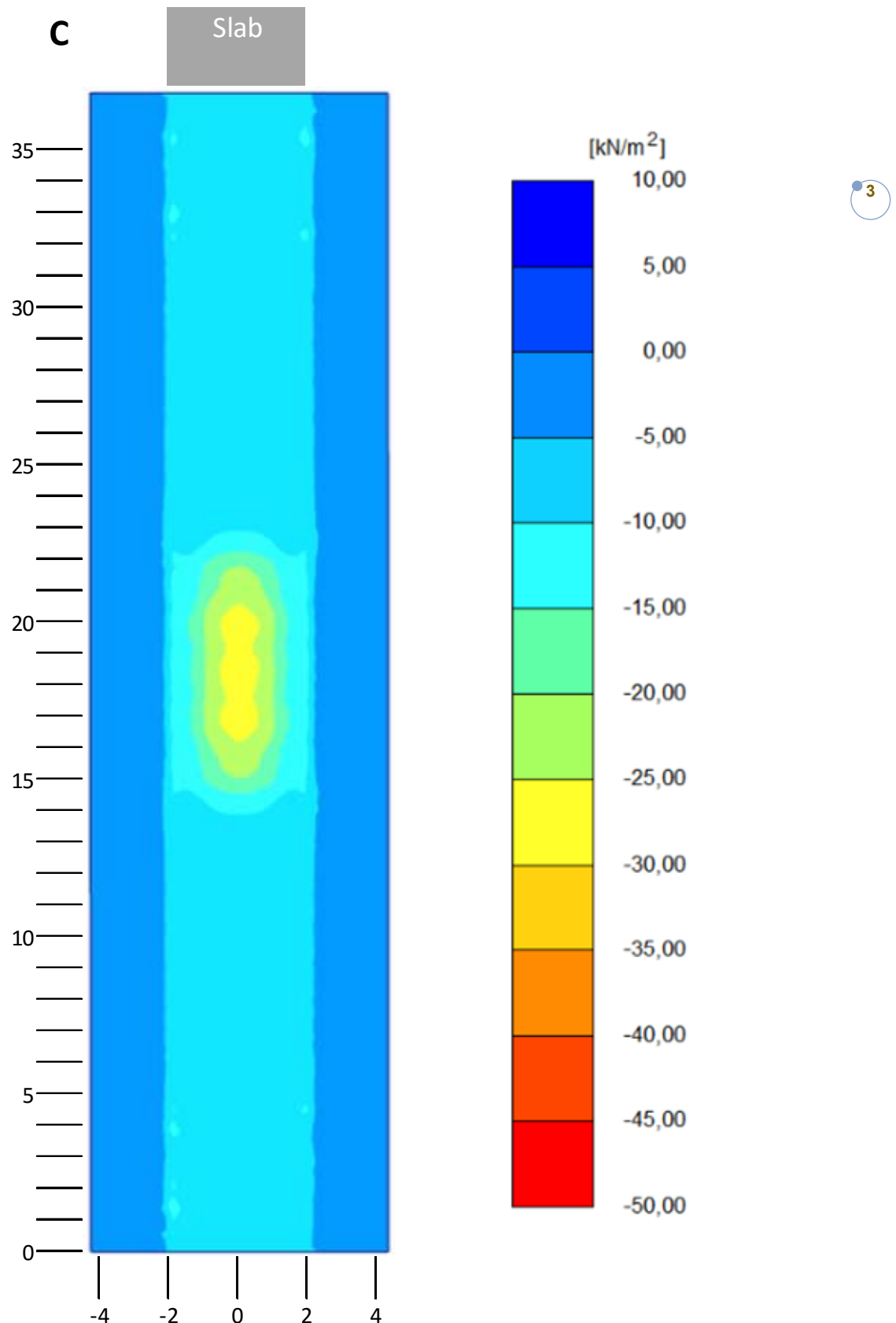


Figure 3. Longitudinal stresses, load model C, slab installation depth 1.4 meters, characteristic load.

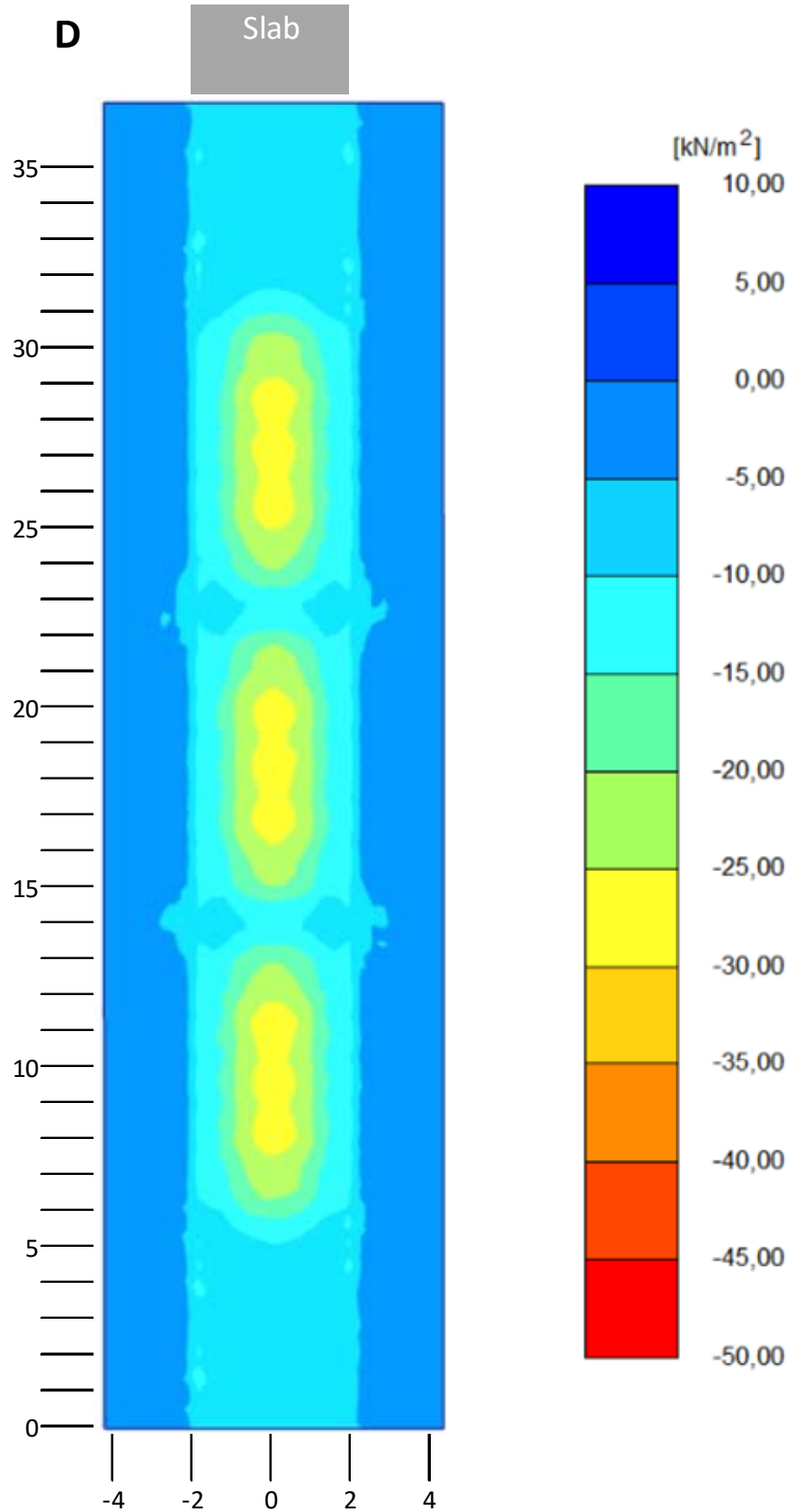


Figure 4. Longitudinal stresses, load model D, slab installation depth 1.4 meters, characteristic load.

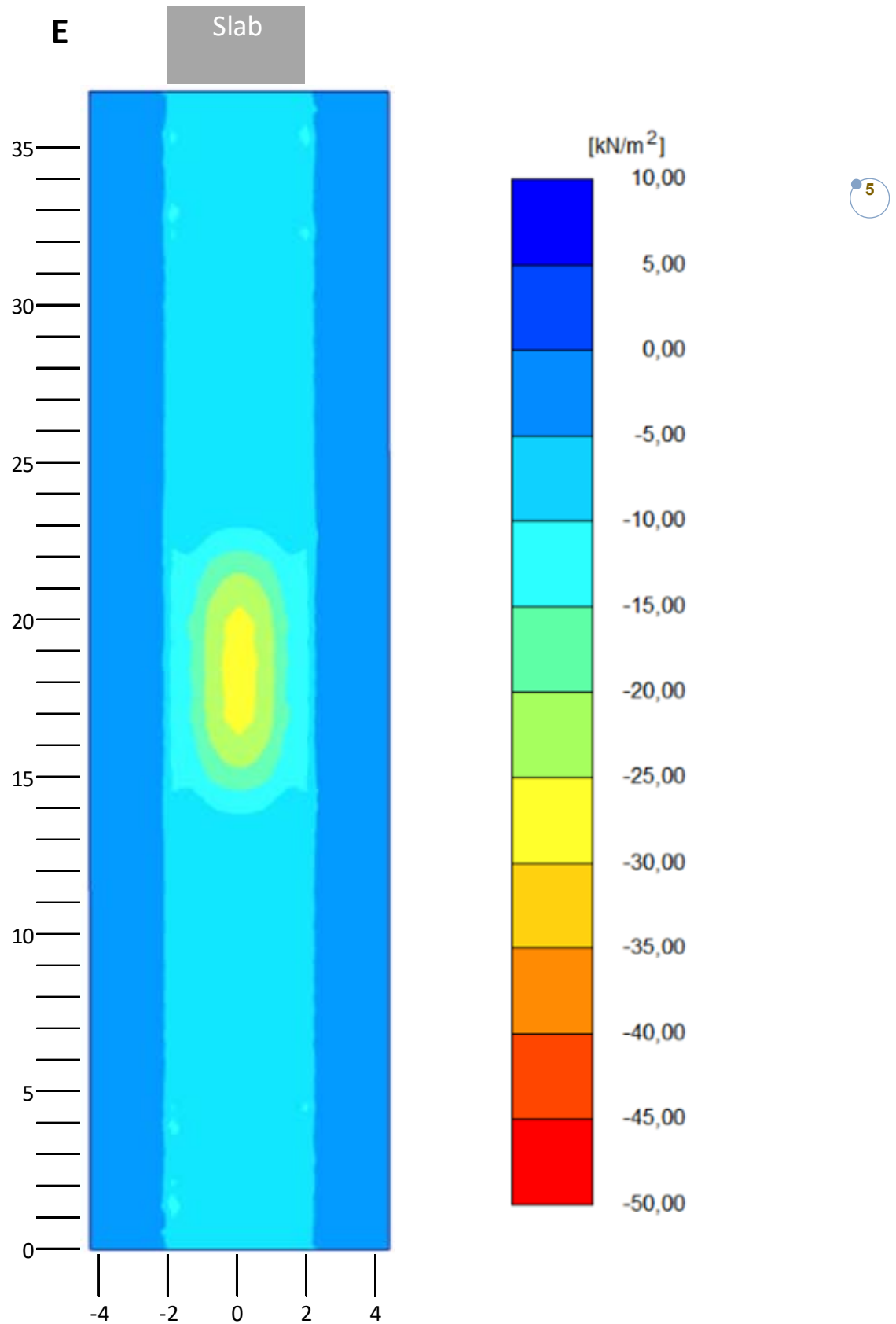


Figure 5. Longitudinal stresses, load model E, slab installation depth 1.4 meters, characteristic load.

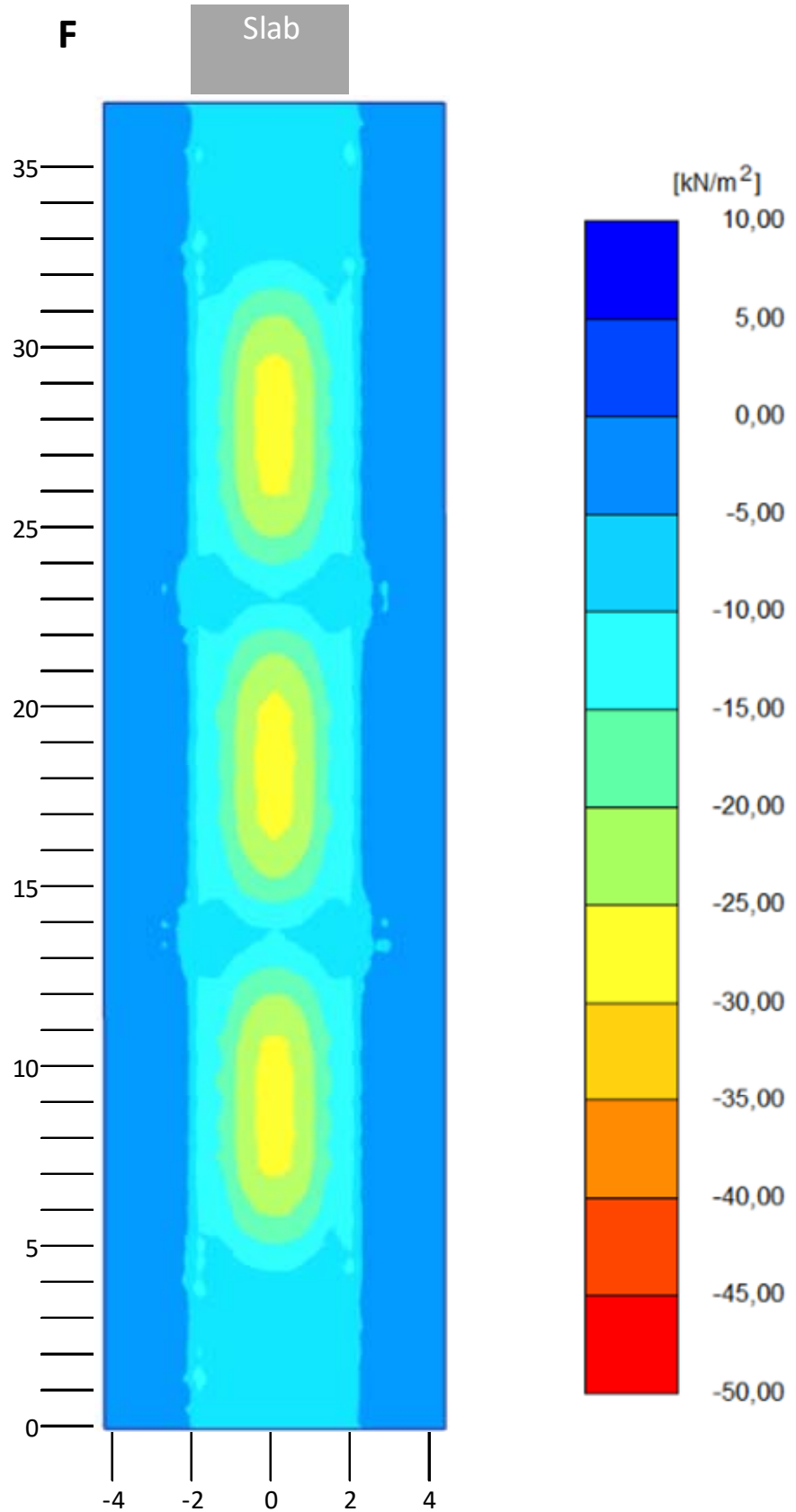


Figure 6. Longitudinal stresses, load model F, slab installation depth 1.4 meters, characteristic load.

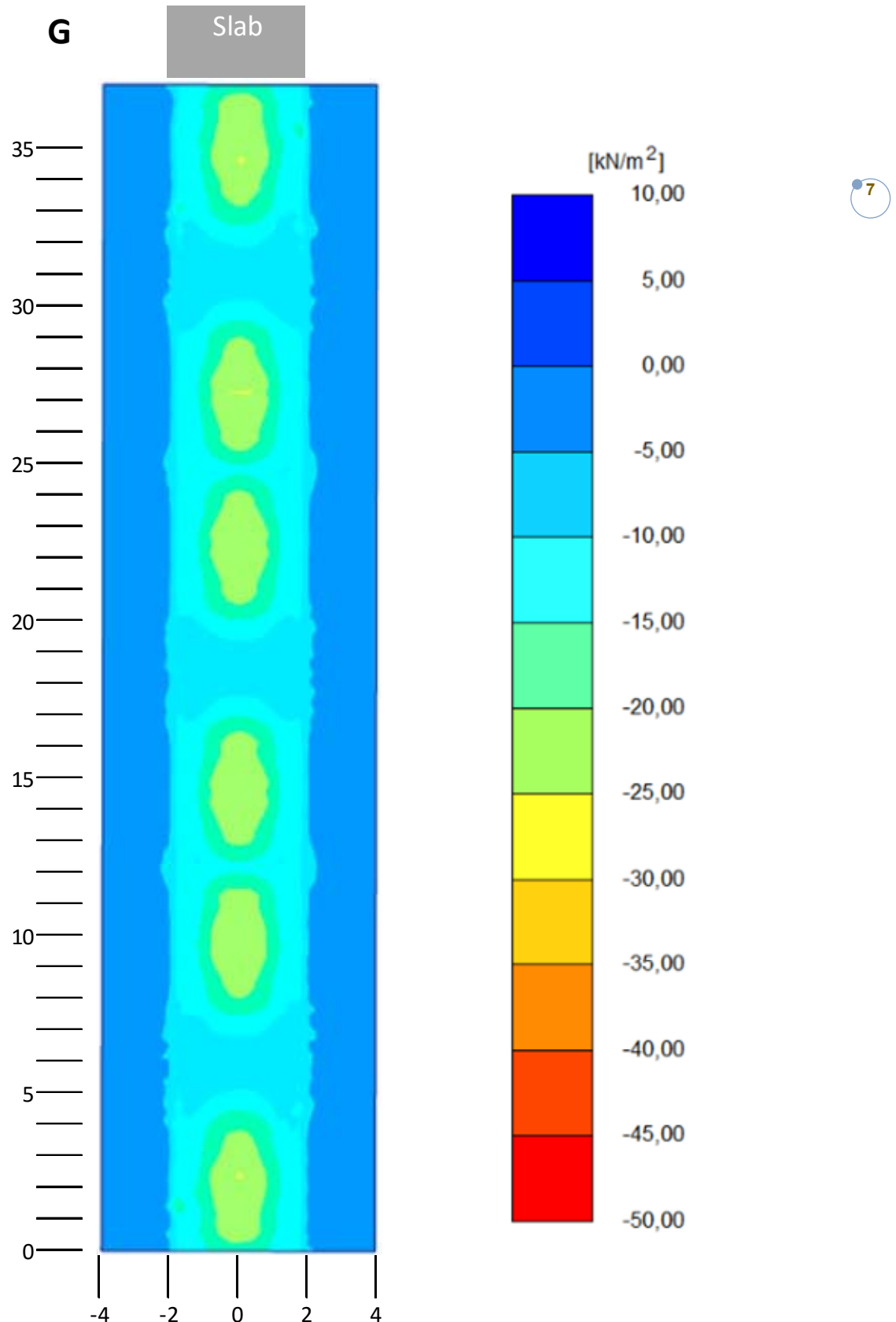


Figure 7. Longitudinal stresses, load model G, slab installation depth 1.4 meters, characteristic load.

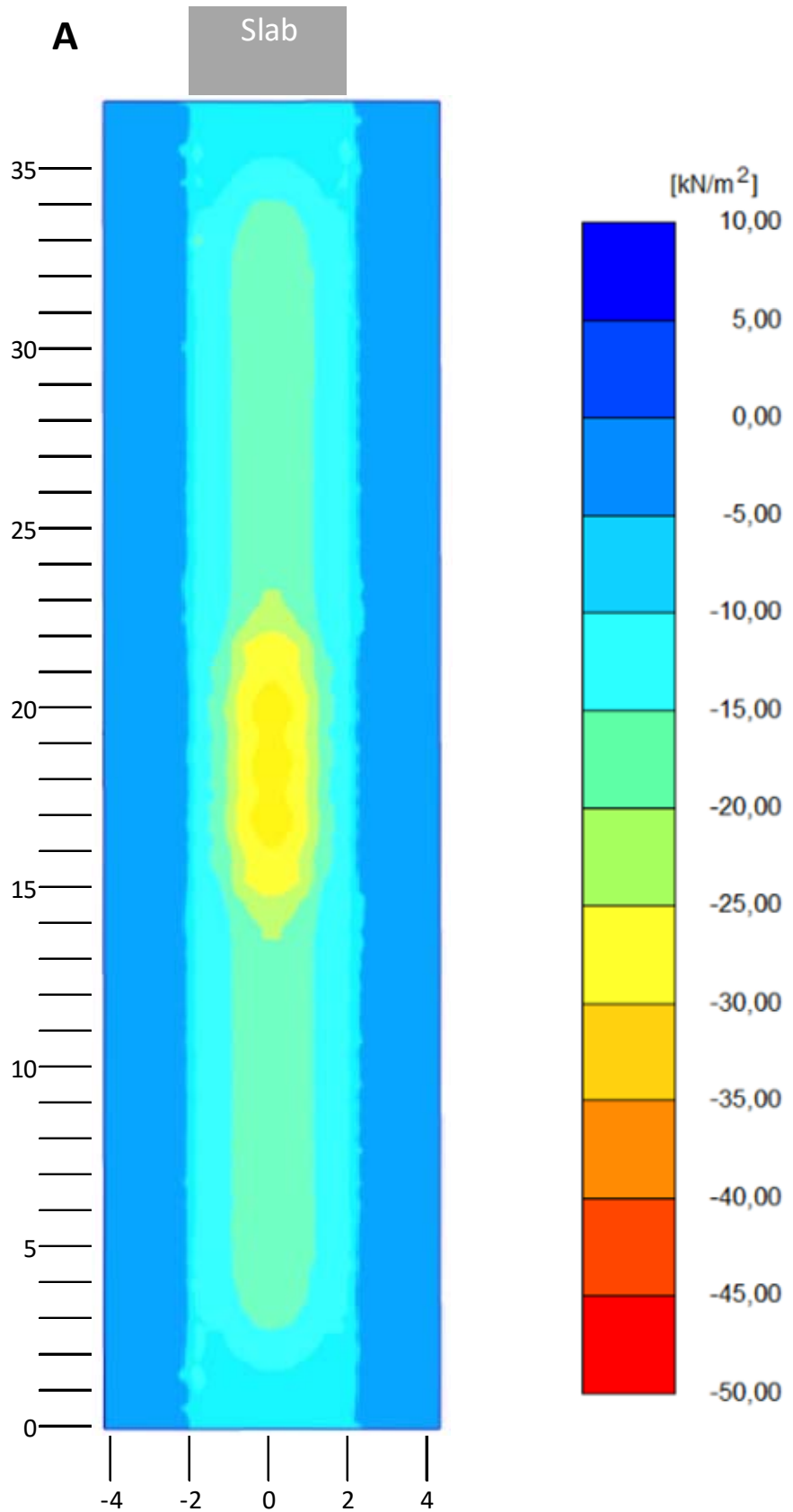


Figure 8. Longitudinal stresses, load model A, slab installation depth 1.4 meters, including dynamic load factor 1.25.

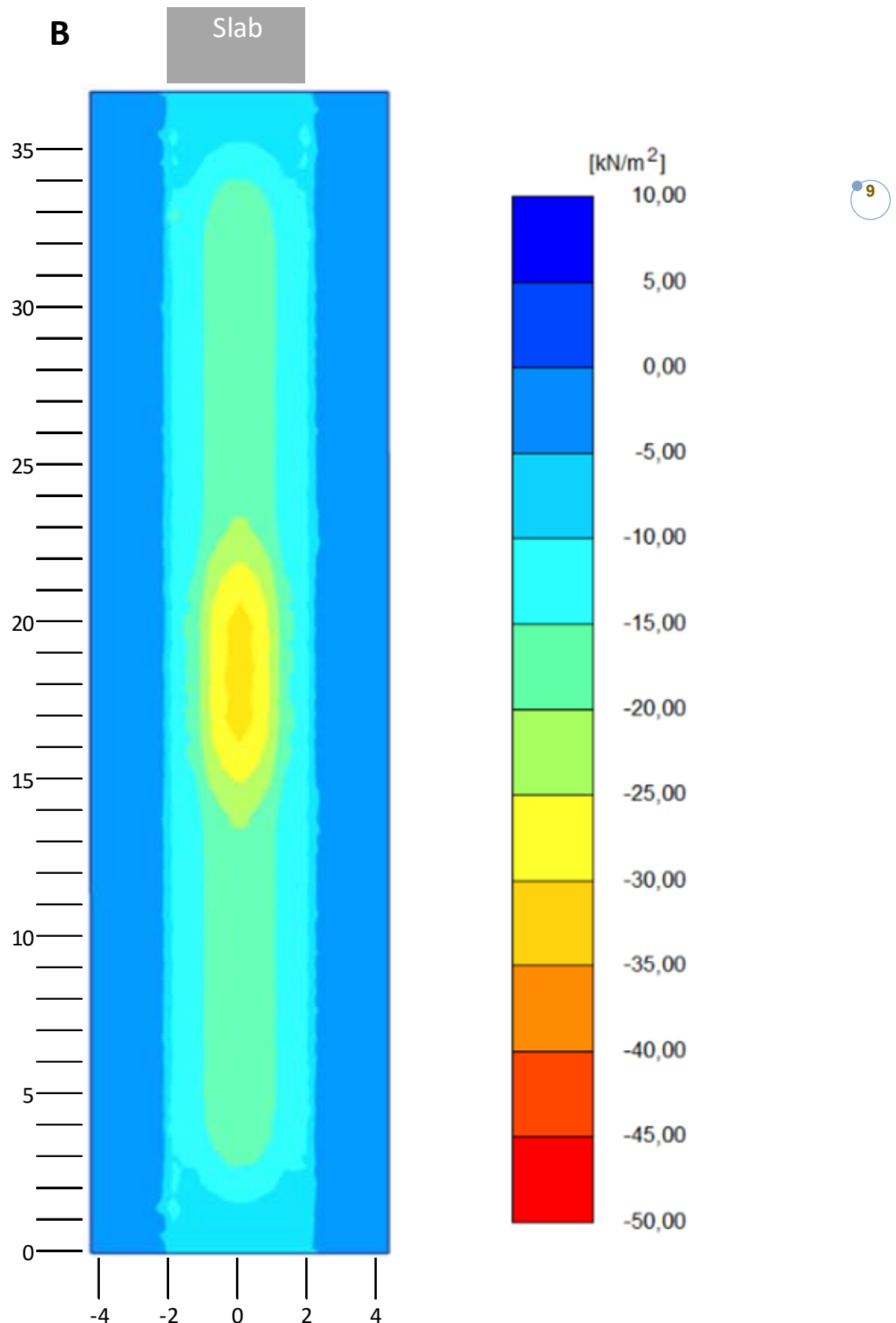


Figure 9. Longitudinal stresses, load model B, slab installation depth 1.4 meters, including dynamic load factor 1.25.

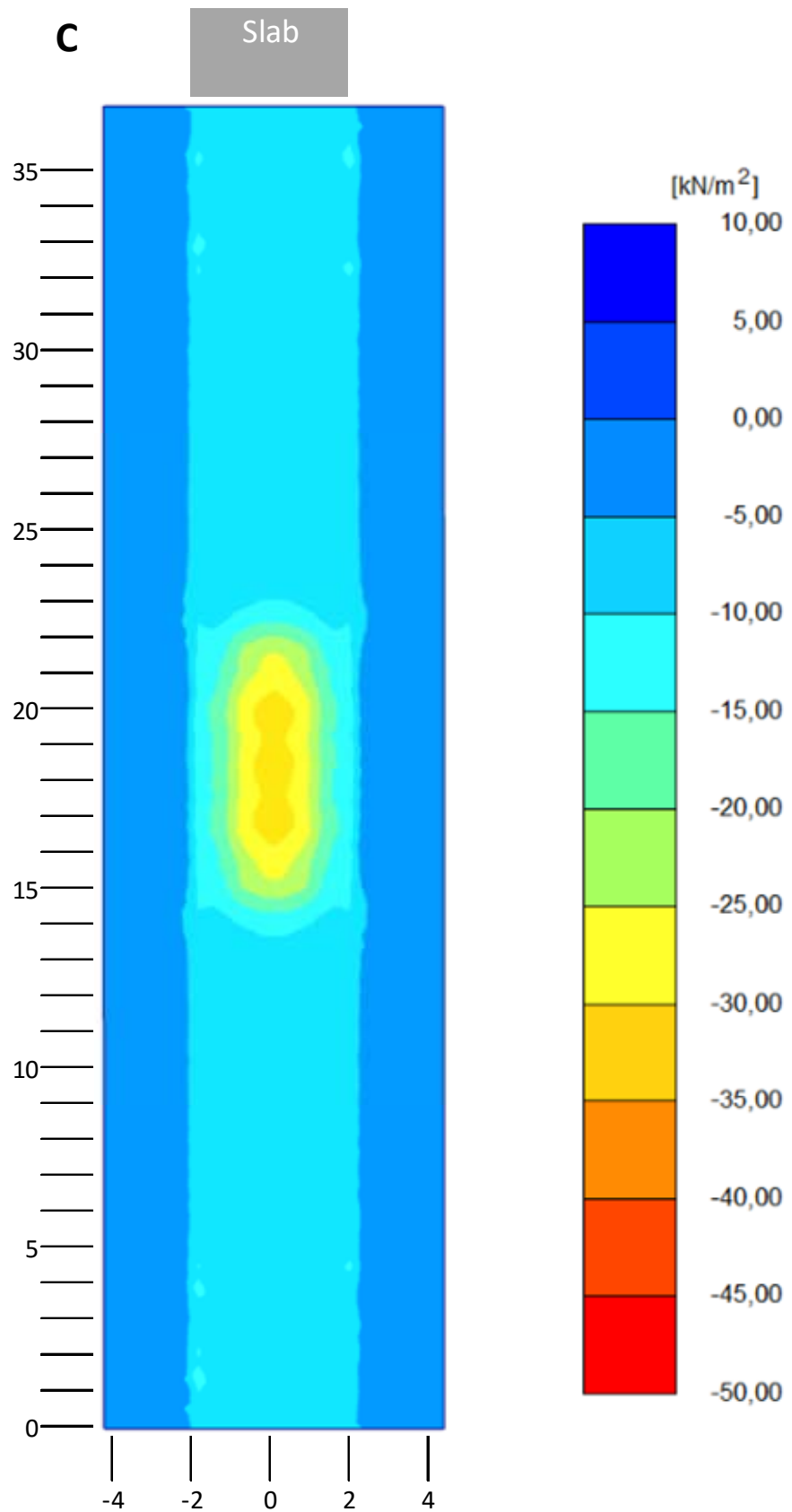


Figure 10. Longitudinal stresses, load model C, slab installation depth 1.4 meters, including dynamic load factor 1.25.

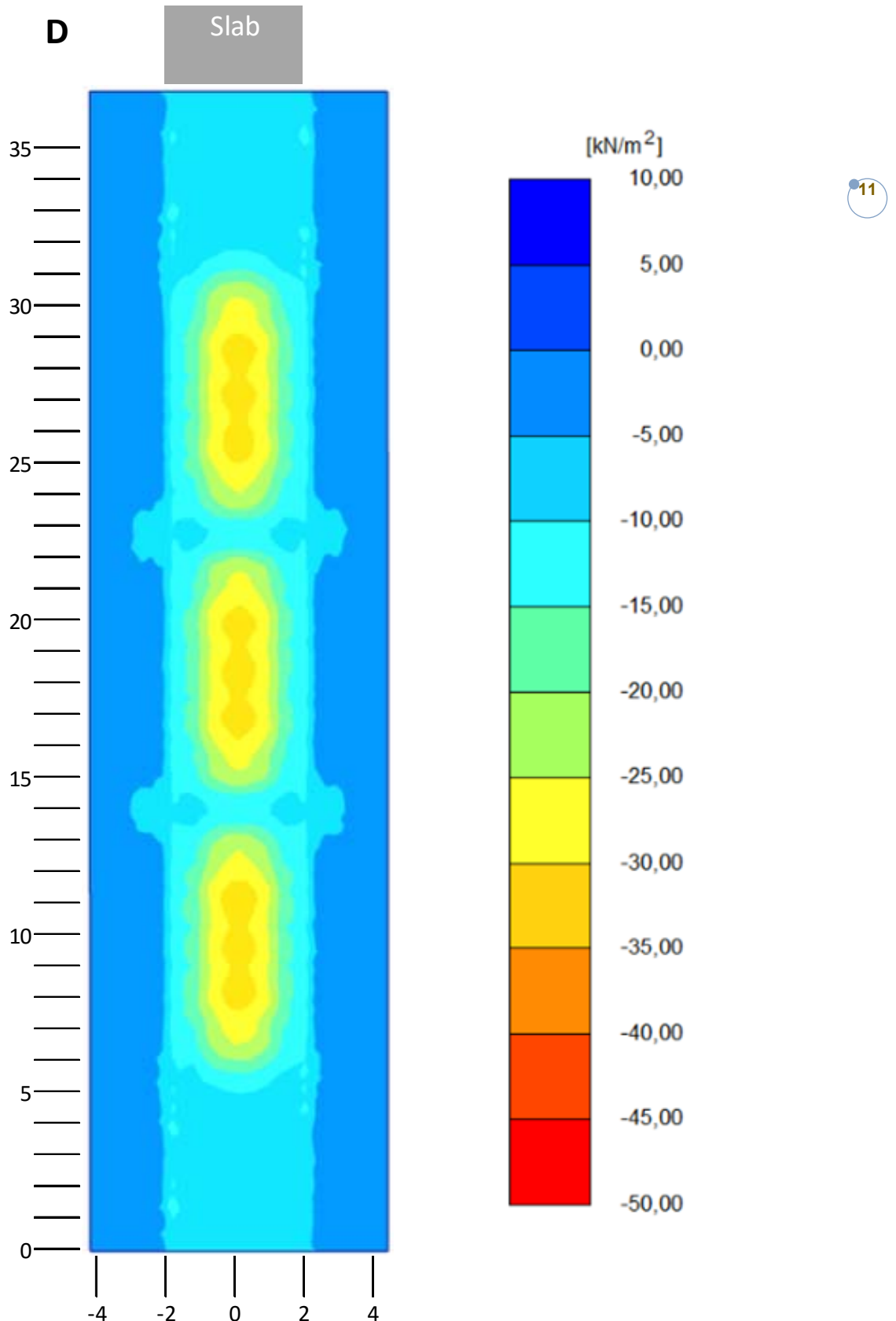


Figure 11. Longitudinal stresses, load model D, slab installation depth 1.4 meters, including dynamic load factor 1.25.

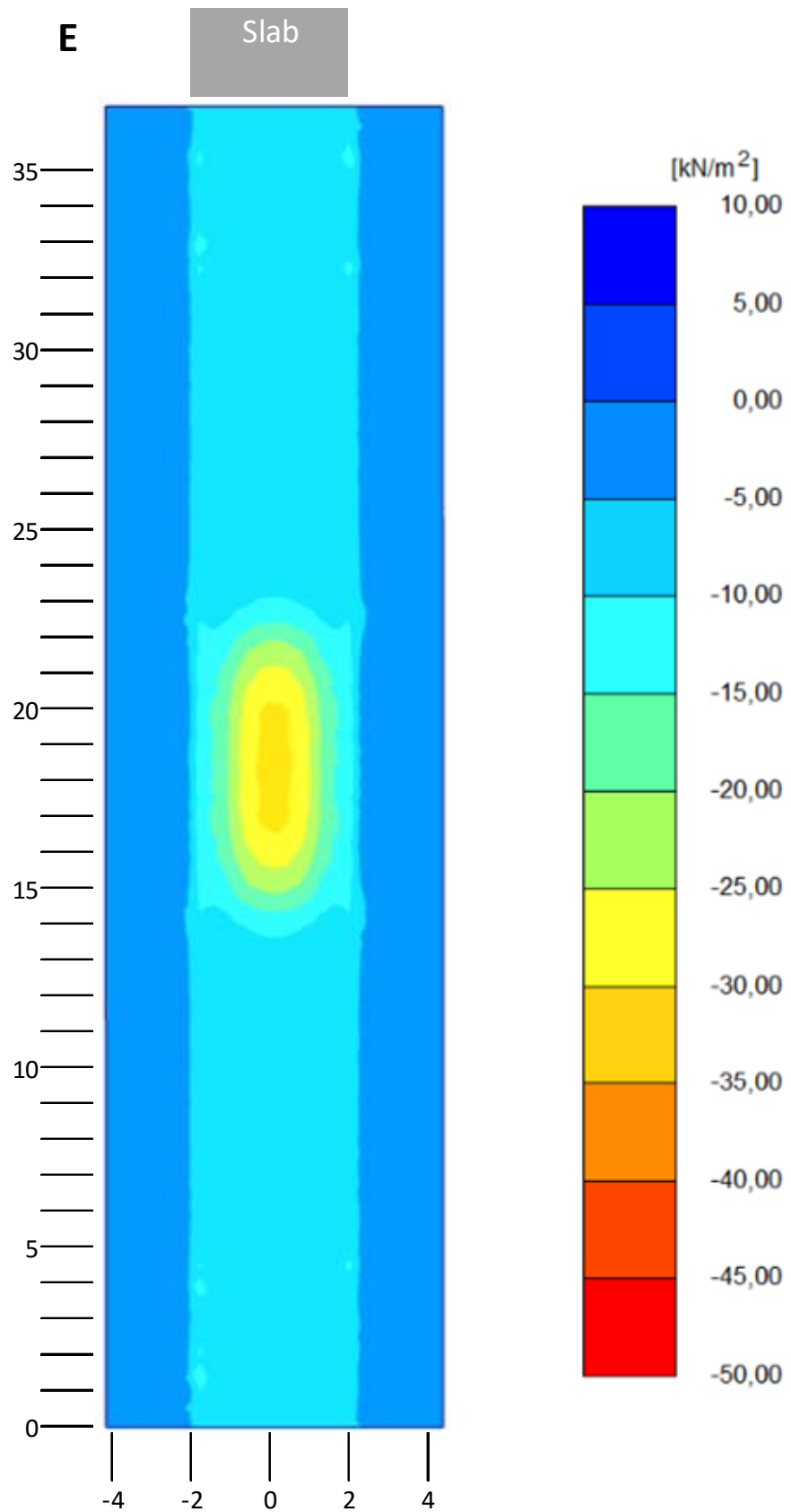


Figure 12. Longitudinal stresses, load model E, slab installation depth 1.4 meters, including dynamic load factor 1.25.

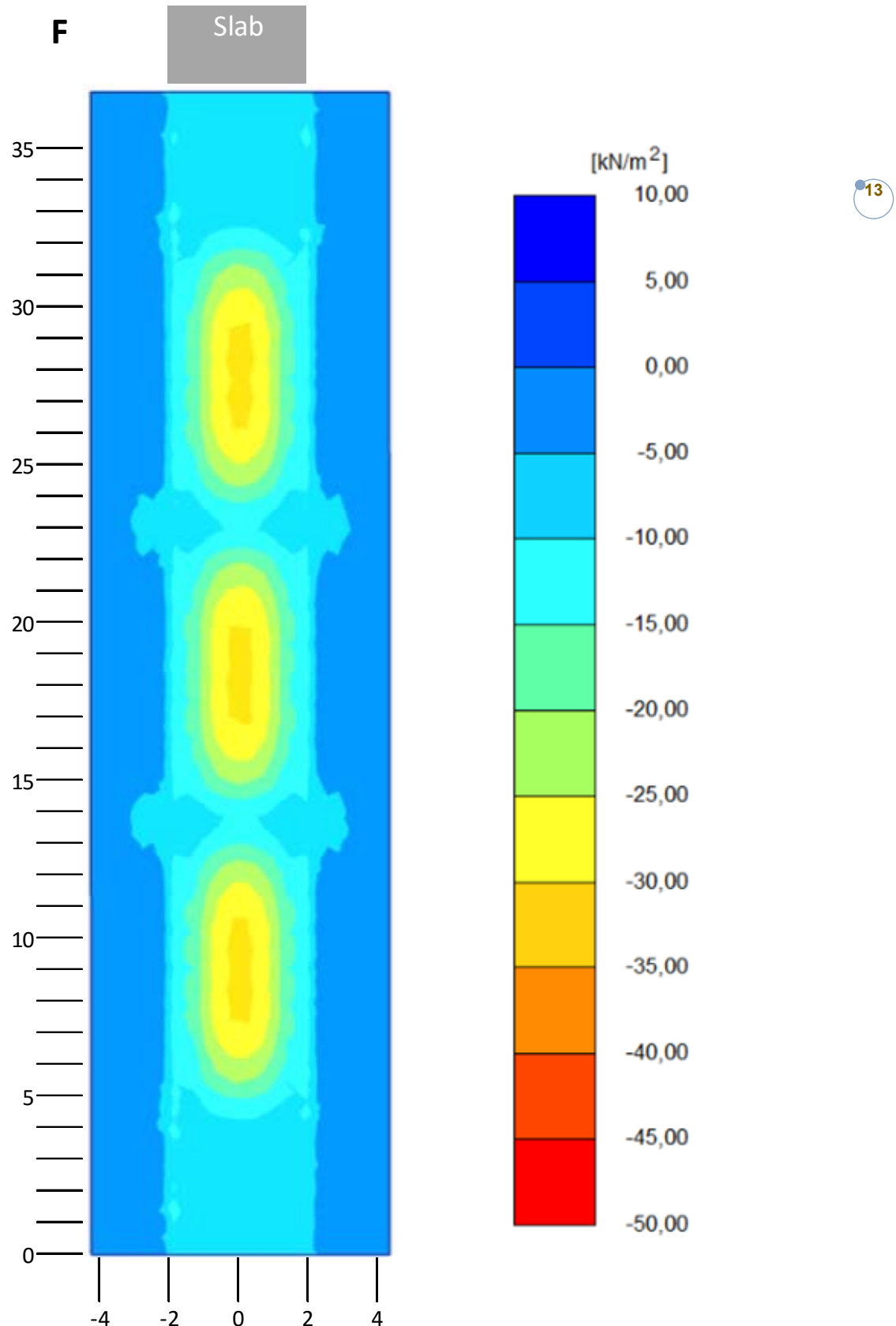


Figure 13. Longitudinal stresses, load model F, slab installation depth 1.4 meters, including dynamic load factor 1.25.

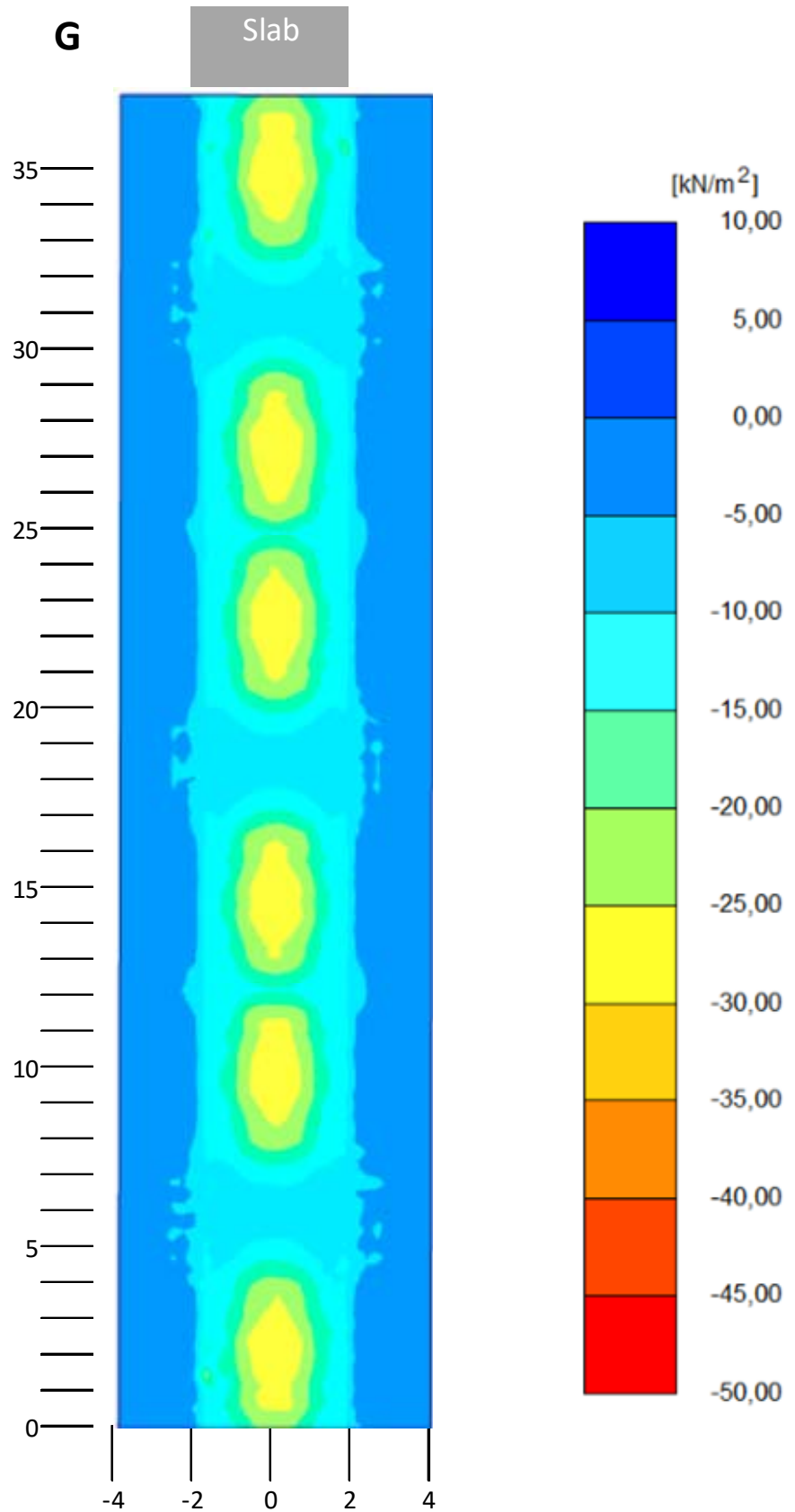


Figure 14. Longitudinal stresses, load model G, slab installation depth 1.4 meters, including dynamic load factor 1.25.

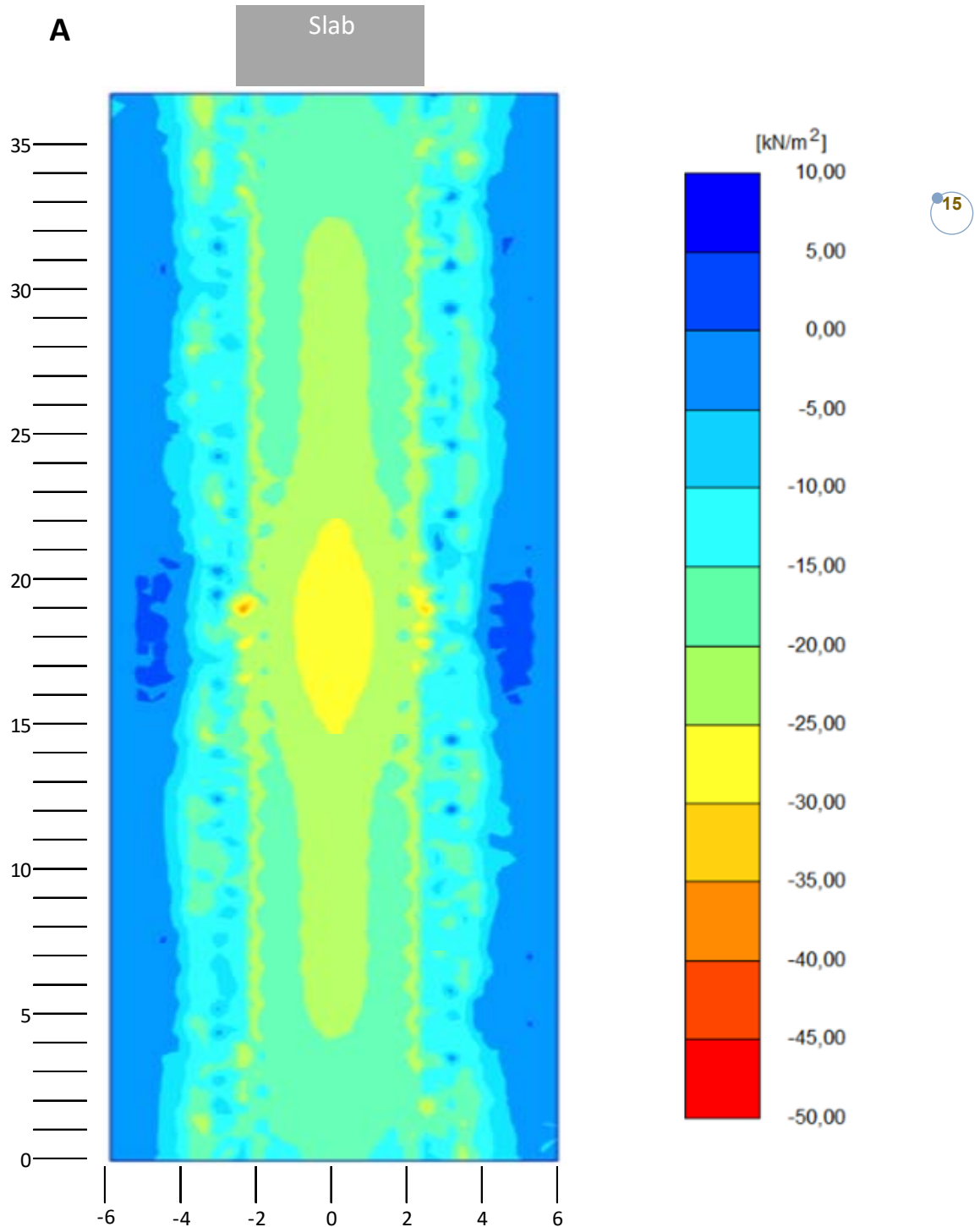


Figure 15. Longitudinal stresses, load model A, slab installation depth 2.5 meters, characteristic load.

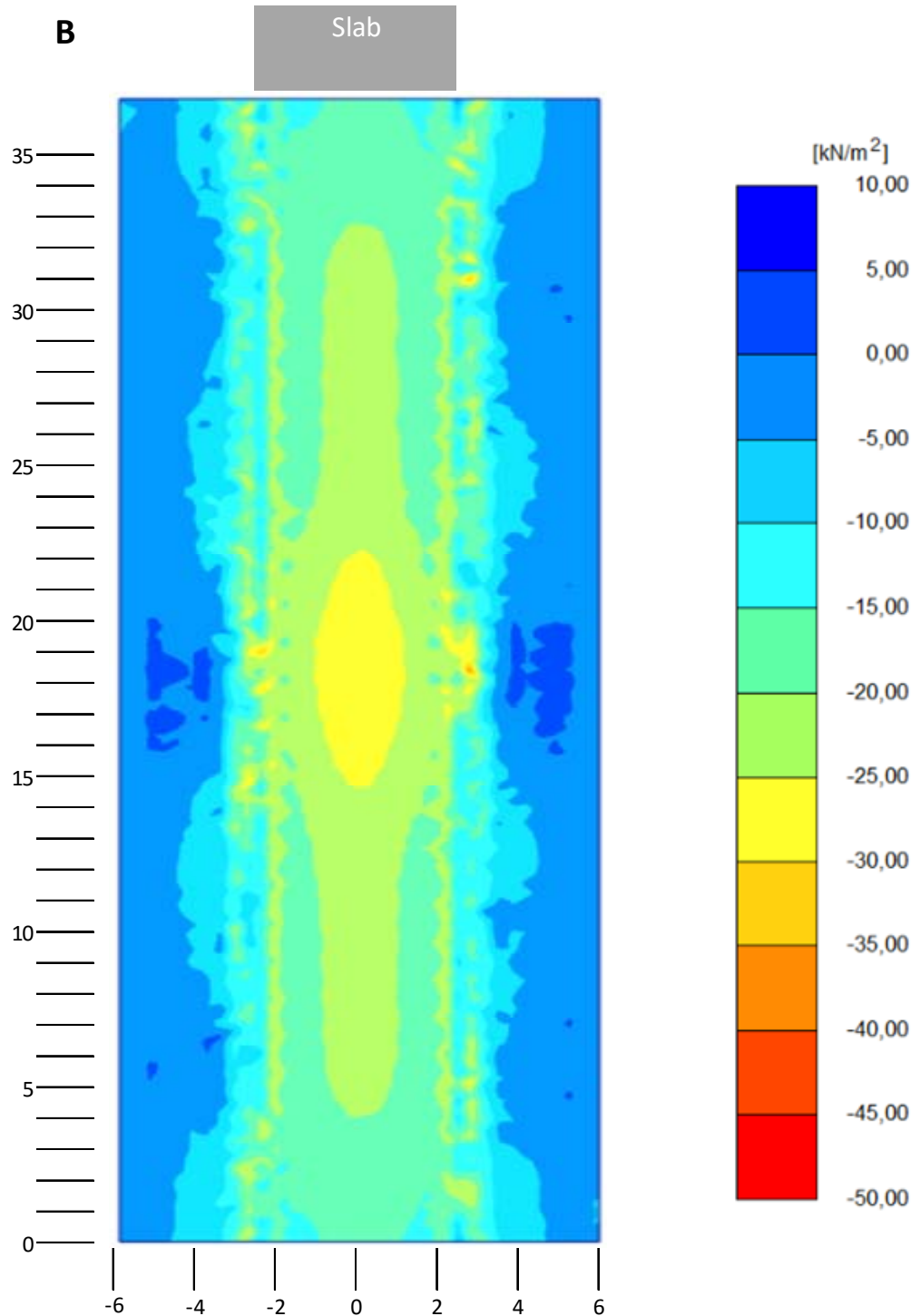


Figure 16. Longitudinal stresses, load model B, slab installation depth 2.5 meters, characteristic load.

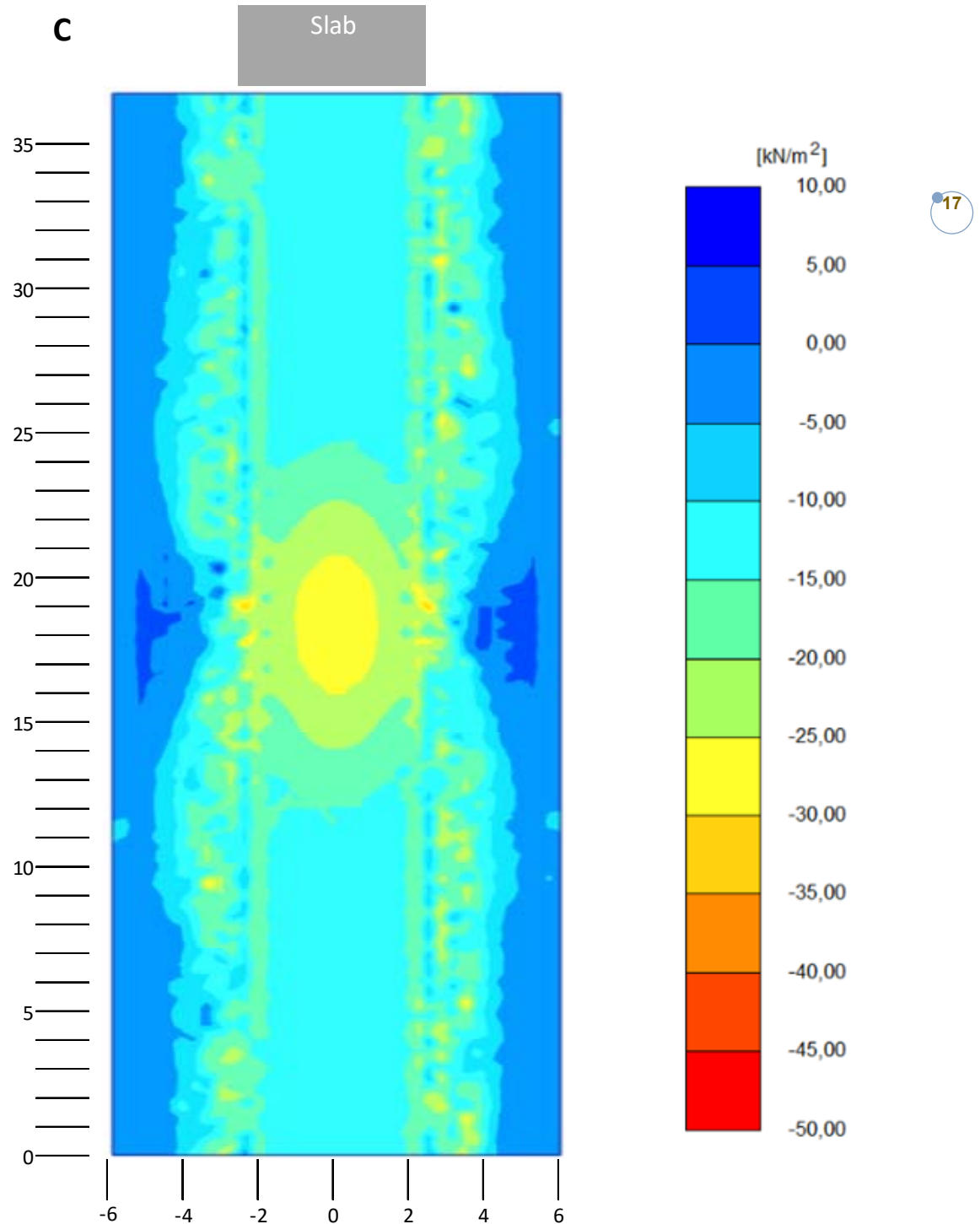


Figure 17. Longitudinal stresses, load model C, slab installation depth 2.5 meters, characteristic load.

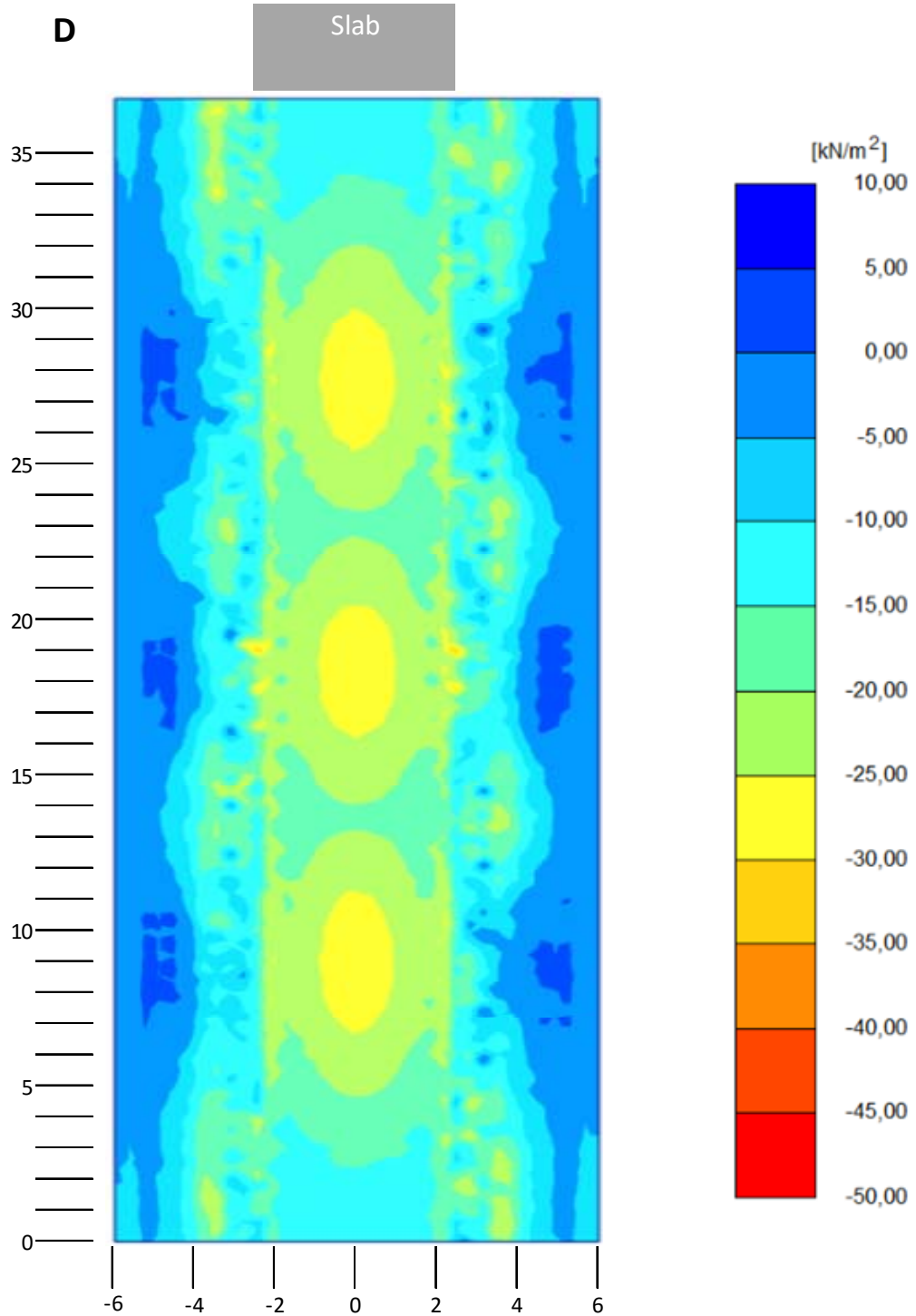


Figure 18. Longitudinal stresses, load model D, slab installation depth 2.5 meters, characteristic load.

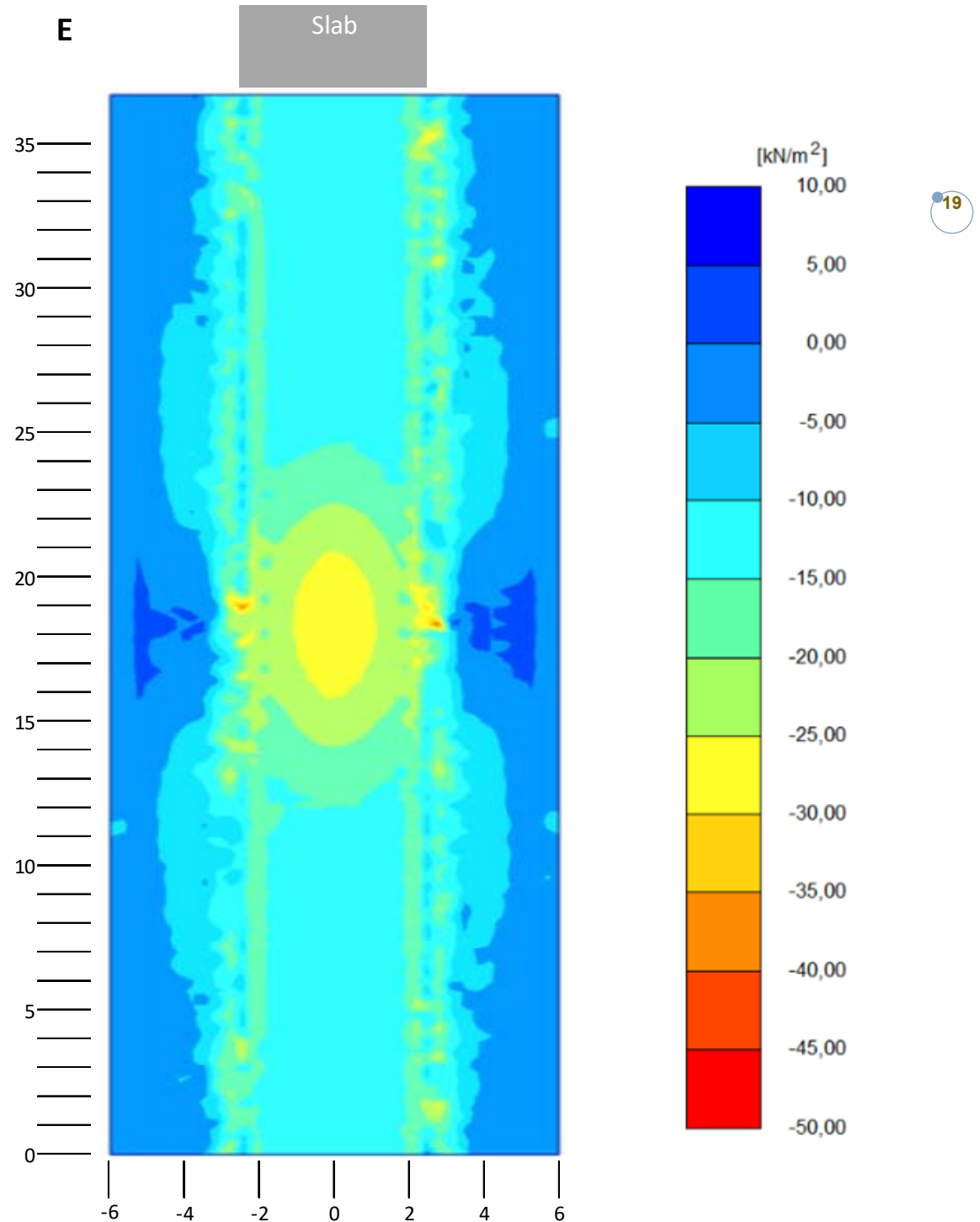


Figure 19. Longitudinal stresses, load model E, slab installation depth 2.5 meters, characteristic load.

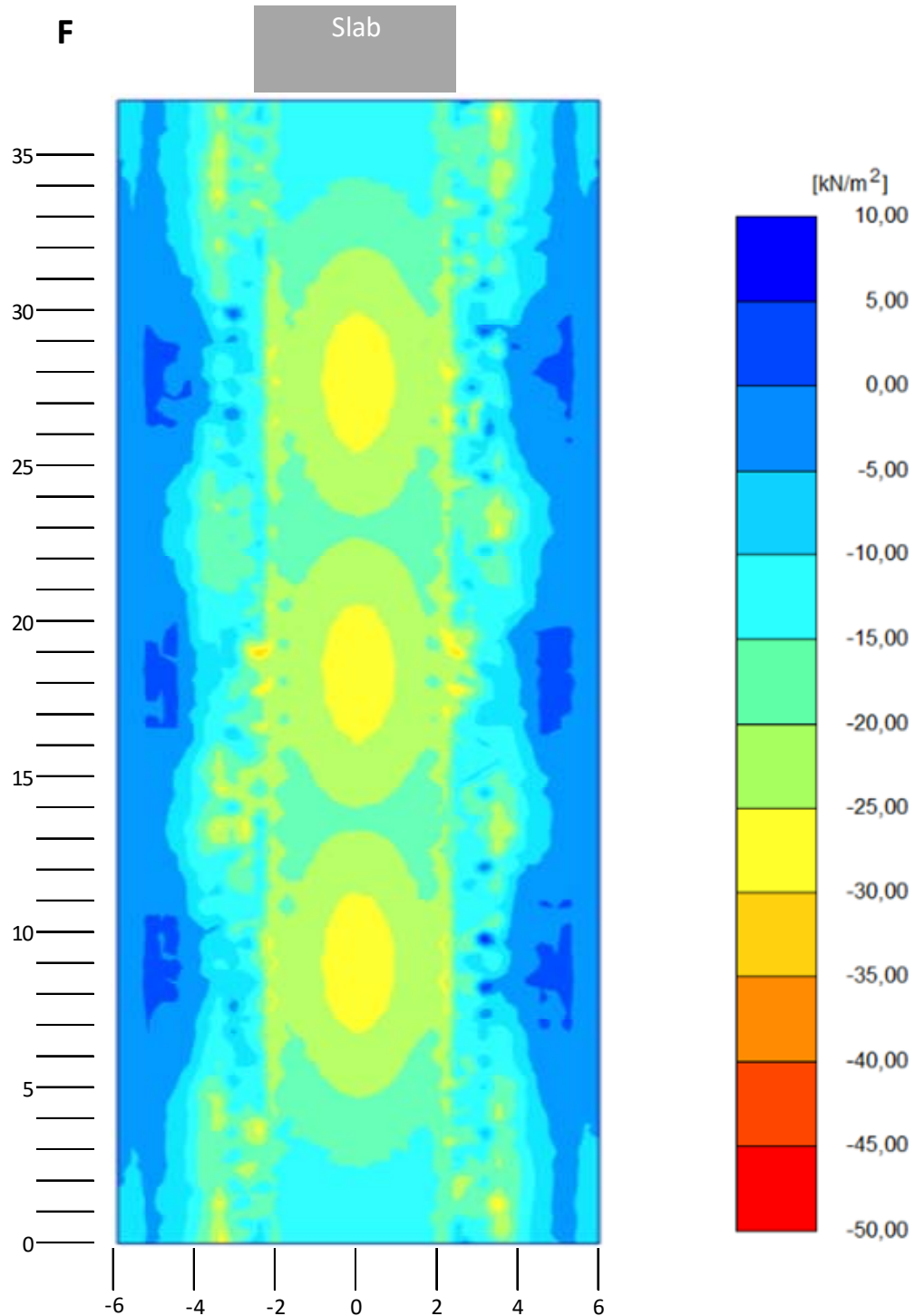


Figure 20. Longitudinal stresses, load model F, slab installation depth 2.5 meters, characteristic load.

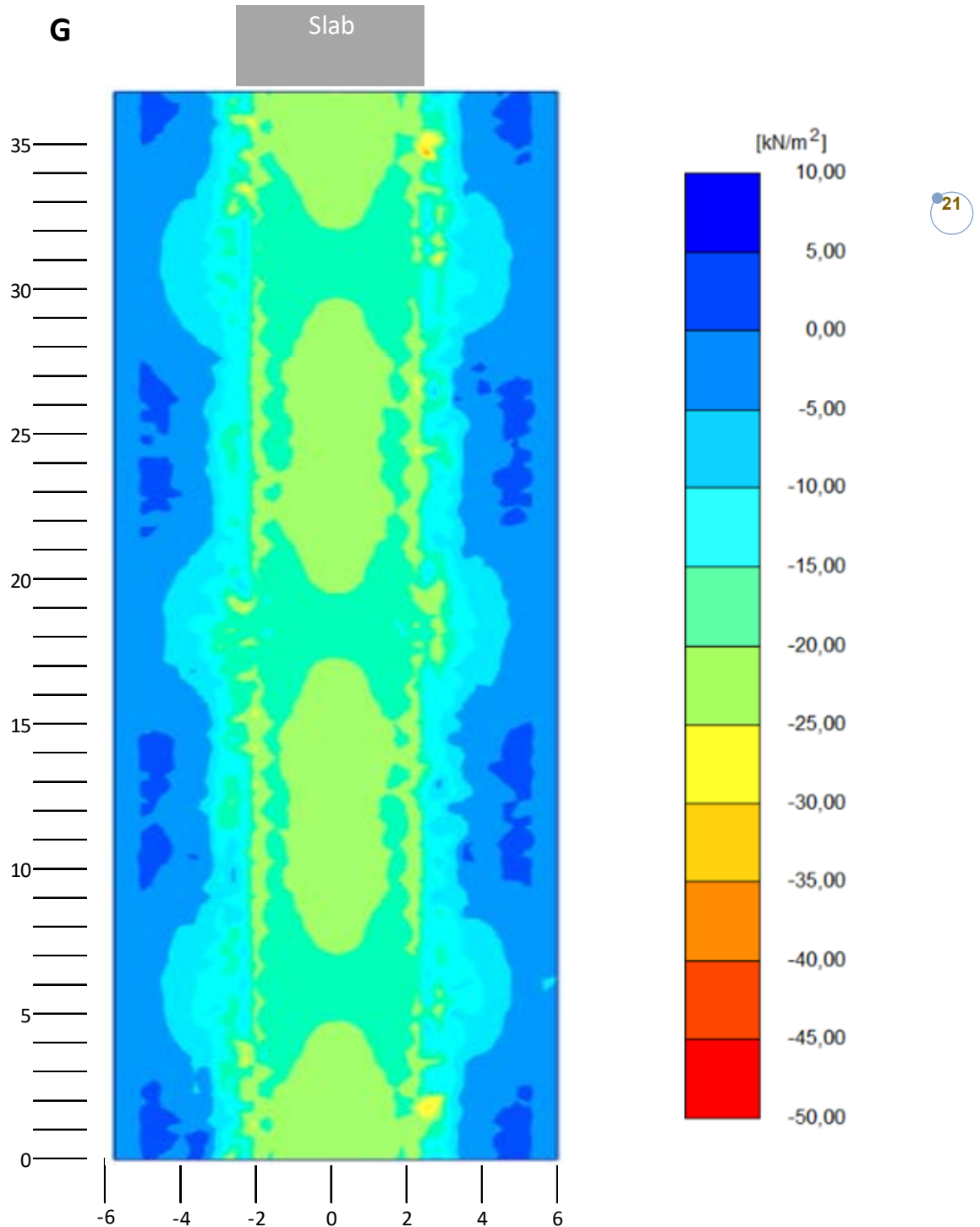


Figure 21. Longitudinal stresses, load model G, slab installation depth 2.5 meters, characteristic load.

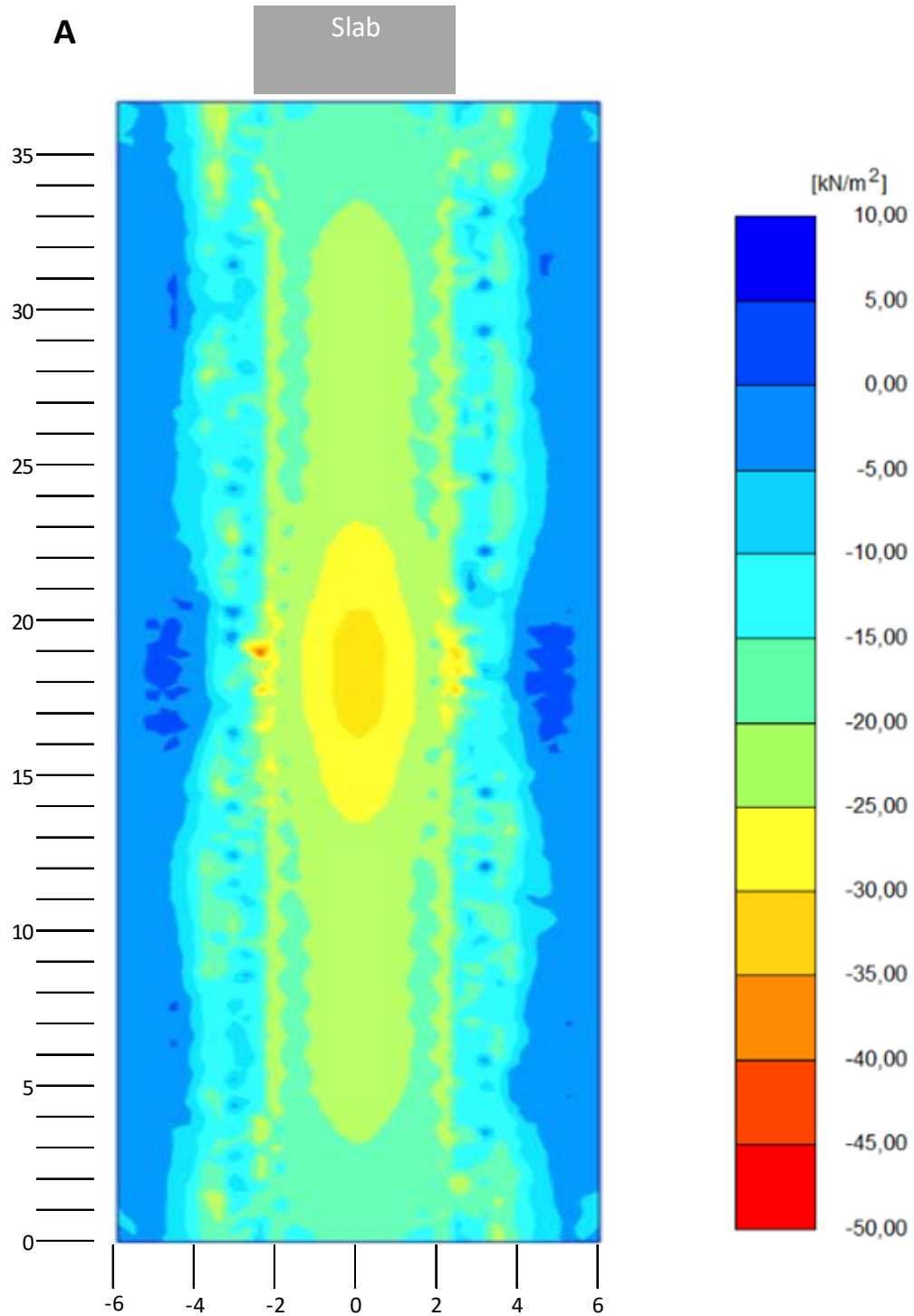


Figure 22. Longitudinal stresses, load model A, slab installation depth 2.5 meters, including dynamic load factor 1.25.

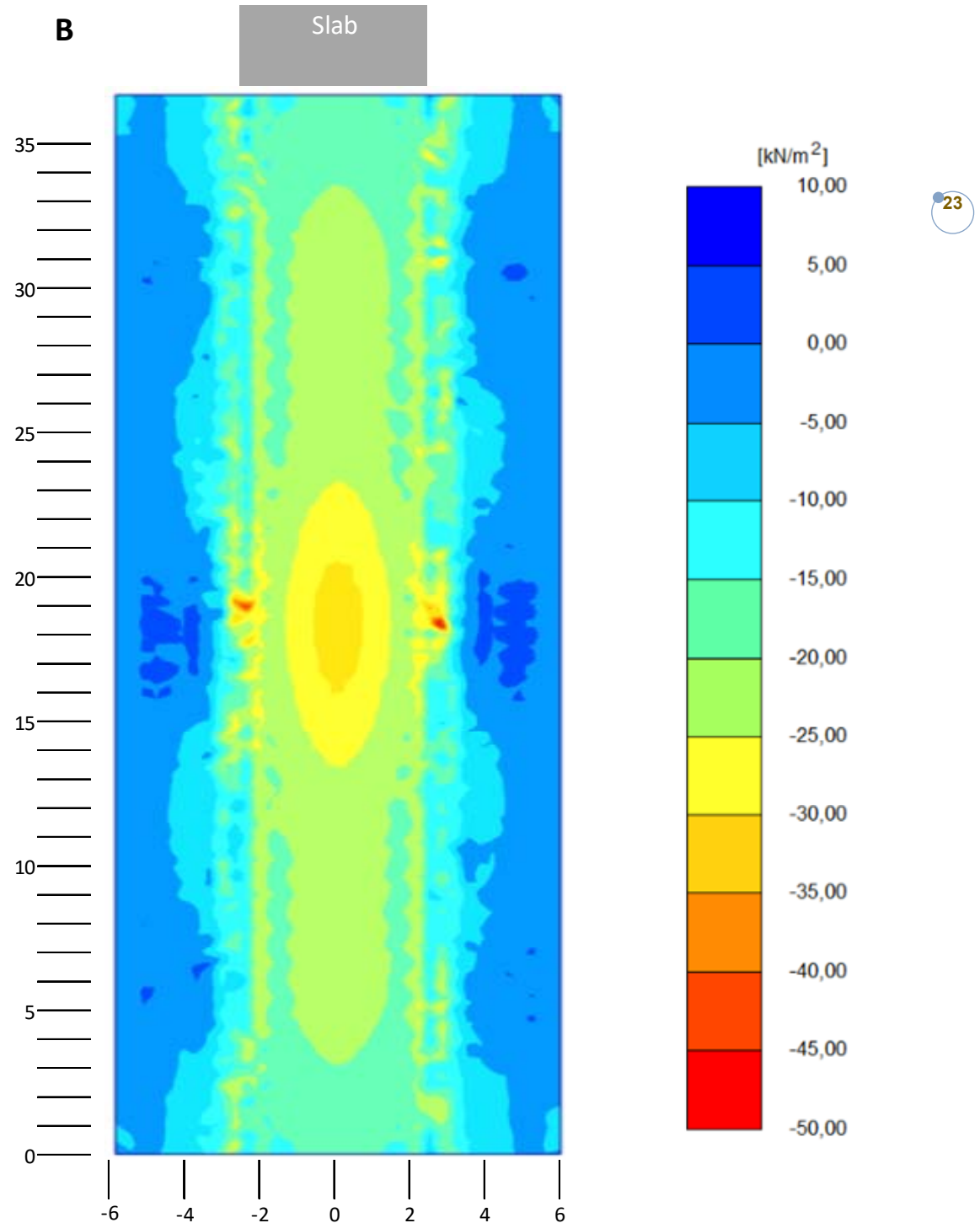


Figure 23. Longitudinal stresses, load model B, slab installation depth 2.5 meters, including dynamic load factor 1.25.

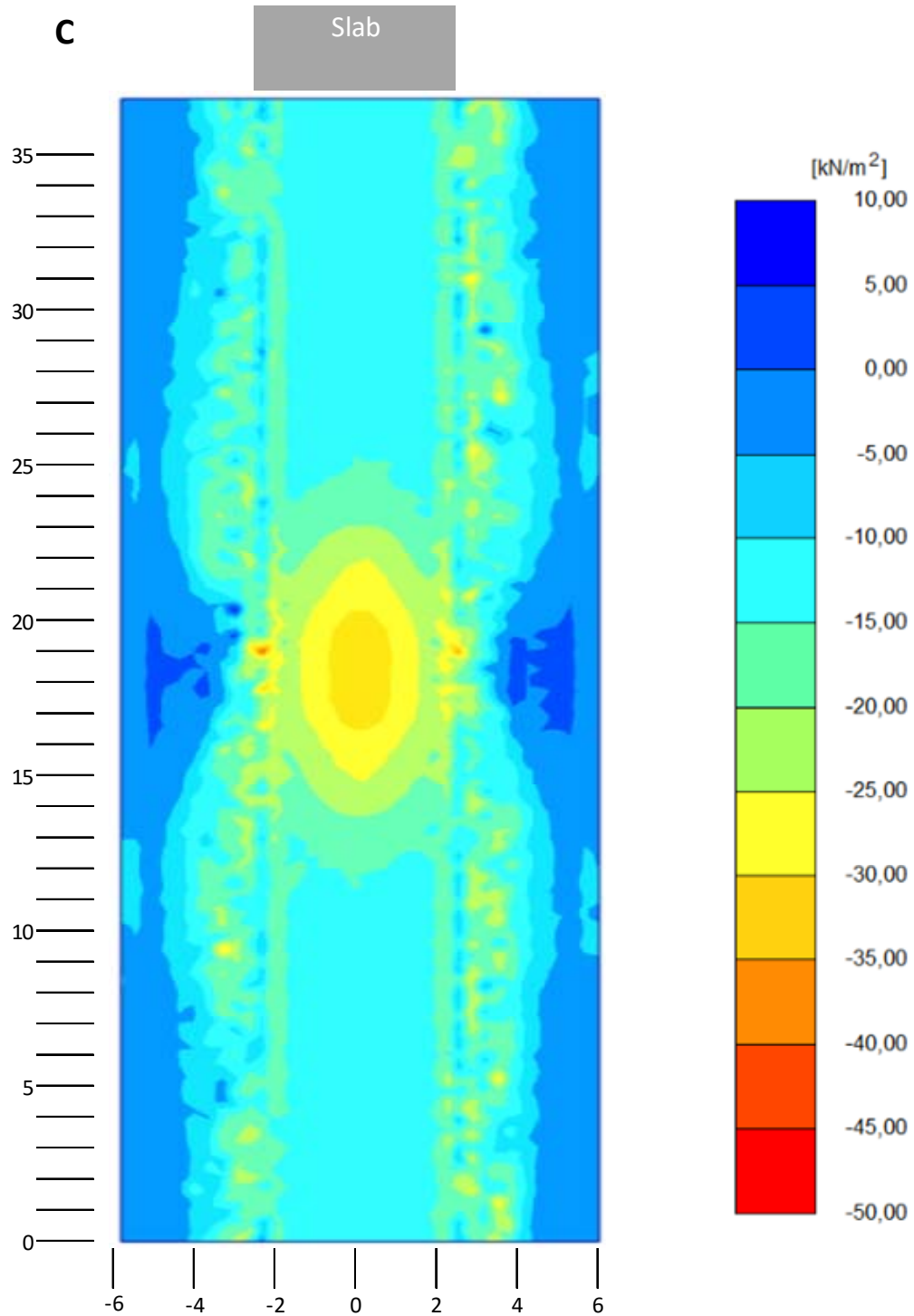


Figure 24. Longitudinal stresses, load model C, slab installation depth 2.5 meters, including dynamic load factor 1.25.

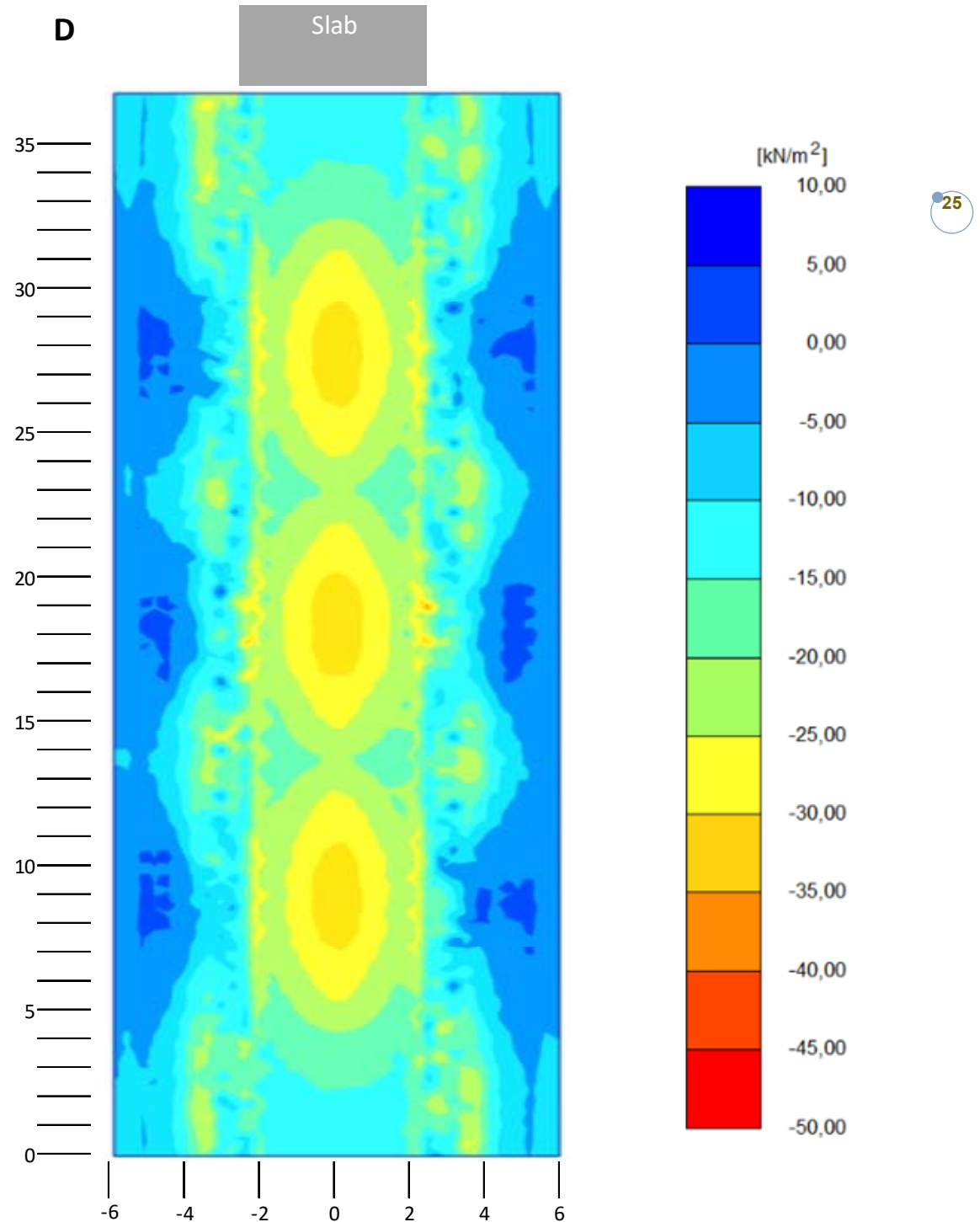


Figure 25. Longitudinal stresses, load model D, slab installation depth 2.5 meters, including dynamic load factor 1.25.

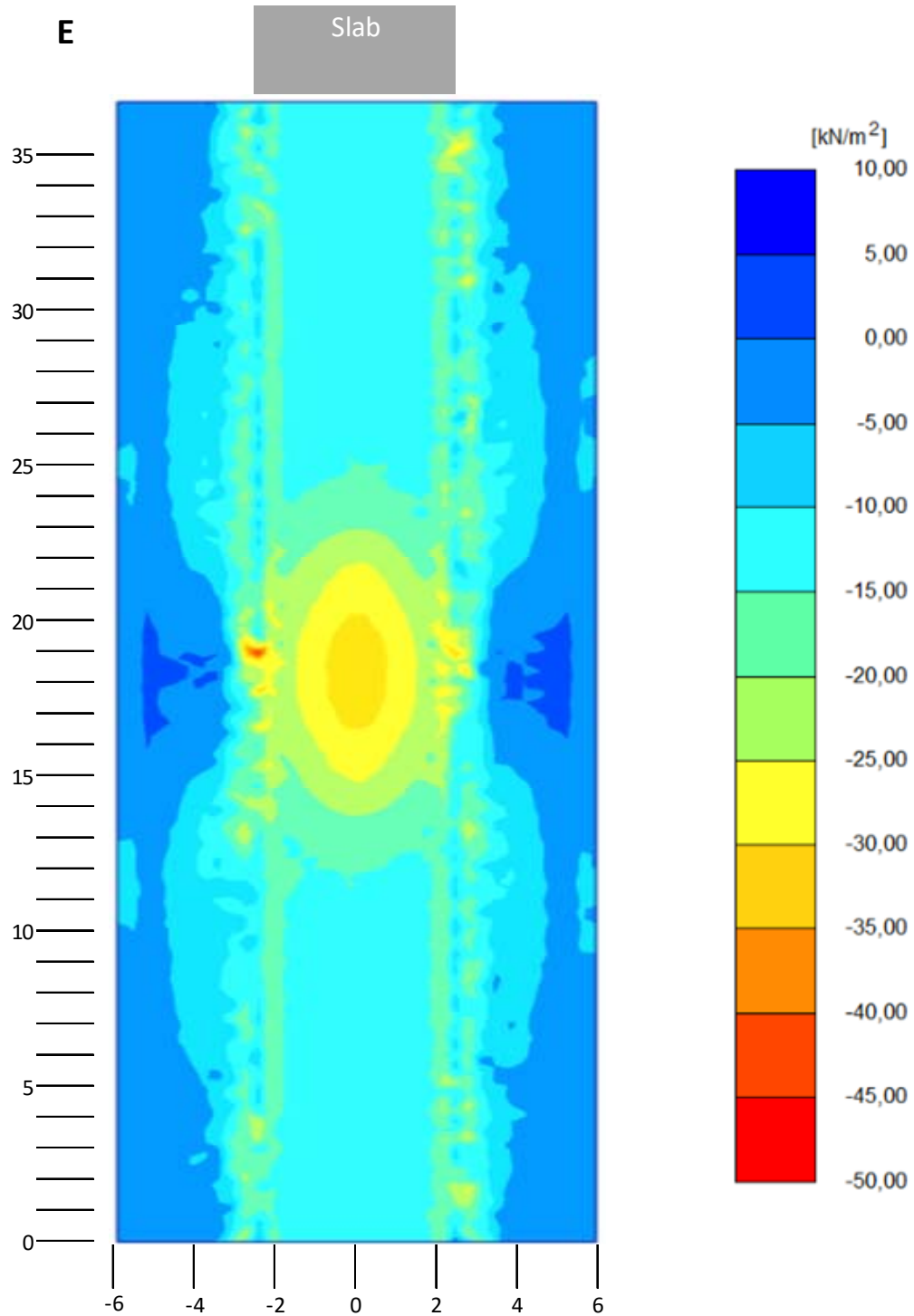


Figure 26. Longitudinal stresses, load model E, slab installation depth 2.5 meters, including dynamic load factor 1.25.

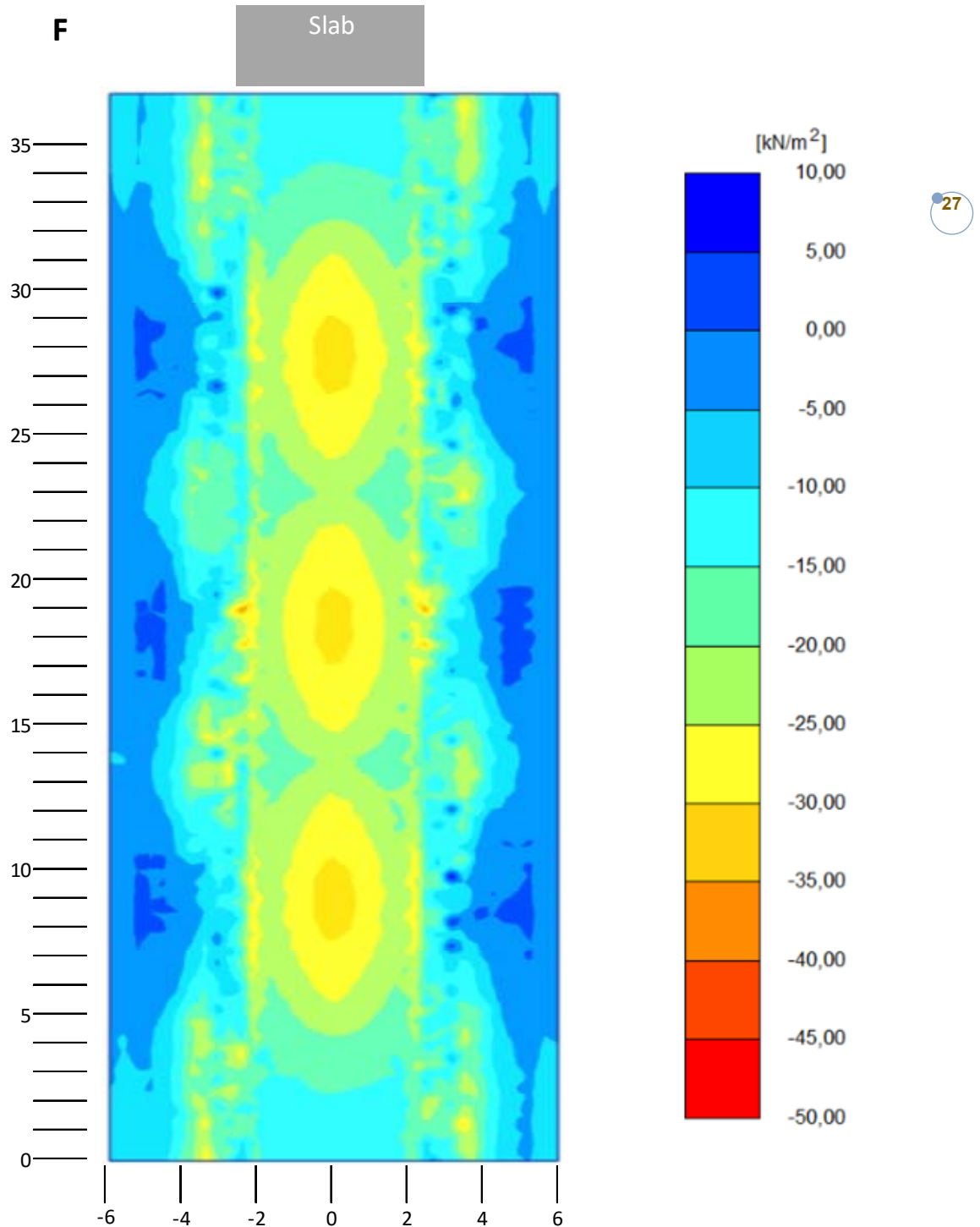


Figure 27. Longitudinal stresses, load model F, slab installation depth 2.5 meters, including dynamic load factor 1.25.

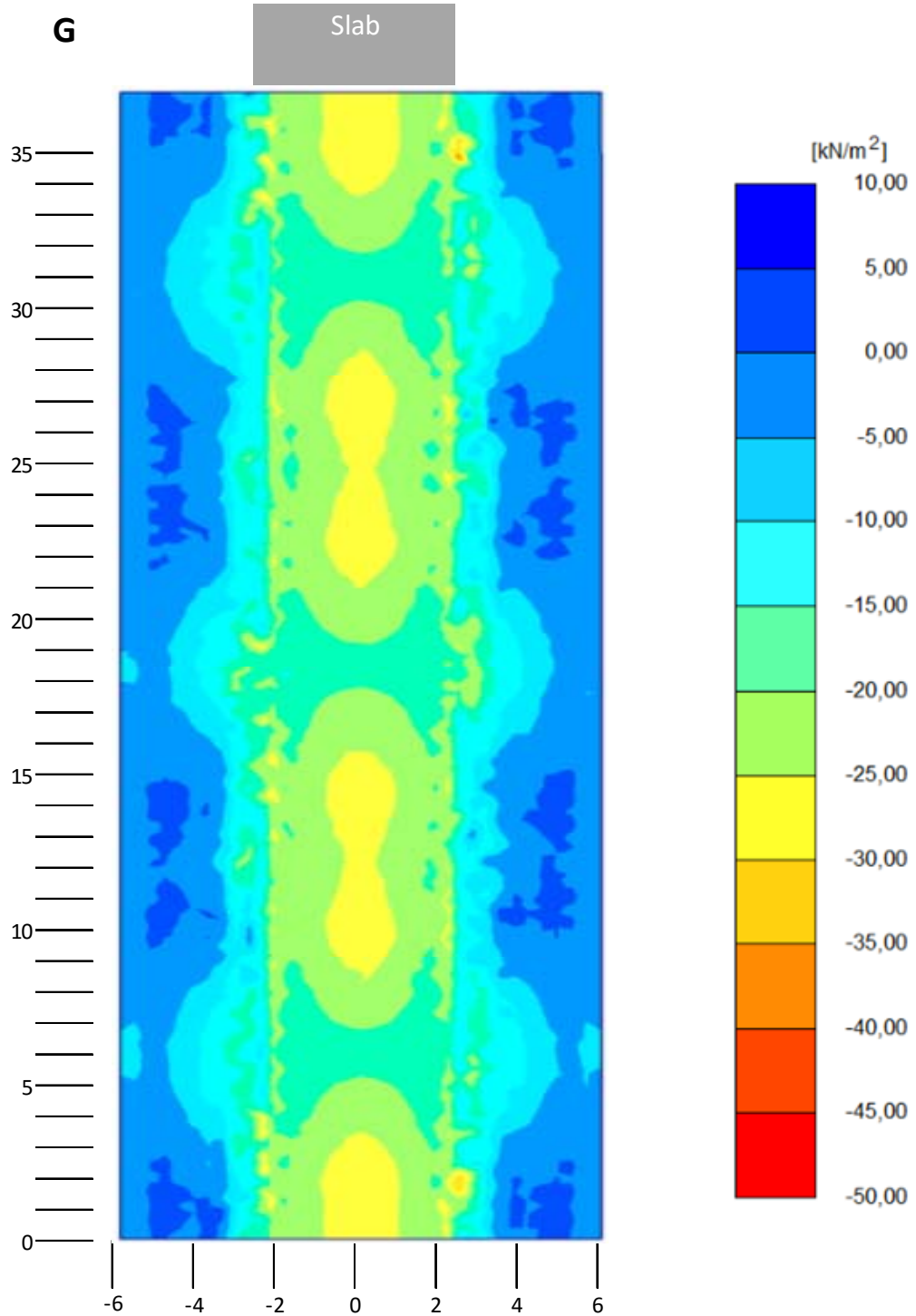


Figure 28. Longitudinal stresses, load model G, slab installation depth 2.5 meters, including dynamic load factor 1.25.

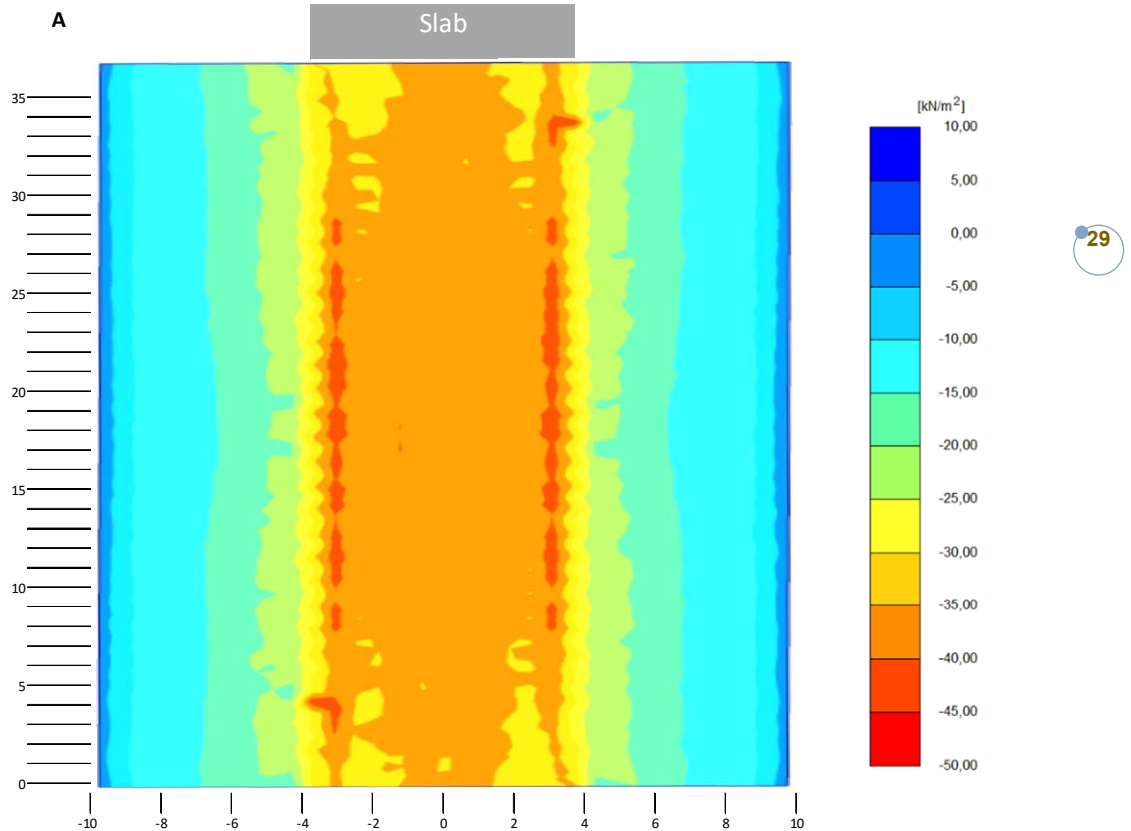


Figure 29. Longitudinal stresses, load model A, slab installation depth 5 meters, characteristic load.

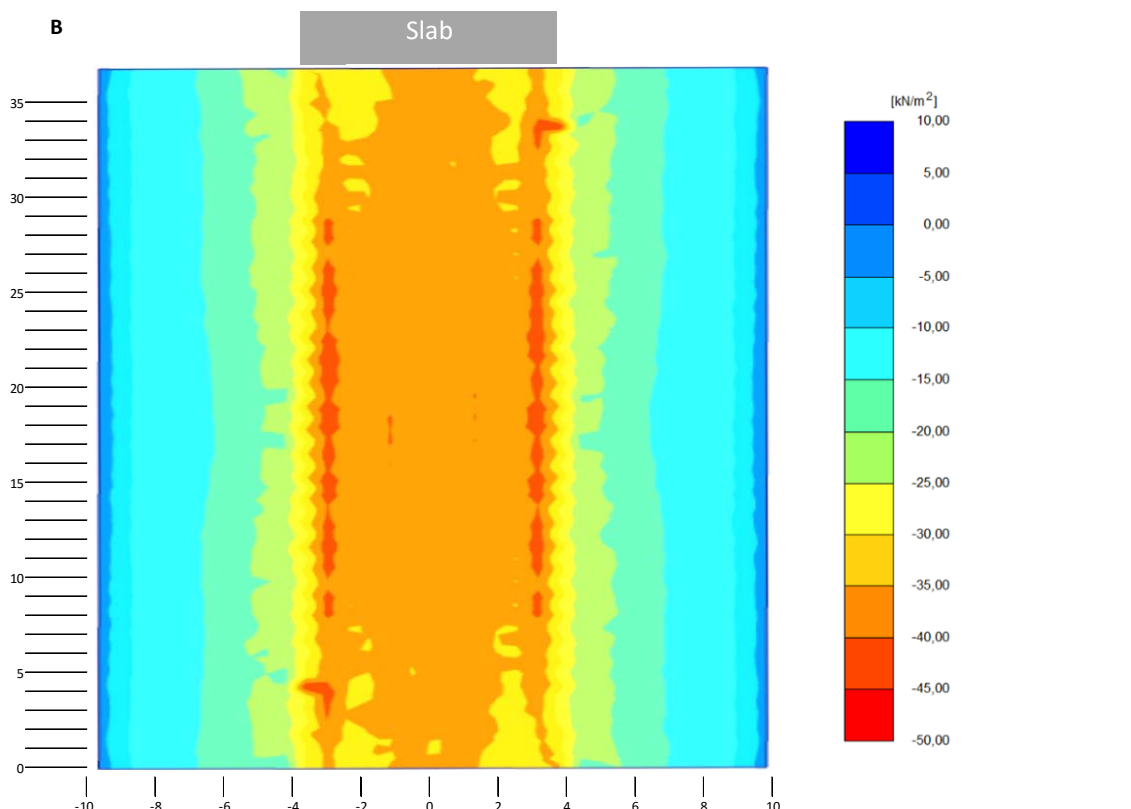


Figure 30. Longitudinal stresses, load model B, slab installation depth 5 meters, characteristic load.

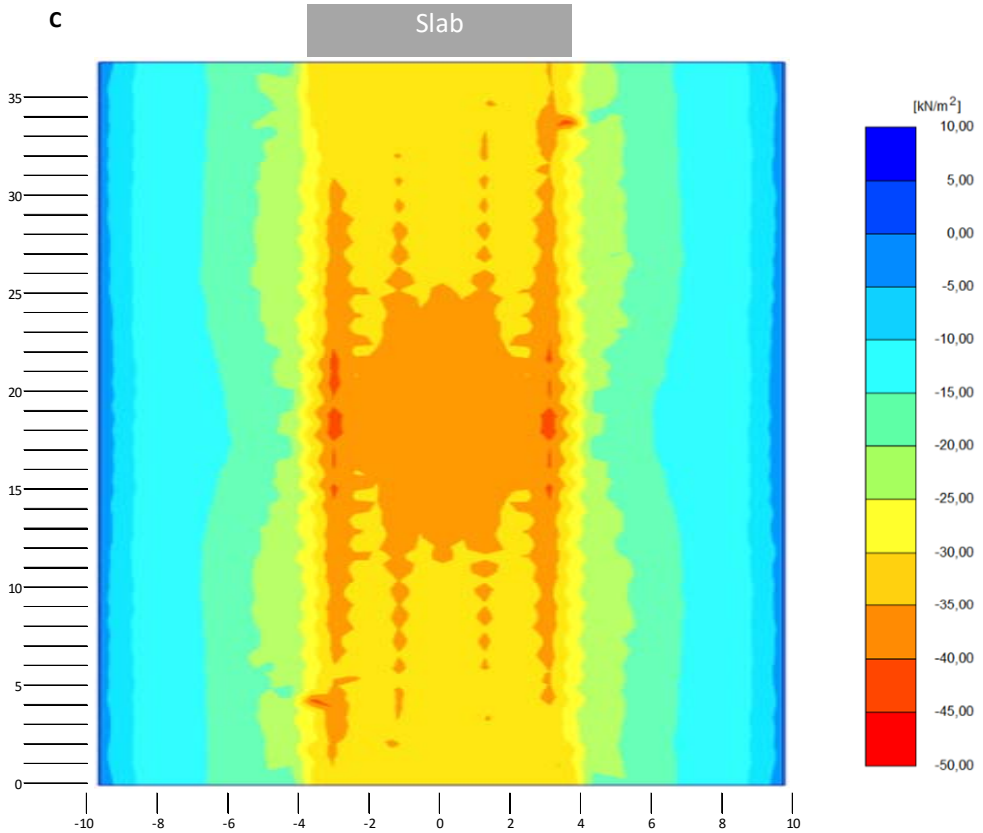


Figure 31. Longitudinal stresses, load model C, slab installation depth 5 meters, characteristic load.

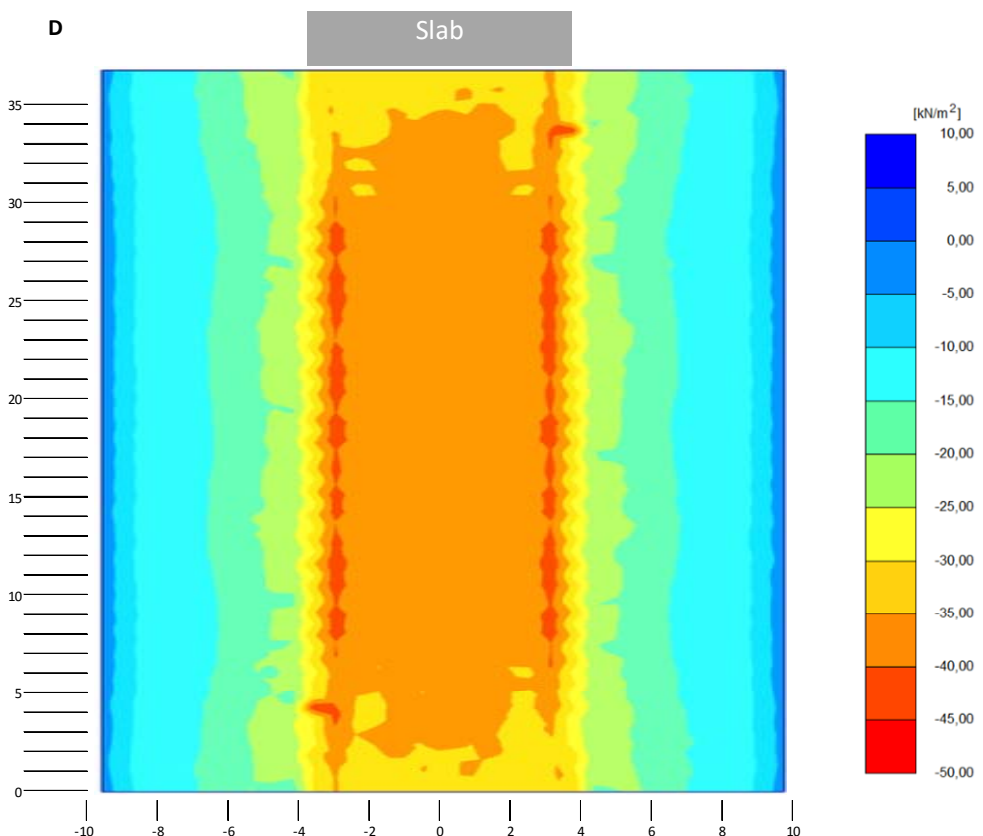


Figure 32. Longitudinal stresses, load model D, slab installation depth 5 meters, characteristic load.

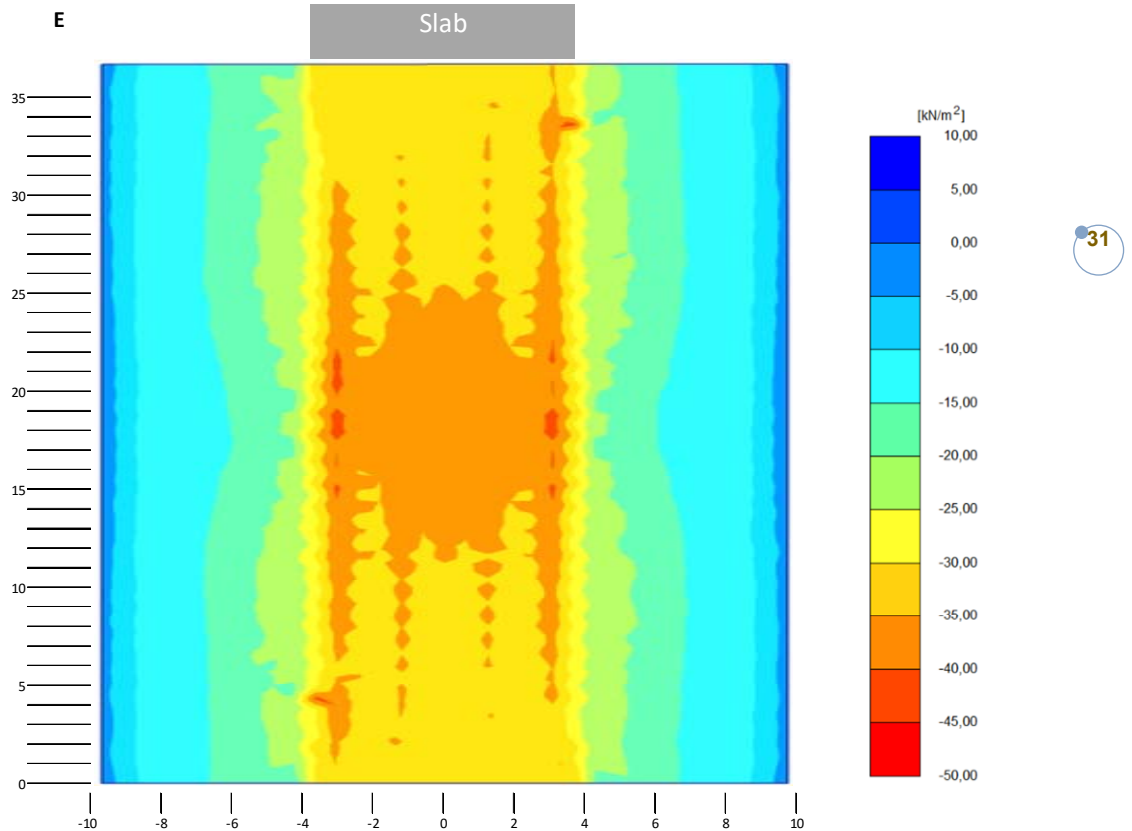


Figure 33. Longitudinal stresses, load model E, slab installation depth 5 meters, characteristic load.

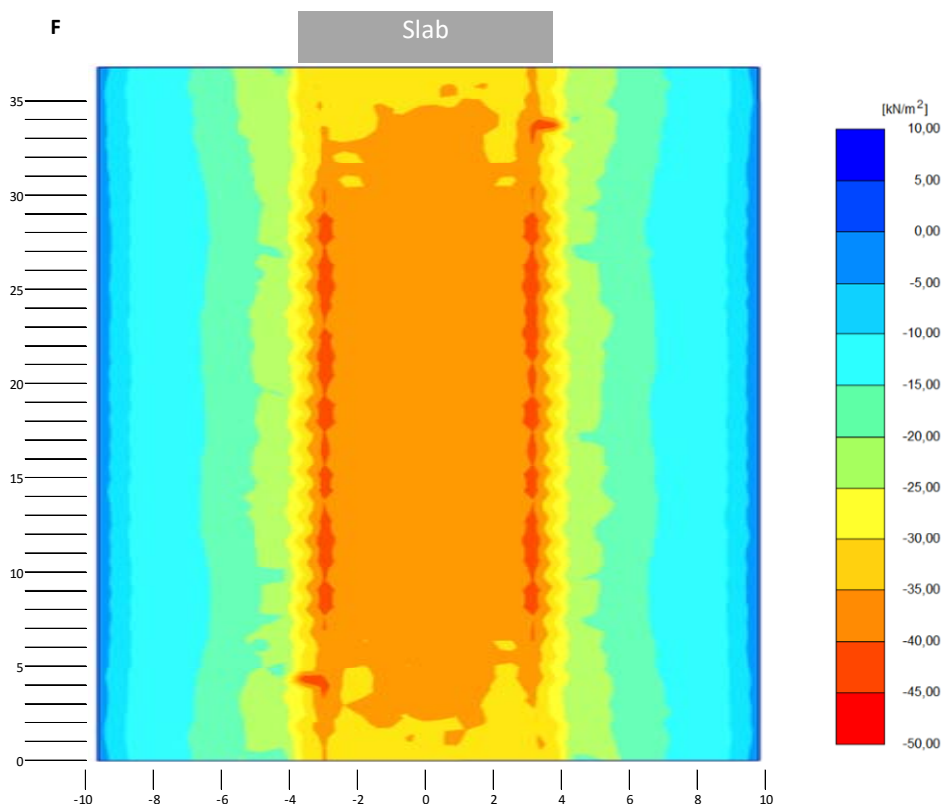


Figure 34. Longitudinal stresses, load model F, slab installation depth 5 meters, characteristic load.

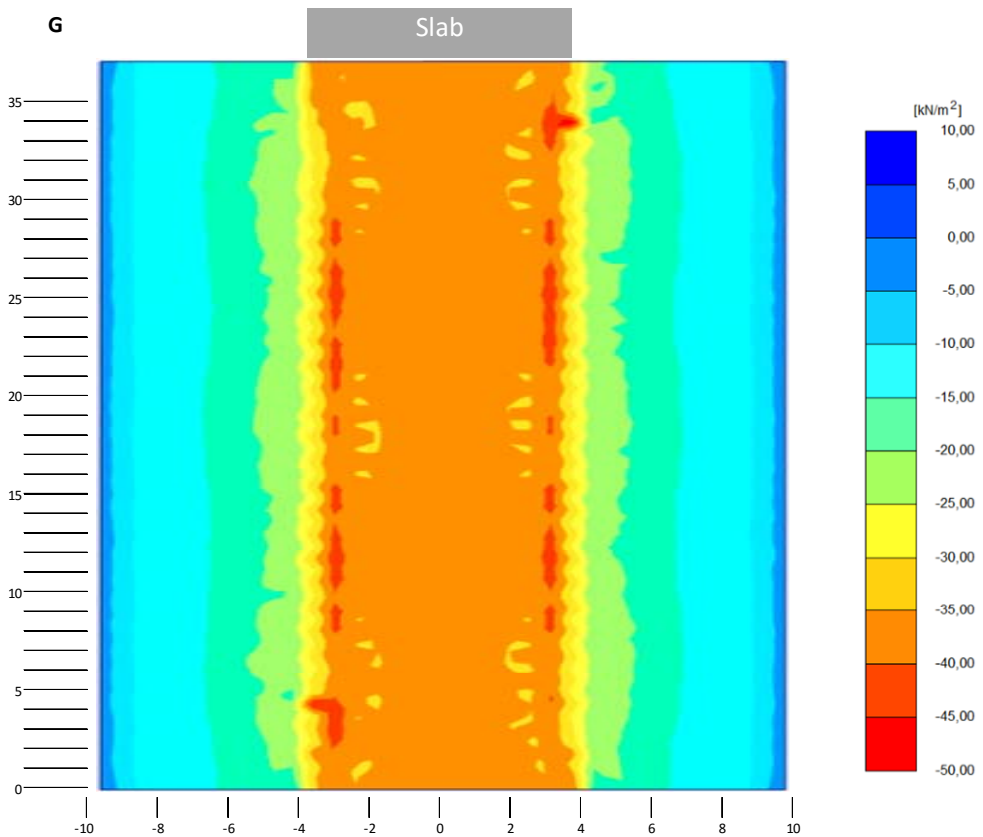


Figure 35. Longitudinal stresses, load model G, slab installation depth 5 meters, characteristic load.

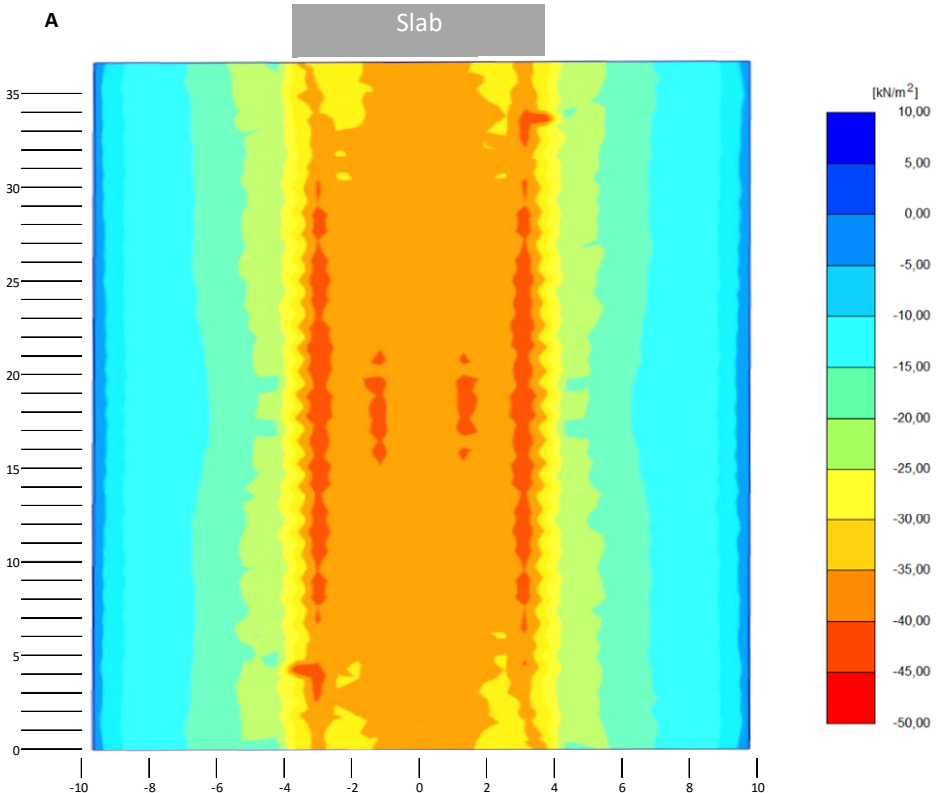


Figure 36. Longitudinal stresses, load model A, slab installation depth 5 meters, including dynamic load factor 1.25.

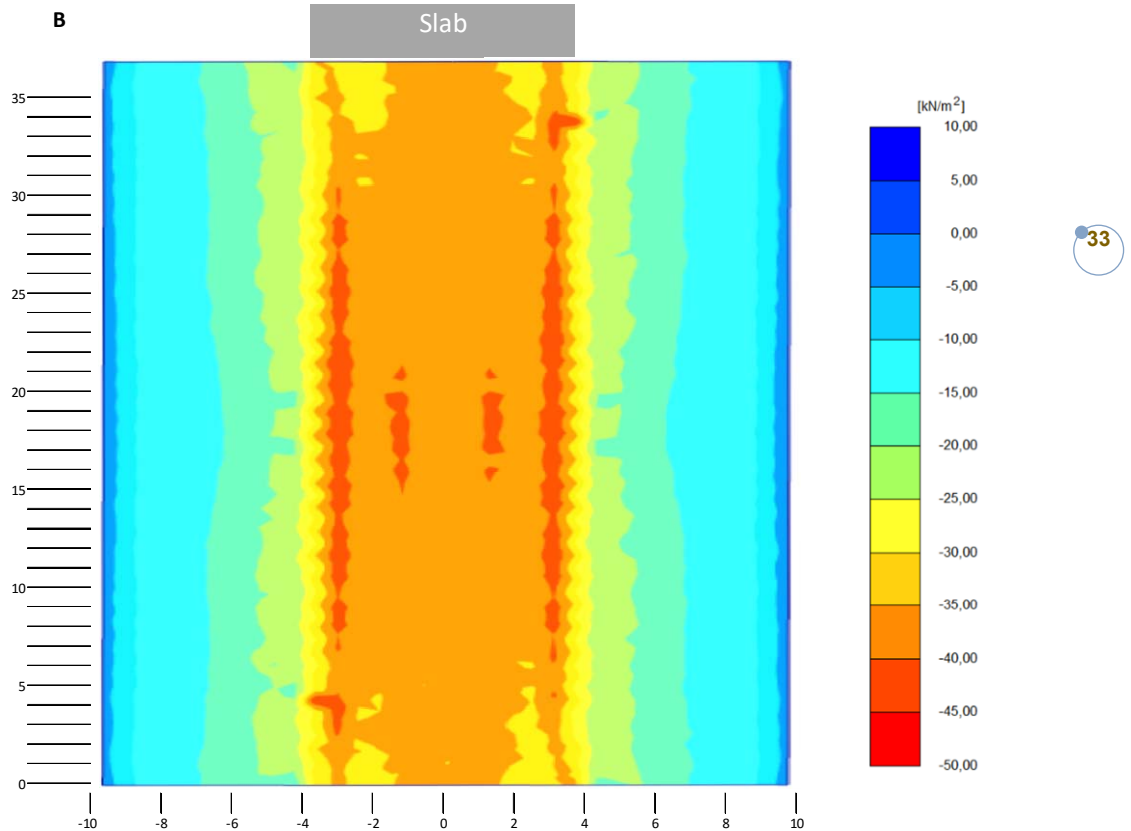


Figure 37. Longitudinal stresses, load model B, slab installation depth 5 meters, including dynamic load factor 1.25.

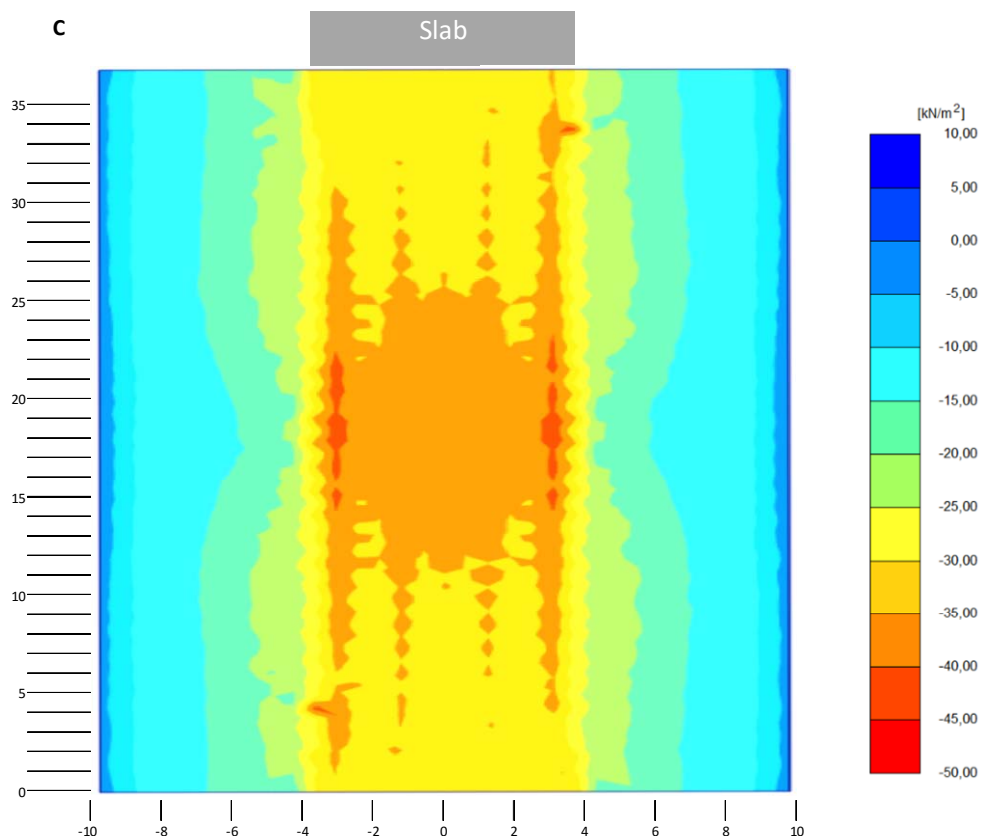


Figure 38. Longitudinal stresses, load model C, slab installation depth 5 meters, including dynamic load factor 1.25.

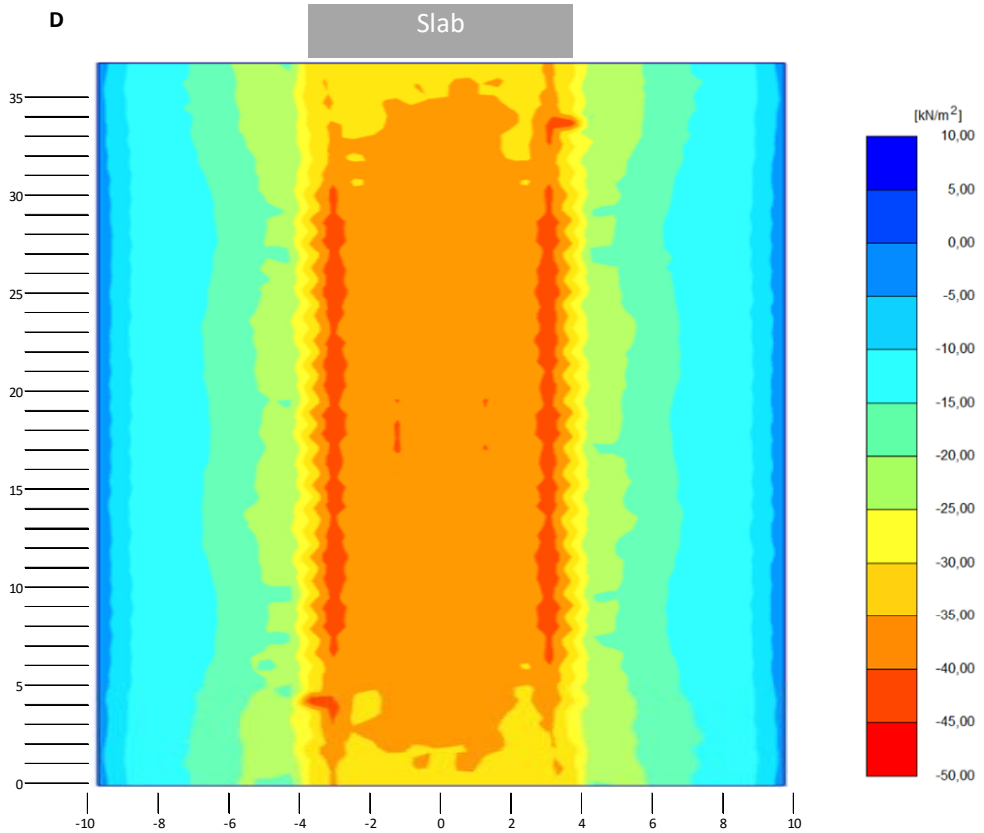


Figure 39. Longitudinal stresses, load model D, slab installation depth 5 meters, including dynamic load factor 1.25.

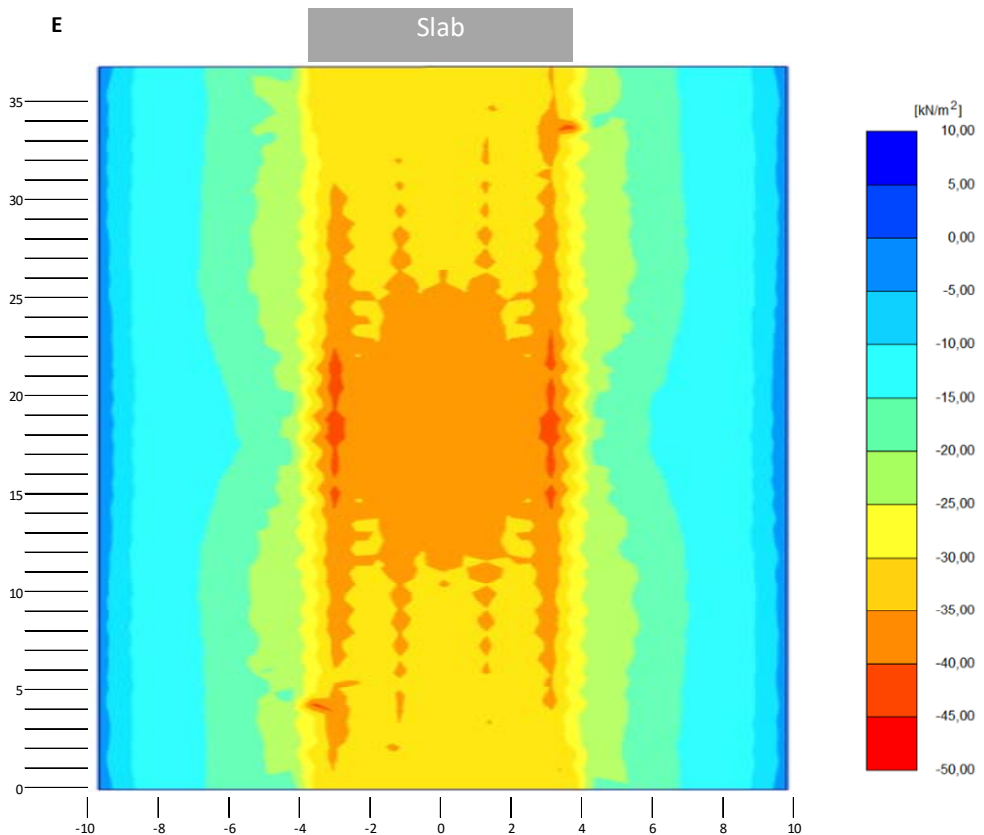


Figure 40. Longitudinal stresses, load model E, slab installation depth 5 meters, including dynamic load factor 1.25.

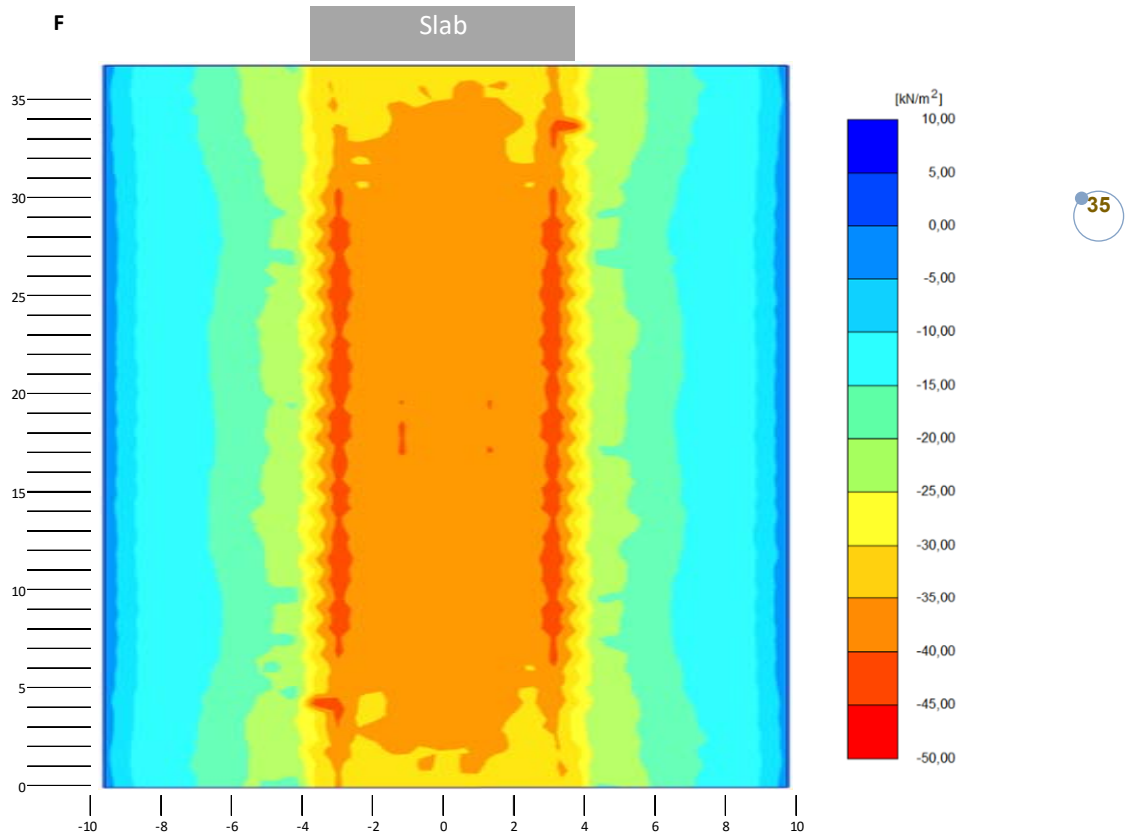


Figure 41. Longitudinal stresses, load model F, slab installation depth 5 meters, including dynamic load factor 1.25.

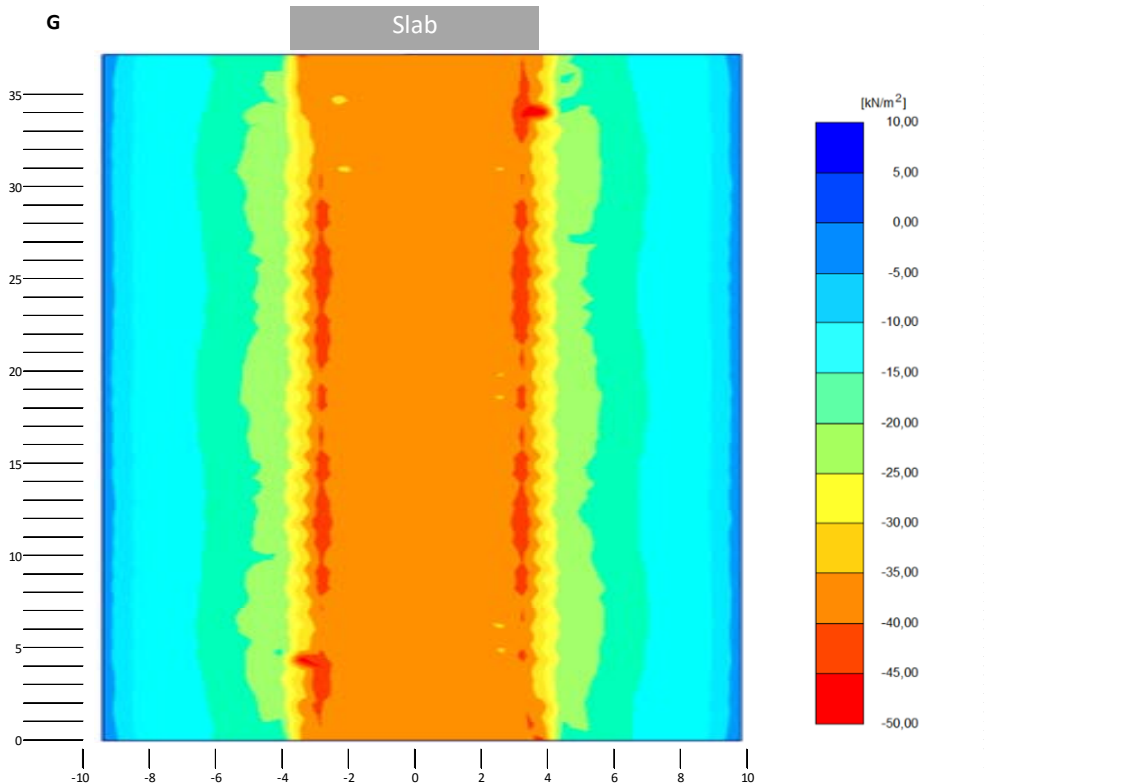


Figure 42. Longitudinal stresses, load model G, slab installation depth 5 meters, including dynamic load factor 1.25.

ISSN-L 1798-6656
ISSN 1798-6664
ISBN 978-952-317-416-0
www.liikennevirasto.fi

**Liik
enne
vira
sto**
Finnish Transport Agency